



<https://theses.gla.ac.uk/>

Theses Digitisation:

<https://www.gla.ac.uk/myglasgow/research/enlighten/theses/digitisation/>

This is a digitised version of the original print thesis.

Copyright and moral rights for this work are retained by the author

A copy can be downloaded for personal non-commercial research or study, without prior permission or charge

This work cannot be reproduced or quoted extensively from without first obtaining permission in writing from the author

The content must not be changed in any way or sold commercially in any format or medium without the formal permission of the author

When referring to this work, full bibliographic details including the author, title, awarding institution and date of the thesis must be given

Enlighten: Theses

<https://theses.gla.ac.uk/>
research-enlighten@glasgow.ac.uk

**STUDIES ON BACTERIAL TYPE II
DEHYDROQUINASES AND SHIKIMATE
DEHYDROGENASES**

Lewis David Brett Evans

Doctor of Philosophy Degree in Biochemistry



**UNIVERSITY
of
GLASGOW**

Division of Biochemistry and Molecular Biology, Institute of Biomedical and Life
Sciences

May, 2003.

ProQuest Number: 10391038

All rights reserved

INFORMATION TO ALL USERS

The quality of this reproduction is dependent upon the quality of the copy submitted.

In the unlikely event that the author did not send a complete manuscript and there are missing pages, these will be noted. Also, if material had to be removed, a note will indicate the deletion.



ProQuest 10391038

Published by ProQuest LLC (2017). Copyright of the Dissertation is held by the Author.

All rights reserved.

This work is protected against unauthorized copying under Title 17, United States Code
Microform Edition © ProQuest LLC.

ProQuest LLC.
789 East Eisenhower Parkway
P.O. Box 1346
Ann Arbor, MI 48106 – 1346

GLASGOW
UNIVERSITY
LIBRARY

13218

Copy 2

DECLARATION

This thesis has been written in accordance with the University regulations, has not been presented for a degree at any other university and is original except where indicated by reference in the text. The work contained within is the author's own except where work was done in collaboration as indicated. This thesis does not exceed 60,000 words.

© Lewis David Brett Evans, May 2003

Signed

Date

1/16/2003

ABSTRACT

The enzymes dehydroquinase and shikimate dehydrogenase catalyse the third and fourth steps of the biosynthetic shikimate pathway, respectively. The work in this thesis investigates the active sites and overall structure of bacterial type II dehydroquinases, shikimate dehydrogenases and related proteins using biochemical and biophysical techniques.

The active site of *Streptomyces coelicolor* type II dehydroquinase (SCDHQase) was characterised by site-directed mutagenesis of the residues: Arg113, His106, Glu104, Ser108 and Tyr28, proposed to be important in previous structural studies of the enzyme. None of the mutations significantly altered the secondary or tertiary structure of the enzyme as shown by circular dichroism. All five mutations significantly decreased the catalytic activity; the most effective mutation was the Y28F mutation with a 4700-fold reduction in activity. This has provided strong evidence of the role of each of the residues within the active site.

To date *Bacillus subtilis* is the only organism known whose genome encodes proteins that resemble both types of dehydroquinase. The type I dehydroquinase was shown to be the active form in cell extracts of *B. subtilis* by sodium borohydride trapping of the Schiff base involved in the mechanism of all type I dehydroquinases. The YqhS protein from *B. subtilis* has 47% identity to the *S. coelicolor* type II dehydroquinase. However, YqhS has been found to have an extremely low level of dehydroquinase activity ($k_{\text{cat}} < 10^{-4} \text{ s}^{-1}$). YqhS has a phenylalanine in place of the highly conserved tyrosine residue found to be catalytically important and implicated in proton abstraction at C2 of the substrate. Site-directed mutagenesis of the phenylalanine to a tyrosine (F23Y) effected a 2000-fold increase in k_{cat} . Growth experiments on the disruption mutant of the *yqhS* gene (YqhSd) produced by the Japanese *Bacillus* Consortium show that the gene is essential for growth in minimal medium.

Detailed studies of the pII dependence, effects of salts on catalytic activity and the inhibitory effect of polyanions were performed on the type II dehydroquinases of *S. coelicolor*, *Mycobacterium tuberculosis* (MUDHQase), *Helicobacter pylori* (HPDHQase) and *B. subtilis* (F23Y mutant). pH-dependence studies on all the dehydroquinases tested show that there is a seven-fold increase in k_{cat} between pH 6.5 and 8.0 indicating that all of these type II DHQases share the same catalytic

mechanism. Low concentrations of chloride cause a moderate increase the catalytic activity of MTDHQase and a 4-fold increase in k_{cat} for HPDQase. In contrast, the k_{cat} of both SCDHQase and *B. subtilis* (F23Y mutant) decreases in the presence of low concentrations of chloride. The differences in the effect of chloride are thought to arise from variations in the flexibility of dehydroquinase structures. Polyanions (sulphate and phosphate) are competitive inhibitors of SCDHQase and HPDQase. The interactions are more complex in MTDHQase and *B. subtilis* YqhS (F23Y). Analysis of the X-ray structures of SCDHQase and MTDHQase reveals contrasting modes of binding of polyanions between the two enzymes. The differences between the interactions and binding of polyanions in type II dehydroquinases may help to explain the relative potencies of rationally designed inhibitors.

The *Haemophilus influenzae* paralogs; shikimate dehydrogenase (HIAroE) and shikimate dehydrogenase related protein (HIYdiB) have been investigated using steady-state kinetics and detailed analysis of their sequences in relation to the published X-ray structures of *Escherichia coli* shikimate dehydrogenase and YdiB protein. Both HIAroE and HIYdiB are NADPH-dependent dehydrogenases and catalyse the oxidation of shikimate to form dehydroshikimate, with k_{cat} values of 194 and 19 s^{-1} , respectively. HIAroE is also able to oxidise quinate as part of the catabolic quinate pathway (k_{cat} of 50 s^{-1}). Fluorescence quenching studies have demonstrated that shikimate is able to bind to HIAroE in the absence of cofactor. HIAroE is likely to follow a random sequential mechanism. The function of HIYdiB is still unclear as the catalytic activity of the HIYdiB protein is significantly lower than the HIAroE enzyme for all the substrates tested. The N-terminal amino acid sequence of the HIYdiB protein is significantly different from the *E. coli* YdiB and other members of the shikimate dehydrogenase family and it is proposed that the N-terminal region defines the function of this protein.

To my Parents

ACKNOWLEDGEMENTS

This project would not have been possible without the help and direction of Prof. John Coggins, Prof. Nick Price and Dr. Adrian Laphorn who have all given me their guidance; knowledge, advice and ideas which have been invaluable.

In the Joseph Black building, I would like to thank my colleagues in B4-17, Bernhard Lohkamp for his immeasurable help with the many aspects of this project as well as his encouragement; David Robinson for the purification of the *M. tuberculosis* and *H. pylori* dehydroquinases and many useful discussions. I would also like to thank Lorna Noble for the production of extremely pure dehydroquinase; Alex Herbert for the purified YqhS protein and Kirsten Fleming for her assistance with western blot experiments. In the circular dichroism laboratory I would like to thank Dr. Sharon Kelly for her valuable technical support and introduction to Opera and Dr. Eleanora Cerasoli for her interesting conversation.

In the Davidson building, I would like to thank John Greene who has kept me smiling throughout my project with his pure protein and insightful comments; Dr. Samantha Campbell for the *H. influenzae aroE* clone and Prof. Les Fixter for several helpful discussions on the YqhS protein.

At the University of Strathclyde I would like to thank Prof. Iain Hunter and his group for help with molecular biology and Dr. Craig Roberts for the production of the YqhS antibodies.

I am extremely grateful to Prof. T. Sato and Michio Takeuchi at the Tokyo University of Agriculture and Technology for the disruption mutant of the *yqhS* gene; Rick Ye at Dupont for the invaluable microarray data and Dr. Malcolm Horsburgh at the University of Sheffield for useful advice on the growth of *B. subtilis*.

I would like to thank Gillian, Wendy and Janet whose organisational skills helped me to find time in John's busy schedule. I am also indebted to the BBSRC for financial support.

Finally I would like to give my special thanks to Polly who has believed in me and supported me throughout this project.

ABBREVIATIONS

ATP	adenosine triphosphate
BSA	bovine serum albumin
CAPS	cyclohexylaminopropane sulphonic acid
CD	circular dichroism
CIAP	calf intestine alkaline phosphatase
Da	dalton
DHQase	dehydroquinase
DMF	dimethylformamide
DMSO	dimethyl sulphoxide
DNA	deoxyribonucleic acid
DNase	deoxyribonuclease
dNTP	deoxynucleotide
DTT	dithiothreitol
ϵ	absorption coefficient
ECL	electrochemiluminescence
ECYdiB	<i>Escherichia coli</i> YdiB protein
EDTA	ethylenediaminetetraacetic acid
GdmCl	Guanidine hydrochloride
IIIAroE	<i>Haemophilus influenzae</i> shikimate dehydrogenase
HIYdiB	<i>Haemophilus influenzae</i> YdiB protein
HPDHQase	<i>Helicobacter pylori</i> dehydroquinase
HPLC	High pressure liquid chromatography
HRP	horse radish peroxidase
IEF	isoelectric focusing

IPG	immobilisation pH gradient
K_m	Michaelis constant
LB	luria broth
MADLI-tof	matrix-assisted laser desorption ionization-time of flight
mRNA	messenger ribonucleic acid
MTDHQase	Mycobacterium tuberculosis dehydroquinase
MW	molecular weight
NAD^+	nicotinamide adenine denucleotide (oxidised form)
NADH	nicotinamide adenine denucleotide (reduced form)
$NADP^+$	nicotinamide adenine denucleotide phosphate (oxidised form)
NADPH	nicotinamide adenine denucleotide phosphate (reduced form)
NB	nutrient broth
PBS	Phosphate Buffer saline
PCR	polymerase chain reaction
PGO	phenylglyoxal
psi	pounds per square inch
PVDF	polyvinylidene difluoride
rpm	revolutions per minute
SCDHQase	Streptomyces coelicolor dehydroquinase
TCA	tricarboxylic acid
Tris	tris (hydroxymethyl) aminomethane
U	units of enzyme activity
UV	ultraviolet
X-gal	5-bromo-4-chloro-3-indoyl- β -d-galactoside

CONTENTS

DECLARATION.....	2
ABSTRACT	3
ACKNOWLEDGEMENTS.....	6
ABBREVIATIONS	7
CHAPTER 1 INTRODUCTION.....	21
<i>1.1 The shikimate pathway.....</i>	<i>21</i>
1.1.1 Enzymes of the shikimate pathway.....	24
1.1.1.1 3-deoxy-D-arabino-heptulosonate-7-phosphate synthase (DAHPS) (EC 4.1.2.15)	24
1.1.1.2 Dehydroquinase synthase (EC 4.6.1.3)	26
1.1.1.3 Dehydroquinase (EC 4.2.1.10).....	28
1.1.1.4 Shikimate dehydrogenase (EC 1.1.1.25).....	29
1.1.1.5 Shikimate kinase (EC 2.7.1.71).....	29
1.1.1.6 5-enolpyruvylshikimate 3-phosphate synthase (EC 2.5.1.19)	31
1.1.1.7 Chorismate synthase (EC 4.6.1.4).....	33
1.1.2 Branches of the shikimate pathway.....	35
1.1.2.1 Chorismate mutase (EC 5.4.99.5)	36
1.1.2.2 Anthranilate synthase/ Isochorismate synthase (EC 5.4.99.6).....	36
1.1.3 Organisation of enzymes.....	36
<i>1.2 Quinate Pathway.....</i>	<i>40</i>
<i>1.3 Two types of dehydroquinase</i>	<i>41</i>
1.3.1 Distribution of types.....	42
1.3.2 Selective inhibition.....	43
1.3.3 Type I DHQase	43
1.3.4 Type II DHQase	46
<i>1.4 Shikimate Dehydrogenase.....</i>	<i>48</i>

1.4.1	Quinate-shikimate dehydrogenase	49
1.4.2	Isozymes of shikimate dhydrogenase.....	49
1.5	<i>Project aims</i>	49
CHAPTER 2 MATERIALS AND METHODS		52
2.1	<i>General Reagents</i>	52
2.2	<i>Reagents for molecular biology</i>	52
2.2.1	Enzymes for molecular biology	52
2.2.2	Bacterial strains.....	52
2.2.3	Plasmids	54
2.2.4	Genomic DNA	55
2.3	<i>Growth media and supplements</i>	55
2.3.1	Media.....	55
2.3.2	Antibiotics.....	57
2.3.3	Induction and chromogenic supplements.....	57
2.4	<i>General laboratory methods</i>	58
2.4.1	pH Measurements.....	58
2.4.2	Storage of bacteria.....	58
2.5	<i>Growth of bacteria</i>	58
2.5.1	<i>E. coli</i>	58
2.5.2	<i>B. subtilis</i>	58
2.5.3	Cell lysis.....	58
2.6	<i>Polymerase Chain Reaction (PCR)</i>	59
2.6.1	Primer Design.....	59
2.6.2	PCR reactions.....	60
2.6.3	Site-directed mutagenesis strategies	61
2.6.3.1	Two stage PCR using Vent polymerase.....	61
2.6.3.2	Site-directed mutagenesis using Quikchange™ site-directed mutagenesis kit from Stratagene	63
2.7	<i>DNA cloning procedures</i>	63
2.7.1	Electrophoresis of DNA on agarose gel.....	63

2.7.2	Isolation of Plasmid DNA from bacteria cells	63
2.7.3	Endonuclease restriction of plasmid DNA and PCR product	64
2.7.4	Purification of restriction digested DNA and PCR product.....	64
2.7.5	Ligation of digested fragments and PCR product	65
2.7.6	Dephosphorylation of plasmid DNA	66
2.8	<i>Preparation of competent cells and transformation</i>	66
2.8.1	Preparation of competent cells	66
2.8.2	Transformation protocol.....	67
2.8.3	Blue-white screening using the <i>lacZ</i> gene	67
2.9	<i>Sequencing of plasmid DNA</i>	67
2.10	<i>Over Expression of proteins in E. coli</i>	68
2.11	<i>Sodium dodecyl sulphate poly-acrylamide gel electrophoresis (SDS PAGE)</i>	69
2.11.1	Protein staining.....	69
2.12	<i>Purification of proteins</i>	69
2.12.1	<i>S. coelicolor</i> type II dehydroquinase.....	69
2.12.1.1	Step 1: Extraction and centrifugation.....	69
2.12.1.2	Step 2: Anion exchange chromatography on DEAE-Sepacel ...	70
2.12.1.3	Step 3: Hydrophobic interaction chromatography on phenyl-Sepharose.....	70
2.12.1.4	Step 4: Gel filtration Chromatography on Sephacryl 200.....	70
2.12.2	<i>B. subtilis</i> YqhS (dehydroquinase related protein) mutant F23Y	71
2.12.2.1	Step1: Extraction, heat treatment and centrifugation.....	71
2.12.2.2	Step 2: Anion exchange chromatography on Q-Sepharose.....	71
2.12.2.3	Step 3: Gel filtration Chromatography on Sephacryl 200.....	72
2.12.3	Purification of <i>H. influenzae</i> shikimate dehydrogenase.....	72
2.12.3.1	Step 1: Extraction and centrifugation.....	72
2.12.3.2	Step 2: Fractionation with ammonium sulphate.....	72
2.12.3.3	Step 3: Anion exchange chromatography on DEAE-Sepacel...	72
2.12.3.4	Step 4: Gel filtration Chromatography on Sephacryl 200.....	73
2.12.3.5	Step 5: Affinity chromatography on 2'5' ADP Sepharose	73
2.13	<i>Protein estimation</i>	73

2.14	<i>Western blotting</i>	74
2.14.1	Preparation of Antibodies	76
2.15	<i>Mass spectrometry</i>	76
2.15.1	Two-dimensional electrophoresis (2-DE)	77
2.15.2	Immunoprecipitation	78
2.15.3	Protein Digests	79
2.15.4	MALDI-tof and electrospray Mass spectrometry	79
2.16	<i>Enzyme assays</i>	80
2.16.1	Type II dehydroquinase assay	80
2.16.2	Shikimate dehydrogenase assays	80
2.17	<i>Preparation of substrates</i>	81
2.17.1	3-dehydroquinate.....	81
2.17.2	Substrates for shikimate dehydrogenase assays	81
2.18	<i>Analysis of kinetic data</i>	81
2.19	<i>Stopped Flow assays</i>	82
2.20	<i>Denaturation experiments on Type II dehydroquinases</i>	83
2.21	<i>Fluorescence spectroscopy</i>	83
2.22	<i>Circular dichroism</i>	84
2.23	<i>Dynamic light scattering</i>	84
2.24	<i>Protein Crystallisation</i>	85
CHAPTER 3 SITE-DIRECTED MUTAGENESIS OF <i>S. COELICOLOR</i> TYPE II DEHYDROQUINASE.		87
3.1	<i>Introduction</i>	87
3.1.1	The active site and proposed catalytic mechanism	87
3.1.2	Site-directed mutagenesis as a tool	93
3.1.3	Target residues for site-directed mutagenesis.....	94
3.2	<i>Construction and over-expression of site-directed mutants. of <i>S. coelicolor</i> type II dehydroquinase.</i>	95
3.3	<i>Protein structure comparisons</i>	103

3.3.1	Mass spectrometry	103
3.3.2	Circular dichroism.....	106
3.4	<i>Functional assays of mutants</i>	108
3.5	<i>Chapter summary</i>	109
CHAPTER 4 CHARACTERISATION OF <i>BACILLUS SUBTILIS</i> TYPE II DEHYDROQUINASE RELATED PROTEIN (YqhS)		112
4.1	<i>Introduction</i>	112
4.2	<i>Construction, over expression and purification of site-directed mutant of <i>B. subtilis</i> type II dehydroquinase related protein (YqhS)</i>	115
4.3	<i>Structural studies of YqhS using circular dichroism, fluorescence and dynamic light scattering</i>	120
4.3.1	Unfolding experiments on YqhS.....	120
4.3.1.1	Circular Dichroism results	120
4.3.1.2	Fluorescence spectroscopy results	121
4.3.2	Dynamic light scattering of YqhS in the presence of low concentrations of guanidine hydrochloride	123
4.3.3	Interaction of YqhS with dehydroquinate as revealed by fluorescence.....	124
4.3.4	Comparison of YqhS with site-directed mutant F23Y YqhS by circular dichroism.....	126
4.4	<i>Kinetic comparison of wild type and mutant enzymes</i>	127
4.5	<i>Detection of YqhS in <i>B. subtilis</i> cell extract</i>	128
4.5.1	Western blotting	128
4.5.2	Proteomics approach	130
4.5.2.1	2-DE of <i>B. subtilis</i> cell extract	131
4.5.2.2	Protein A immunoprecipitation of <i>B. subtilis</i> cell extract.....	133
4.5.2.3	Mass Spectrometry.....	134
4.5.3	Disruption mutant (YqhSd).....	134
4.5.3.1	Growth experiments on the YqhSd mutant.	136
4.6	<i>Inactivation of <i>B. subtilis</i> type I dehydroquinase from cell extract</i>	138

4.7	<i>Chapter summary</i>	141
CHAPTER 5 KINETIC AND STRUCTURAL STUDIES OF TYPE II DEHYDROQUINASES FROM DIFFERENT BACTERIAL SPECIES 146		
5.1	<i>Introduction</i>	146
5.2	<i>Structural comparison of Type II dehydroquinases</i>	149
5.3	<i>Unfolding of Type II dehydroquinase from H. pylori</i>	149
5.3.1	Structural analysis using circular dichroism.....	150
5.3.2	Structural analysis using fluorescence.....	151
5.3.3	Catalytic activity.....	151
5.3.4	Structural analysis using dynamic light scattering.....	152
5.3.5	Structural analysis using differential scanning calorimetry (DSC)...	153
5.4	<i>Kinetic characterisation of type II dehydroquinases</i>	154
5.4.1	pH dependence of the kinetic parameters of type II dehydroquinases.....	154
5.4.2	Stopped flow assay experiments.....	157
5.4.3	Effects of salts on catalytic activity.....	157
5.4.4	Temperature effect on catalytic activity.....	163
5.4.5	Characterisation of effects of phosphate and sulphate on type II dehydroquinases.....	163
5.5	<i>Chapter summary</i>	170
CHAPTER 6 HAEMOPHILUS INFLUENZAE SHIKIMATE DEHYDROGENASE AND RELATED YdiB PROTEIN..... 177		
6.1	<i>Introduction</i>	177
6.1.1	Substrate binding domain and reaction mechanism.....	179
6.1.2	Binding specificity of the cofactor.....	182
6.1.3	Inhibitor and analogue studies of shikimate dehydrogenase.....	184
6.2	<i>Construction, over expression and purification of H. influenzae shikimate dehydrogenase and the related YdiB protein</i>	187
6.2.1	Purification of <i>H. influenzae</i> shikimate dehydrogenase.....	187
6.2.2	Cloning and over-expression of <i>H. influenzae</i> of YdiB protein.....	189

6.2.3	Purification of YdiB protein.....	192
6.3	<i>Dynamic light scattering of HIAroE and HIYdiB</i>	196
6.4	<i>Crystallization of HIAroE and HIYdiB</i>	198
6.5	<i>Structural comparisons using circular dichroism</i>	201
6.6	<i>Kinetic Comparisons of AroE and YdiB enzymes</i>	203
6.7	<i>Fluorescence binding experiments of H. influenzae shikimate dehydrogenase</i>	209
6.8	<i>Chapter summary</i>	210
CHAPTER 7 GENERAL DISCUSSION.....		215
REFERENCES.....		220
APPENDIX A.....		246
APPENDIX B.....		250
APPENDIX C.....		252

LIST OF FIGURES (Short titles)

Figure 1. Schematic of the biosynthetic shikimate pathway and the catabolic quinate pathway.	22
Figure 2. Schematic of the 3-deoxy-D-arabino-heptulosonate-7-phosphate synthase (DAHPS) reaction.	24
Figure 3. Schematic of the dehydroquinate synthase (DHQS) reaction.	26
Figure 4. The reversible dehydration of dehydroquinate to dehydroshikimate.	28
Figure 5. Schematic of the reaction catalysed by shikimate dehydrogenase.	29
Figure 6. Schematic of phosphorylation of shikimic acid to form shikimate-3-phosphate by shikimate kinase.	29
Figure 7. Schematic of the 5-enolpyruvoylshikimate 3-phosphate synthase (EPSP synthase) reaction.	31
Figure 8. Structure of glyphosate (<i>N</i> -phosphonomethyl glycine, (commercially known as 'Tumbleweed [®] ' or 'Roundup [®] ').	32
Figure 9. Schematic of the elimination of phosphoric acid from EPSP to form chorismate catalysed by Chorismate synthase.	33
Figure 10. Organisation of shikimate pathway enzyme in different species and Taxonomies.	38
Figure 11. Proposed mechanism of type I dehydroquinase for the enzymic conversion of dehydroquinate	45
Figure 12. PCR two stage site-directed mutagenesis strategy.	62
Figure 13. Schematic of western blot apparatus.	75
Figure 14. Solid ribbon representation of the X-ray structure of <i>S. coelicolor</i> type II dehydroquinase.	89
Figure 15. Schematic representation of the proposed mechanism of <i>S. coelicolor</i> type II dehydroquinase.	90
Figure 16. 1% DNA agarose gels of pT7.7 <i>S. coelicolor</i> <i>aroQ</i> construct, two-stage site-directed mutagenesis (H106A), first round of PCR.	96
Figure 17. 1% DNA agarose gels of pT7.7 <i>S. coelicolor</i> <i>aroQ</i> construct, two-stage site-directed mutagenesis (H106A), second round of PCR.	97
Figure 18. Stratagene Quikchange [™] site-directed mutagenesis strategy of pT7.7 <i>S. coelicolor</i> <i>aroQ</i> construct.	100

Figure 19.	SDS PAGE analysis of expression time course of <i>S. coelicolor</i> type II dehydroquinase mutant Y28F	101
Figure 20.	Elution gradient profile of <i>S. coelicolor</i> mutant Y28F (A) DEAE-Sephacel and (B) phenyl-Sepharose.....	102
Figure 21.	15% SDS PAGE of purified <i>S. coelicolor</i> mutant type II dehydroquinases.....	103
Figure 22.	Electrospray mass spectrometry data of <i>S. coelicolor</i> wild-type and mutant type II dehydrogenases.....	104
Figure 23.	Superimposed circular dichroism spectra of wild type and mutant <i>S. coelicolor</i> dehydroquinases.....	107
Figure 24.	Taxonomic tree of bacteria showing the distribution of classes dehydroquinases.....	113
Figure 25.	Overlay of subunits from <i>Bacillus subtilis</i> (green), <i>Mycobacterium tuberculosis</i> (orange) and <i>Streptomyces coelicolor</i> (blue).....	114
Figure 26.	1% DNA agarose gels of pTB361 <i>B. subtilis</i> <i>yqhS</i> construct, two-stage site-directed mutagenesis, first round of PCR.....	116
Figure 27.	1% DNA agarose gels of pTB361 <i>B. subtilis</i> <i>yqhS</i> construct, two-stage site-directed mutagenesis, second round of PCR.....	117
Figure 28.	SDS PAGE analysis of the time course expression of expression of <i>B. subtilis</i> dehydroquinase related protein YqhS (F23Y).....	118
Figure 29.	The elution profile from Q sepharose column during purification of <i>B. subtilis</i> YqhS mutant F23Y.....	118
Figure 30.	SDS PAGE analysis of the purification of <i>B. subtilis</i> YqhS (F23Y) from Q Sepharose.....	119
Figure 31.	SDS PAGE analysis of the purification of <i>B. subtilis</i> YqhS (F23Y) from Sephacryl 200.....	120
Figure 32.	Far UV circular dichroism spectra of the unfolding of <i>B. subtilis</i> YqhS.....	121
Figure 33.	Percentage change in fluorescence emissions at 308 nm during unfolding of <i>B. subtilis</i> YqhS protein	122
Figure 34.	<i>B. subtilis</i> YqhS protein trimer of subunits.....	123
Figure 35.	Fluorescence binding of <i>B. subtilis</i> YqhS protein.....	125
Figure 36.	The far UV CD spectra of <i>B. subtilis</i> wild type YqhS protein.....	126
Figure 37.	Activity assay of <i>B. subtilis</i> YqhS wild type and F23Y mutant.....	128

Figure 38.	Western blot of purified <i>B. subtilis</i> wild type and F23Y mutant YqhS protein.....	129
Figure 39.	Western blots of <i>B. subtilis</i> (derivative 168) cell extract.....	130
Figure 40.	2-dimensional SDS PAGE of <i>B. subtilis</i>	132
Figure 41.	SDS PAGE (15% acrylamide) analysis of protein A immunoprecipitation of <i>B. subtilis</i> cell extract.....	133
Figure 42.	Integration of pMUTIN vector into a target gene.....	135
Figure 43.	Western blot of <i>B. subtilis</i> derivative 168 and YqhSd cell extracts..	136
Figure 44.	Overlay of subunits from <i>Streptomyces coelicolor</i> (green), <i>Mycobacterium tuberculosis</i> (orange) and <i>Helicobacter pylori</i> (blue).....	147
Figure 45.	Far UV circular dichroism spectra of the unfolding of <i>H. pylori</i> type II DHQase by guanidine hydrochloride.....	150
Figure 46.	Fluorescence data of the unfolding of <i>H. pylori</i> type II dehydroquinase by guanidine hydrochloride (GdmCl).....	151
Figure 47.	Steady-state kinetics pH-dependence studies effect on (A) k_{cat} and (B) K_m of type II DHQases from <i>S. coelicolor</i> (green), <i>H. pylori</i> (blue), <i>M. tuberculosis</i> (orange), <i>A. nidulans</i> (purple) and <i>B. subtilis</i> YqhS F23Y mutant (red).....	155
Figure 48.	Catalytic activity of <i>S. coelicolor</i> (green), <i>H. pylori</i> (blue), <i>M. tuberculosis</i> (orange) DHQase and <i>B. subtilis</i> YqhS F23Y mutant (red) in the presence of low concentration denaturants and salt (A) GdmCl (B) Urea (C) NaCl.....	158
Figure 49.	The affect of salts from the Hofmeister series on the catalytic activity.....	163
Figure 50.	Inhibition of <i>S. coelicolor</i> and <i>H. pylori</i> type II dehydroquinases by phosphate and sulphate.....	166
Figure 51.	Inhibition of <i>M. tuberculosis</i> type II dehydroquinases and <i>B. subtilis</i> YqhS (F23Y) by phosphate and sulphate.....	168
Figure 52.	Comparison of the two active sites of the two DHQases.....	169
Figure 53.	3-dimensional structure of <i>M. tuberculosis</i> dehydroquinase in complex with 2,3-anhydro-quinic acid and chloride ions.....	172
Figure 54.	X-ray structure of ECARoE-NADP ⁺ complex substrate binding pocket with bound sulphate (S1) and DTT molecules.....	180

Figure 55.	Comparison of the cofactor recognition and binding site of (A) ECARoE and (B) ECYdiB	183
Figure 56.	Substrate analogues and inhibitors of the shikimate dehydrogenase family.....	186
Figure 57.	SDS PAGE analysis of the time course of expression of <i>H. influenzae</i> shikimate dehydrogenase	188
Figure 58.	The elution profile from DEAE Sephacel column during purification of <i>H. influenzae</i> shikimate dehydrogenase.....	188
Figure 59.	SDS PAGE of Sephacryl 200 fractions during purification of <i>H. influenzae</i> shikimate dehydrogenase.....	189
Figure 60.	1% DNA agarose gel of <i>H. influenzae</i> PCR	190
Figure 61.	SDS PAGE analysis of the time course expression of expression of <i>H. influenzae</i> shikimate dehydrogenase related protein YdiB.....	191
Figure 62.	SDS PAGE analysis of ammonium sulphate saturation experiment.	193
Figure 63.	Elution profile of the purification of <i>H. influenzae</i> shikimate dehydrogenase related protein YdiB on Sephacryl 200 column.....	195
Figure 64.	SDS PAGE analysis of Sephacryl 200 elution fractions.....	195
Figure 65.	Crystals of HIAroE	198
Figure 66.	Crystals of <i>H. influenzae</i> shikimate dehydrogenase related protein YdiB	200
Figure 67.	CD spectra of HIAroE (red) and HIYdiB (blue).....	202
Figure 68.	Steady state kinetics double reciprocal plot of <i>H. influenzae</i> shikimate dehydrogenase (HIAroE) with NAD ⁺ and shikimate.....	205
Figure 69.	Absorbance spectrum of 0.1 mM vanillin.....	208
Figure 70.	Fluorescence binding of <i>H. influenzae</i> shikimate dehydrogenase (HIAroE).....	209
Figure 71.	<i>S. coelicolor</i> type II dehydroquinase (SCDHQase) aligned against representatives of type II dehydroquinases.....	Error! Bookmark not defined.
Figure 72.	<i>E. coli</i> shikimate dehydrogenase (ECARoE) aligned against representatives of the shikimate dehydrogenase family.....	Error! Bookmark not defined.

LIST OF TABLE (Short titles)

Table 1. Bacterial strains used for general cloning expression and <i>in vivo</i> studies.....	53
Table 2. Plasmids used for molecular cloning	54
Table 3. Growth media.....	55
Table 4. Standard PCR reaction mixture.....	60
Table 5. K_i values (μM) for inhibitors against type I and II dehydroquinases.....	92
Table 6. Secondary structure estimates (%) of SCDHQase mutants.	106
Table 7. Catalytic parameters of <i>S. coelicolor</i> DHQase site-directed mutants. .	108
Table 8. Dynamic light scattering data of <i>B. subtilis</i> YqhS protein.....	124
Table 9. Secondary structure estimates (%) of <i>B. subtilis</i> YqhS and YqhS F23Y mutant using SELCON.	126
Table 10. <i>B. subtilis</i> disruption mutant (YqhSd) growth experiment.4	137
Table 11. Sodium borohydride (NaBH_4) chemical modification experiments on <i>E. coli</i> and <i>B. subtilis</i> cell extracts and purified <i>E. coli</i> type I dehydroquinase and <i>S. coelicolor</i> type II dehydroquinase.....	140
Table 12. Dynamic light scattering data for type II dehydroquinases in the presence of various denaturants and salts.	153
Table 13. pH-dependence steady-state kinetics studies on bacterial type II DHQases.	156
Table 14. Catalytic kinetic parameters of bacterial type II DHQases in the presence of 0.5 M NaCl and GdmCl.....	160
Table 15. Inhibition by polyanions on the kinetic properties of type II DHQases.164	
Table 16. Dynamic light scattering data of <i>H. influenzae</i> shikimate dehydrogenase and YdiB protein.	197
Table 17. Crystallisation conditions for HIYdiB.	199
Table 18. Secondary structure estimates (%) using SELCON of HIAroE and HIYdiB.....	201
Table 19. Summary of concentration ranges used for two substrate assays performed on HIAroE and HIYdiB.....	204
Table 20. Steady-state kinetic analysis of <i>H. influenzae</i> shikimate dehydrogenase.....	206
Table 21. Steady-state kinetic analysis of <i>H. influenzae</i> shikimate YdiB protein.207	

CHAPTER 1 INTRODUCTION

1.1 The shikimate pathway

The products of the shikimate pathway are the aromatic amino acids phenylalanine, tyrosine, and tryptophan, as well as vitamins E and K, folic acid, ubiquinone and plastoquinone and certain metal chelators, such as enterochelin (Bentley, 1990; Pittard, 1987). These products are assembled by the condensation of the carbohydrates; phosphoenolpyruvate (PEP) and D-erythrose 4-phosphate in a series of seven biosynthetic steps (Dewick, 1998; Knaggs, 2001) that form the basic “trunk” of the pathway (Figure 1).

D-Erythrose 4-phosphate is a product of the Calvin cycle or the pentose phosphate pathway and PEP is a product of glycolysis (Mousdale and Coggins, 1993). The branching point of the “common shikimate pathway” occurs after the formation of chorismate; this leads to several diverse terminal pathways (Pittard, 1987; Haslam, 1974). L-Tryptophan is formed from chorismate *via* anthranilate. L-Phenylalanine and L-tyrosine are formed either *via* prephenate, 4-hydroxyphenylpyruvate or L-arogenate, depending on the organism concerned. It is often possible for an organism to utilise more than one of these routes; this may be connected to the availability of active enzymes (Dewick, 1998). Vitamin K and enterochelin branch from isochorismate (Bentley, 1990).

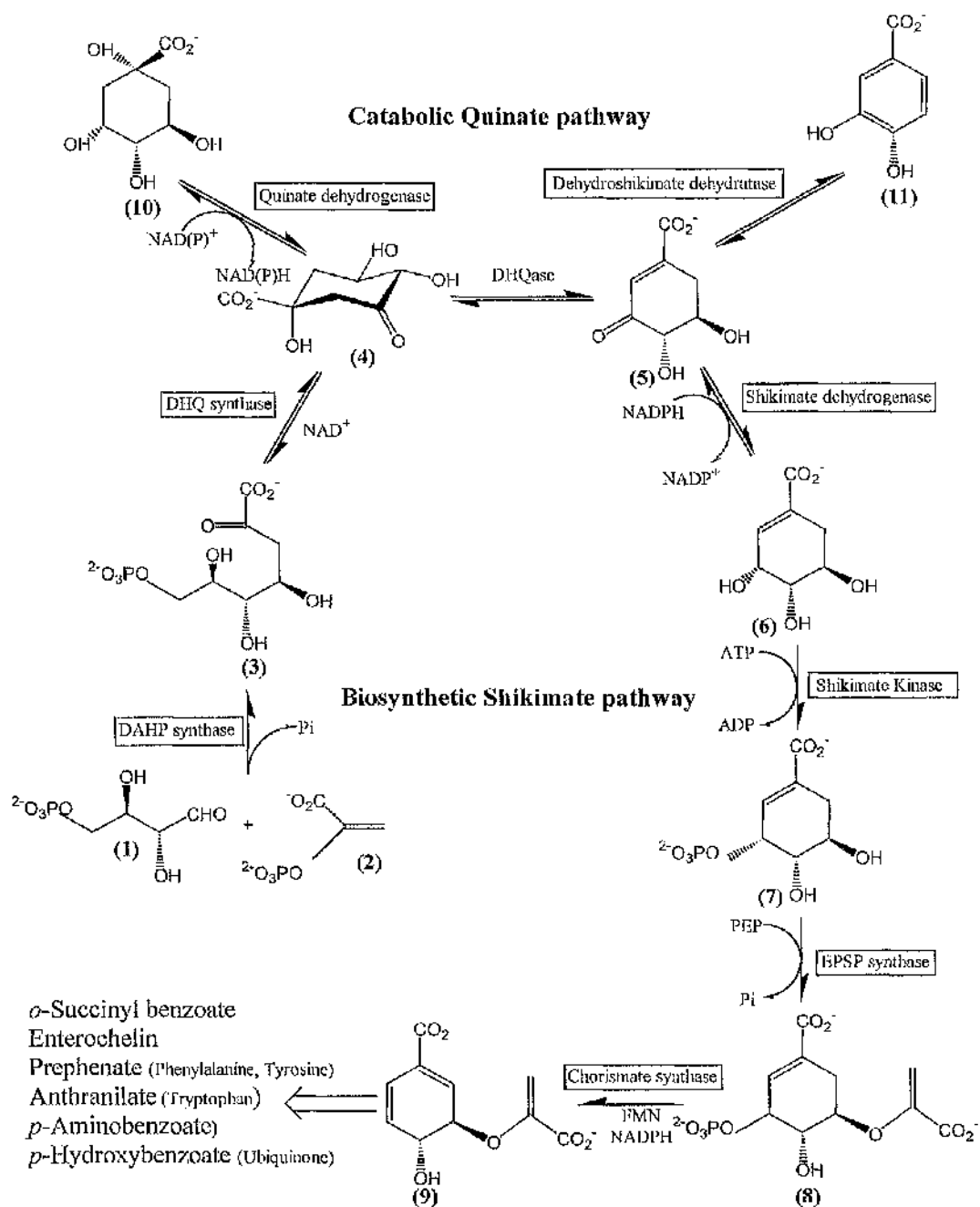


Figure 1. Schematic of the biosynthetic shikimate pathway and the catabolic quinate pathway. The substrate intermediates of both pathways are: (1) erythrose-4-phosphate, (2) phosphoenolpyruvate (PEP), (3) 3-deoxy-D-arabino-heptulosonic acid -7-phosphate (DAHP), (4) dehydroquinate (DHQate), (5) dehydroshikimate, (6) shikimate, (7) shikimate-3-phosphate, (8) 5-enolpyruvylshikimate 3-phosphate (EPSP), (9) chorismate, (10) quinate, (11) protocatechuate.

The delineation of the pathway is a classic example of the combined use of auxotrophic mutants and isotopically labelled precursors. Analysis of the sequence of steps in the biosynthetic pathway is facilitated by the fact that each mutant may accumulate in its culture fluid the substrate for the enzymic reaction that is blocked and may utilise later members of the sequence to replace the required metabolites (Haslam, 1974).

The shikimate pathway was first studied by Eykman in 1885 (Eykman, 1885; 1891). The pathway is present in plants, fungi, bacteria (Bentley, 1990; Mousdale and Coggins, 1993; Haslam, 1974) and has been recently discovered in protozoa (Ranganathan and Mukkada, 1995; Roberts *et al.*, 1998; McConkey, 1999).

The shikimate pathway is not present in vertebrates such as mammals. These organisms lack the capacity for aromatic biosynthesis, other than the aromatization of the steroid ring A. Mammals depend on their diet to obtain the products of the shikimate pathway, therefore any anti-metabolites of this pathway will not act on humans making the shikimate pathway enzymes promising targets for the design of antimicrobials. (Bentley, 1990; Payne *et al.*, 2000). The *aroA* (1.1.1.6) gene of *Aeromonas hydrophila* was inactivated by the insertion of a DNA fragment containing kanamycin resistance into the *aroA* gene by means of a suicide vector. This resulted in a highly attenuated strain which was unable to survive *in vivo* and cause infection. The attenuated mutant strain confers significant protection against the wild type strain when used as a live vaccine in rainbow trout (Moral *et al.*, 1988). Preliminary studies to isolate a disruption mutant of the *aroK* (1.1.1.5) gene of *Mycobacterium tuberculosis* proved unsuccessful this was attributed to the difficulty in gene replacement in all slow growing mycobacteria. The construction of a merodiploid strain containing an L5- integrated copy of the *aroK* gene allowed the disruption of the wild type *aroK* allele. Even in media with aromatic amino acids supplemented, *M. tuberculosis* was not viable demonstrating that the shikimate pathway is essential in *M. tuberculosis* (Parish and Stoker, 2002).

1.1.1 Enzymes of the shikimate pathway

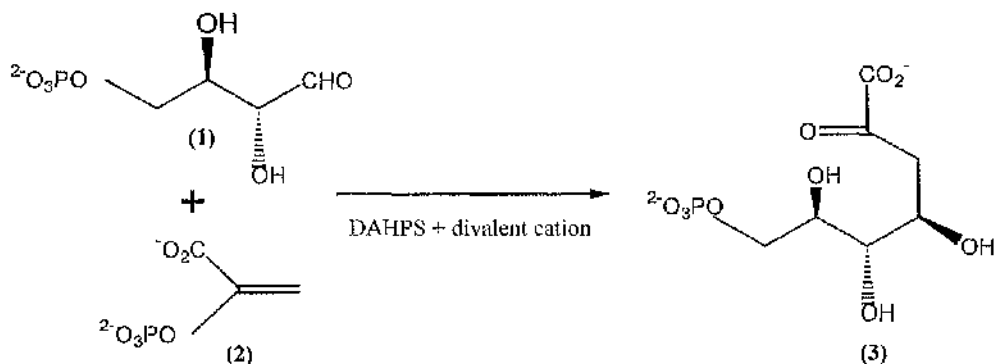
1.1.1.1 3-deoxy-D-*arabino*-heptulosonate-7-phosphate synthase (DAHPS) (EC 4.1.2.15)

Figure 2. Schematic of the 3-deoxy-D-*arabino*-heptulosonate-7-phosphate synthase (DAHPS) reaction.

The first enzyme in the shikimate pathway is DAHPS which catalyses the aldol-like condensation of PEP (2) with D- erythrose 4-phosphate (1) giving 3-deoxy-D-*arabino*-heptulosonate-7-phosphate (DAHPS) (3) (Figure 2) (Srinivasan *et al.*, 1955; Srinivasan *et al.*, 1958). The enzyme mechanism is ordered with PEP binding first to the active site, possibly involving a ping-pong mechanism. ^{18}O -labelled substrates have shown that the formation of DAHP is associated with C-O cleavage of the PEP phosphate group (DeLeo and Springson, 1968). This C-O cleavage of PEP is analogous to that observed in 3-deoxy-D-manno-octulosonate-8-phosphate synthase (Hedstrom and Abeles, 1988). It has been suggested that the condensation is preceded by C-O cleavage and may involve an additional enzyme-thiol group bound to PEP as many DAHPSs have been shown to be susceptible to inhibition by thiol modifying reagents (Gancm, 1987).

Kinetic studies on the three *E. coli* DAHPSs isozymes using substrate analogues of D- erythrose 4-phosphate in which the C-O-P group was replaced by either C-P or C-CH₂-P led to significantly different reaction rates with the isosteric homophosphate analogue the better of the two analogues (Le Maréchal *et al.*, 1980). The stereochemistry of DAHPS, involves the *cis* (*si*) attack of the C3 of PEP and the *trans* (*re*) attack of the C1 of D- erythrose 4-phosphate (Floss *et al.*, 1972). Kinetic studies using PEP analogue (*Z*)-phosphoenol-3-fluoropyruvate (F-PEP) showed that F-PEP bound to DAHPS with a similar affinity to PEP. However, the V_{\max} is 85-fold lower

for DAHPS with F-PEP as substrate than DAHPS with PEP as substrate. Additional kinetic experiments showed F-PEP to be a competitive inhibitor of DAHPS (Pilch and Somerville, 1976).

The regulation of DAHPS is different between plants and microorganisms. Isozymes from the latter are characterised by differential feedback inhibition by the aromatic amino acids. This plays an important part in the regulation of the pathway. Wild-type *Escherichia coli* has been shown to produce three feedback inhibitor-sensitive DAHPSs, namely a Phe-sensitive (DAHPS(Phe)), a Tyr-sensitive (DAHPS(Tyr)) and a Trp-sensitive (DAHPS(Trp)) enzyme (Doy, 1968). DAHPS(Phe), a homotetramer encoded by the *aroG* gene, is the major isoform, constituting nearly 80% of the total activity of the DAHPSs. DAHPS(Tyr) (*aroI'*) and DAHPS(Trp) (*aroH*) are both homodimers, constituting around 20 and 1% of the total activity of the DAHPSs, respectively (Schoner and Hermann, 1976). This arrangement provides the cell with the ability to modulate the overall rate of synthesis in response to changes in the availability of particular aromatic amino acids. Whereas the inhibition of Tyr-sensitive and Phe-sensitive isozymes by tyrosine and phenylalanine respectively is as high as 95%, inhibition of DAHPS (Trp-sensitive) by tryptophan is only 40% (Doy, 1968). Different species of bacteria have different dominant isozymes (DeLeo *et al.*, 1973; Ahmad and Jensen, 1989). Random and site-directed mutagenesis of the aromatic amino acid-regulated DAHPSs of *E. coli* show that mutations leading to inactivation of feedback inhibition are not found in a specific region of the polypeptide chain, suggesting that feedback inhibition of the DAHPSs probably arose by divergent evolution rather than domain recruitment (Ray *et al.*, 1988; Kikuchi *et al.*, 1997). The distribution of the three isozymes in microorganisms varies considerably; in some microorganisms such as *Anabaena variabilis* only two isozymes of DAHPS have been detected, one of which is tyrosine sensitive and the other sensitive to phenylalanine (Niven *et al.*, 1988). DAHPS(Phe) isozyme is thought to have evolved most recently since it is absent in most Gram-negative bacteria which possess the other two isoforms (Ahmad and Jensen, 1989). *B. subtilis* possesses a bifunctional enzyme complex which exhibits DAHPS and chorismate mutase (1.1.2.1) activity. This bifunctional polypeptide is also associated with the shikimate kinase (1.1.1.5) from this species forming a trifunctional enzyme complex (Nakatsukasa and Nester, 1972). Plant DAHPS isozymes are differentiated by their

requirements for divalent cations Mn^{2+} or Co^{2+} ; the DAHPS which requires Co^{2+} has a higher pH optimum than the DAHPS Mn^{2+} -requiring isozyme (Suzuki *et al.*, 1996; Mousdale and Coggins, 1993).

The DAHPS isozymes require a divalent metal ion for activity. The identity of the activating metal is unclear, however there is evidence for both Fe^{2+} and Cu^{2+} . Metal variation significantly affects the apparent affinity for the substrate, D-erythrose phosphate, but not for the second substrate PEP (Stephens and Bauerle, 1991). The 3-dimensional X-ray structure of DAHPS(Phe) from *E. coli* complexed with PEP and Pb^{2+} revealed that mutations which reduce feedback inhibition are clustered about a cavity close to the dimer interface. The Pb^{2+} (which is only a weak activator) is bound at the active site, coordinating PEP. The binding position of PEP may be different in the presence of more active divalent cations such as Cu^{2+} (Shumilin *et al.*, 1999). Preliminary X-ray structural analysis has been performed on the DAHPS(Tyr) from *S. cerevisiae* complexed with Zn^{2+} and PEP (Schneider *et al.*, 1999).

1.1.1.2 Dehydroquinase synthase (EC 4.6.1.3)

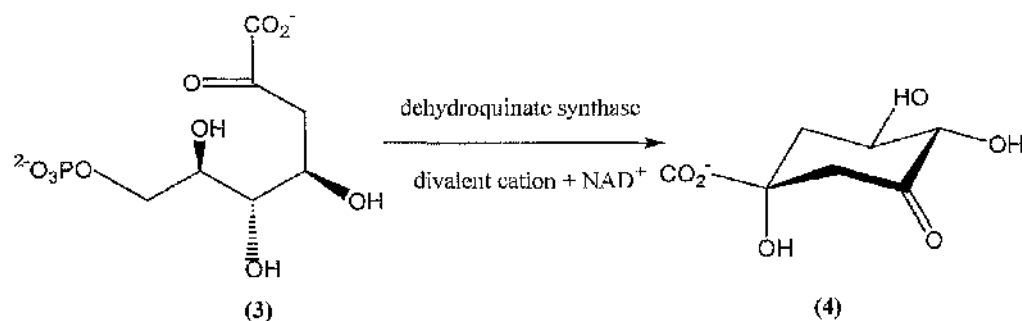


Figure 3. Schematic of the dehydroquinase synthase (DHQS) reaction.

Dehydroquinase synthase (DHQS) is a NAD^+ -dependent metalloenzyme that converts DAHP (3) to dehydroquinic acid (4), the first cyclic intermediate of the shikimate pathway (Figure 3).

This catalytic conversion was first proposed by Sprinson *et al.*, (1963). DAHP (the first intermediate of the shikimate pathway) was chemically synthesized to study the enzymic conversion. On structural grounds it would be assumed that the conversion of DAHP to dehydroquinase would be mediated by several stable intermediates. However, the rate of formation of dehydroquinase is equal to the rate of disappearance of DAHP suggesting that there are no stable intermediates (Srinivasan

et al., 1963). Millar and Coggins (1986) characterised the amino acid sequence of the *aroB* from *E. coli* and calculated the molecular weight to be approximately 39 kDa.

The complex multistep mechanism of DHQS involves a sequence of several reactions: alcohol oxidation, a β -elimination (Widlanski *et al.*, 1987), a reduction and an intramolecular exchange of the DAHP ring oxygen with C7, driven by the cleavage of the phosphoester, and an intramolecular aldol condensation (Srinivasan *et al.*, 1963). It has been proposed that the phosphate catalyses its own elimination and that the final steps in the mechanism could occur spontaneously (Rotenberg and Sprinson, 1978; Bartlett and Satake, 1988; Widlanski *et al.*, 1989a; Widlanski *et al.*, 1989b).

In the first step of the mechanism, C5 of DAHP is oxidised by NAD^+ (Rotenberg and Sprinson, 1978). The divalent metal ion may play a role in facilitating hydride transfer between the C5 hydroxyl and NAD^+ (Carpenter *et al.*, 1998).

The second step in the mechanism is β -elimination of the phosphate group at C6. Kinetic isotope effects studies using labelled substrate analogues revealed that the phosphate group is essential for the conversion (Rotenberg and Sprinson, 1978). The DHQS domain of the pentafunctional AROM enzyme from *Neurospora crassa* was shown to require Zn^{2+} for activity (Lambert *et al.*, 1985) where as, the *E. coli* enzyme requires Co^{2+} for activity (Srinivasan *et al.*, 1963). The 3-dimensional X-ray structure of the DHQS domain of the AROM protein (1.1.3) from *Aspergillus nidulans* complexed with Zn^{2+} and carbaphosphonate (a substrate analogue of DAHP and an inhibitor of DHQS (Bender *et al.*, 1989) was solved by Carpenter *et al.*, (1998). The position of the inhibitor shows a phosphate-binding pocket and the interactions from the phosphate oxygens could remove the proton from C6 (Bender *et al.*, 1989).

In the third step, a proton shuffling system is used: the C5 of a substrate intermediate is reduced by NADH (Rotenberg and Sprinson, 1978). This is a reversal of the first step with the hydride ion from C4 being transferred back to C5.

The two final steps of the reaction consist of ring opening and intramolecular aldol condensation. The ring-opening step involves deprotonation of the hydroxyl at C2. A water molecule is implicated in this part of the mechanism as it is the only neighbouring species (Carpenter *et al.*, 1998). Ring opening is followed by a rotation

around the C5-C6 bond and an intramolecular aldol condensation to re-form the ring. These two steps can occur spontaneously in solution (Bartlett and Satake, 1988; Widlanski *et al.*, 1989a; Widlanski *et al.*, 1989b). However, unwanted by-products such as 1-*epi*-dehydroquinate are also formed, which are not present in the DHQS-catalysed formation of dehydroquinate. It is thought that DHQS channels the reaction to prevent the formation of side products (Bartlett *et al.*, 1994; Carpenter *et al.*, 1998).

1.1.1.3 Dehydroquinase (EC 4.2.1.10)

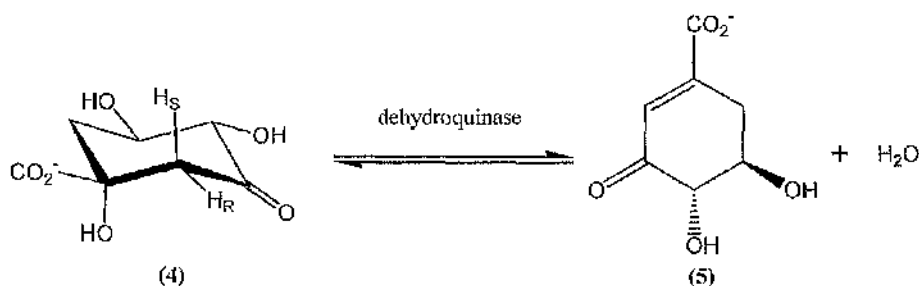


Figure 4. The reversible dehydration of dehydroquinate to dehydroshikimate.

The enzyme dehydroquinase (3-dehydroquinate dehydratase; DHQase) catalyses the reversible dehydration of dehydroquinic acid (4) to form dehydroshikimic acid (5) (Figure 4) (Mitsuhashi and Davis, 1954; Grewe and Haendler, 1966).

This reaction is part of two metabolic pathways, the shikimate pathway, and the quinac pathway (1.1.3) (Giles *et al.*, 1968; Chaleff, 1974; Hawkins *et al.*, 1982).

The dehydroquinase reaction, will be discussed in more detail in a later part of this chapter (1.3).

1.1.1.4 Shikimate dehydrogenase (EC 1.1.1.25)

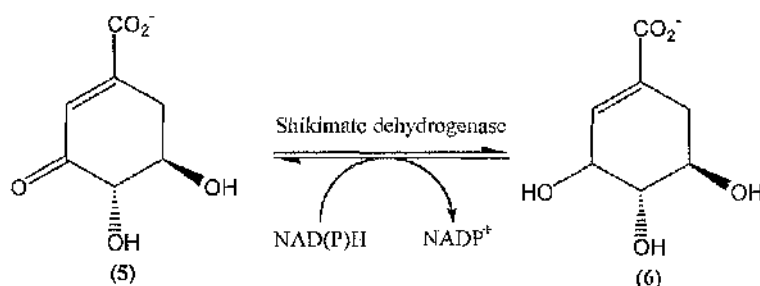


Figure 5. Schematic of the reaction catalysed by shikimate dehydrogenase.

The fourth step in the shikimate pathway is the reduction of dehydroshikimic acid (5) to shikimic acid (6) (Figure 5) (Salamon and Davis, 1953; Yaniv and Gilvarg, 1955). This reaction is also part of the two metabolic pathways associated with DHQase: the shikimate pathway, and the quinate pathway (1.1.3) (Chaleff, 1974; Hawkins *et al.*, 1982).

The *E. coli* isozyme is catalyzed by an NAD(P)H-dependent shikimate dehydrogenase with a molecular weight of 29 kDa. Isozymes found in other microorganisms are pyrrolo-quinoline quinone dependent (Duine, 1991).

The shikimate dehydrogenase reaction will be discussed in more detail in a later part of this chapter (1.4).

1.1.1.5 Shikimate kinase (EC 2.7.1.71)

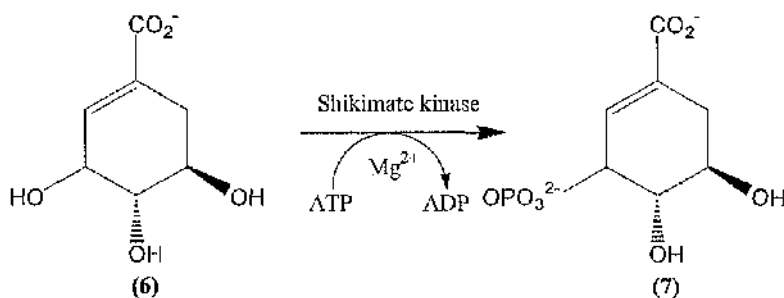


Figure 6. Schematic of phosphorylation of shikimic acid to form shikimate-3-phosphate by shikimate kinase.

Shikimate kinase catalyses the fifth step of the shikimate pathway, namely the transfer of phosphate from ATP to the C-3 hydroxyl group of shikimate (6) forming shikimate-3-phosphate (7) (Figure 6). There are two isozymes of shikimate kinase in *E. coli* and *S. typhimurium*: shikimate kinase I and II encoded by *aroK* and *aroL*

genes, respectively. The two isozymes are of comparable polypeptide chain length and molecular weight (approximately 19.5 kDa) but only share 30% sequence identity (Millar *et al.*, 1986; Løbner-Olesen and Marinus, 1992, Whipp and Pittard, 1995). The K_m value for shikimate of shikimate kinase I is approximately 100 times greater than shikimate kinase II (20 mM compared with 200 μ M) (DeFeyter and Pittard, 1986b). It is suggested that isozyme I may not be a true shikimate kinase and has another function(s) within the cell. A random insertional mutagenesis study of *E. coli* revealed that mutation of the *aroK* gene confers mecillinam resistance. Mecillinam is a β -lactam antibiotic specific to penicillin-binding protein 2 in *E. coli*, which blocks cell wall elongation and indirectly cell division. Shikimate kinase I possibly has some role in cell division (Vinella *et al.*, 1996).

Gene expression of shikimate kinase II (*aroL*) is regulated by cooperation between the *trpR* and *tyrR* repressor genes and is associated with a second gene designated as *aroM*, the function of which is unclear (DeFeyter and Pittard, 1986a; DeFeyter *et al.*, 1986). However, shikimate kinase I (*aroK*) regulation is independent of amino acid concentration and the *trpR* and *tyrR* repressors (Ely and Pittard, 1979). It has been suggested that this enzyme is at a branch point of two distinct pathways (Millar *et al.*, 1986). In *B. subtilis* there is a single shikimate kinase which forms a trifunctional complex with the bifunctional DAHPS/chorismate mutase enzyme. When this complex is dissociated, shikimate kinase becomes inactive (Nakatsukasa and Nester, 1972).

Shikimate kinase II has been shown to require Mg^{2+} as a cofactor, this involves the direct interaction with two protein side-chains (Krell *et al.*, 1998). The optimum pH of the enzyme is alkaline (8.6-9.6) (Mousdale and Coggins, 1993). The three dimensional structure of shikimate kinase from *Erwinia chrysanthemi* has been determined by X-ray crystallography using multiple isomorphous replacement (Krell *et al.*, 1998). The enzyme undergoes substantial conformational modifications during catalysis, with two flexible domains shifting to fit the substrate (Krell *et al.*, 1998). Site-directed mutagenesis of *E. chrysanthemi* shikimate kinase identified lysine residue (K15) as an essential residue in the phosphorylation of shikimic acid. The 3-dimensional X-ray structure of the K15M mutant *E. chrysanthemi* shikimate kinase showed as well as the role in catalysis Lys15 has a role in the structural organisation of the P-loop (Krell *et al.*, 2001). Shikimate kinase in archaea is part of the GHMP-

kinase superfamily and shares no homology with bacterial or eukaryotic shikimate kinases (Daugherty *et al.*, 2001).

1.1.1.6 5-enolpyruvoylshikimate 3-phosphate synthase (EC 2.5.1.19)

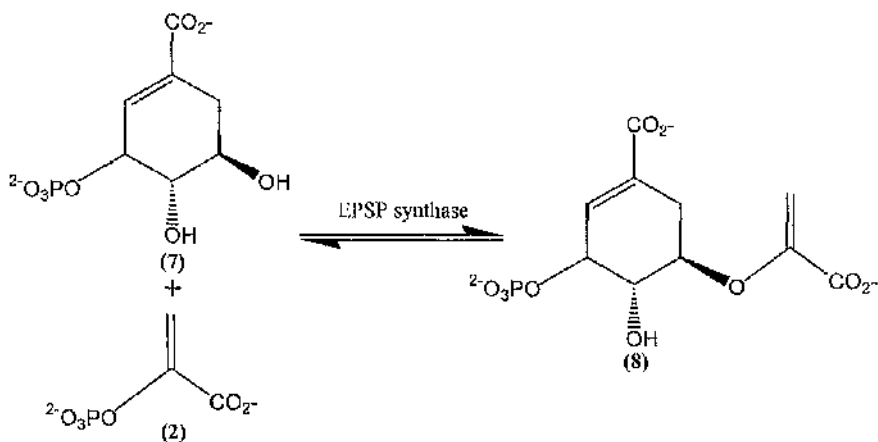


Figure 7. Schematic of the 5-enolpyruvoylshikimate 3-phosphate synthase (EPSP synthase) reaction.

The enzyme, 5-enolpyruvoylshikimate 3-phosphate synthase (EPSP Synthase) catalyses the condensation of shikimate 3-phosphate (7) with a second PEP (2) to produce the enol ether, 5-enolpyruvoylshikimate-3-phosphate (EPSP, 8) (Figure 7) (Levin and Sprinson, 1964). The *E. coli* gene *aroA* encodes for EPSP synthase (Duncan *et al.*, 1984a), a monomeric enzyme with a molecular weight of 49 kDa (Duncan *et al.*, 1984b). The 3-dimensional structure of EPSP synthase from *E. coli* has been determined by Stallings *et al.*, (1991). The protein has two domains, each of which comprises two parallel α helices and four β strands. The active site is located near the inter-domain crossover region of the protein.

The mechanism of EPSP synthase involves cleavage of a C-O bond of PEP. Labelled substrate studies revealed, a reversible addition-elimination mechanism where protonation of C3 of PEP is associated with nucleophilic attack on C2 by C5 of shikimate-3-phosphate (Bondinell *et al.*, 1971; Grimshaw *et al.*, 1982). This reaction introduces the three-carbon fragment that is designated to become the main chain of phenylalanine and tyrosine and which is removed during the synthesis of tryptophan (Pittard, 1987). The mechanism of EPSP synthase is thought to proceed via a moderately stable tetrahedral intermediate formed from shikimate-3-phosphate and PEP by means of an ordered BiBi mechanism. There have been extensive studies

involving the identification, characterisation and isolation of the enzyme intermediates of EPSP synthase (Anderson and Johnson, 1990)

The billion dollar broad-spectrum herbicide glyphosate [*N*-(phosphonomethyl) glycine] (commercially known as 'Tumbleweed[™]' or 'Roundup[™]') (Figure 8) was first reported to act on *Lemna gibba* by the Jaworski group at Monsanto (1972). On addition of *L*-phenylalanine the growth inhibition of glyphosate was reduced. The precise target of for glyphosate, EPSP synthase was identified by Steinrucken and Amrhein (1980). It is an analogue of the PEP and the kinetic patterns are consistent with an ordered sequential mechanism in which either PEP or glyphosate can bind to an enzyme-shikimate-3-phosphate complex (Boocock and Coggins, 1983). Glyphosate is a competitive inhibitor with respect to PEP of EPSP synthase. Of several known PEP-dependent enzyme reactions, EPSP synthase is the only known enzyme inhibited by glyphosate. The PEP binding region of EPSP synthase therefore appears to be unique (Padgett *et al.*, 1991).

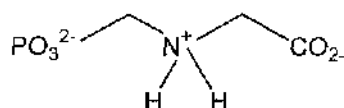


Figure 8. Structure of glyphosate (*N*-phosphonomethyl glycine, commercially known as 'Tumbleweed[®]' or 'Roundup[®]').

Site-directed mutagenesis has identified several amino acid side chains as being essential in the catalytic mechanism of EPSP synthase. There is a conserved arginine (R104) in the *B. subtilis* enzyme which plays a key role in the discrimination between glyphosate and PEP. Site-directed mutagenesis of this side chain, in particular the loss of guanidium chain reduces the K_i by 14-fold (K_i 5 μ M) (Selvapandiyar *et al.*, 1995). Further site-direct mutagenesis was performed to characterise the active site residues of the *E. coli* EPSP synthase, including the identification of an essential arginine residue, and a lysine residue that increased the K_m for PEP significantly (Shuttleworth *et al.*, 1999). Furthermore a critical glycine residue that interacts with the phosphate moiety of PEP has also been identified (Padgett *et al.*, 1991). Despite over 20 years of extensive use of glyphosate the occurrence of spontaneous resistance to glyphosate in plants is rare. Recently goosegrass (*Eleusine indica*) was found to have developed resistance to glyphosate. Sequence analysis of the strain which had

developed resistance showed two amino acids changes from the sensitive goosegrass strain (Baerson *et al.*, 2002).

The X-ray structure of shikimate-3-phosphate and glyphosate bound to EPSP synthase has been reported and allows a detailed visualisation of the interactions of the ligands with their target however, it is unclear whether glyphosate and PEP occupy the same binding site. It is thought that upon ligand binding the tertiary structure of EPSP synthase changes from an 'open' form to 'closed' form. It is also thought that the 'closed' form is not readily transported into plant chloroplasts (Alibhai and Stallings, 2001).

1.1.1.7 Chorismate synthase (EC 4.6.1.4)

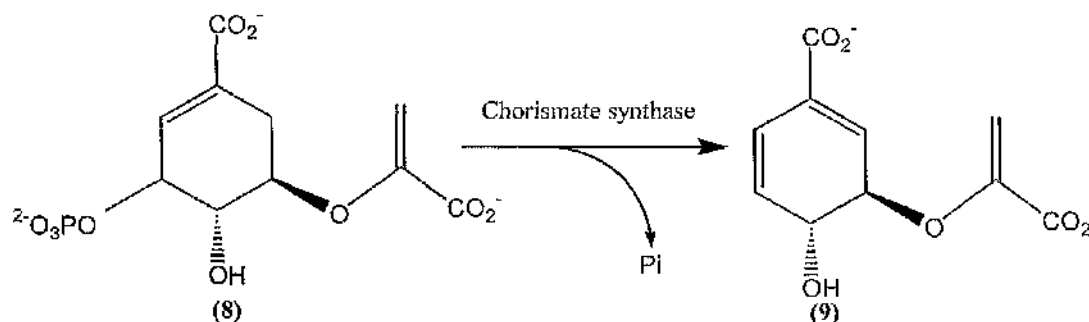


Figure 9. Schematic of the elimination of phosphoric acid from EPSP to form chorismate catalysed by 5-enolpyruvylshikimate 3-phosphate-lyase (Chorismate synthase).

Chorismate synthase (5-enolpyruvylshikimate 3-phosphate-lyase) catalyses the 1,4-elimination of phosphate from EPSP (8) to give chorismate (9, Figure 9), introducing the second double bond into the aromatic ring system (Morell *et al.*, 1967). The mechanism of chorismate synthase involves the *trans*-1,4-conjugate elimination of the phosphate group. Studies using labelled substrates showed that the chorismate synthase reaction is stereospecific involving the *anti* elimination of the *pro*-6R hydrogen (Hill and Newkome, 1969; Onderka and Floss, 1969; Floss *et al.*, 1972). The elimination requires a reduced flavin and NAD(P)H, although there is no change in oxidation state of the reduced flavin. FMN is the preferred flavin cofactor over FAD. The role of the flavin is unclear, but it appears to be directly involved in catalysis. Studies using reduced 5-deaza-FMN gave conflicting results. In some studies reduced 5-deaza-FMN reconstituted the catalytic activity of inactive *E. coli*

and *N. crassa* chorismate synthases, while other studies showed a significant decrease in catalytic activity in the presence of reduced 5-deaza-FMN (Bornemann *et al.*, 1995; Osborne *et al.*, 2000). Pre-steady state kinetics studies do not show a burst or a lag phase in the reaction. It is thought that release of the phosphate occurs in parallel with the rate-limiting step of the reaction (Hawkes *et al.*, 1990). The *aroC* gene encodes chorismate synthase in *E. coli* and *N. crassa*. Both purified enzymes are tetramers with subunit molecular masses of 38 kDa and 50 kDa, respectively (Millar *et al.*, 1986; White *et al.*, 1988).

There are two types of chorismate synthase defined by whether they are active in anaerobic or aerobic conditions. *E. coli* chorismate synthase is oxygen sensitive and requires an anaerobic environment, whereas the *Bacillus subtilis* enzyme is aerobic. The essential difference between the isozymes is that the anaerobic type contains a diaphorase (flavoprotein) catalysing the redox reaction between a reduced pyridine nucleotide and a suitable acceptor (Mousdale and Coggins, 1993). Chorismate synthase is found in the chloroplasts of *Pisum sativum* L. and is likely to contain an amino terminal extension to direct chloroplast import (Mousdale and Coggins, 1986). Two distinct chorismate synthases have been identified in tomato (*Lycopersicon esculentum* L.); there is 85% cDNA sequence similarity between the isozymes and both sequences contain regions involved in plastidic transit. The two isozymes are expressed at different levels one gene (LeCS1) has significantly higher expression levels compared with that of the other gene (LeCS2) (Görlach *et al.*, 1993).

Initially chorismate synthase was thought to form the intermediate iso-EPSP. Bartlett *et al.*, (1986) chemically synthesized this potential intermediate and found it be a competitive inhibitor of *N. crassa* chorismate synthase rather than an intermediate with a K_i of 8.7 μM (compared with a $K_m(\text{EPSP})$ of 2.7 μM).

Attempts to produce rational designed inhibitors of the shikimate pathway enzyme led Sutherland *et al.* (1989) to make the two stereoisomers of 6-fluoroshikimic acid. These compounds were designed to be substrates of shikimate kinase and EPSP synthase (Duggan *et al.*, 1995). The substrate analogue (6S)-6-fluoro-FPSP is a competitive inhibitor of *Neurospora crassa* chorismate synthase (Balasubramanian *et al.*, 1991). This substrate analogue is converted into 6-fluorochorismate at a rate two orders of magnitude lower than the normal substrate. The spectral characteristics of the fluoro-substrate are different from the true substrate. (6S)-6-fluoroshikimic acid

is more likely to be an inhibitor of 4-aminobenzoic acid synthesis (Bornemann *et al.*, 1995). The results are consistent with the antimicrobial effect of 6-fluoroshikimate (Davis *et al.*, 1994). Unfortunately spontaneous resistance to (6S) arose in *E. coli* and other enterobacteria at high frequencies. The uptake of (6S)-6-fluoroshikimate by *E. coli* was studied by performing exchange-diffusion experiments with [C^{14}]shikimate (Jude *et al.*, 1996). A loss of susceptibility to (6S)-6-fluoroshikimate was caused by a loss of activity of the shikimate transport system as a result of genetic changes at the *shiA* loci (Ewart *et al.*, 1995). These compounds have also been shown to have an inhibitory effect on *Plasmodium falciparum* which can be reversed by the supplementation of PABA (McConkey, 1999). Recently a series of 2(Z)-2-benzylidene-6,7-dihydroxybenzofuran-3[2H]-ones have been identified by extensive chemical library screening as potential inhibitors of bacterial chorismate synthase (Thomas *et al.*, 2003).

1.1.2 Branches of the shikimate pathway

Chorismate is the major branch point of the synthesis of the aromatic amino acids L-phenylalanine, L-tyrosine and L-tryptophan (Figure 1). Chorismate is a substrate for several different enzymes including chorismate mutase (1.1.2.1) and anthranilate synthase/ isochorismate synthase (1.1.2.2).

There are also several other branch points of the shikimate pathway before the chorismate intermediate. A novel variant of the shikimate pathway involving 3-amino-5-hydroxybenzoic acid (AHBA) has been described; this pathway leads to rifamycin and other related antibiotics. A variety of antibiotics, notably the ansamycins that include rifamycin contain a biosynthetically unique moiety, called a mC₇N unit. Production of the mC₇N units is thought to involve DAHP synthase and shikimate dehydrogenase (Kim *et al.*, 1992). The branch point for this compound is the intermediate dehydroshikimate and the pathway has been characterised in *Amycolatopsis mediterranei* by Kim *et al.* (1998). Shikimate dehydrogenase is also the branch point for the synthesis of hydrolysable tannin from gallic acid. Hydrolysable tannins are involved in insect resistance in plants (Ossipov *et al.*, 2003) (6.1.3).

Two more unusual branch points of the shikimate pathway also found in *Streptomyces* appear to involve the dehydroquinase-catalysed reaction. They are the

formation of cyclohexanecarboxylic acid and dihydroxycyclohexanecarboxylic acid, which are respectively an anti-fungal agent and a precursor of the immunosuppressant ascomycin (Wilson *et al.*, 1998).

1.1.2.1 Chorismate mutase (EC 5.4.99.5)

The first branch of the main trunk of the shikimate pathway occurs at the chorismate mutase reaction. This enzyme catalyses the Claisen-like arrangement of chorismate to prephenate. Prephenate is a precursor of L-phenylalanine and L-tyrosine. The PEP-derived side chain changes to form a direct bond to the carbocycle (Dewick, 1998). Prephenate is a relatively unstable compound and can be converted into phenylpyruvate at an acidic pH. The enzyme is a homodimer with a subunit molecular weight of about 42 kDa (Mousdale and Coggins, 1993; Pittard, 1987).

E. coli chorismate mutase has been purified to homogeneity, and is present as part of a bifunctional polypeptide along with prephenate dehydrogenase (Sampathkumar and Morrison, 1982).

1.1.2.2 Anthranilate synthase/ Isochorismate synthase (EC 5.4.99.6)

Anthranilate synthase exhibits significant amino acid sequence homology with isochorismate synthase and *p*-aminobenzoate synthase (which forms the precursor to ubiquinone) suggesting a common mechanism (Dewick, 1998). These enzymes are involved in the biosynthetic pathways to anthranilate and *p*-aminobenzoate respectively. A glutamine amidotransferase activity provides ammonia from glutamine, which then reacts with chorismate to form 4-amino-4-deoxychorismate or 2-amino-2-deoxyisochorismate. Anthranilate is an intermediate for the synthesis of L-tryptophan (Ganem, 1978; Dewick, 1998).

1.1.3 Organisation of enzymes

Although the same chemical intermediates are involved, the organisation of the enzymes concerned in the pathway varies considerably between organisms. In most bacteria, reactions two to six of the shikimate pathway are catalysed by five separate monofunctional enzymes, but in fungi, a single polypeptide called the *arom* protein which is a pentafunctional polypeptide, serves the same purpose (Figure 10) (Lumsden and Coggins, 1977; Coggins *et al.*, 1985; Coggins and Boocock, 1986).

Arom proteins have been studied from *N. crassa* (Giles *et al.*, 1967; Lumsden and Coggins, 1977), *A. nidulans* (Charles *et al.*, 1985), *Saccharomyces cerevisiae* (Duncan *et al.*, 1987), *Schizosaccharomyces pombe*, *Cryphonectria parasitica* (Lakshman *et al.*, 1998) and *Pneumocystis carinii* (the pathogen that is the principal cause of death in AIDS patients) (Banerji *et al.*, 1993). No examples of the *arom* pentafunctional polypeptides are known in photosynthetic organisms (Coggins *et al.*, 1987). The pentafunctional polypeptide chains have a mosaic structure and are essentially the five monofunctional enzymes found in bacteria fused together to form a multifunctional polypeptide chain (Coggins and Boocock, 1986). Studies of controlled proteolysis by trypsin and subtilisin have shown the presence and location of distinct protein domains (Smith and Coggins, 1983; Coggins and Boocock, 1986). The *N. crassa arom* complex is also Zn^{2+} dependent, with 1 atom per subunit of tightly bound zinc (Lambert *et al.*, 1985).

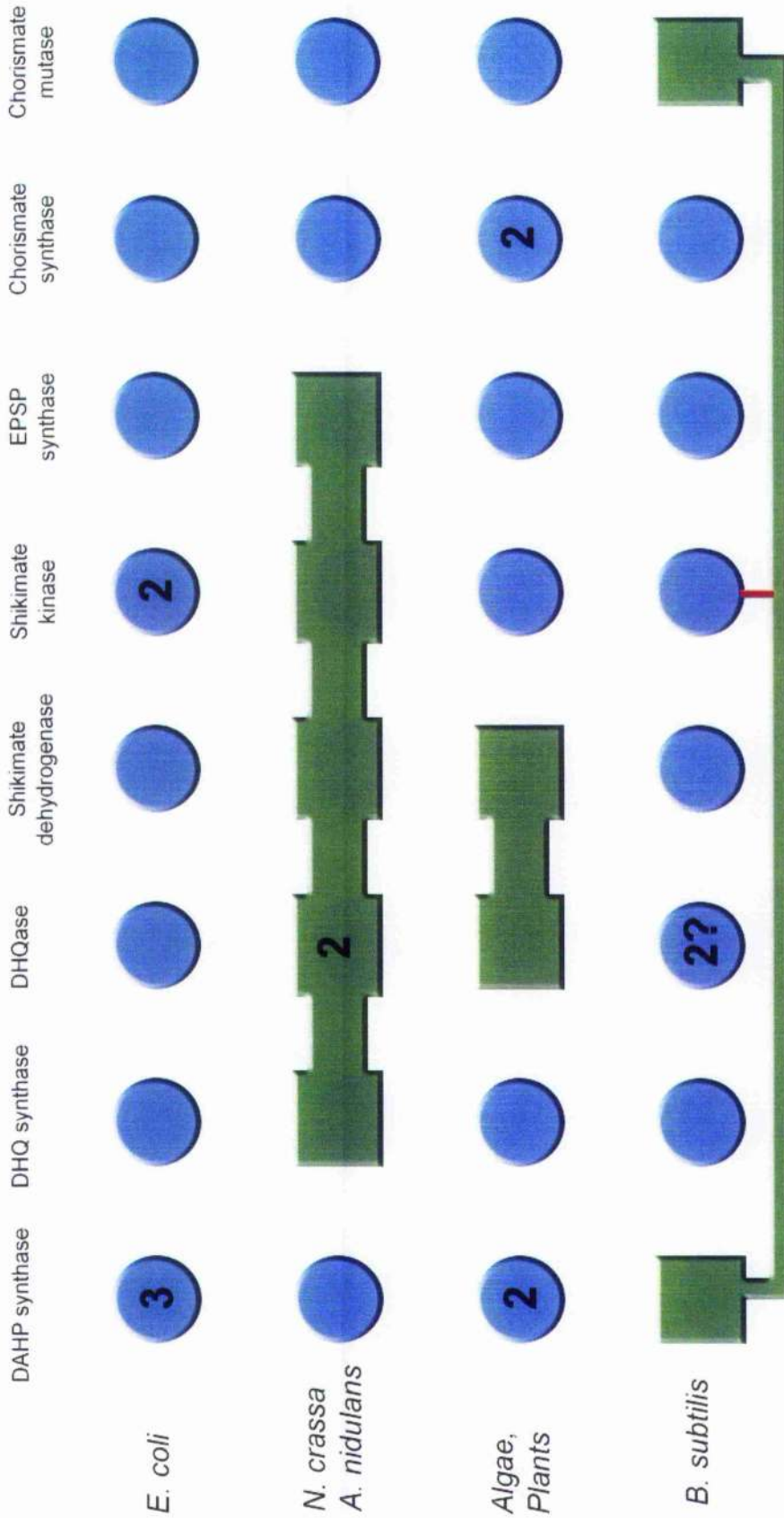


Figure 10 See following page for details.

Figure 10. Organisation of shikimate pathway enzyme in different species and Taxonomies. Blue circles indicate monofunctional enzymes and green linked squares indicate multifunctional polypeptides. The red line indicates a functional complex is formed between these proteins. The numbers indicate the number of the known isozymes for a given enzyme in a specific organism.

In these complexes, the order of the enzymes along the polypeptide chain differs from the sequence of the reactions in the pathway. Components of protein domains corresponding to DHQ synthase and EPSP synthase form the N-terminal element, whereas the domains corresponding to shikimate kinase, dehydroquinase, and the shikimate dehydrogenase form the C terminal portion (Smith and Coggins, 1983; Coggins and Boocock, 1986). One of the advantages of multifunctional enzymes is that the 'gene cluster' encoding the multifunctional polypeptide supplies a mechanism which regulates the expression of the functional domains so that equal amounts of each polypeptide are made and only one set of control sequences are required to regulate the expression of the pathway (Coggins *et al.*, 1987). There are a number of other proposed advantages of multifunctional enzymes, including the channelling of the substrate (Lamb *et al.*, 1992), the protection of unstable intermediates and enhancement of catalytic activity.

In higher plants such as *Phaseolus mungo*, *Physcomitrella patens*, *Nicotiana tabacum* and *Pisum sativum*, reactions three and four of the shikimate pathway are catalysed by a bifunctional enzyme (3-dehydroquinate dehydratase-shikimate dehydrogenase) (Koshihara, 1978; Polley, 1978; Mousdale *et al.*, 1987; Bonner and Jensen, 1994; Deka *et al.*, 1994). The dehydration site is located in the amino terminal half of the polypeptide. The partial cDNA sequence encodes a type I dehydroquinase (Bonner and Jensen, 1994). The inhibition by sodium borohydride in the presence of the substrate indicates that the bifunctional enzyme catalyses the dehydration of dehydroquinate via a Schiff base mechanism (Deka *et al.*, 1994) and is therefore a type I dehydroquinase (1.3.3). The shikimate dehydrogenase domain of the bifunctional enzyme is homologous with the catabolic quinate dehydrogenase (*qutB*) of *A. nidulans* and *N. crassa* (Bonner and Jensen, 1994).

Enzymes catalysing the remaining three reactions of the shikimate pathway are structurally homologous to those found in prokaryotes. Plant shikimate kinase cDNA

encodes an additional amino terminal sequence encoding plastid import (Schmid *et al.*, 1992). Shikimate kinase is localised in the chloroplasts of plants and appears to be activated by the energy charge (Schmidt *et al.*, 1990).

B. subtilis possesses a bifunctional polypeptide which has two domains with DAHP synthase and chorismate mutase activity, respectively (Figure 10). The shikimate kinase of *B. subtilis* is only active when complexed with this bifunctional enzyme (Nakatsukasa and Nester, 1972) (1.1.1.1 and 1.1.2.1).

There are three isozymes of DAHP synthase and two isozymes of shikimate kinase in *E. coli* (Figure 10); these are discussed in sections 1.1.1.1 and 1.1.1.5.

The organisation of the shikimate pathway genes is very diverse. Several species have a cluster of genes associated with the shikimate pathway including *Enterococcus faecalis*, *Clostridium acetobutylicum* and *Streptococcus pneumoniae*.

1.2 Quinate Pathway

Quinic acid is an abundant plant metabolite constituting 2-10% of the dry mass of higher plants (Bentley, 1990). *A. nidulans* is a heterotrophic ascomycete, which plays a role in the decay of humus, and decaying leaves. Quinate is present in this decaying vegetation and *A. nidulans* has the ability to grow solely on this carbon source (Hawkins *et al.*, 1982).

Three enzymatic reactions have been isolated *in vitro*:- a dehydrogenase (*qutB*) converting quinate to dehydroquinate, a dehydroquinase (*qutE*) converting 3-dehydroquinate to 3-dehydroshikimate, and a dehydratase (*qutC*) converting 3-dehydroshikimate to protocatechuate. These genes seem to be regulated by the product of a tightly linked third gene (*qutA*) (Valone *et al.*, 1971; Hawkins *et al.*, 1982; Da Silva *et al.*, 1986; Beri *et al.*, 1990). In the *A. calcoaceticus* chromosome the genes are part of the PCA operon (Hawkins *et al.*, 1993; Elsemore and Ornston, 1995). A number of organisms have quinate-shikimate dehydrogenases or shikimate dehydrogenase which can also act as a quinate dehydrogenase (1.4.1). Studies on mutant strains of *N. crassa arom*⁻¹ which encodes the shikimate dehydrogenase domain of the pentafunctional enzyme are able to grow on minimal medium since the *qa-3* quinate pathway shikimate dehydrogenase is able to catalyse the reaction disrupted by the mutation of the *arom* complex (Case *et al.*, 1972). Dehydroshikimate is converted to protocatechuate by dehydroshikimate

dehydratase; the stereochemistry of the catalysis was determined using the crude extract of mutant *N. crassa arom*⁻¹ and stereospecifically labelled substrate at C6 (Scharf *et al.*, 1971) this revealed that the reaction mechanism of dehydroshikimate dehydratase proceeds via the elimination of the *pro*-6R hydrogen together with the hydroxyl group at C5. Protocatechuate can be processed by the β -ketoadipate pathway eventually feeding into the TCA cycle (Giles *et al.*, 1985) (Figure 1).

The repressor proteins which regulate quinate catabolism in *N. crassa* (*qutR*) and the C-terminal domain of *A. nidulans* and *S. cerevisiae arom* protein have similar physical characteristics (Anton *et al.*, 1987; Lamb *et al.*, 1996). It is thought that both these proteins evolved from the three functional domains of the pentafunctional protein corresponding to dehydroquinase, dehydroshikimate dehydrogenase and shikimate kinase (Bonner and Jensen, 1994; Lamb *et al.*, 1996). *N. crassa* and *A. nidulans* both also possess a type II DHQase encoded by the genes: *qa-2* and *qutE*, respectively (Hawkins *et al.*, 1993).

Some fungi (*N. crassa* and *A. nidulans*) have both a type I domain within the *arom* pentafunctional enzyme and a type II dehydroquinase (1.3). In such organisms the type I enzyme is considered the anabolic form from the shikimate pathway and the type II enzyme the catabolic form in the quinate pathway (Giles *et al.*, 1967; Hawkins *et al.*, 1993; Dewick, 1998). The biosynthetic pathway enzyme is expressed constitutively and the catabolic enzyme is inducible. This allows the fungi to maintain flux through the shikimate pathway and respond to high levels of quinate in the environment (Giles *et al.*, 1985).

1.3 Two types of dehydroquinase

3-Dehydroquinase (dehydroquinase dehydratase; DHQase) catalyses the conversion of 3-dehydroquinase to 3-dehydroshikimate (Figure 4). Two distinct classes of dehydroquinase (types I and II) are responsible for catalysing the dehydration of dehydroquinase by different mechanisms and they also show no significant sequence similarity (Giles *et al.*, 1968; Charles *et al.*, 1985; Moore *et al.*, 1992; Lalonde *et al.*, 1994). It appears that the two types of dehydroquinase have arisen independently (Gourley *et al.*, 1999). They have very different amino acid sequences, subunit molecular weights, secondary, tertiary and quaternary structures, thermal stability and catalytic mechanisms. The two DHQases are generally well conserved within each

type (Gourley *et al.*, 1999). These biophysical properties have been studied using the *E. coli* type I and the *A. nidulans* type II DHQases. The type I DHQase is a homodimer of approximately 56 kDa. The type II DHQase is a homododecamer of 190 kDa. Thermal stability studies show that the Type I DHQase unfolds at 57°C while the type II DHQase unfolds above 82°C. The type II enzyme unfolds at concentrations of guanidinium chloride 4-times greater than are required for the type I enzyme. The type I enzyme unfolds in one transition while type II DHQase unfolds through a series of transitions (Kleanthous *et al.*, 1992, Price *et al.*, 1999). Stereochemical studies, using deuterated dehydroquinate and fluorinated substrates show that the reaction catalysed by the type II enzyme proceeds via an *anti* stereochemistry; in contrast in the type I DHQase the stereochemistry of the elimination is *syn* (Haslam *et al.*, 1971; Shneier *et al.*, 1993; Harris *et al.*, 1993a; Parker *et al.*, 2000). The substrate analogues 5-deoxy- and 4,5-dideoxy-dehydroquinic acid were used to test differences in substrate specificity between type I and type II DHQases. 4,5-dideoxy-dehydroquinic acid was found to be a poor substrate of *M. tuberculosis* type II DHQase with a k_{cat}/K_m of $5 \text{ M}^{-1} \text{ s}^{-1}$ and was not a substrate for the *E. coli* type I DHQase, highlighting the importance of the C4 hydroxyl group in the type I mechanism (Harris *et al.*, 1996).

Enzymes are generally considered to catalyse reactions by optimised mechanisms. It is therefore very interesting, when two mechanistically distinct enzymes are found which catalyse the same reaction.

1.3.1 Distribution of types

NCBI Genbank (<http://www.ncbi.nlm.nih.gov/BLAST>), EBI Genbank (<http://www.ebi.ac.uk>) and TIGR Comprehensive Microbial Resource (CMR) (<http://www.tigr.org/tigr-scripts/CMR2/CMRHomePage.spl>) web sites were used to reveal approximately 50 DHQases from different species, comparisons of the primary structures were performed using <http://prodes.toulouse.inra.fr/multalin/multalin.html> (Corpet, 1988). There is a demographic representation of the distribution of type I and II DHQases across a variety of species in Chapter 4 Figure 24. The type I DHQases have only been found in the context of the shikimate pathway whereas type II enzymes have been found to be involved in both the shikimate and quinate pathways. It should be noted that *Bacillus subtilis* has both forms of the enzyme. There does not seem to be any significant correlation between possession of either

type of DHQase and gene clustering. However in certain species the type I DHQase gene (*aroD*) is found to be neighbouring that of the shikimate dehydrogenase (*aroE*) (data not shown). This may have some evolutionary link to the formation of the bifunctional enzyme found in photoautotrophic organisms.

1.3.2 Selective inhibition

The availability of these two types of DHQase opens the way for the design of highly specific enzyme inhibitors with a potential importance as selective therapeutic agents (Gourley *et al.*, 1999). The stereochemical differences in the mechanism between the two types have been exploited in the design of specific inhibitors. (2*R*)-2-Bromo-3-dehydroquinic acid and (2*R*)-2-Fluoro-3-dehydroquinic acid are both substrates of the *M. tuberculosis* type II DHQase, while in the *E.coli* type I DHQase they are both irreversible inhibitors with K_i values of 3.7 mM and 80 μ M, respectively (Bello *et al.*, 2000).

A variety of known pathogens contain the type II enzyme, notably *Helicobacter pylori* (thought to cause stomach ulcers), *M. tuberculosis* (cause of tuberculosis) and *Campylobacter jejuni* (causes food poisoning) this makes it an interesting and novel antibiotic target. Since multiple drug resistance has evolved in *M. tuberculosis* it is of great importance that new drugs against this pathogen are found (Nachega and Chaisson, 2003). As more pathogenic organisms such as *P. falciparum* (McConkey, 1999) and *Chlamydia trachomatis* (Stephens *et al.*, 1998) are found to have the shikimate pathway the stronger the case becomes to develop novel drug compounds that inhibit the pathway.

Although both types of enzyme are likely to have similar substrate recognition elements in the active site a greater understanding of their mechanisms may suggest a rational basis for selective drug design. Several inhibitors of type II DHQases which are poor inhibitors of the type I class have been identified (Frederickson *et al.*, 1999; 2002) and are discussed in Chapter 3 (3.1.1).

1.3.3 Type I DHQase

The amino acid sequence of type I enzyme was deduced from the nucleotide sequence of the *aroD* gene in *E. coli* by Duncan *et al.* (1986b) and the subunit molecular mass was calculated as 26 kDa. The *E. coli* enzyme exists in solution as a dimer. The enzyme has also been characterised as part of a bifunctional enzyme in

Pisum sativum (Deka *et al.*, 1994). In the presence of guanidine hydrochloride the bacterial enzyme unfolds in one continuous transition suggesting that the dimer unfolds in a single co-operative step (Kleanthous *et al.*, 1991; 1992).

pH dependence studies on the *E. coli* type I dehydroquinase show that the enzyme is active over a broad range from pH 7.0 to 9.0 (Balinsky and Davies, 1961c). The type I enzymes catalyse a *cis*-dehydration of dehydroquinate involving elimination of the *pro-R* hydrogen along with the C1 hydroxyl group via a covalent imine (Schiff base) intermediate (Butler *et al.*, 1974; Chaudhuri *et al.*, 1991) (Figure 11), the formation of which is thought to be the rate limiting step of the reaction (Rotenberg and Sprinson, 1978; Harris *et al.*, 1996a; Gourley *et al.*, 1999). Using sodium borohydride trapping, the mechanism of *E. coli* type I dehydroquinase and the dehydroquinase component of the pentafunctional *arom* enzyme from *N. crassa* were shown to involve the formation of a Schiff base (Butler *et al.*, 1974) between dehydroquinate and an active site lysine of the enzyme (Chaudhuri *et al.*, 1991). Stability studies using circular dichroism, guanidine hydrochloride (GdmCl) denaturation, susceptibility to proteolysis and differential scanning calorimetry, showed that type I dehydroquinase from *E. coli* with covalently bound ligand was significantly more stable than unmodified enzyme. The concentration of GdmCl required to unfold the modified enzyme being 3-4-fold greater than for the unmodified native enzyme (Kleanthous *et al.*, 1991).

Radioactive labelling studies using iodo(2-¹⁴C)acetic acid were performed to identify residues in the active site of *E. coli* type I DHQase. This was achieved by sequencing radiolabelled peptide fragments isolated after proteolytic digestion (Kleanthous *et al.*, 1990a). Two residues, Met23 and Met205 were located in the active site pocket (Kleanthous *et al.*, 1990b). The covalently linked imine product is linked at the centre of the barrel attached to Lys170 (Figure 11), which is located on the β -strand. This location is similar to that in several enzymes proceeding via a Schiff base intermediate (Gourley *et al.*, 1999).

In order to investigate the mode of binding of dehydroquinate to the *E. coli* type I DHQase, a series of affinity labels were synthesized. These were used to characterise the active site general base, the carboxylate binding site and the C4 hydroxyl binding site (Bugg *et al.*, 1988). Type I DHQase will tolerate the absence of the C-5 hydroxy group, however the substrate specificity is significantly reduced suggesting that this

group forms an important binding interaction with the enzyme (Harris *et al.*, 1996a). The loss of the C-4 hydroxyl group of dehydroquinone completely abolishes the catalytic activity. It is thought that the C4 hydroxyl group is important for imine formation by the type I enzyme. Studies on the type II DHQase show the C4 hydroxyl group does not contribute significantly to specificity of the enzyme. Kinetic studies show that the absence of the C5 hydroxyl group reduces the specificity of the enzyme. An apparent binding energy (ΔG_{app}) for the 5-hydroxyl group was calculated from the k_{cat}/K_m values for dehydroquinone and 5-deoxy-dehydroquinone to be 17.2 kJ mol^{-1} . This suggests that the 5-hydroxyl group makes a strong interaction with a charged side chain either a lysine or arginine (Harris *et al.*, 1996b). Parker *et al.*, (2000) have highlighted some of the differences between the two enzymes using fluoro-analogues of the substrate ((6*R*)- and (6*S*)-6-fluoro-3-dehydroquinone). These analogues enable the enzyme-substrate imine to be trapped on the type I enzyme on treatment with sodium borohydride rather than the usual enzyme product imine.

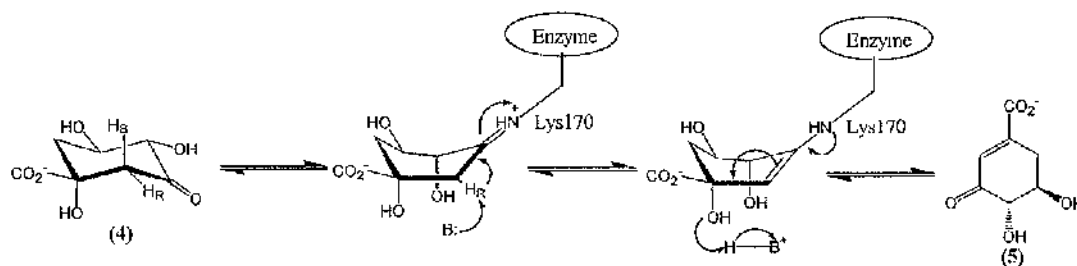


Figure 11. Proposed mechanism for the enzymic conversion of dehydroquinone (4) into dehydroshikimate (5) catalysed by type I dehydroquinase (Harris *et al.*, 1993; 1996b; Gourley *et al.*, 1999).

Mutagenesis of the active site residues performed by Leech *et al.* (1995) showed that mutation of Lys170 to an alanine almost totally abolishes the activity. This makes it clear that formation of the Schiff base is indispensable for the catalysis in the enzyme. Chemical modification experiments using the group specific reagent diethyl pyrocarbonate (DEPC) implicated His143 as the putative general base (B in Figure 11) in the breakdown of the imine intermediate. Furthermore pH-dependence studies identified a single ionised group with a pK_a of 6.2 (Deka *et al.*, 1992). His146 was also thought to be a candidate for this role; accordingly both of these side chains were mutated to alanine. The H143A mutant gave a similar K_m to the wild type whereas

there was a 5-6-fold reduction in k_{cat} . However, the catalytic activity and K_m were not affected by the H146A mutation (Lecch *et al.*, 1995). The 3-dimensional X-ray structure of *Salmonella typhi* type I DHQase reveals that His143 lies at the centre of a hydrogen bonded triad with Lys170 and Glu86 (Boys *et al.*, 1992; Gourley *et al.*, 1999). His143 and Glu86 residues interact through the protonated amine side chain of Lys170 (Gourley *et al.*, 1999). Studies using protein engineering and 2-dimensional 1H , ^{13}C NMR and additional pH-dependence studies by Lecch *et al.*, (1998) proved that His143 does not ionise over the pH range 6-9.5.

Glu86 is strictly conserved in type I DHQases suggesting an important functional role possibly in orientating His143. Chemical modification experiments on *E. coli* type I DHQase using the arginine-directed reagent phenylglyoxal (PGO) revealed that Arg213 was hyper-reactive (Krell *et al.*, 1996). The X-ray structure shows that Arg213, which is located on a distorted helix at the subunit interface binds to the C1 carboxylate (Gourley *et al.*, 1999).

The subunit architecture of type I DHQase is an eight-stranded α/β -barrel, a very common fold that was first reported for triosephosphate isomerase.

1.3.4 Type II DHQase

Type II DHQase has been characterised from *Actinobacillus pleuropneumoniae* (Lalonde *et al.*, 1994), *Streptomyces coelicolor* (White *et al.*, 1990), *H. pylori* (Bottomley *et al.*, 1996b; Kwak *et al.*, 2001), *Streptomyces hygroscopicus* (Florova *et al.*, 1998) and several other organisms. The structure of the type II enzyme from the human pathogen *M. tuberculosis* has been solved using multiple isomorphous replacement (MIR) to 2.0 Å resolution (Gourley *et al.*, 1994; 1999). A type II DHQase subunit consists of a five-stranded parallel β -sheet core flanked by four α -helices arranged with a similar overall topology to flavodoxin (Burnett *et al.*, 1974). The enzyme is a homododecamer and the subunits are arranged tetrahedrally as a tetramer of trimers. This type of dodecameric structure has also been observed in the catabolic ornithine carbamoyltransferase from *Pseudomonas aeruginosa* (Villeret *et al.*, 1995; Nguyen *et al.*, 1996).

The thermal stability of the enzyme is substantially higher than the type I enzyme with unfolding commencing at 80°C (Kleanthous *et al.*, 1992). Unfolding in the presence of guanidine hydrochloride occurs in three stages. Low concentrations (0.5

M) of guanidinium chloride are thought to cause the enzyme to dissociate into trimeric units, with little or no change in the secondary and tertiary structure. In *S. coelicolor* DHQase there is a 15% loss in activity while in *M. tuberculosis* DHQase there is a 55% increase in activity (Price *et al.*, 1999) in the presence of 0.5 M guanidinium chloride. The effect of addition of metal chelators and unfolding during refolding of the enzyme was examined by Bottomley *et al.*, (1996b). These experiments showed that the type II DHQases are not metal-dependent dehydratases. The subunit of type II DHQase has a molecular weight of approximately 16.5 kDa. The position of the active site was suggested by the cluster of conserved residues near the C-termini of the β strands (Gourley *et al.*, 1999).

Initial localization of the active site was performed using chemical modification in conjunction with electrospray mass spectrometry (Krell *et al.*, 1996). These experiments identified that the type II enzymes have an essential hyper-reactive arginine residue (Arg23 in *S. coelicolor* DHQase) and an essential tyrosine residue (Tyr28 in *S. coelicolor* DHQase). The role of the arginine residue was proposed to be in stabilising the carbanion intermediate. The active site has also been characterised using the fluorescent properties of a single tryptophan (Trp66 in *S. coelicolor* DHQase). It was thought that this residue was unlikely to be involved in the catalytic mechanism but might help to identify the active site (Boam *et al.*, 1997).

Type II DHQase catalyses an exclusively *anti* elimination of the *pro-S* hydrogen along with the C1 hydroxyl group. Due to the fact that there is no conserved lysine residue in sequence alignments, and treatment of the type II enzyme with sodium borohydride or cyanoborohydride does not lead to the inactivation it can be concluded that a Schiff base mechanism is not involved (Harris *et al.*, 1993). It is proposed that the type II enzyme adopts the step wise E₁CB (elimination unimolecular via conjugate base) mechanism and involves an enolate intermediate (Harris *et al.*, 1996a). The process involves a base-catalysed abstraction of the axial proton at the C2 leading to enolate formation (Gourley *et al.*, 1999; Harris *et al.*, 1996a). Elucidation of the enzyme mechanism is discussed in detail in Chapter 3 (3.1.1) and has been reported in Roszak *et al.*, (2002).

1.4 Shikimate Dehydrogenase

Shikimate dehydrogenase catalyses the reversible reduction of dehydroshikimate to shikimate (Salamon and Davis, 1953; Yaniv and Gilvarg, 1955) (Figure 5). Both the plant and bacterial enzymes require NADPH as a cofactor. A hydride is transferred from the nicotinamide ring of the cofactor to the C3 position of the substrate and a proton is also acquired stabilising the hydroxyl group at C3. Hydride transfer takes place from the A-side of the nicotinamide ring of NADPH (Dansette and Azcrad, 1974).

Shikimate dehydrogenase encoded by the *aroE* gene (Anton and Coggins, 1988) has been purified to homogeneity from *E. coli* (Chaudhuri and Coggins, 1985), and was shown to be monomeric (Maclean *et al.*, 2000) with a molecular mass of 32 kDa. The enzyme shows a strong preference for NADP⁺ over NAD⁺. The 3-dimensional X-ray structure of *E. coli* shikimate dehydrogenase reveals a novel binding site for NADP⁺ (Maclean *et al.*, 2000; Michel *et al.*, 2003). The plant shikimate dehydrogenase is part of a bifunctional polypeptide which requires NADPH for catalysis (Mousdale *et al.*, 1987; Deka *et al.*, 1994).

Much of the work on this enzyme has been carried out by assaying the enzyme in the reverse direction of the biosynthetic pathway; this is because shikimate is readily available and dehydroshikimate is not. Several inhibitors of shikimate dehydrogenase have been synthesized. The analogues of dehydroshikimate including 1,6-dihydroxy-2-oxoisonicotinic acid were found to be fairly potent inhibitors of the reverse reaction of shikimate dehydrogenase (Baillie *et al.*, 1972). Analogues lacking the C4 and C5 hydroxyl group of the substrate have helped identify the mode of substrate binding (Bugg *et al.*, 1988). Kinetic isotope studies and cofactor dissociation constants determined for the *Pisum sativum* enzyme suggest that shikimate dehydrogenase proceeds via an ordered BiBi mechanism, with the cofactor binding to the enzyme first (Balinsky *et al.*, 1971; Dowsett *et al.*, 1972). These inhibitors, analogues and isotope studies are discussed in more detail in Chapter 6 section 6.1.3.

1.4.1 Quinate-shikimate dehydrogenase

Quinate-shikimate dehydrogenases are thought to be distinct from the biosynthetic shikimate dehydrogenases catalysing the first step in the quinate pathway (1.2), namely the oxidation of quinate and shikimate to dehydroquinate and dehydroshikimate, respectively (Lopez Barea and Giles, 1978; Giles *et al.*, 1985). The cofactor specificity of this group of enzymes varies between species. The largest group that includes enzymes from fungi such as *A. nidulans* (Hawkins *et al.*, 1982) and *N. crassa* (Hawkins *et al.*, 1993) and bacterial enzymes such as that from *R. rhodochrous* (Bruce and Cain, 1990) are NAD⁺ specific. The NAD⁺ cofactor is normally associated with catabolic functions. The NADP⁺ specific shikimate dehydrogenase from some organisms may also be able to catalyse the oxidation of both quinate and shikimate. In *A. calcoaceticus* the reaction is catalysed by an unrelated pyrrolo-quinoline quinone (PQQ) dependent enzyme (Elsomore and Ornston, 1994).

1.4.2 Isozymes of shikimate dehydrogenase

Two isozymes of shikimate dehydrogenase have been isolated in a variety of plant species including tomato (*Lycopersicon esculentum*) loblolly pine (*Pinus taeda*) and pea (*Pisum sativum*). Some species of plants have three isozymes (Koshiba, 1978; Lourenco and Neves, 1984; Ossipov *et al.*, 2000). These genes have been used as genetic markers in agriculture.

Several bacterial genome projects have also identified a protein with some sequence homology to the shikimate dehydrogenase family, these proteins are denoted YdiB. The function of this group of proteins is unknown. The 3-dimensional structure of the *E. coli* YdiB protein (25% identity to *E. coli* shikimate dehydrogenase) has been recently solved (Michel *et al.*, 2003). The *E. coli* YdiB has the same overall fold as *E. coli* shikimate dehydrogenase (Michel *et al.*, 2003). However, the YdiB protein is dimeric in contrast with the *E. coli* shikimate dehydrogenase, which is monomeric. The structures and catalytic parameters of both these proteins are discussed in detail in Chapter 6 (6.1).

1.5 Project aims

The studies performed in this thesis were undertaken to investigate in more detail the mechanism, inhibition and substrate specificities of bacterial type II dehydroquinases

and shikimate dehydrogenases. This work should provide a greater understanding of the species specific differences in the enzymes and improve the prospect of rational drug design. The major experiments undertaken are outlined below.

- Several amino acid side chains were proposed to be located in the active site and involved in catalysis in type II DHQases. This was tested by site-directed mutagenesis on the *S. coelicolor* enzyme using a clone (pT7.7 *aroQ* (SCDHQase)) donated by Prof. Iain Hunter, University of Strathclyde. The residues mutated were Arg113, His106, Glu104, Ser108 and Tyr28. Characterisation of these mutant enzymes has provided strong evidence of the role of each of the residues within the active site (CHAPTER 3).
- The tyrosine residue shown by mutagenesis to be involved in proton abstraction at C2 of the substrate is conserved in all type II dehydroquinases except the enzyme from *B. subtilis* (YqhS). *B. subtilis* YqhS has a phenylalanine residue in this position. The *B. subtilis* protein has been purified (A. Herbert) and fully characterised by site-directed mutagenesis, kinetics and biophysical studies (CHAPTER 4).
- The type II DHQases which have been previously characterised kinetically appear to fall into two main groups. The enzymes from organisms such as *S. coelicolor* and *Aspergillus nidulans* have relatively high values of k_{cat} , in the range 100 to 1000 s^{-1} . By contrast, the enzymes from *Helicobacter pylori*, *M. tuberculosis* and *Neurospora crassa* have much lower values of k_{cat} in the range 10 s^{-1} or lower. Detailed studies of the pH dependence, pre-steady state kinetics, effects of salts on catalytic activity and the inhibitory effect of polyanions were performed on the enzymes of *S. coelicolor*, *M. tuberculosis*, *H. pylori* and *B. subtilis* (F23Y mutant). This has provided a better overall understanding of these enzymes (CHAPTER 5).
- The gene encoding shikimate dehydrogenase from *Haemophilus influenzae* has been cloned into an expression vector pTB361 *aroE* (donated by Dr. S. Campbell, University of Glasgow). Several species of bacteria possess an isozyme of shikimate dehydrogenase called YdiB which has a significantly different N-terminal amino acid sequence. The 3-dimensional structure of the YdiB protein from *E. coli* has recently been solved and shown to be NAD^+

dependent. *H. influenzae* also possesses the isozyme YdiB, however the N-terminal region of this protein differs significantly from the *E.coli* YdiB and other shikimate dehydrogenases. The YdiB protein from *H. influenzae* has been cloned, over expressed purified and characterised by a variety of techniques including steady-state kinetics, dynamic light scattering, circular dichroism and fluorescence (CHAPTER 6).

CHAPTER 2 MATERIALS AND METHODS

2.1 General Reagents

Chemicals and biochemicals were generally either analytical grade or the highest grade available. Unless otherwise stated all reagents were purchased from Sigma Aldrich Company Ltd., Fisher Scientific or Gibco BRL. See Appendix B for addresses of companies. Elga deionised water was used to make all buffers.

2.2 Reagents for molecular biology

Reagents used for molecular biology were supplied from Invitrogen Life Technologies, Promega, New England Biolabs, Amersham Pharmacia, Boehringer Mannheim and Difco. DNA markers used on agarose gels were EZ Load 100bp Molecular Ruler DNA marker and DNA Markers X and XIV (Roche). Protein markers used were Mark 12™ Novex wide range protein standard, low-range marker from Boehringer Mannheim and Promega Low-range protein molecular weight marker. See Appendix B for addresses of companies.

2.2.1 Enzymes for molecular biology

Restriction enzymes and their buffers were obtained from New England Biolabs Incorporated, Promega Corporation and Boehringer Mannheim. Several polymerases were used: Vent DNA polymerase was obtained from New England Biolabs, *pfu* turbo was obtained from Stratagene and Taq polymerase from Promega. Bacteriophage T4 DNA ligase was obtained from Boehringer Mannheim and Invitrogen. Calf intestine alkaline phosphatase (CIAP) (1 U/μl) was supplied by Promega. Restriction enzymes, polymerases and ligases were stored at -20°C. Sequencing grade modified trypsin (0.54 mg/ml) supplied from Promega was stored at -70°C.

2.2.2 Bacterial strains

The bacterial strains used in this project are listed with genotype and antibody resistance in Table 1.

Table 1. Bacterial strains used for general cloning expression and *in vivo* studies

Strain	Relevant genotype	Notes
<i>Escherichia coli</i>		
BL21 (DE3)	<i>HsdS gal OmpT lon⁻ (λclts857 ind1 Sam7 nin5 lacUV5-T7 gene l)</i>	High level expression of genes cloned into expression vectors containing bacteriophage T7 promoter (Studier and Moffatt 1986) (gifted by B. Lohkamp).
DH5α	<i>SupE44 ΔlacU169(φ80 lacZ ΔM15) hsR17 recA1 endA1 gyrA96 thi-1 relA1</i>	Plating and growth of plasmids (Hanahan 1983) (gifted by B. Lohkamp).
JM109	<i>e14⁻(McrA⁻) recA1 endA1 gyrA96 thi-1 hsdR17 (r_s⁻m_k⁺) SupE44 relA1 Δ(lac-proAB) F⁺[traD36 proAB⁺ lacI^q lacZ ΔM15]</i>	Plating, growth of plasmids and allows blue-white screening on X-gal (Yanisch-Perron <i>et al.</i> , 1985) (Stratagene).
PIR1	<i>F⁻ Δlac169 rpoS(Am) robA1 creC510 hsdR514 endA1 recA1 uidA(ΔmluI)::pir-116</i>	Also called PIR1 One Shot™ competent cells part of Invitrogen Echo™/TOPO® cloning system (2.7.5).
XL1-Blue	<i>SupE44 hsR17 recA1 endA1 gyrA96 thi-1 relA1 lac⁻ F⁺[proAB⁺ lacI^q lacZ ΔM15 Tn10 (tet^r)]</i>	Competent Cells part of QuikChange™ site-directed mutagenesis kit (Bullock <i>et al.</i> , 1987) (Stratagene)

Strain	Relevant genotype	Notes
<i>Bacillus subtilis</i>		
Derivative 168	ATCC Number: 33234	(Gifted by Dr. Blackburn)
Disruption mutant YqhSd	Inserted pMUTIN 3: Erythromycin antibiotic resistance	(Gifted by Prof. Sato)

2.2.3 Plasmids

The plasmids used in this project are listed with antibody resistance and promoters in Table 2.

Table 2. Plasmids used for molecular cloning

Plasmid	Source	Selection	Promoters	Notes
pGEM [®] 5Zf(+/-)	- S. Campbell	Ampicillin	T7/SP6	(Summerton <i>et al.</i> , 1983; Promega) Used for blue/white screening (2.8.3)
pLysS	S. Campbell	Chloramphenicol	T7	(Moffatt and Studier, 1987)
pT7.7	I. Hunter	Ampicillin	T7/SP6	(Tabor and Richardson, 1985)
pTB 361	A. Herbert	Tetracycline	T7	(Horsburgh, 1995)
pUni/V5-His- TOPO [®]	Invitrogen	Kanamycin	Uni1 forward/ reverse	Used to clone <i>ydib</i> from <i>H. influenzae</i> (2.7.5).

2.2.4 Genomic DNA

S. Campbell gifted genomic DNA for *Haemophilus influenzae* (ATCC 51907). Genomic DNA was stored at -20°C at a concentration of 0.5 ng/ μl (total of 10 ng)

2.3 Growth media and supplements

2.3.1 Media

The preparation of growth media and 1.5% agar growth media plates is described in Table 3.

Table 3. Growth media

Media	Composition per litre	Notes
Luria-Bertani (LB) ¹	10g NaCl 10g tryptone 5g yeast extract	Adjust pH to 7.0 and autoclave. For standard growth of <i>E. coli</i> strains
Spizizen minimal medium (SMM)	2g ammonium sulphate 14g dipotassium phosphate 6g monopotassium phosphate 1g sodium citrate·2H ₂ O 0.2g magnesium sulphate·7H ₂ O Following autoclave add: 20 ml filter-sterilised 25% (w/v) glucose.	Filter sterilise, final concentration of glucose is 0.5% (w/v). (Anagnostopoulos and Spizizen 1960).

¹ 1.5%(w/v) Bacto-agar for solid media plates

Media	Composition per litre	Notes
Nutrient broth (NB) ²	15g Standard II nutrient broth Final pH of 7.5.	For standard growth of <i>B. subtilis</i> (section 2.5.2).
NZY+ Broth	10g NZ (caesein hydrolysate) 5g yeast extract 5g NaCl. Following autoclave add: 12.5 ml 1M MgCl ₂ 12.5 ml 1M MgSO ₄ 10 ml 2M glucose, (filter-sterilised).	Filter sterilise. For growth of super-competent <i>E. coli</i> cells (Stratagene).
SOC medium	20g tryptone 5g yeast extract 0.5g NaCl. Following autoclave add: 10 ml 1M MgCl ₂ 10 ml 1M MgSO ₄ 10 ml 2M glucose, (filter-sterilised).	Filter sterilise. For growth of competent <i>E. coli</i> cells (section 2.8).

² 1.5%(w/v) Bacto-agar for solid media plates

2.3.2 Antibiotics

Antibiotics were used at the following final concentrations: ampicillin 100 µg/ml, tetracycline 12.5 µg/ml, kanamycin 50 µg/ml, erythromycin 1 µg/ml and chloramphenicol 34 µg/ml. A stock solution of 100 mg/ml of ampicillin was dissolved in distilled water and was sterilised by filtration through a 0.2 µm filter. A stock solution of 12.5 mg/ml of tetracycline was made up in 70% ethanol; filter sterilisation was not required. A 1 mg/ml stock solution of erythromycin was dissolved in 100% ethanol; filter sterilisation was not required. A 100 mg/ml stock solution of chloramphenicol was dissolved in 100% ethanol; filter sterilisation was not required. Kanamycin was made up as a 10 mg/ml stock in distilled water and filter sterilised. The antibiotic stock solutions were all stored at -20°C.

When making Agar plates which required antibiotics, the medium was allowed to cool to 50°C before the antibiotic was added. After mixing the medium was poured on to 90 mm petri dishes. All plates were stored at 4°C and if not used within four weeks were discarded.

2.3.3 Induction and chromogenic supplements

Isopropyl-β-D-thiogalactoside (IPTG) is an analogue of lactose, which targets *lac O* regulation and triggers expression of T7 RNA polymerase. IPTG was used at a final concentration of 0.8 mM. A 0.8 M stock solution was filter sterilised and stored at -20°C.

Bacteria with a non-functional β-galactosidase protein (*lacZΔM15*) can be reactivated by the addition of a plasmid containing the *lacZ* gene this codes for an amino-terminal fragment of the β-galactosidase protein. The combined peptide fragments make a functional β-galactosidase protein; a process termed α-complementation. 5-bromo-4-chloro-3-indoyl-β-D-galactoside (X-gal) is hydrolysed by β-galactosidase and produces a dark blue colour; this is used in blue-white screening of bacterial constructs (section 2.8.3). X-gal was used at a final concentration of 80 µg/ml. A stock solution of 80 mg/ml of X-gal was prepared in dimethylformamide (DMF) and stored at -20°C.

2.4 General laboratory methods

2.4.1 pH Measurements

pH measurements were made with a Orion model 420A+ pH meter with a Orion 81-72BN probe, calibrated at 20°C.

2.4.2 Storage of bacteria

Bacterial strains were stored as glycerol stocks. These were made by the addition of 0.5 ml of 50% (v/v) glycerol and deionised water (filter sterilised) to 0.5 ml of a rapidly growing culture ($A_{600} > 0.6$) to give a final concentration of glycerol of 25% (v/v). Glycerol stock cultures were stored at -80°C. Some cultures were temporarily stored by streaking onto Agar plates and kept at 4°C for up to four weeks.

2.5 Growth of bacteria

2.5.1 *E. coli*

E. coli was grown in liquid culture by taking a single colony from a LB Agar plate and inoculating LB medium (Table 3) containing the appropriate antibiotic. Cultures were grown at 37°C with vigorous shaking (~200 rpm) either overnight or for the planned induction time course (section 2.3.3). Incubation was performed either on a Grant shaking water bath (model OLS 200) or on a large shaker incubator (Gallenkamp). Cultures were monitored by measuring the optical density at 600 nm. Bacteria were harvested by centrifugation at $5,000 \times g$ for 15 minutes at 4°C using a Beckman model J-6B centrifuge fitted with a swinging bucket rotor. Smaller scale cultures were harvested in an Eppendorf (model 5415C) centrifuge at $16,000 \times g$ for 4 minutes at room temperature; pellets were either used immediately or were stored at -20°C. Agar plate cultures of *E. coli* were grown overnight at 37°C in a Eurotherm controls model 2216L incubator.

2.5.2 *B. subtilis*

B. subtilis was grown in either NB or minimal media (Table 3) under the same conditions as *E. coli* (section 2.5.1); some growth periods were extended to 32 hours.

2.5.3 Cell lysis

All steps during and after cell lysis were carried out at 4°C unless otherwise stated. Cells were resuspended in 10 ml of appropriate extraction buffer maintained at 0°C.

Cells were lysed by two passages through an automatic French pressure cell D118-00106 (Aminco®) at 15,000 psi. The pressure cell was pre-chilled on ice before use.

Lysis of volumes of less than 1 ml of bacterial cells for crude extract experiments involved a rapid freeze-thaw method followed by sonication in a 1.5 ml Eppendorf tube. The cells were subjected to 5 cycles of rapid freezing and thawing using liquid nitrogen and a Grant QBT2 heat block set at 25°C. Bacterial cells were further disrupted by five 1-minute cycles of sonication and incubation on ice a Decon model FS 100 water bath sonicator.

2.6 Polymerase Chain Reaction (PCR)

2.6.1 Primer Design

PCR Primers were designed to be at least 25 bases in length and the melting temperature (T_m) of the primers were matched with the primer on the opposite strand.

The following formula was used for Calculating T_m :

$$T_m = 81.5 + 0.41(\%GC) - 675/N - \% mismatch$$

Where %CG refers to the percentage of cytosine and guanine within the primer, N is the primer length in bases and % mismatch is applicable only for site-directed mutagenesis. Further details of this formula can be obtained from Stratagene (Appendix B).

Both mutagenic oligonucleotide primers contained the desired mutation (1-3 base changes within a codon) and anneal to the same sequence on the opposite strand of the plasmid. The mutation was always placed in the middle of the primer. Primers external to the gene had restriction sites incorporated to facilitate cloning of the PCR product into a vector. The 3' end was designed not to finish with a thymine or a run of 3 or more cytosine or guanine bases. It was not always possible to meet all of these criteria in every case especially because of the high GC content of the gene encoding *S. coelicolor* DHQase (approximately 70%GC).

Primers were supplied by MWG-Biotech at a concentration of approximately 45 pmol/ μ l having been purified by HPLC and phosphorylated at 3' end.

2.6.2 PCR reactions

PCR reactions were carried out using several different polymerases along with the buffers and salts provided by the manufacturer. The reaction was set up to have a total volume of 50 μ l comprising the following:

Table 4. Standard PCR reaction mixture

Reagent	Concentration of stock	Volume
Polymerase	2000 U/ml	1 μ l
Buffer and salts	as supplied	5 μ l
dNTPs	80 mM	1 μ l
Primers	10 pmol/ μ l	5 μ l
Varying quantities of template DNA (genomic or plasmid).	N/A	N/A

Varying quantities of enhancing agents were used in the PCR reaction for example $MgSO_4$ at final concentrations ranging between 0.5-2 mM, DMSO and glycerol at final concentrations of 1-10% (v/v) (Chakrabarti and Schutt, 2002). The total volume was made up to 50 μ l with sterile water; reactions were set up in 0.2 ml BioRad thin walled PCR tubes.

BioRad Gene cycler™ version 1.7 was used for all thermal cycles. Programs varied but usually comprised an initial 'hot start' step at 94-95°C for 5 minutes, followed by 30 cycle repeats of a 1 minute annealing step (temperature depending on T_m), an elongation step at 68-72°C (time depending on length in bases of desired PCR product) and a denaturation step at 94-95°C for 1 minute. A final elongation step of between 5 and 10 minutes at the elongation temperature was performed at the end of the amplification reaction to ensure that all amplified material was full length.

2.6.3 Site-directed mutagenesis strategies

2.6.3.1 Two stage PCR using Vent polymerase

PCR was used in a two-stage procedure to generate site-directed mutants (Higuchi *et al.*, 1988). To reduce primer-dimer and non-specific priming a hot start polymerase was employed (Vent[®] polymerase from NEB.)

The template for all these reactions was plasmid DNA. External primers P1 and P2 (Figure 12) were designed to include restriction sites within the original multiple cloning site of the plasmid. Internal primers (P2 and P3) (Figure 12) with the mismatch were designed with a T_m similar to that of the external primers so that any mismatch would not generate problems during thermal cycling.

The first step was to generate two overlapping fragments with the desired mutation; these were made in independent reactions as described in section 2.6.2. The products from the PCR reaction were analysed on a 1% (w/v) agarose gel as described in section 2.7.1. The PCR product of the correct size was excised and purified using QIAquick[®] spin purification system (2.7.4) and used as the template DNA for the second round of PCR.

The second step of the PCR strategy was to anneal these fragments together and extend at the 3' end to generate a full-length cDNA with the mutation (Figure 12). PCR was again carried out as described in section 2.6.2. The full length mutated DNA fragment was visualised by staining with ethidium bromide on a 1% (w/v) agarose gel (section 2.7.1) excised and purified with QIAquick[®] spin purification system (section 2.7.4). The purified DNA was then digested by the appropriate restriction endonuclease(s) using the sites present in the external primers (section 2.7.3) and ligated to an expression vector (section 2.7.5).

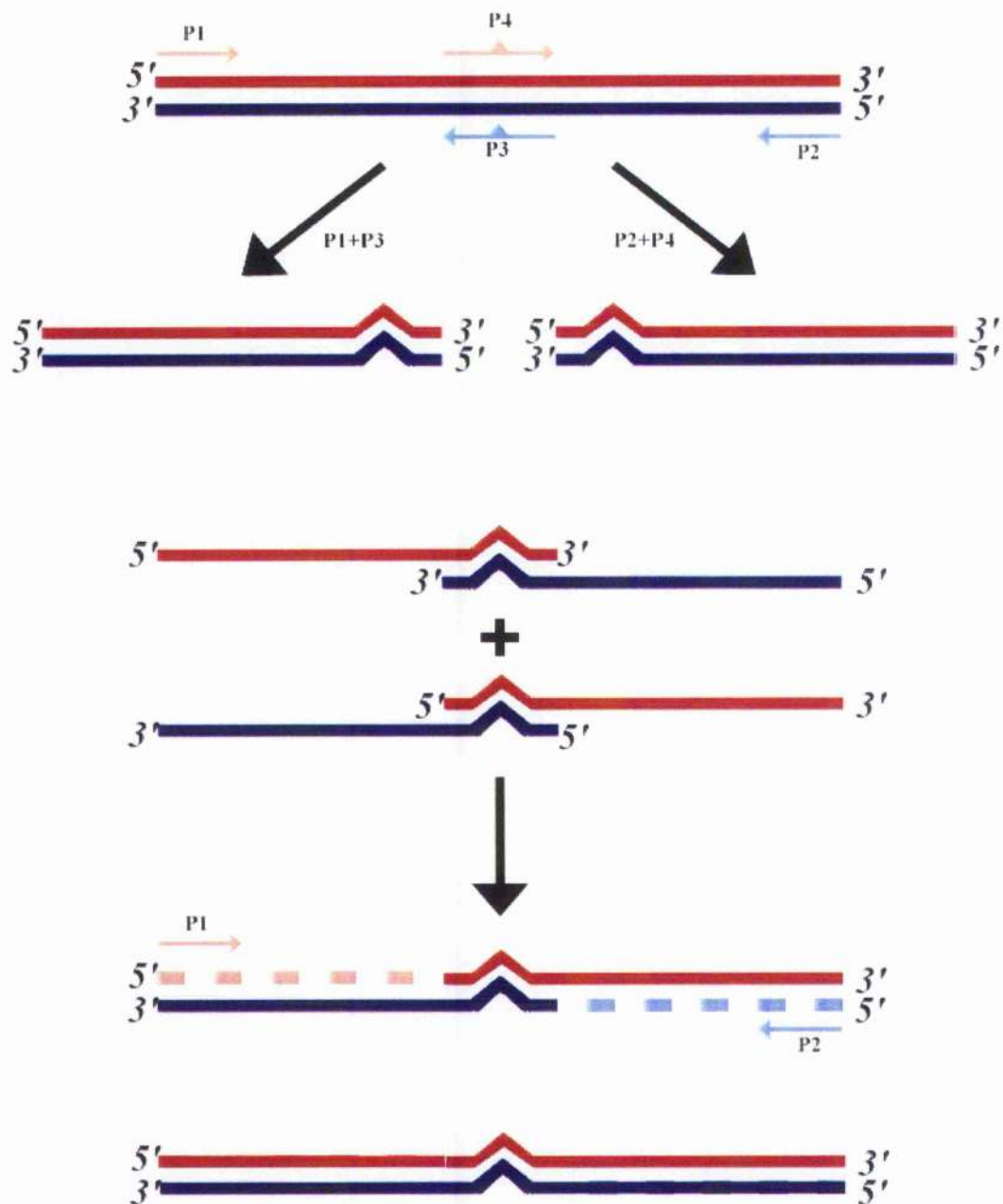


Figure 12. PCR two stage site-directed mutagenesis strategy (Higuchi *et al.*, 1988). Primers are shown as red and blue arrows, the black arrows represent PCR reactions.

2.6.3.2 Site-directed mutagenesis using Quikchange™ site-directed mutagenesis kit from Stratagene

The two stage site-directed mutagenesis strategy described in section 2.6.3.1 proved to be rather inefficient; hence in the majority of the work the Quikchange™ site-directed mutagenesis kit from Stratagene was employed. Two mutagenic primers each complementary to opposite strands of the template plasmid DNA are extended to amplify the whole length of the plasmid during temperature cycling by *pfuTurbo* DNA polymerase. Incorporation of the mutagenic primers generates a mutated circular plasmid containing staggered nicks. *Dpn I* is then used to digest parental template DNA as the parental DNA retains its methyl groups. The nicked mutated plasmid can then be transformed into XL1-blue competent cells. Further details of this procedure are can be obtained from Stratagene (Appendix B).

2.7 DNA cloning procedures

2.7.1 Electrophoresis of DNA on agarose gel

DNA strands were separated by electrophoresis using TAE (Appendix A) agarose gels ranging from 0.7-1.5% (w/v) depending on the size of the DNA strands; the gel also contained 0.5 µg/ml of ethidium bromide to visualise the DNA under UV light. Samples were loaded with a 1:10 dilution of agarose gel sample loading buffer (Appendix A). A variety of standard markers were used to estimate the size and quantity of separated bands. Gels were run at 80V at 20°C in a Mini-sub® cell GT BioRad tank until the bromophenol blue in the agarose gel sample-loading buffer had migrated at least two thirds of the way down the gel. The DNA was then visualised using a UVP Bio Doc-It™ system and UVP camera model J6 × 11 Macro. Prints were produced when appropriate using a Sony video graphic printer UP-895CE.

2.7.2 Isolation of Plasmid DNA from bacteria cells

Bacterial colonies growing on selective media were picked and grown overnight in from 1.5 to 5 ml of LB at 37°C shaking at 200 rpm with the relevant antibiotic. Plasmids were then isolated by the alkaline lysis procedure (Birnboim and Doly, 1979) using either the Qiagen QIAprep® Spin Mini prep kit or the Sigma Genelute® Miniprep system. Bacterial cells are lysed under alkaline conditions, the lysate is subsequently neutralised and adjusted to high salt conditions favourable for plasmid

DNA to bind to silica-based resins. Plasmid DNA is eluted in a low salt buffer. Plasmid yield with both systems varies depending on the copy number per cell, the individual insert in a plasmid, factors that affect growth of the bacterial culture, the elution volume and the elution incubation time. Typically a 1.5 ml culture will yield from 5 to 15 μg of plasmid DNA (maximum of 20 μg of plasmid DNA). Further details of these procedures are can be obtained by contacting Qiagen or Sigma (Appendix B).

2.7.3 Endonuclease restriction of plasmid DNA and PCR product

DNA was digested using restriction enzymes from Boehringer Mannheim, Promega or New England Biolabs. Typical digests contained target DNA (plasmid or PCR product); the amount of DNA depended on the downstream application.

The digests were performed using between 1-50 units of restriction enzyme and the appropriate restriction enzyme buffer. If two restriction enzymes were used in the reaction, the buffer best suited to both enzymes was used or Promega multicore[®] buffer. The mixture was made up to its final volume with sterile water. Digestion reactions were incubated at 37°C for at least 1 hour. Analysis of digested DNA was performed by agarose gel electrophoresis (section 2.7.1) and if necessary DNA was purified by excising the relevant band from an agarose gel (2.7.4).

2.7.4 Purification of restriction digested DNA and PCR product

The restriction digested DNA and PCR product are separated from contaminants such as primer-dimers, amplification primers or restriction enzymes by agarose gel electrophoresis (section 2.7.1). 45 μl of the PCR product was separated on a 1% (w/v) agarose gel and excised with a scalpel on a Clare chemical research Dark reader UV box and purified using Qiagen QIAquick[®] spin purification procedure. The excised gel fragment is solubilized in a binding buffer at 50°C for 10 minutes. The QIAquick[®] uses the same purification technique for DNA as is used in the isolation of plasmid DNA from bacterial cells (2.7.2) involving salt exchange on a silica membrane (Birnboim and Doly, 1979). The purified DNA was eluted in 50 μl of sterile water for use in further cloning procedures. This procedure yielded approximately 10 μg of DNA depending on the concentration of DNA within the PCR product or restriction digest.

2.7.5 Ligation of digested fragments and PCR product

The concentration of DNA was estimated by agarose gel electrophoresis using molecular weight standards of known concentrations (section 2.7.1). After the DNA has been prepared for ligation the following calculation was applied to work out the molar ratio of vector and insert (Further information on this formula can be obtained by contacting Promega: Appendix B):

$$\text{ng of insert} = \frac{\text{ng of vector} \times \text{kb size of insert}}{\text{kb size of vector}} \times \text{molar ratio of } \frac{\text{insert}}{\text{vector}}$$

Typically several ratios of vector DNA and insert DNA were used in separate ligations. Ligation reactions used between 50-200 ng of vector DNA. Ligations were performed in a total volume of either 10 or 20 μl . Between 1-3 units of T4 ligase from Promega, Boehringer Mannheim or Invitrogen were incubated at room temperature overnight with the relevant buffer and sterile water was added to correct the volume if required. The ligation mixture (1 to 20 μl) was used to transform competent cells (section 2.8.2). pGEM[®] -5Zf(+/-) vector digested with restriction endonuclease *EcoRV* was used in blunt end ligations; insertion of blunt ended fragments into the *lacZ* gene allowed for blue-white screening in *E. coli* JM109.

A one-step cloning strategy (TOPO[®] cloning, Invitrogen) was also utilised for direct insertion of A-tailed PCR products into recombinant plasmid. The TOPO[®] cloning procedure involves topoisomerase I from *Vaccinia* virus that binds to specific DNA sites and cleaves the phosphodiester backbone after 5'-CCCTT. The energy from the broken bond is conserved by the formation of a covalent phospho-tyrosyl bond between the 3' phosphate of the cleaved DNA and Tyr274 of topoisomerase I. This forms a linearized vector (pUni/V5-his-TOPO[®]) with a overhanging 3' deoxythymidine; the phospho-tyrosyl bond can subsequently be attacked by 5' hydroxyl of a PCR product releasing the topoisomerase I. This allows efficient ligation of PCR product without the use of ligase. The reaction mixture contains between 0.5 to 4 μl of PCR product (dependent on DNA concentration), 1 μl of 200 mM NaCl, 10 mM MgCl₂, 1 μl of pUni/V5-his-TOPO[®] and the volume is then adjusted to 6 μl with sterile water (all reagents are supplied by Invitrogen). Further details of this procedure are can be obtained by contacting Invitrogen (Appendix B).

2.7.6 Dephosphorylation of plasmid DNA

Removal of 5' phosphates from linearised vector DNA can help prevent self-ligation and improve ligation efficiency. Alkaline phosphatase (Promega) was used to dephosphorylate restricted plasmid DNA. 1 µl of calf intestinal alkaline phosphatase (CIAP)(10 U/µl) diluted 1:10 with CIAP buffer were added to the plasmid restriction digest and made up to the final volume with distilled water. The volume was corrected with sterile water. The reaction was incubated for 40 minutes at 37°C. DNA was then purified by agarose gel electrophoresis (2.7.4).

2.8 Preparation of competent cells and transformation

2.8.1 Preparation of competent cells

An adaptation of the method of Hanahan (Hanahan and Meselson, 1980; Hanahan *et al.*, 1980) was used to make competent cells; this involved employing potassium chloride rather than rubidium chloride in the buffers. 10 ml of LB was inoculated with an *E. coli* strain from an -80°C glycerol stock and was grown at 37°C shaking at 200 rpm overnight (with antibiotic if required). The absorbance at 600 nm of the overnight culture was measured and the culture diluted to 0.1 OD in 80 ml of LB. The cells were then grown at 37°C shaking at 200 rpm for 1 hour or until they reached mid log phase (A_{600} in the range of 0.35-0.6). The cells were then placed on ice for 15 minutes and were kept below 4°C throughout the rest of the procedure. The culture was then transferred to chilled centrifuge tubes and centrifuged at 3000 × g in a Beckman model J2-21 using a JA-20 rotor for 15 minutes to pellet the cells. The pellet was then resuspended in 30 ml of ice cold RF1 (Appendix A) and incubated on ice for 1 hour after which the cells were re-pelleted by centrifugation. The pellet was resuspended in 7 ml of ice cold RF2 (Appendix A) and incubated on ice for 15 minutes. The cell suspension was then divided into 200 µl aliquots in 1.5 ml Eppendorf tubes and each aliquot was either used for transformation or flash frozen in a dry-ice/ ethanol bath and stored at -80°C.

Competent cells can be stored indefinitely at -80°C, without showing any significant reduction in transformation efficiency.

2.8.2 Transformation protocol

An Eppendorf tube containing a 200 μ l aliquot of cells was allowed to thaw on ice or was used directly from a preparation of competent cells made immediately before transformation. Plasmid DNA or ligation mixture was added to cells and mixed by inverting gently after which the cells were incubated on ice for 1 hour. The cells were heat shocked at 42°C for 45 seconds and were then returned to ice for a further 30 minutes. 0.8 ml of either SOC or NZY+ broth (Table 3) was added to the transformation mixture and was incubated at 37°C for 45 minutes to aid recovery. The cells were then pelleted in an Eppendorf centrifuge at 16,000 \times g for 3 minutes and were re-suspended in 100 μ l of the same media and plated out on selective plates.

2.8.3 Blue-white screening using the *lacZ* gene

Blue-white screening was used to identify successfully ligated plasmid within bacterial cells. It is necessary to use a bacterial strain which has the *lacZ* Δ M15 gene on the F' episome, such as JM109 and a vector which has the *lacZ* gene like pGEM V and the chromogenic supplement; X-gal (2.3.3). The ligated gene disrupts the *lacZ* gene, so that the bacteria are unable to hydrolyse X-gal. Therefore the bacterial cell colony will not exhibit a blue phenotype. The *lacZ* gene in pGEM V can be disrupted using the blunt end restriction site EcoRV.

2.9 Sequencing of plasmid DNA

Sequencing of recombinant genes was carried out by the Functional Genomics Sequencing Facility at the University of Glasgow. Typically a total of 600 ng of DNA was supplied for sequencing. The concentration of sequencing primers used was between 3.2 to 5 μ M (pmol/ μ l). Sequencing reactions were set up using varying volumes of deionised water and plasmid DNA depending on DNA concentration, 4 μ l of the Big Dye, dideoxynucleotide (ddNTPs) reaction mixture (Applied Biosystems), and 1 μ l of sequencing primer in a total volume of 10 μ l. All components were added to a 96-well plate and centrifuged at 16000 \times g for 30 seconds. Sequencing reactions were carried out in a PCR machine PE9700, hot start (95°C) for 5 minutes, then 30 cycles of 50°C for 5 minutes, 60°C for 4 minutes and 95°C for 10 seconds. DNA samples were then precipitated using 2 μ l of 1.5 M sodium acetate, 0.25 M EDTA (pH 8.0) and 80 μ l analytical grade ethanol, and centrifuged for 60 minutes at 4°C at 16000 \times g and then washed in 200 μ l 70% ethanol and centrifuged again for 20

minutes. Samples were resuspended using 2 μ l of loading buffer (25 mM EDTA, 25 mg/ml blue dextran, 50 % (v/v) deionised formamide) and loaded on to a 4.5 % acrylamide sequencing gel using Long Ranger XL PreMix Gel Solution and run using TBE buffer. Each ddNTPs contains a specific fluorescent dye that can be excited by a laser. The signals are then collected and a coloured electropherogram is produced which is analysed by Sequencing Analysis Version 3.4.1 ABI PRISM[®] (Applied Biosystems) software.

2.10 Over Expression of proteins in *E. coli*

The BL21 (DE3) strain *from E. coli* was used for over expression of proteins. This strain is deficient in the *OmpT* and *lon* genes which code for proteases that could degrade expressed protein. BL21 (DE3) also has the gene for T7 RNA polymerase integrated into its chromosome under the control of a *lac* promoter and operator. This will specifically recognize the T7 promoter region of an expression plasmid and will not efficiently transcribe from other promoters. T7 RNA polymerase can also be induced by the lactose analogue, IPTG. The pLysS plasmid encodes T7 lysozyme which binds and inhibits T7 RNA polymerase; this controls the basal levels of the expressed protein prior to induction with IPTG.

The strain BL21 (DE3) pLysS transformed with the relevant expression vector was used to inoculate (from a plate) a 2 litre conical flask containing 500 ml LB, chloramphenicol and the relevant antibiotic for the expression vector. The culture was grown overnight at 37°C with continuous shaking at ~200 rpm. The following day, eleven 2-litre flasks containing 500 ml LB, chloramphenicol and the relevant antibiotic for the expression vector were inoculated with the overnight culture to a starting optical density of 0.1 A_{600} ; these cultures were grown at 37°C with continuous shaking at 200 rpm until the A_{600} reached between 0.4-0.6. Adding IPTG and growing the cells for a further 5-6 hours induced protein expression. *E. coli* cells were then harvested, as outlined in section 2.5.1. The typical wet weight of the harvested cells from 11 flasks was between 10 and 15g. The cell pellet was stored at -20°C until required.

2.11 Sodium dodecyl sulphate poly-acrylamide gel electrophoresis (SDS PAGE)

Sodium dodecyl sulphate polyacrylamide gel electrophoresis (SDS-PAGE) was used to identify and characterise proteins as described by Laemmli (1970) using a BioRad mini gel apparatus with a 5% acrylamide stacking gel and separation gels of either 12 or 15%. Samples were loaded in SDS-PAGE sample loading buffer (Appendix A). A variety of protein markers were used to estimate the molecular weight of protein bands. Unless otherwise stated Low molecular weight markers from Boehringer Mannheim were diluted 1:10 with the loading buffer. Gels were usually run at 30 mA for 45 minutes or until the dye front (bromophenol blue) reached the bottom of the gel.

2.11.1 Protein staining.

After electrophoresis, proteins on a SDS-PAGE were visualised by staining with Coomassie Blue. The staining reagent was 0.05% (w/v) Coomassie brilliant blue R-250 in 50% (v/v) methanol and 10% (v/v) acetic acid for at least 30 minutes at 40°C. Destaining was carried out at 40°C in 10% (v/v) methanol and 10% (v/v) glacial acetic acid until the background was fully destained and the protein bands clearly visible.

2.12 Purification of proteins

All purification steps following cell breakage were performed at 4°C unless otherwise stated.

2.12.1 *S. coelicolor* type II dehydroquinase

The type II dehydroquinase from *Streptomyces coelicolor* was purified using an adaptation of the method of White *et al.*, (1990) as outlined below.

2.12.1.1 Step 1: Extraction and centrifugation

The type II DHQase was over expressed in *E. coli* strain BL21 (DE3) pLysS using the expression vector pT7.7 (2.3.3). The Cells were suspended in 20 ml of 50 mM Tris·HCl, pH 7.5 containing 0.4 mM DTT and a Complete™ EDTA free protease inhibitor cocktail tablet (600 mg) (buffer A). Cells were lysed using a French pressure cell (2.5.3). The volume of the lysed cells was increased to 80 ml. 0.5 mg

of DNase was added and the lysate was stirred on ice for 45 minutes. The lysate was then centrifuged at $40,000 \times g$ for 1 hour in a MSE high speed-18 centrifuge; type II dehydroquinase was purified from the resulting supernatant fraction.

2.12.1.2 Step 2: Anion exchange chromatography on DEAE-Sephacel

The supernatant was loaded on to a DEAE-Sephacel (Amersham Pharmacia) anion exchange column (11.5×5.0 cm diameter) equilibrated in buffer A at a flow rate of 80 ml/hour. The column was washed with buffer until the A_{280} of the eluate was less than 0.1. The column was then washed with 100 mM NaCl until the A_{280} of the eluate was again less than 0.1. A linear gradient of 100 mM to 400 mM NaCl in 800 ml of buffer A was set up to elute the protein (flow rate of 30 ml/hour). 10 ml fractions were collected and A_{280} and enzyme activity were monitored (2.16.1). Fractions containing activity $>1.2 \Delta A_{234} \text{min}^{-1} \mu\text{l}^{-1}$ were pooled and dialysed into 50 mM Tris-HCl, pH 7.5 containing 0.4 mM DTT and 1M ammonium sulphate (buffer B) overnight or concentrated to 20 ml using an AMICON[®] protein concentrator with a 30 kDa filter and were adjusted to 1 M ammonium sulphate.

2.12.1.3 Step 3: Hydrophobic interaction chromatography on phenyl-Sepharose

The dialysed material was applied to a phenyl-Sepharose hydrophobic interaction column (8.0×4.5 cm diameter) equilibrated in buffer B at a flow rate of 40 ml/hour. A 1.0-0M gradient of ammonium sulphate was applied to the column in 600 ml of 50 mM Tris-HCl, pH 7.5 (flow rate of 10-40 ml/hour). The column was washed with a further 300 ml of 50 mM Tris-HCl, pH 7.5 (flow rate of 40ml/hour). 5 ml fractions were collected and analysed as before, samples containing high activity were pooled and dialysed overnight against 50 mM Tris-HCl, pH 7.5 to remove ammonium sulphate.

2.12.1.4 Step 4: Gel filtration Chromatography on Sephacryl 200

The dialysis buffer was then changed to 50 mM Tris-HCl, pH 7.5 containing 150 mM NaCl (buffer C) and dialysed for 3 hours. The dialysed material was then concentrated to a volume of 1.5 ml using an Amicon[™] concentrator. The concentrate was applied to a Sephacryl 200 Size separation (Gel filtration) column (165×2.5 cm diameter) equilibrated in buffer C at a flow rate of 10 ml/hour. The protein was eluted using buffer C in 2 ml fractions. After assaying for DHQase activity

appropriate fractions were pooled and concentrated. A sample of the concentrate was analysed by SDS-PAGE (section 2.12.1.1) to check the purity of the dehydroquinase and then dialysed into 50 mM Tris·HCl, pH 7.5 containing 50% (v/v) glycerol for 24 hours and stored at -20°C .

2.12.2 *B. subtilis* YqhS (dehydroquinase related protein) mutant F23Y

The *B. subtilis* YhqS mutant F23Y, was overexpressed in BL21 (DE3) pLysS using expression vector pTB361 (section 2.10). The purification protocol was similar to that for *S. coelicolor* dehydroquinase. Some adjustments to the protocol were made, as it was not possible to monitor the dehydroquinase activity of the *B. subtilis* YqhS mutant F23Y during the purification.

2.12.2.1 Step 1: Extraction, heat treatment and centrifugation

The heat stability of the protein was exploited by heat-treating the cell extract after step 1 (section 2.12.1.1) prior to loading on to the DEAE-sephacel column. The soluble cell extract was heated to 65°C for 10 minutes in a stainless steel beaker using a Grant OLS 200 water bath and then kept on ice for 10 minutes. The heat-treated lysate was then centrifuged at $40,000 \times g$ for 40 minutes in a MSE high speed-18 centrifuge. The supernatant was collected and dialysed against 50 mM Tris·HCl, pH 7.5 containing 100 mM NaCl and for 2 hours.

2.12.2.2 Step 2: Anion exchange chromatography on Q-Sepharose

The dialysed material was applied to a Q-Sepharose (Pharmacia Biotech) anion exchange column (24.5×2.5 cm diameter) equilibrated in 50 mM Tris·HCl, pH 7.5 containing 50 mM NaCl, 0.4 mM DTT and a Complete™ EDTA free protease inhibitor cocktail tablet (600 mg) at a flow rate of 60 ml/hour. The column was washed with buffer until the A_{280} of the eluate was less than 0.1. A linear gradient from 50 mM to 500 mM NaCl in 500 ml of buffer A was set up to elute the protein (flow rate of 70 ml/hour). 10 ml fractions were collected and A_{280} measurements and analysed by SDS-PAGE (section 2.11) were performed to locate the desired protein fractions. These fractions were pooled and dialysed against 50 mM Tris·HCl, pH 7.5 containing 150 mM NaCl.

2.12.2.3 Step 3: Gel filtration Chromatography on Sephacryl 200

Purification of the *B. subtilis* YqhS F23Y using Sephacryl 200 gel filtration column followed the same purification protocol as *S. coelicolor* DIIQase see section 2.12.1.4. Detection of the appropriate fractions was performed using A_{280} measurements and analysed by SDS-PAGE (section 2.11). Fractions were concentrated to 5 ml and dialysed into 50 mM Tris·HCl, pH 7.5 containing 50% (v/v) glycerol for one day and stored at -20°C .

2.12.3 Purification of *H. influenzae* shikimate dehydrogenase

Shikimate dehydrogenase from *Haemophilus influenzae* was purified using the methods described for the purification of *E. coli* shikimate dehydrogenase by of Chaudhuri and Coggins, (1985) and Maclean *et al.* (2000), as outlined below.

2.12.3.1 Step 1: Extraction and centrifugation

Shikimate dehydrogenase from *Haemophilus influenzae*, was over-expressed in BL21 (DE3) pLysS using expression vector pTB361 (section 2.10). The cells were suspended in 20 ml of 100 mM Tris·HCl, pH 7.5 containing 1.3 mM EDTA, 0.4 mM DTT and a Complete™ EDTA free protease inhibitor cocktail tablet (600 mg) (Extraction buffer). Cells were lysed and centrifuged as in section 2.5.3. Shikimate dehydrogenase was purified from the supernatant fraction.

2.12.3.2 Step 2: Fractionation with ammonium sulphate

Benzamidine was added to a final concentration of 1 mM and the crude extract was then adjusted slowly to 30% saturation with solid ammonium sulphate stirring on ice, for 20 minutes. The precipitate was then removed by centrifugation at $40,000 \times g$ for 30 minutes in a MSE high speed-18 centrifuge. The supernatant was adjusted to 55% saturation with ammonium sulphate and stirred on ice for 20 minutes. The resulting precipitate was collected by centrifugation at $40,000 \times g$ for 30 minutes in a MSE high speed-18 centrifuge. The precipitate was re-dissolved in 100 mM Tris·HCl, pH 7.5 containing 0.4 mM DTT (buffer D) and dialysed over night in buffer D with 50 mM KCl.

2.12.3.3 Step 3: Anion exchange chromatography on DEAE-Sephacel

The dialysed material was applied to a DEAE-Sephacel (Amersham Pharmacia) anion exchange column (11.5×5.0 cm diameter) that had been pre-equilibrated in

buffer D with 50 mM KCl at a flow rate of 80 ml/hour. The column was washed with buffer D with 100 mM KCl until the A_{280} of the eluate was less than 0.2. A linear gradient of 100 mM to 400 mM KCl in 800 ml of buffer D was set up to elute the protein (flow rate of 30 ml/hour). 10 ml fractions were collected and A_{280} and assays (2.16.2) were performed. Fractions containing activity $>0.15 \Delta A_{340} \text{min}^{-1} \mu\text{l}^{-1}$ were pooled and dialysed into buffer D and 500 mM KCl overnight.

2.12.3.4 Step 4: Gel filtration Chromatography on Sephacryl 200

Purification of the *H. influenzae* shikimate dehydrogenase using a Sephacryl 200 gel filtration column followed the same purification protocol as *S. coelicolor* DHQase see section 2.12.1.4. Detection of the appropriate fractions was performed using A_{280} measurements and enzyme assays (section 2.16.2). Fractions containing shikimate dehydrogenase activity were pooled and dialysed against 100 mM Tris-HCl, pH 7.5 containing 150 mM KCl (buffer E).

2.12.3.5 Step 5: Affinity chromatography on 2'5' ADP Sepharose

The dialysed enzyme was concentrated to 5 ml and applied to an ADP-Sepharose column (3 × 3.5 cm diameter) (Pharmacia Biotech) that had been pre-equilibrated in buffer E. The column was washed in buffer E until the A_{280} of the eluate was less than 0.1 (flow rate of 10 ml/hour; 4 ml fractions). A solution of 1 mM NADP⁺ in buffer E (flow rate of 1 ml/hour; 1 ml fractions) was then used to elute the shikimate dehydrogenase. The pooled fractions with shikimate dehydrogenase activity were concentrated to 5 ml. A sample of the concentrate was analysed by SDS-PAGE (section 2.11) to check the purity. The concentrated enzyme was dialysed into 100 mM Tris-HCl, pH 7.5 containing 50% (v/v) glycerol for 24 hours and stored at -20°C.

2.13 Protein estimation.

Protein concentrations were determined using the methods of Bradford (1976) and Lowry (1951) using BSA as a standard. Six standard points were used from dilutions of a 100 mg/ml BSA stock.

Protein concentration was also estimated using a JASCO (model V-550) spectrophotometer in a 1 ml, 1 cm path length quartz cuvette. Absorbance was measured at 280 nm. The absorbance of a protein at 280 nm depends on the content

of tryptophan, tyrosine residues and cystine disulphide bonds; the extinction coefficient at 280 nm was calculated by using the frequency of these chromophores in the protein (Pace *et al.*, 1995; Edelhoch, 1967). The sample protein concentration was calculated in terms of mg/ml.

2.14 Western blotting.

Following SDS-PAGE as described in section 2.11, proteins separated on a gel can be transferred to a positively charged polyvinylidene difluoride (PVDF) membrane (Matsudaira, 1987). The proteins can then be probed with specific antibodies.

The transfer of proteins on to the PVDF membrane (Hybond-P from Amersham) was performed in a Bio-Rad mini trans blot apparatus in which the gel and the membrane are sandwiched between foam and filter paper with the membrane closest to the anode (Figure 13). The filter paper (BioRad 1 mm) and foam were pre-soaked in transfer buffer (CAPS) (Appendix A) for 30 minutes. The PVDF membrane was pre-soaked first in 100% methanol for 50 seconds and then washed in distilled water for 30 minutes changing the distilled water every 10 minutes. Finally the membrane was pre-soaked in transfer buffer (CAPS) for 45 minutes. The gel was washed in transfer buffer (CAPS) for 30 minutes. All soaks and washes were conducted on a Stuart Scientific (model STR9) 3D rocking platform. The transfer components were arranged in a transfer sandwich shown in Figure 13. Air bubbles were removed by gently rolling a test tube over each layer. Cutting the corner of the PVDF membrane marked the orientation of the gel. Proteins were transferred onto the membrane at 60V for 90-120 minutes in transfer buffer (CAPS).

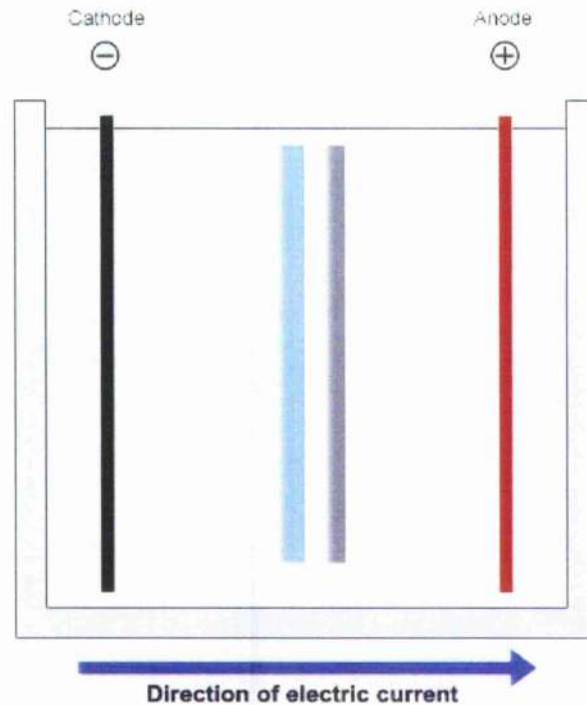


Figure 13. Schematic of western blot apparatus, the sponge and filter paper are shown in cream and light grey, respectively. The gel is represented in light blue and the PDVF membrane is in dark grey.

Once transfer was complete, the membrane was rinsed in distilled water for 10 minutes and then blocked in PBS (Appendix A) 0.1%(v/v) Tween-20 and 3%(w/v) Marvel for 45 minutes to prevent non-specific binding. The membrane was then incubated with primary antibody supplied by Dr. Craig Roberts at the University of Strathclyde (section 2.14.1) at a 1/500-1/2000 dilution in PBS 0.1%(v/v) Tween-20 and 3%(w/v) Marvel for at least 1 hour (usually overnight) on a Stuart Scientific (model STR9) 3D rocking platform. The membrane was then washed extensively in PBS 0.1%(v/v) Tween-20 for 45minutes with 3 buffer changes. The horseradish peroxidase (HRP)-conjugated secondary antibody (section 2.14.1) which is directed against the species of origin of the primary antibody was then applied at a 1/2500 dilution in PBS 0.1%(v/v) Tween-20 and 3%(w/v) Marvel for 45 minutes. The membrane was then washed in PBS 0.1%(v/v) Tween-20 for 15minutes with 3 changes of buffer.

Immunoreactive products were visualised using an electrochemiluminescence (ECL) detection kit (Pierce) using Super Signal[®] West Pico chemiluminescence substrate. Equal volumes of each ECL solution were mixed and then applied to the membrane for 1 minute. Konica medical film (18 × 24 cm) was exposed to the membrane inside an X-ray film cassette for 30-60 second exposure or until bands are visible. X-ray films were developed using a Kodak X-OMAT 2000 processor. This procedure was carried out in a dark room to minimise background film exposure

Membranes were stained with Coomassie brilliant blue to ensure transfer on to membrane after ECL visualisation. Gels were stained as in section 2.11.1. All steps were carried out at room temperature.

2.14.1 Preparation of Antibodies

Antibodies against *B. subtilis* type II dehydroquinase were supplied by Dr. Craig Roberts at the University of Strathclyde. Antibodies were raised by injecting 0.1 ml of *B. subtilis* F23Y dehydroquinase (YqhS) (0.5 mg/ml) in PBS buffer into 3 BALB/C mice and 3 C57BL6 mice. After a period of approximately 4 weeks, polyclonal antibodies termed IgG (immunoglobulin G) that react specifically with the introduced protein were harvested from the animal's serum.

Specific polyclonal antibodies against denatured *E. coli* type I dehydroquinase were raised in rabbits by A. Tikidilid (MSc project 1989). The *E. coli* type I dehydroquinase was denatured by reduction and carboxymethylation. Antiserum was raised in a New Zealand white rabbit. An initial immunisation of 400 µg of protein followed by a second (boost) after 6 weeks of 200 µg of protein. Polyclonal antibodies that react with denatured *E. coli* type I dehydroquinase were produced.

HRP-conjugated secondary antibodies for mice were donated by Dr. Craig Roberts and also supplied by Pierce Scientific. Pierce Scientific also supplied Immuno Pure[®] antibody goat-anti-rabbit IgG (H+L) HRP labelled. All antibodies were stored in 50 % (v/v) glycerol in 40 µl aliquots at -20°C.

2.15 Mass spectrometry

To identify a cellular protein by mass spectrometry it is necessary to separate the protein of interest from the complex protein mixture extracted from the cell. Two approaches are outlined below for the protein separation:

2.15.1 Two-dimensional electrophoresis (2-DE)

This technique sorts proteins according to two independent properties in two steps: The first-dimension step, isoelectric focusing (IEF), separates proteins according to their isoelectric points (pI); the second-dimension step, SDS PAGE separates proteins according to their molecular weight (2.11) (O'Farrell, 1975). Each spot corresponds to a single protein species in the sample. All 2-DE separations were performed in duplicate.

All electrophoresis equipment and reagents for 2-DE were supplied by Amersham Pharmacia Biotech Ltd unless otherwise stated. Frozen Bacterial cell pellets (approximately 200 µg of protein) were disrupted in 40 µl of lysis solution containing 8 M urea, 4% (w/v) CHAPS, 40 mM Tris (stored at -20°C) and subjected to 5 cycles of rapid freeze and thawing using liquid nitrogen and a Grant QBT2 heat block set at 25°C. Bacterial cells were further disrupted by five 1-minute cycles of sonication and incubation on ice a Decon model FS 100 water bath sonicator. Solubilisation was aided by subsequent addition of a rehydration buffer containing 8 M urea, 2% (w/v) CHAPS, 22 mM DDT, 0.5% (v/v) immobilisation pH gradient (IPG) buffer and a trace quantity of bromophenol blue, to a final sample volume of 125 µl. Insoluble material was removed by centrifugation at 16000 × g for 5 minutes at 20°C.

Proteins were separated in the first dimension using IPGphor™ isoelectric focusing system, employing a 7 cm immobilised pH 4-7 linear gradient immobilisation strip. The sample in rehydration buffer was loaded into a ceramic strip holder and the IPG strip was placed gel side down orientating the anodic end of the strip towards the pointed end of the strip holder. The IPG strip was covered with IPG cover fluid to minimise evaporation and placed on the electrode pads of the IPGphor™ system. The protocol for the isoelectric focusing was optimised by A. Foucher (University of Glasgow) and included a rehydration step of 15 hours at 20°C series and three voltage steps that gradually increased from 500 V to 6000 V over 18 hours. After the IPG strip had been treated for 15,000-20,000 voltage hours (Vh), the proteins focused on the IPG strip were equilibrated for the second dimension separation by soaking the strip in 10 ml of SDS equilibration buffer (50 mM Tris-HCl, 6M urea, 30% (v/v) glycerol, 2% SDS) containing 100mg DTT for 15 minutes. A second equilibration

was performed with equilibration buffer containing 250 mg of iodoacetamide instead of DTT for 15 minutes.

After equilibration, the proteins were separated in the second dimension by SDS PAGE (2.11). The equilibrated IPG strip was applied to a 15% acrylamide gel without a stacking gel and sealed using agarose sealing solution (SDS PAGE running buffer (Appendix A), 0.5% (w/v) agarose NA, trace quantity of bromophenol blue). After second dimension electrophoresis the duplicate 2-DE gels were analysed separately one Coomassie stained (2.11.1) and the other western blotted (2.14).

2.15.2 Immunoprecipitation

Using the Pierce Seize™ Classic (A) Immunoprecipitation kit, all reagents and disposable spin cartridge apparatus were supplied within the kit.

Frozen Bacterial cell pellets (3 ml of culture grown for 48 hours and then centrifuged at $16,000 \times g$ for 4 minutes at 20°C) were disrupted by sonication in 200 μl of Tris-HCl (pH 7.5) and subjected to 5 cycles of rapid freeze and thawing using liquid nitrogen and a Grant QBT2 heat block at 25°C . Bacterial cells were further disrupted by five 1-minute cycles of sonication and incubation on ice using a Decon model FS 100 water bath sonicator. Disrupted cells were centrifuged for 5 minutes at $16,000 \times g$ to remove cell debris. The supernatant was incubated with approximately 1.5 mg/ml of antibody (2.14.1) for 1 hour at 20°C on a Stuart Scientific (model STR9) 3D rocking platform. 0.4 ml of ImmunoPure® Plus Immobilized Protein A (50% slurry) was equilibrated with 3 washes of BupH™ binding/wash buffer (0.14 M NaCl, 8 mM Na_2PO_4 , 2 mM potassium phosphate, 10 mM KCl pH 7.4). All washes were performed in a spin X cup and centrifuged at $16,000 \times g$. The immune complex (antibody and cell lysate) was added to the equilibrated immobilized Protein A and incubated for 30 minutes at 20°C on a rocking platform. The spin X cup containing the immune complex and protein A was washed 3 times with Binding/wash buffer and then eluted with 190 μl of ImmunoPure® Elution buffer (pH 2.8) containing primary amine, the elution step was repeated two further times. Both the washes and the eluants were analysed by SDS PAGE (2.11).

Preliminary experiments with the Seize™ X Protein A immunoprecipitation kit were performed using a similar method to the Seize™ Classic (A) immunoprecipitation kit.

In this method antibodies were cross-linked to the immobilized Protein A overcoming the problem of antibody contamination in the eluant.

2.15.3 Protein Digests

After 2-DE (2.15.1) or immunoprecipitation (2.15.2) separated proteins of interest were recovered from SDS PAGE, for *in situ* proteolytic digestion (Hellman *et al.*, 1995). Proteins were excised from a destained polyacrylamide gel (1 mm × 1 mm square) and washed for 1 hour in 500 µl of 100 mM ammonium bicarbonate. The wash was discarded and the gel fragment was washed in 50% (v/v) acetonitrile, 100 mM ammonium bicarbonate for 1 hour. The wash was discarded and the gel fragment was shrunk in 50 µl of 100% acetonitrile for 10 minutes. The solvent was removed and the gel fragment was dried in a fume hood for 25 minutes at 20°C. Proteolytic digestion was performed using 0.2 µg of sequencing grade modified trypsin (Promega) in 30 µl of 20 mM ammonium bicarbonate and the solution was incubated for 16 hours at 37°C shaking at 200 rpm using a Grant OLS 200 shaker/water bath. Digested protein samples were then either stored at -20°C or analysed directly using mass spectrometry.

2.15.4 MALDI-tof and electrospray mass spectrometry

Protein masses were determined using a QStar Pulsar mass spectrometer running AnalystQS software (Applied Biosystems) fitted with a Protana nanospray source (Protana) or an API 3000 Triple Quadrupole instrument. Buffers salts were first removed from the sample on a C18 ZipTip (Millipore) (before use ZipTips were conditioned by washing three times with each of the following: (1) 10 µl of acetonitrile in 0.5% formic acid, (2) 50% acetonitrile in 0.5% formic acid and finally (3) 0.5% formic acid). Protein samples were absorbed on to the tip by repeated pipetting of the solution. The pH of the adsorbed proteins was approximately pH 3.5 due to the formic acid. The samples were then desalted by extensive washing with 0.5% formic acid (at least 10 x 10 µl). Proteins were then eluted from the tip with 2-3 µl of 50% acetonitrile in 0.5% formic acid and loaded immediately into the nanospray tip (Protana). Samples for electrospray ionisation (ESI) were spotted on to a gold plate for ionisation and left to dry for 30 minutes. Key parameter settings were for the QStar Pulsar: spray voltage 1000V, curtain gas 25, declustering potential 85, and pulsar settings of 5 and 6 for IRD and IRW respectively. Data were collected from

400-2000 m/z using settings optimised for horse heart myoglobin, and deconvoluted to zero charge using the BioAnalyst software. Deconvolution was performed using a step mass of 0.5 Da running 20 iterations. Mass accuracies were estimated at +/- 0.01%.

2.16 Enzyme assays

All assays were carried out at 25°C in a 1 ml quartz cuvette, 1 cm path length on a Jasco V-550 dual beam spectrophotometer unless otherwise stated.

2.16.1 Type II dehydroquinase assay

Type II dehydroquinase activity was determined by monitoring the formation of dehydroshikimate at 234 nm ($\epsilon = 12 \times 10^3 \text{ M}^{-1} \text{ cm}^{-1}$) (Salamon and Davis, 1953; Mitsunashi and Davis, 1954; White *et al.*, 1990). Assays were performed using 50 mM Tris-acetate buffer, pH 7.0 in a total volume of 1 ml. Reactions were initiated by the addition of enzyme (0.015 μg , 0.5 μg , 3 μg and 34 μg of SCDHase, MTDHase, HPDHase, and *B. subtilis* YqhS (F23Y) respectively). Kinetic parameters were determined by varying the substrate (3-dehydroquinate) concentration over an appropriate range (between 10 μM and 2 mM).

2.16.2 Shikimate dehydrogenase assays

Shikimate dehydrogenase and shikimate dehydrogenase related protein (YdiB) activity was measured by following the conversion of NADP⁺ to NADPH or NAD⁺ to NADH at 340 nm ($\epsilon = 6.18 \times 10^3 \text{ M}^{-1} \text{ cm}^{-1}$) (Chaudhuri and Coggins, 1985) during the either the oxidation of either shikimate to dehydroshikimate (reverse direction of the shikimate pathway) or quinate to dehydroquinate (forward direction of the quinate pathway). Assays were performed using 100 mM Glycine NaOH buffer, (pH 10) in a total volume of 1 ml. Reactions were initiated by the addition of enzyme (0.1 μg and 1.0 μg of *H. influenzae* shikimate dehydrogenase and YdiB protein, respectively). Each substrate of the reaction (NADP⁺ or NAD⁺ and either shikimate or quinate) was varied in turn over an appropriate range. The ranges were between 25 μM and 60 mM for shikimate, between 10 mM and 200 mM quinate, 25 μM and 1.5 mM NADP and between 2.5 mM and 20 mM for NAD keeping the concentration of the other substrate constant.

2.17 Preparation of substrates

2.17.1 3-dehydroquinate

3-dehydroquinate was gifted by Prof. John Coggins from a batch prepared in 1991 using the method of Grewe and Haendler (1966). The principle of the method is to oxidise quinic acid with nitric acid and then crystallise dehydroquinate as an ammonium salt. The substrate may be purified using ion exchange resin. Substrate prepared by this method proved unsatisfactory for studying enzymes with low activity for two reasons: - (i) there was high background absorption at 234 nm and (ii) both the 5- and the 3- forms of dehydroquinate are produced. It is thought that 5-dehydroquinate could have an inhibitory effect on dehydroquinases. The dehydroquinate also proved difficult to handle as it forms a sticky solid.

An alternative preparation was performed by Lorna Noble via a multi-stage chemical synthesis (Evans *et al.*, 2002). This yielded extremely pure DHQate which in solution had a very low A_{234} and which was stable for at least one hour at 25°C. 2 and 20 mM stocks of substrate were kept at -20°C; once defrosted stocks were kept for up to four weeks at 4°C.

The concentration of solutions of substrate were determined on the basis of the limiting change in absorbance at 234nm, on addition of 1 µg of SCDIIQase, taking into account the equilibrium constant for the reaction which is 15 (Kleanthous *et al.*, 1991).

2.17.2 Substrates for shikimate dehydrogenase assays

Substrates for the shikimate dehydrogenase assays were bought from Sigma and Boehringer Mannheim.

2.18 Analysis of kinetic data

The values K_m and V_{max} were obtained by performing a non-linear regression plot, fitting the change in absorbance per minute (ΔA_{min}^{-1}) against a range of substrate concentrations ([S]) to the Michaelis-Menten equation (1913) using Microcal Origin software version 5.0. Values of k_{cat} were calculated from the V_{max} data by dividing by the enzyme concentration. For inhibition studies Lineweaver-Burk (Lineweaver and Burk, 1934) plots were drawn in which the inverse of ΔA_{min}^{-1} ($1/v$) was plotted

against the inverse [S] ($1/[S]$) which gives a straight line with an intercept at the x-axis equal to $-1/K_m$ and an intercept on the y-axis equal to $1/V_{max}$.

$$v = \frac{V_{max}[S]}{K_m + [S]}$$

(Michaelis-Menten equation)

$$\frac{1}{v} = \frac{K_m}{[S]} \cdot \frac{1}{V_{max}} + \frac{1}{V_{max}}$$

(Lineweaver-Burk transformation of Michaelis-Menten equation)

Two substrate reactions are more complex and are categorised depending on the order in which the enzyme substrate complexes are formed. SDHase is thought to involve a ternary complex where the enzyme binds to both substrates before the products are formed. The initial rate (v) of the reaction is calculated from the equation:

$$v = \frac{V_{max}[A][B]}{K'_A K_B + K_D[A] + K_A[B] + [A][B]}$$

(Ternary complex mechanism equation Huang, (1979))

Values of 16.5, 18.0, 20.6 and 16 kDa were used for the subunit molecular masses of SCDHase, MIDHase, HPDHase, and (F23Y) BSDHase respectively. Using a his-tag purification system David Robinson purified the HPDHase and the MIDHase the his-tag is included in the molecular weight calculations. The kinetic parameters of these enzymes were very similar to those previously reported for the corresponding native enzymes (Bottomley *et al.*, 1996a).

The subunit molecular masses for *H. influenzae* SHDase and YdiB are 29.76 and 29.9kDa respectively.

2.19 Stopped Flow assays

Pre-steady state kinetics of *S. coelicolor* DHase, *H. pylori* DHase and *B. subtilis* YqhS (F23Y) were measured by stopped flow using an Applied Photophysics stopped flow reaction analyser. Absorbance at 234nm was measured with a path length of the observation chamber 2 mm. These measurements were carried out at room temperature (20°C) the two syringes (A and B) are mixed in less than 2

milliseconds with a mixing ratio of 1:10 respectively. Syringe A was filled with a known dilution of enzyme, syringe B was filled with the appropriate buffer and substrate typically 50 mM Tris-acetate, pH 7.0 and 1 mM 3-dehydroquinase.

2.20 Denaturation experiments on Type II dehydroquinases

The stability of proteins was studied using denaturation reagents. 0.1-0.5 mg/ml protein samples were incubated for between 1-24 hours at 20°C with either the denaturant guanidine hydrochloride (GdmCl) or urea at a range of concentrations (0.25-8 M GdmCl and 0.5-4 M urea). Concentration of denaturant was determined using refractive index measurements (Nozaki, 1972; Pace 1986).

2.21 Fluorescence spectroscopy

Changes in the quantum yields and emission maxima of intrinsic fluorescence can be used to monitor conformational changes in protein structure and their interaction with ligands.

When a molecule is exposed to electromagnetic radiation it is transformed from a 'ground' state to an 'excited' state. The energy of the absorbed photon of light corresponds to the energy difference between these two states. The molecule can return to its 'ground' state by the emission of a photon of light which corresponds to the energy difference of the 'excited' state this emission is known as fluorescence (Szabo, 2000).

Fluorescence scans were carried out during denaturation of proteins and ligand binding experiments. The fluorimeter was set up to selectively excite either tryptophan or tyrosine residues at a wavelength of 290 nm or 280 nm, respectively. Emission was monitored either between 340 and 350 nm if the tryptophan was solvent exposed or between 308 and 340 nm if the tryptophan was buried in the interior of a native protein (Eftink and Shastry, 1997). The tyrosine emission signal is much weaker and therefore the environment of the tyrosine residues is more difficult to analyse. Fluorescence measurements were made at 20°C with 1 cm path length cell with a 1 ml volume and with the slits set at 5.0 nm bandpass using a Perkin-Elmer LS50B spectrofluorimeter.

2.22 Circular dichroism

Circular dichroism (CD) measures the difference in absorption of left and right circularly polarised radiation. Plane-polarised light is split into two components by subjecting the radiation to an alternating (50 kHz) electric field using a modulator containing a piezoelectric quartz crystal tightly coupled to a thin quartz plate. When left and right circularly polarised light passes through a protein sample the chirality of secondary and tertiary structures of the protein results in one of the components of the circular polarised light being absorbed to a greater extent than the other resulting in elliptically polarised light. CD data are presented as ellipticity in degrees (θ).

In the far UV region (240-190 nm), which corresponds to absorption of peptide bonds, spectra can be analysed to give an indication of secondary structure content. The CD spectrum in the near UV region (320-260 nm) reflects the environments of the aromatic amino acids and thus gives information about the tertiary structure of the protein, it can also give information about disulphide bonds and non-protein cofactors which might absorb in this spectral region (Kelly and Price, 2000; Kuwajima, 1995).

CD spectra were recorded at 20°C on a JASCO J-600 spectropolarimeter at protein concentrations ranging from 0.5 to 1.5 mg/ml in 100 mM potassium phosphate buffer (pH 7.0). All spectra were recorded in at a path length of either 0.02 cm (near UVCD) or 0.5 cm (far UVCD). All spectra were recorded by Dr. S. Kelly (University of Glasgow). The spectra were analysed for secondary structure content using SELCON (Sreerama and Woody, 1994a; 1994b).

2.23 Dynamic light scattering

Dynamic light scattering can be used to analyse single species protein solutions to determine quaternary structure and the effect of different metal ions, pH or salt concentrations on the aggregation states. If the molecular weight of the protein is known, predictions about the shape and density of the protein can be made by taking into account that the predicted mass from light scattering relies on the assumption that the protein in question is spherical and has an average protein density.

When a polarised light beam from a monochromatic laser passes through a solution it interacts with the particles and causes the electron distribution to oscillate. This oscillation results in the scattering of light of the same wavelength as the incident

beam. When the diameter of the particles is significantly less than the incident beam this type of scattering is termed Rayleigh scattering. However, macromolecules in solution are subject to Brownian motion and this can cause fluctuations in the scattered light intensity. When measuring static light scattering on a second time-scale the information about the fluctuations is lost as they are averaged. These fluctuations result in a deviation from Rayleigh scattering, which can be used to calculate the diffusion coefficient. It is possible to measure these fluctuations using a highly sensitive detector, which measures on a microsecond time-scale, this is termed dynamic light scattering (Santos *et al.*, 1996). A DynoPro™ system was used to measure dynamic scattering samples of 200 µl with a protein concentration between of between 0.5-2.5 mg/ml of protein were injected into the observation chamber (20°C). From the diffusion coefficient, the hydrodynamic radius can be calculated using the Stokes-Einstein equation (Santos *et al.*, 1996):

$$D = \frac{kT}{6\pi\eta R}$$

(Stokes-Einstein equation)

Where D is the diffusion coefficient, k is the Boltzmann constant, T is the temperature, η is the solvent viscosity and R is the hydrodynamic radius.

Using the radius of gyration the mass of the protein can be estimated assuming that the protein is spherical and of an average protein density.

2.24 Protein Crystallisation

Protein crystals were grown using the sitting drop vapour diffusion method. Using a Crystchem™ 24 well plate (Hampton Research) a sparse matrix screen was set up. Sparse matrix screens cover a wide range of crystallisation conditions, varying the precipitant, buffer and additives over a series of concentrations and types of precipitant and additives; and pH levels.

A 2 µl drop composed of 1 µl of 10-20 mg/ml protein solution (>95% purity, section 2.12) and 1 µl of crystallisation reagent from the sparse matrix screen is placed in the concave depression on a raised post; 0.8 ml of the same crystallisation reagent is placed in the reservoir. The drop contains a lower crystallisation reagent concentration than the reservoir. The wells are then sealed with Crystal Clear Sealing

Tape (Hampton Research). The Crystallisation screen is left at 20°C for an indefinite amount of time screening for crystal growth intermittently using an Olympus microscope model S240. Pictures were taken of the crystals using a JVC TK-1280E colour video camera.

The formation of crystals depends on the solubility of the protein solution which can be manipulated using a precipitant. It is necessary for the protein to be supersaturated to form crystals, this is achieved by the equilibration between the protein solution and crystallisation reagent. To achieve equilibrium, water vapour leaves the drop and eventually ends up in the reservoir. As water leaves the drop, the sample undergoes an increase in relative supersaturation (McPherson, 1989).

Once a condition is found that produces crystals it can be optimised to produce larger crystals, which maybe easier to handle and yield better results from X-ray diffraction.

Protein crystals were tested by X-ray diffraction at the Daresbury synchrotron on Beam Line 9/6 by B. Lohkamp and A. McEwen.

CHAPTER 3 SITE-DIRECTED MUTAGENESIS OF *S. COELICOLOR* TYPE II DEHYDROQUINASE.

3.1 Introduction

The type II dehydroquinase from *S. coelicolor* was first purified by White *et al* (1990); this was the first micro-organism to be found to possess a biosynthetic type II dehydroquinase rather than a type I. The differences between the two types of enzyme are discussed in detail in section 1.3. It is well known that the catalytic mechanism of type I dehydroquinase involves the formation of a Schiff base between the substrate and the active site lysine 170 (*Salmonella typhi* numbering of amino acids) (Chaudhuri *et al.*, 1991). This is not the case in type II dehydroquinases which do not have a conserved lysine and in which no imine intermediate can be demonstrated by borohydride trapping experiments (Kleanthous *et al.*, 1992). The stereochemistry also differs between the two types, type I enzymes catalyse a *syn* elimination of water with the loss of the *pro-R* hydrogen from C-2, whereas type II enzymes catalyse an *anti* elimination reaction with the loss of the more acidic axial *pro-S* hydrogen from C-2. To demonstrate this, ¹H NMR experiments were performed using dehydroquinone labelled in either the C-2 *pro-R* or *pro-S* positions with deuterium and used as the substrate for both type I and II dehydroquinase (Shneier *et al*, 1993). Type II enzymes are thought to proceed via an enolate intermediate (Harris *et al*, 1996a). Studies with (6*S*)/(6*R*)-6-fluoro-3-dehydroquinone and *E. coli* type I dehydroquinase also revealed an imine intermediate by ¹⁹F NMR (Parker *et al*, 2000). Understanding the catalytic mechanism and the differences in the mechanism between the two mechanistically and structurally distinct forms of dehydroquinase is important for the development of novel selective therapeutic agents.

3.1.1 The active site and proposed catalytic mechanism

The identification of an essential hyper-reactive arginine residue (Arg23 in *S. coelicolor*) using the arginine-specific reagent phenylglyoxal (PGO) in conjunction with electrospray mass spectrometry led to the identification of the active site of type II dehydroquinase (Krell *et al.*, 1995 and 1996). Three site-directed mutants of Arg23 were constructed; R23K, R23Q and R23A. All three mutants had significantly lower k_{cat} with R23A being 30,000 times less active than the wild-type enzyme.

Arg23 was attributed to a role in substrate recognition as well as a possible catalytic role. Chemical modification with tetranitromethane (TNM) also identified Tyr28 as being at or close to the active site (Krell *et al.*, 1995).

The 3-D X-ray crystal structures of *M. tuberculosis* (Gourley *et al.*, 1999), *S. coelicolor* and mutant *S. coelicolor* R23A dehydroquinases (Roszak *et al.*, 2002) confirmed the location of the active site. The SCDHQase R23A structure was solved with dehydroshikimate bound within the active site. The active site is located in the cleft formed at the carboxy edge of the β sheet between strands $\beta 1$ and $\beta 3$ (Figure 14). The active site is partially covered by helix $\alpha 3$ from the neighbouring subunit forming a salt bridge between Arg117 and Asp92* (*S. coelicolor* numbering of amino acids with residues from a neighbouring subunit denoted with an asterisk). This intersubunit salt bridge maintains the orientation of a flexible loop that forms a lid domain (residues 21-31) over the active site (Price *et al.*, 1999), which includes residues Arg23 and Tyr28. In addition residues Gly21 and Asp31 show a significant hinged movement resulting in a difference of over 5 Å between apo and complexed structures of the *S. coelicolor* enzyme (Roszak *et al.*, 2002).

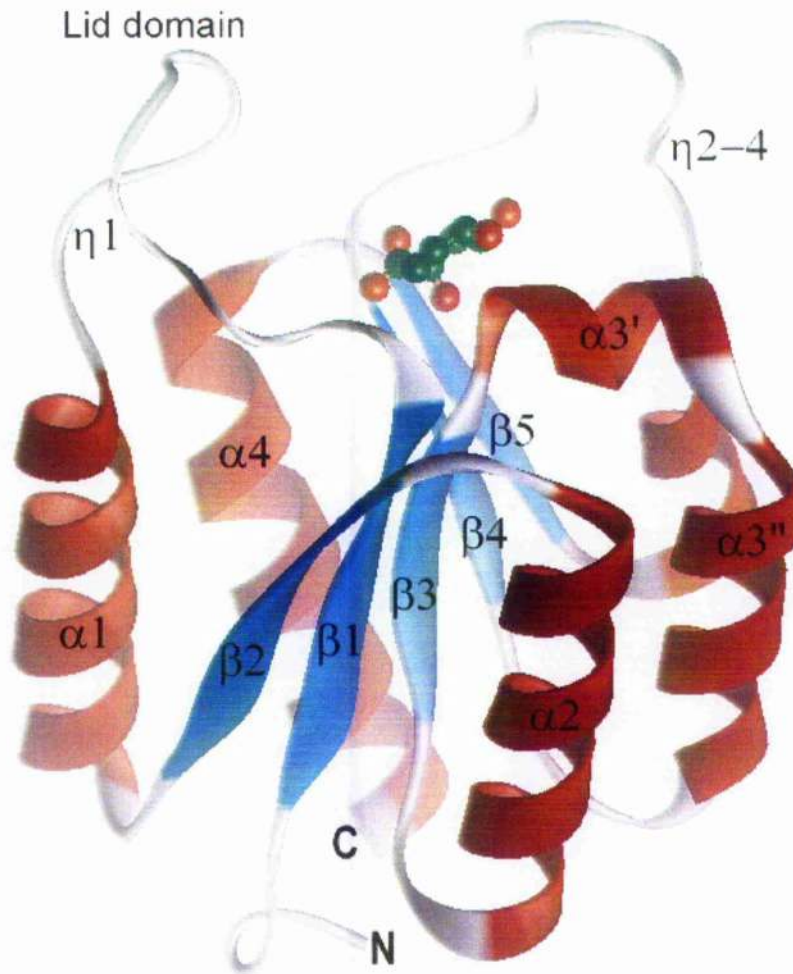


Figure 14. Solid ribbon representation of the X-ray structure of *S. coelicolor* type II dehydroquinase. α helix (red) are labelled $\alpha 1$ - $\alpha 4$ and β strands (blue) labelled $\beta 1$ - $\beta 5$ and 3_{10} helices are labelled $\eta 1$ -4. The ligand 2,3-anhydroquinic acid is shown as a ball and stick representation to highlight the location of the active site.

The proposed catalytic mechanism for type II dehydroquinase utilises a stepwise E_1CB (elimination unimolar via conjugate base) mechanism proposed to involve an enolate intermediate. This was first suggested by substrate and solvent isotope studies, where the proton abstraction was shown to be rate limiting for *M. tuberculosis* and *A. nidulans* type II dehydroquinase (Harris *et al.*, 1996b).

Analysis of the crystal structure of *S.coelicolor* dehydroquinase with various ligands bound in the active site, such as phosphate, transition state analogue 2,3-anhydro-

quinic acid and dehydroshikimate (R23A mutant SCDHQase) revealed that the carboxylate group of the substrate is bound to the main chain of Ser108 and Ile107. The phosphate ion, which is a competitive inhibitor of SCDHQase, mimics the carboxylate group. The hydroxyl of Ser108 also binds to the C1 carboxylate of dehydroquininate (Roszak *et al.*, 2002; Evans *et al.*, 2002 and section 5.4.5).

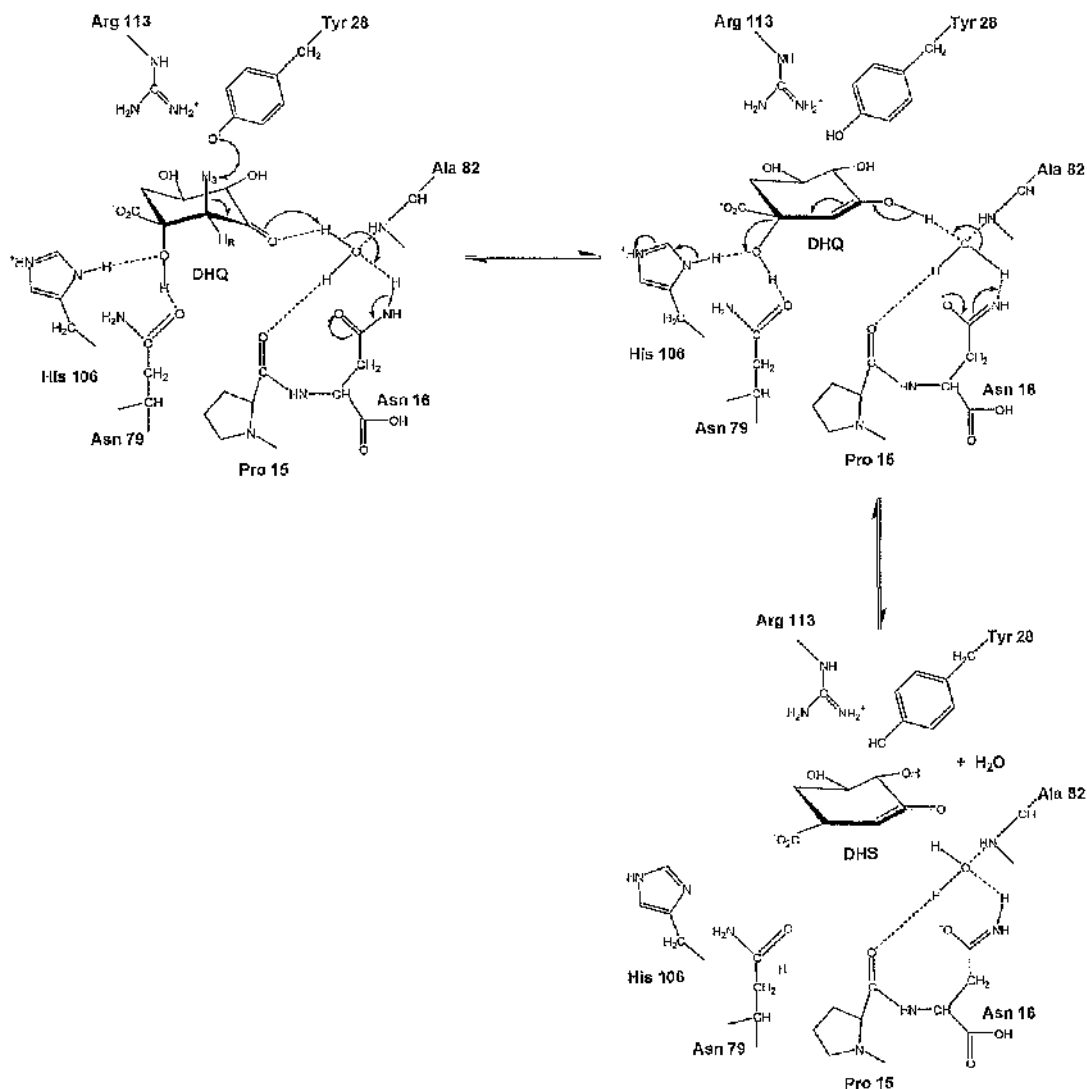


Figure 15. Schematic representation of the proposed mechanism of *S. coelicolor* type II dehydroquinase.

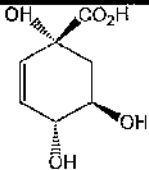
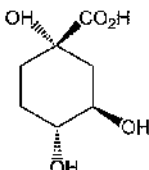
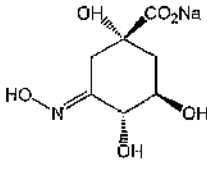
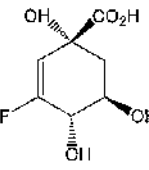
The substrate and solvent isotope effects show that proton abstraction is partially rate limiting and occurs at or before the highest transition state (Harris *et al.*, 1996b). Abstraction of the more acid axial *pro S* hydrogen from C2 of dehydroquininate by the side chain of Tyr28 is thought to be the first step in the mechanism. Since the

hydroxyl group of free tyrosine has a pK_a of 10.0, it would be expected that the tyrosine residue would be fully protonated at pH 7.0. It is thought that the pK_a of the tyrosine is shifted by the proximity of Arg113 and perhaps to a lesser extent by Arg23 (Figure 15). This environmental shift of the pK_a of a tyrosine residue has been observed in human aldose reductase (Tarle *et al.*, 1993) where a neighbouring lysine residue forms a hydrogen bond to the tyrosine thought to be involved in proton abstraction. A similar interaction with two lysine residues is thought to alter the environment of the active site in Class C β -lactamase from *Citrobacter freundii* lowering the pK_a of a tyrosine residue (Oefner *et al.*, 1990). The side chains of Tyr28 and Arg113 in SCDHQase are thought to be orientated by the side chain of Ser108. It is proposed that the transition state produced by the abstraction of the *pro S* hydrogen will lead to a double bond being formed between C2 and C3 presumably forming an enolate intermediate (Figure 15). The intermediate is characterized by a flattening of the carbocyclic ring and is likely to involve stronger hydrogen bonding to the enolate oxygen in the transition state. However, the absence of a positively charged amino acid to interact with the oxygen at C3 makes an enolate intermediate unlikely. A conserved water molecule (present in all *S. coelicolor* enzyme-ligand X-ray structures) is positioned to form an enol intermediate. The water molecule is held in a specific orientation 2.8 Å away from the carbonyl of dehydroshikimate by invariant residues Asn16 and the carbonyl of Pro15 and the main chain amide of Ala82. The next step is the elimination of the hydroxyl group at C1 with His106 acting as a proton donor (Figure 15). The side chain of Asn79 orientates the hydroxyl group at C1 to accept the proton.

It was originally thought that the His106 formed a His-Glu pair with the invariant residue Glu104 and could act as base in the removal of the *pro S* hydrogen at C2 of the substrate (Gourley *et al.*, 1999). But crystallographic studies on SCDHQase in complex with 2,3-anhydro-quinic acid show that His106 interacts with the C1 hydroxyl of the substrate and does not have a role in proton abstraction (Roszak *et al.*, 2002).

The release of the products (dehydroshikimate and water) is probably triggered by the fact that the active site is not large enough for both to occupy the cavity: on removal of the hydroxyl from C1, the intermediate undergoes a structural change and becomes planar as the product dehydroshikimate is formed.

Table 5. K_i values (μM) for inhibitors against type I and II dehydroquinases from Frederickson *et al.* (1999 and 2002)

	<i>S. typhimurium</i>	<i>A. nidulans</i>	<i>M. tuberculosis</i>	<i>S. coelicolor</i>
	type I DHQase	type II DHQase	type II DIIQase	type II DHQase
	(K_i μM)			
 2,3-anhydroquinic acid	3000 ± 1000	60 ± 10	200 ± 20	30 ± 10
 3-deoxyquinic acid	4500 ± 500	1500 ± 200	1200 ± 200	600 ± 200
 Oxime	> 25000	15 ± 1	20 ± 2	500 ± 0.2
 Vinyl fluoride	1500 ± 500	50 ± 5	10 ± 2	15 ± 2

Inhibitors of type II dehydroquinase were designed exploiting the two key differences between type I and II dehydroquinases: the stereochemistry of the initial elimination of the proton at C2 and the formation of different intermediates (Frederickson *et al.*, 1999). 2,3-anhydroquinic acid and 3-deoxyquinic acid were synthesized; they are both structurally similar to the substrate but lack the C3 carbonyl group needed to

form the imine intermediate formed in type I dehydroquinases. 2,3-anhydro quinic acid possesses a double bond between C2 and C3 and thus acts as a mimic for the planar ring of the transition-state. An oxime was synthesized exploiting the carboxylate-binding pocket with the aim of decrease the K_i of the inhibitor. Recent studies by Frederickson (2002) have developed a vinyl fluoride that closely mimics the geometric and electronic features of the transition-state. These compounds were tested on both type I and II dehydroquinases with the results summarised in Table 5.

3.1.2 Site-directed mutagenesis as a tool

Substitution of amino acids by site-directed mutagenesis is a powerful tool in testing hypotheses in regard to the importance of a particular residue in catalysis. 3-D structures of type II dehydroquinase were used to select amino acid residues to be replaced.

The first site-directed mutagenesis strategy that was adopted was developed by Higuchi (1988), outlined in section 2.6.3.1. Unfortunately this method proved to be time consuming, as it required the optimisation of three PCRs for each mutation. The fragments in the first stage that were generated were very small and thus difficult to process. The fact that two rounds of PCR were necessary to produce the desired mutation within the gene meant that there was more chance of introducing unwanted mismatches. The high G + C content of the *S. coelicolor* genome (Wright and Bibb, 1992) made the optimisation of these PCRs more difficult (for example, the G+C content of the *S. coelicolor aroQ* gene is 70%). Dimethyl sulphoxide (DMSO) has been shown to increase the level of amplification of PCRs; it is thought that DMSO enhances PCR by hydrogen bonding to the major and minor grooves of the template DNA and destabilising the double helix (Pomp and Medrano, 1991; Chakrabarti and Schutt, 2002). DMSO was used as an additive in the site-directed mutagenesis PCRs of the G+C rich *aroQ*; other additives such as glycerol were also tested, but was found to be less potent.

The second site-directed mutagenesis strategy was the Stratagene® QuikChange™ site-directed mutagenesis kit (2.6.3.2). This strategy had many advantages over the two-stage PCR strategy including the replication of the whole vector with the desired mutation in one round of PCR and the direct transformation of the PCR DNA into *E. coli* without a ligation step. The Stratagene® procedure also used *Pfu* turbo DNA

polymerase that has 2-fold higher fidelity in DNA synthesis than *Vent* polymerase (Cline *et al.*, 1996). The Invitrogen® ExSite™ mutagenesis kit was also tested but was not successfully used.

3.1.3 Target residues for site-directed mutagenesis

The residues chosen for site directed mutagenesis were Glu104, His106, Arg113, and Ser108 and were all mutated to alanine; Tyr28 was mutated to phenylalanine. These residues are highly conserved across the type II dehydroquinase family (Appendix C: **Error! Reference source not found.**). Alanine was chosen for the first four mutations, as its small side chain would not be expected to disrupt the tertiary structure. In addition, the methyl group of the alanine residue would also not be able to perform the same function as the residues that being were replaced.

Phenylalanine was chosen to replace Tyr28, as it lacks the hydroxyl group in the aromatic ring and thus would not be able to act as a proton donor or acceptor in the catalytic mechanism. Phenylalanine was also chosen as sequence alignments had already revealed the *B. subtilis* YqhS (that shows 47% identity to *S. coelicolor* DHQase) possessed a phenylalanine in this position (4.1).

As previously described in section 3.1.1 Arg113 is believed to alter the environment of Tyr28 and lower pK_a of this residue. Thus exchanging this residue for an alanine should affect the pK_a of the tyrosine and reduce the k_{cat} of the enzyme. The role of the invariant Glu104 in the catalytic mechanism is not established; originally it had been thought to be involved in abstraction of the *pro S* proton of dehydroquinone and hence, it was mutated to establish whether the residue was directly involved in catalysis or played a structural role. The mutation of His106 was designed to establish its importance in the catalytic mechanism as a possible proton donor to the hydroxyl at C1 of dehydroquinone. Ser108 is thought to be involved in substrate recognition and orientation by binding to the carboxylate group at C1 of dehydroquinone. Hence substituting this residue should lead to an increase in the K_m of the enzyme.

3.2 Construction and over-expression of site-directed mutants. of *S. coelicolor* type II dehydroquinase.

A two-stage site directed mutagenesis strategy was followed for the H106A mutation of *S. coelicolor* type II DHQase as outlined in section 2.6.3.1, using a construct of pT7.7 with *S. coelicolor aroQ* inserted into the multiple cloning site between the *Nde*I and *Hind* III, (gifted by Prof. Iain Hunter, Strathclyde University) as the template for the amplification. The four primers for the procedure were as follows:

P1 5'GATATACATATGCCCCGCAGCCTGGC 3'

P2 5'CGTC'IGCAGAAGC'TTC'IGCACAGGAAC 3'

P3 5'GTGGTGGAGGTCGCCATCTCCACCATCCAC 3'

P4 5'ATGTTGGAGATGGCGACCTCCACCACCGG 3'

The mutagenesis primers (P3+4) were designed with the desired codon change (shown in bold) to allow the substitution of the histidine by an alanine. The first step generated two fragments of *aroQ* cDNA, the first fragment was 257 bp (P1+4) and the second was 342 bp (P2+3). The PCR reaction for the P2 + P3 fragment contained ≈ 3 ng of template DNA, 50 pmol of both primers, 0.2 mM of each dNTPs, 2 units Vent_R[®] polymerase (NEB), 1:10 dilution of 10 \times ThermoPol reaction buffer (10mM KCl, 10mM ammonium sulphate, 20mM Tris-HCl pH 8.8, 2 mM MgSO₄ and 0.1% (v/v) Triton X-100) an additional 1 μ l of 0.5 mM MgSO₄ and 10% (v/v) DMSO in a total volume of 50 μ l made up with sterilised water. The P1 + P4 PCR reaction was the same apart from the addition of MgSO₄ to a final concentration of 80 μ M.

The BioRad Gene Cycler program included 3 elements: a hot start at 94°C for 5 minutes, 35 cycles of amplification consisting of an annealing temperature of 68°C for one minute, an extension period of 1 minute at 72°C and a denaturation step of 94°C for 1 minute followed by a segment of annealing for 1 minute and elongation for 4 minutes. 5 μ l of the PCR product was separated and analysed by agarose gel electrophoresis using XIV DNA marker (Roche) and EZ Load 100 bp Molecular

Ruler (BioRad) (Figure 16). Fragments of the appropriate size were purified by extraction from the gel (2.7.4).

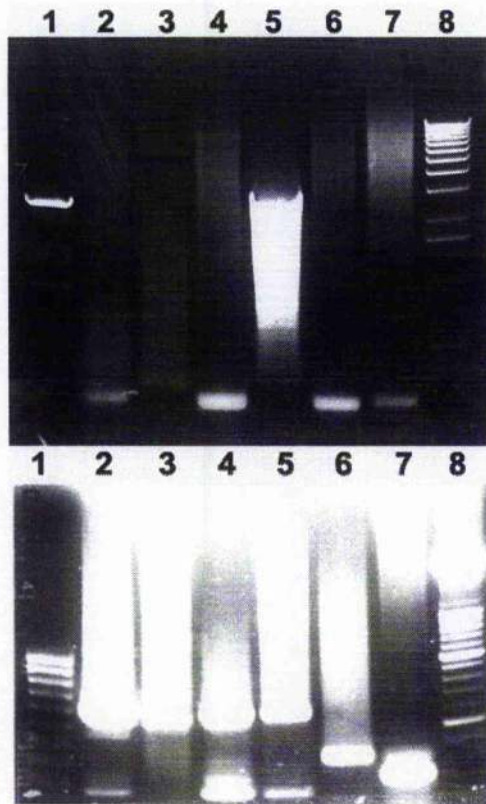


Figure 16. 1% DNA agarose gels of pT7.7 *S. coelicolor aroQ* construct, two-stage site-directed mutagenesis (H106A), first round of PCR. (A) Lane 1: XIV DNA marker (Roche), lanes 2-7: PCR fragment P1 + P4, lane 8: DNA molecular weight marker X (Roche). (B) Lane 1: EZ Load 100 bp Molecular Ruler (BioRad), lanes 2-3: PCR fragment P2 + P3, lane 8: XIV DNA marker (Roche). (5 μ l of PCR product).

The two fragments of PCR product (P1 + P4 and P2 + P3) were used as the template for the second stage of PCR. The second stage PCR reaction contained ≈ 5 ng of both of the fragments from the first stage, 50 pmol of both external primers (P1+2), 0.2 mM of each dNTP, 10% (v/v) DMSO, 2 enzyme units Vent_R[®] polymerase, 1 \times ThermoPol reaction buffer with an additional 1 μ l of 0.25mM MgSO₄ in a total volume of 50 μ l made up with sterilised water. The BioRad Gene Cyclor program included 3 elements: a hot start at 94°C for 5 minutes, 30 cycles of amplification consisting of an annealing temperature of 64°C for one minute, an extension period

of 1 minute at 72°C and a denaturation step of 94°C for one minute followed by a final step of annealing for 1 minute and elongation for 5 minutes. 4 µl of the PCR product was separated and analysed by agarose gel electrophoresis using DNA Marker X and XIV (Roche) (Figure 17).

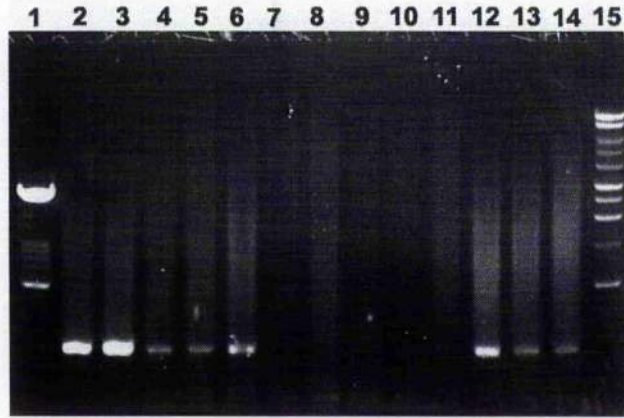


Figure 17. 1% DNA agarose gels of pT7.7 *S. coelicolor aroQ* construct, two-stage site-directed mutagenesis (H106A), second round of PCR. Lane 1: XIV DNA marker (Roche), lanes 2-14: fused PCR fragments, lane 15: DNA Marker X (Roche), (4 µl of PCR product).

Mutated *aroQ* H106A was ligated into cloning vector pGEM[®]-5Zf(+/-) using the *EcoR* V restriction site. Both pGEM-5 plasmid and the PCR product were digested in a reaction containing 45 µl of the PCR product or 15 µg plasmid DNA, 6 units of *EcoR* V (NEB) with 1×digestion buffer 2 (NEB). The digestion reaction was incubated at 37°C for 3 hours and purified by gel electrophoresis before being used in the ligation reaction (2.7.5). The ligation reaction consisted of ≈100 ng of insert DNA (*aroQ* H106A), ≈50 ng of vector DNA (pGEM-5), 1 unit of T4 DNA ligase with 1×T4 ligase buffer (Boehringer Mannheim) with sterilised water added to a total volume of 10µl. The reaction was incubated for 16 hours at room temperature. 10µl of the ligation reaction product was transformed into JM109 competent cells (as described in section 2.8.2). Plasmid purifications were performed using colonies resistant to ampicillin (100 µg/ml) and which exhibited a white phenotype in the presence of 20 mM IPTG and 80µg/ml of X-gal. Restriction digest analysis was used to identify successful ligations and to establish the orientation of the gene within the vector. The pGEM-5 *aroQ* H106A construct was ligated into expression vector

pT7.7 using the restriction sites *Nde* I and *Hind* III. Both the pGEM-5 *aroQ* H106A construct and pT7.7 with an unknown 1.3 kb insert (gifted by Prof. Hunter) were digested in a reaction containing 150 μ l pGEM-5 *aroQ* H106A or 50 μ l pT7.7 with an unknown 1.3 kb insert, 30 units of each restriction enzyme (*Nde* I and *Hind* III from NEB) with 1 \times digestion buffer 4 (NEB). The digestion reaction was incubated at 37°C for 3 hours and purified by gel electrophoresis before use in the ligation reaction (2.7.5). The ligation reaction consisted of \approx 150 ng insert DNA (*aroQ* H106A), \approx 20 ng vector DNA (pT7.7), 1 unit T4 DNA ligase with 1 \times T4 ligase buffer (Boehringer Mannheim) in a total volume of 10 μ l and was incubated for 16 hours at room temperature. 10 μ l of the ligation reaction was transformed into DH5 α competent cells (2.8.2). Plasmid purifications were performed using colonies resistant to ampicillin. Restriction digest analysis was used to identify successful ligations.

The Stratagene Quikchange™ site-directed mutagenesis kit was used to make the point mutations E104A, R113A, S108A and Y28F in *S. coelicolor* type II dehydroquinase (*AroQ*) as outlined in section 2.6.3.2 (All reagents were supplied by Stratagene unless otherwise stated). Plasmid pT7.7 with *S. coelicolor aroQ* inserted into the multiple cloning site between the *Nde*I and *Hind* III, was used as the template for the amplification. Forward and reverse primers were designed using the criteria outlined in section 2.6.1. The eight primers for the procedure were as follows (MWG) with the desired codon change (shown in bold):

E104A

Forward primer 5'GCTGCCGGTGGTGG**CGG**TCCACATCTCC 3'

Reverse primer 5'GGAGATGTGGACCGCCACCACCGGCAGC 3'

R113A

Forward primer 5'CCAACATCCACCAGGCTGAGCCGTTCCGGCACC 3'

Reverse primer 5'GGTGCCGGAACGGCTCAGCCTGGTGGATGTTGG 3'

S108A

Forward primer 5'GGAGGTCCACATCGCCAACATCCACCAGC 3'

Reverse primer 5'GCTGGTGGATGTTGGCGATGTGGACCTCC 3'

Y28F

Forward primer 5'CCAGCCGGAGATCTTCGGCTCCGACACC 3'

Reverse primer 5'GGTGTCGGAGCCGAAGATCTCCGGCTGG 3'

The PCR reaction contained ≈ 15 ng template DNA, 125 ng of forward and reverse primer for each mutation, 0.2 mM of each dNTPs, 2.5 units *PfuTurbo*[®] DNA polymerase, 1 \times reaction buffer (200 mM Tris-HCl (pH 8.8), 20 mM MgSO₄, 100 mM KCl, 100 mM (NH₄)SO₄, 1% Triton[®] X-100, 1 mg/ml nuclease-free BSA); 8% (v/v) DMSO was added to the recommended reaction. The total volume was made up to 50 μ l with sterilised water.

The BioRad Gene Cyclor program included 2 elements: a hot start at 95°C for 1 minutes, 14 cycles of amplification consisting of a further 30 seconds at 95°C (denaturation step), an annealing temperature of 55°C for one minute, followed by an extension period of 6 minutes at 68°C. 10 μ l PCR product was separated and analysed by agarose gel electrophoresis using X and XIV DNA marker (Roche) (Figure 18) to check for amplification. PCR product was then digested with *Dpn* I and transformed into XL1-Blue super competent cells as described in section 2.8.2.



Figure 18. Stratagene Quikchange™ site-directed mutagenesis strategy of pT7.7 *S. coelicolor aroQ* construct. 1% DNA agarose gels: (A) Lane 1: XIV DNA marker (Roche), lanes 2-6: PCRs, lane 7: DNA Marker X (Roche). (B) Lane 1: XIV DNA marker (Roche), lanes 2-6: PCRs, lane 7: DNA Marker X (Roche), (10 µl of PCR product).

The mutations were checked by the University of Glasgow Functional Genomics Sequencing Facility (section 2.9). The pT7.7 *aroQ* mutant constructs were transformed into the over-expression strain BL21 (DE3) pLysS (as described in sections 2.8.2 and 2.10). Cell growth was monitored by A_{600} and once the absorbance had reached 0.6, the expression of protein was induced by addition of 0.8 mM IPTG; Figure 19 shows the time course of the induction of Y28F mutant. Each of the mutants were grown for a further 5.5 hours after induction, yielding 8.27 g, 12.25 g, 16.37 g, 12.43 g and 12.8 g wet weight of cells for E104A, H106A, R113A, S108A and Y28F respectively from 11×0.5 litres of LB medium.

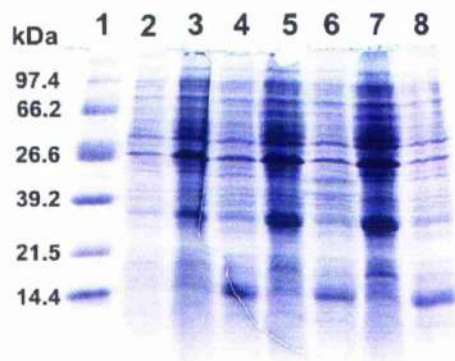


Figure 19. SDS PAGE analysis of expression time course of *S. coelicolor* type II dehydroquinase mutant Y28F in pT7.7 BL21 (DE3) pLys S construct. Lane 1: Boehringer Mannheim marker low-range, lanes 2,4,6,8: induced by addition of 0.8 mM IPTG from 0-6 hours. Lanes 3,5,7: control without 0.8 mM IPTG from 0-6 hours (two hour increments).

The purification protocol is described in section 2.12.1 with the omission of the gel filtration step on Sephacryl 200. It was not possible to locate fractions by the level of catalytic activity. Fractions that had a high absorbance at A_{280} were analysed using SDS PAGE, fractions containing *S. coelicolor* dehydroquinase monomer (molecular mass 16.5 kDa) were pooled and concentrated using an AMICON[®] protein concentrator with a 30 kDa cut-off membrane. Figure 20 shows the DEAE-Sephacel (A) and phenyl-Sepharose (B) elution gradient profile for mutant Y28F dehydroquinase. The purified mutant dehydroquinases were analysed on SDS PAGE to check the purity (Figure 21). The final purified proteins were stored at -20°C in 50% glycerol (v/v). The protein concentration for SCDHQase mutants E104A, H106A, R113A, S108A and Y28F was determined by using the Lowry method (2.13) as 4.3, 6.7, 20.5, 2.1 and 6 mg/ml respectively in the pooled peak fractions.

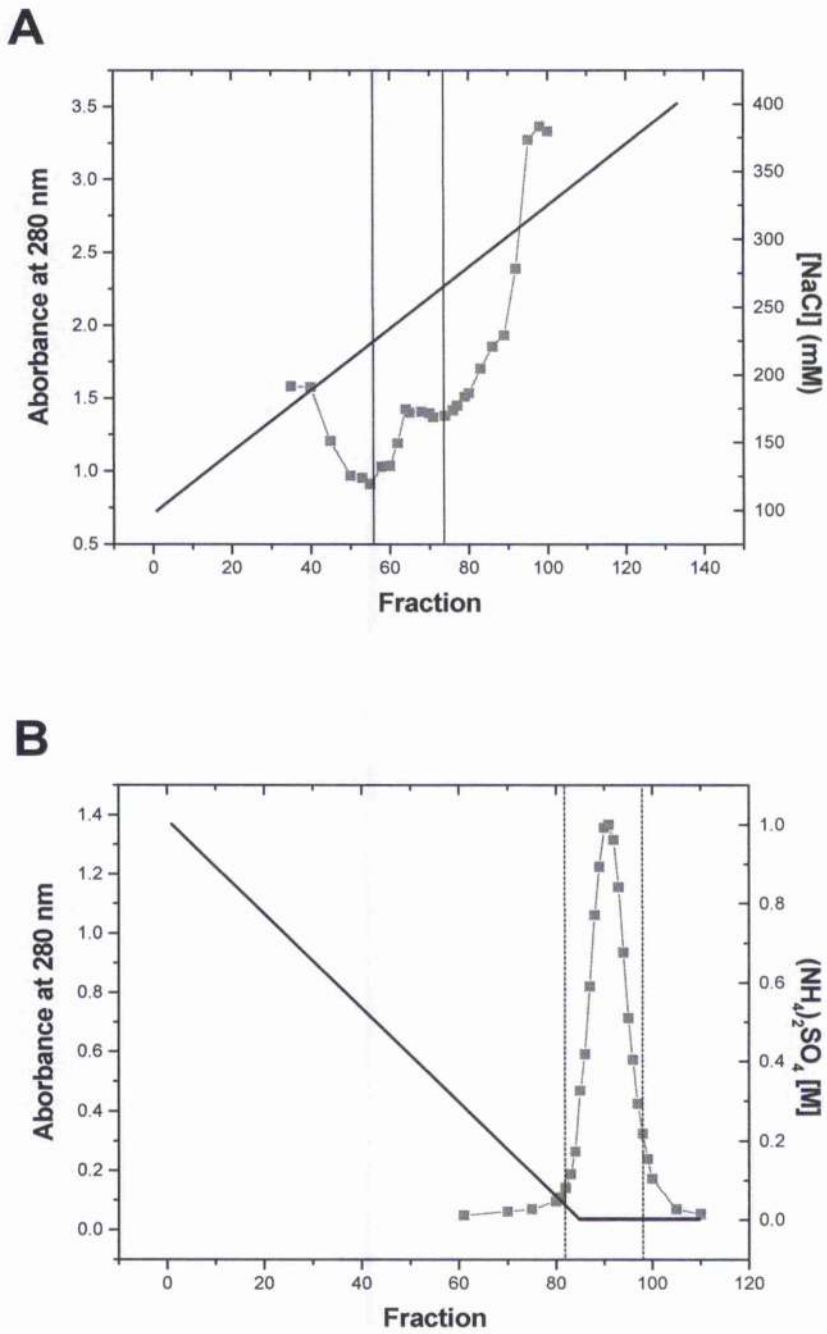


Figure 20. Elution gradient profile of *S. coelicolor* mutant Y28F showing A_{280} measurements (green triangles) and concentration of salt in linear gradient (blue line) (A) DEAE-Sephacel and (B) phenyl-Sepharose. Fractions that were pooled are shown between the black lines.

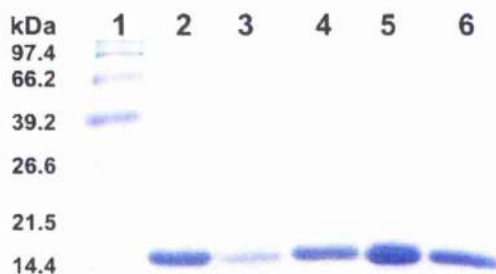


Figure 21. 15% SDS PAGE of purified *S. coelicolor* mutant type II dehydroquinases.

Lane 1: Boehringer Mannheim low-range, lanes 2-6: have between 5 and 10 μg of mutant dehydrogenase H106A, S108A, E104A, R113A and Y28F, respectively.

In early experiments, an initial heat treatment step at 65°C for 10 minutes was tested, as type II dehydroquinases have been shown to be thermally stable. Although the heat treatment was a very effective purification step it was not possible to recover more than 80% of the catalytic activity (results not shown). Hence this step was abandoned for purification of the mutants.

3.3 Protein structure comparisons.

3.3.1 Mass spectrometry

The mass of the purified mutant proteins was determined using electrospray mass spectrometry (2.15). The protein concentration was between 1.1 and 1.8 mg/ml in 50mM Tris acetate (pH 7.0); samples were passed through C18 zip tips to remove ions. The molecular masses of all the dehydroquinases tested showed 100% processing of the N-terminal methionine. N-terminal methionine process in SCDHQase has been reported by Krell *et al.* (1995). The mass of the wild type, type II dehydroquinase from *S. coelicolor* was found to be 16549.68 Da, very close to the theoretical mass of 16550.6 Da (Figure 22A). The Y28F mutant has a mass of 16535.08 Da; 14.6 Da less than the wild type, which corresponds to the difference between a tyrosine and a phenylalanine amino acid residue, i.e. one oxygen atom (Figure 22B).

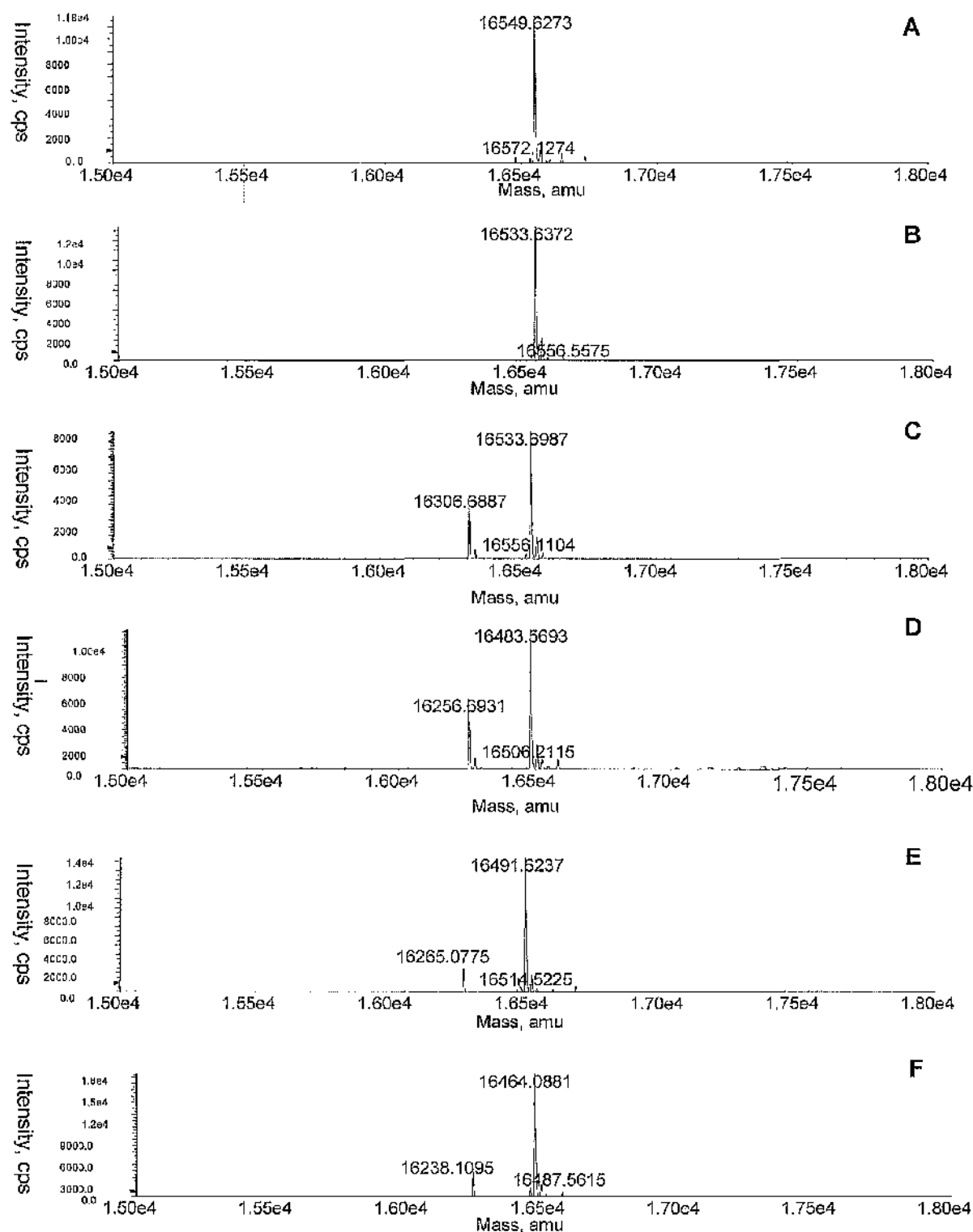


Figure 22. Electro spray mass spectrometry data of *S. coelicolor* wild-type and mutant type II dehydrogenases. (A) Wild type, (B) Y28F, (C) S108A, (D) H106A, (E) E104A and (F) R113A.

The spectrum of the S108A mutant displays two peaks, one at 16533.72 Da, which exactly matches the substitution of serine by alanine. The second peak is at 227 Da less than the major peak and has approximately 50% of its intensity (Figure 22C). Two peaks are also present in the R113A mutant spectrum (Figure 22F) although in this case the minor peak is only about 20% as intense as the major peak. The major peak in the R113A spectrum corresponds precisely to the mutation of arginine to alanine; the minor peak has the same difference in mass (227 Da) as the minor peak in the S108A mutant spectrum. This indicates that the minor peak is not an impurity and is likely to be the result of C-terminal processing as the difference in mass observed is the same as the combined molecular mass of an arginine and alanine, residues present at the C-terminal. Processing at the N-terminus is less likely as the sequence starts with a proline followed by an arginine. Proline residues usually impede cleavage and the combined molecular weight is 26 Da larger than observed difference in mass (227 Da) between the peaks. Analyses of the 3-D X-ray structures of SCDHQase suggest that loss of two amino acids at C-terminal is unlikely to affect the activity. To confirm C-terminal processing the C-terminal sequencing could be performed. Enzymatic C-terminal sequencing based on carboxypeptidase cleavage employing protein digestion using O^{18} -enriched H_2O can be used to identify the C-terminal peptide.

The spectrum of the H106A mutant also displays two peaks (Figure 22D). The major peak is 66 Da smaller (16483.6 Da) than the wild type SCDHQase peak corresponding exactly to the substitution of histidine by alanine. The second minor peak that corresponds to the C-terminal processing of two amino acids makes up about 33% of the protein in solution. The E104A spectrum shows approximately 15% C-terminal processing of the protein in solution. The major peak is equivalent to the substitution of glutamate by alanine (16491.6 Da) (Figure 22E).

Each protein spectra has a small peak on average 22.8 Da larger than the major dehydroquinase peak. This corresponds to the atomic weight of sodium and these small peaks are likely to be a sodium atom bound to the unfolded protein. This is a residual salt contamination as the C18 zip tips are not totally effective.

3.3.2 Circular dichroism

The CD spectrum of the wild type SCDHQase and each of the mutants was recorded in both the near UV (0.5 cm path length) and far UV (0.02 cm path length) at protein concentrations of 1.6 and 0.5 mg/ml respectively in 50mM potassium phosphate buffer pH 7.0. Evidence from the far UV CD spectroscopy demonstrated that the secondary structure of the protein was not altered significantly in any of the mutants (Figure 23A). The differences in the percentage distribution of secondary structural features were calculated using the SELCON procedure (Sreerama and Woody, 1994a) and are shown in Table 6.

Table 6. Secondary structure estimates (%) using the SELCON procedure of Sreerama and Woody (1994b).

	Alpha helix	Antiparallel beta sheet	Parallel beta sheet	Turns	Other
SC WT	30.7	13.6	8.6	15.1	32.9
E104A	28.8	14.9	8.5	14.4	34.0
H106A	31.1	13.2	8.5	13.5	33.6
R113A	29.9	14.0	7.9	12.7	35.3
S108A	29.9	12.5	9.2	10.9	37.8
Y28F	30.0	13.1	9.0	13.1	34.8

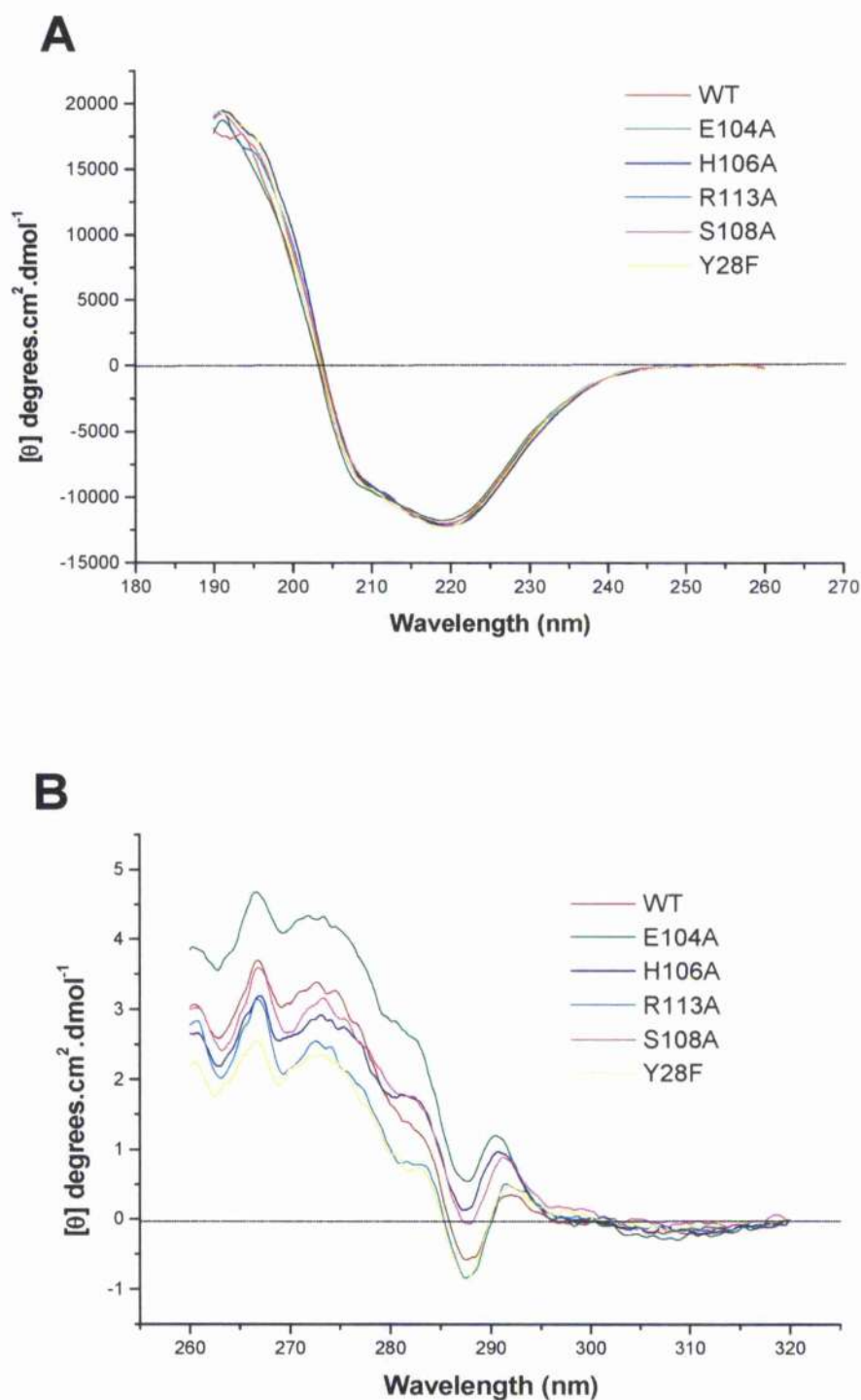


Figure 23. Superimposed circular dichroism spectra of wild type and mutant *S. coelicolor* dehydroquinases. See inserted legend for colour of mutants and wild type (A) Far UV CD (B) near UV CD.

The near UV CD spectrum shows little difference in the environments of the aromatic amino acids between the wild type and the mutant *S. coelicolor* dehydroquinases (Figure 23B). The overall shapes of the spectra are similar throughout, suggesting that the tertiary structure is unaffected by the mutations. Slight alterations in the in the spectra could reflect the conformational mobility of the protein in solution. There is a subtle shift in the peak at 290 nm of mutants; E104A, H106A and S108A, this maybe attributed to a minor change in the environment of the tryptophan, residue 65. The E104A mutant is the only mutation to have a higher intensity than the wild type between 280 and 260 nm; this indicates greater rigidity in the residues that absorb within this region (3 phenylalanine and 3 tyrosine residues).

3.4 Functional assays of mutants.

Enzyme assays were carried out as described in section 2.16.1. 10 µg of enzyme was used for each assay of mutants E104A and H106A, 0.5 µg, 25 µg and 50µg of enzyme were used for each assay of the S108A, Y28F and R113A mutant, respectively and 0.015 µg of wild type SCDIIQase. The kinetic parameters were determined as described in section 2.18, and are summarised in Table 7. The errors in K_m and k_{cat} are less than 5% of the stated values.

Table 7. Catalytic parameters of *S. coelicolor* DHQase site-directed mutants.

	µmol/min/mg	K_m (µM)	k_{cat} (s ⁻¹)	k_{cat}/K_m (s ⁻¹ M ⁻¹)
Wild type	454	99	124.8	1.26×10^6
E104A	1.16	44	0.318	7.16×10^3
H106A	0.5	92	0.137	1.49×10^3
R113A	0.21	360	0.057	1.59×10^2
S108A	14.1	430	3.872	9.00×10^3
Y28F	0.1	100	0.026	2.63×10^2

All of the mutations of *S. coelicolor* type II dehydroquinase resulted in a decrease in k_{cat} . The Y28F mutation reduced the catalytic activity (k_{cat}) by 4700-fold, although

the K_m was not affected. The K_m of the H106A mutant is also unaffected, but shows a 910-fold decrease in k_{cat} from the wild type. The catalytic activity of the S108A mutation is the least affected, but k_{cat} is still 32-fold lower than the wild type, with the K_m showing a 4.3 fold increase. R113A mutation showed an increase in K_m of 3.6-fold and a decrease in k_{cat} of 2200-fold compared with the wild type enzyme. The E104A mutation is the only mutation to exhibit a decrease in K_m of approximately 2-fold; the k_{cat} is also decreased by 33-fold.

3.5 Chapter summary.

All of the site-directed mutants show a loss in catalytic activity. According to the proposed catalytic mechanism (Roszak *et al.*, 2002) Tyr28 is essential for catalytic activity, and this is supported by the very large decline in k_{cat} with no effect on K_m in the Y28F mutant. Arg113 also seems to be involved catalysis as k_{cat} is almost as low as the Y28F mutant. In addition the R113A mutant has an effect on substrate binding a significant increase in K_m which may be due to electrostatic effects of removing a charged residue from the active site. The wild type *S. coelicolor* dehydroquinase shows a seven-fold increase in catalytic activity between pH 6.5 to 8.0 (section 5.4.1). Additional experiments analysing the pH dependence may reveal a different degree of dependence in these mutants. The mutants Y28F and R113A could be used to verify that the chemical modification experiments using TNM and PGO performed by T. Krell (1996) were specifically affecting the mutated residues.

The catalytic properties of the H106A mutant concur with the hypothesis that the residue is the proton donor for the hydroxyl at C1 of the substrate. The reduction in k_{cat} is not as great as either R113A or Y28F. The role of the invariant Glu104 is less clear; the substitution of this residue by alanine caused tighter binding of the substrate and a more radical effect on the k_{cat} than expected. A possible explanation of the effect on catalytic activity is the proximity of Glu104 to His106 (X-ray structure analysis) implying that Glu104 maybe important in the reprotonation of His106 as well as the correct orientation of this residue. Interestingly the near UV CD spectrum of the E104A mutation suggests a greater rigidity in the overall tertiary structure, which could account for the lower K_m . It would be extremely valuable to generate 3-D X-ray structures of each of the mutants bound with a ligand for further characterisation, especially the E104A mutant. It is possible that this mutant would crystallise under similar conditions to the wild type as the secondary structure is

equivalent and the mutated residue is unlikely to be exposed on the surface of the macromolecule, as it is involved in an ionic interaction with His106.

The substitution of Ser108 by alanine supports the proposed mechanism; the role of Ser108 is recognition of the substrate through the binding of the carboxylate group of the substrate. The affinity for substrate becomes weaker as reflected in the K_m and although the turnover is impaired this is not to anything like the same degree as any of the other mutations. The loss in activity of the S108A mutant maybe due to the role of Ser108 in orientating Tyr28 and Arg113. Additional phosphate and inhibitor binding studies should be performed on the S108A mutant to characterise the binding of ligands further.

All of the mutants retain a small amount of activity, even though the major functional groups of the amino acids have either been replaced or completely lost. Site-directed mutants of *Bacillus amyloliquefaciens* subtilisin (a serine protease) also show small amounts of residual activity. Replacement of each of the subtilisin catalytic triad residues Asp32, His64 and Ser221, by alanine reduced the k_{cat} by factors of 3×10^4 , 2×10^6 and 2×10^6 , respectively. A triple mutation of all three residues to alanine also decreases activity by 2×10^6 . The K_m values of all the site-directed mutants of subtilisin were increased by only a factor of two. However, it is unlikely that the residual activity is a result of the presence of a small amount of wild type enzyme, since the mutants are resistant to inhibition by phenylmethanesulfonyl fluoride, an irreversible inhibitor of the subtilisin wild type enzyme. The mechanism of the triple mutant is thought to have changed, as the catalytically important hydroxyl group of the Ser221 is no longer present. The residual activity is thought to be due to direct nucleophilic attack by a water molecule on the substrate (Carter and Wells, 1988). It is possible that the overall properties of the active site of the SCDHQase creates a favourable environment for catalysis and that a bound water molecule may perform the role of a catalytic residue to a certain extent. Detailed analysis of X-ray structures of the mutants may help to answer this problem. It is unlikely that there is contamination of any of the mutants with wild type enzyme, as the mass spectrometry data do not show a peak, corresponding to the mass of the wild type in any of the mutant spectra. Although low levels of contamination of between 0.1-0.01% would be very hard to identify. If mutant that had absolutely no activity, but wild type

enzyme was present at a level of 0.1%, the result would be a 10^3 -fold lower k_{cat} value than the wild type, but the K_m would remain the same.

Alanine was chosen for the majority of the mutations, as it is a small amino acid and would be unlikely to interfere with the tertiary structure. In order to characterise the role of these residues further it would be desirable to mutate them to another residue or perform double or triple mutations. Ser108 could be mutated to an aspartic acid that would be expected to repel the carboxylate at C1 of dehydroquinone and interact with Arg113. Arg113 could be mutated to a lysine and the change in the tyrosine environment could be studied.

There are also several other mutations that would be interesting to study. For example the oxime inhibitor of *M. tuberculosis* dehydroquinase does not bind very well to the *S. coelicolor* dehydroquinase, analysis of the 3-D X-ray structure by D. Robinson has revealed that Ala81, which is a glycine in *M. tuberculosis* dehydroquinase, may cause a steric clash with the inhibitor (Robinson, 2003). It would be interesting to replace Ala81 with a glycine to see if the inhibitor bound more tightly. It is thought that the release of dehydroshikimate from the active site is brought about by the fact that there is not enough space in the active site for both dehydroshikimate and the water molecule. The likely route for the water molecule to exit is through a solvent cavity close to the dimer interface. The cavity is formed by the presence of residues Ser123, Val129 and Ala131 conserved over many dehydroquinases, and it might be possible to block this route by replacing one or more of these amino acids with a larger residue, such as a methionine or lysine, although this could disrupt the tertiary structure. Asn 79 and Ile107 are both implicated in the binding of the carboxylate on C1 of the substrate. It would be interesting to mutate both of these residues in the wild type and perform a double mutation using the S108A mutant, which would be expected this to increase the K_m further. It might be possible to destabilise the enol intermediate by mutating Asn19 (which binds to the water molecule within the active site) to a hydrophobic residue such as a valine or a leucine.

Directed evolution may highlight some previously unidentified contributions from other residues and help to answer the question of why the native enzyme is so large.

CHAPTER 4 CHARACTERISATION OF *BACILLUS SUBTILIS* TYPE II DEHYDROQUINASE RELATED PROTEIN (YqhS)

4.1 Introduction

To date, *Bacillus subtilis* is the only bacterium known to have genes coding for both the type I and type II dehydroquinase enzymes. There are only gene data for four other members of the *Bacillus* family (Figure 24). *B. stearothermophilus* possess a type I DHQase while *B. anthracis* possess a type II DHQase. There does not seem to be any pattern of distribution of type I and type II dehydroquinases and it is thought that this is a result of horizontal gene transfer. The start codon of the *yqhS* gene is GTG, which is quite rare in *B. subtilis*; 9% of genes start with this codon (Kunst *et al.*, 1997). The organisation of shikimate enzymes in *B. subtilis* is distinct from all other organisms in which the shikimate pathway has been studied (Nakatsukasa and Nester, 1972; 1.1.3).

An alignment of the amino acid residues of YqhS shows high homology with the other type II dehydroquinases, for instance there is 45, 47 and 43% identity with MTDHQase, SCDHQase and HPDHDQase, respectively (Appendix C; **Error! Reference source not found.**) (Corpet, 1988; Altschul *et al.*, 1997). All the residues in the active site thought to be involved in the catalytic mechanism are present in YqhS apart from the tyrosine 28 which is substituted by phenylalanine, believed to be involved in proton abstraction (Roszak *et al.*, 2002). In previous work YqhS had been over-expressed in *E. coli* strain BL21 (DE3) pLysS and purified by A. Herbert. Preliminary assays performed by A. Herbert suggested that YqhS was catalytically inactive. The purified YqhS was also crystallised and high resolution structural data were obtained by Dr. Laphorn and D. Robinson; these studies confirmed that the residues thought to be involved in the catalytic mechanism of type II DHQase (apart from the tyrosine) are in the correct orientation (Figure 25). Interestingly it was possible to resolve the active site lid domain in YqhS; this flexible region of the polypeptide chain has not been resolved in MTDHQase or HPDHDQase.

Site directed mutagenesis was used to mutate the phenylalanine (Phe23) of YqhS to a tyrosine in an attempt to restore catalytic activity to YqhS.

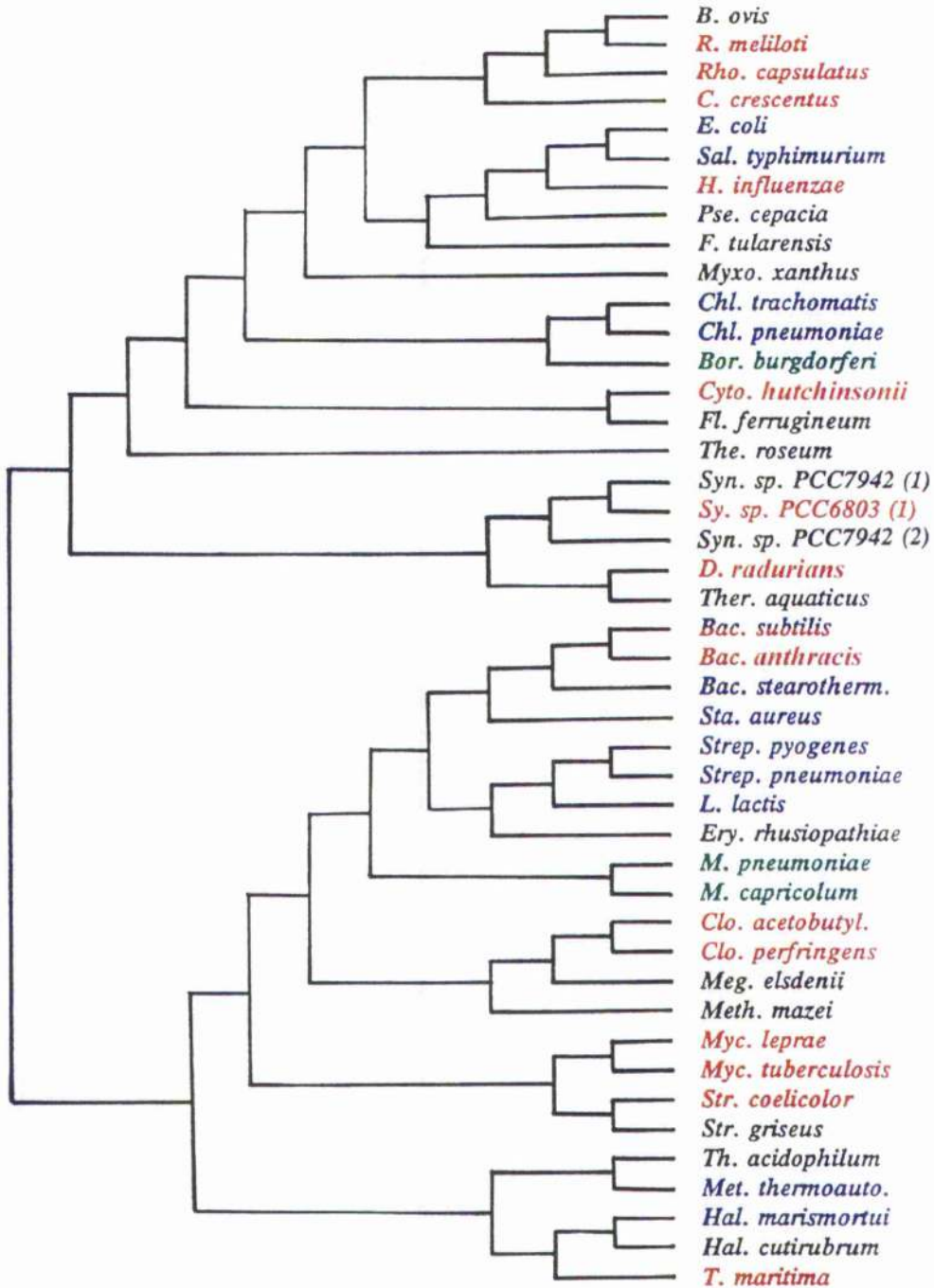


Figure 24. Taxonomic tree of bacteria showing the distribution of classes dehydroquinases the type I DHQase are highlighted in blue, type II in red, parasitic bacteria in green and unknown in black. *B. subtilis* is highlighted in both red and blue. Modified from Consensus neighbour-joining tree for prokaryotic organisms based on Hsp70 protein sequences (Gupta, 1998).

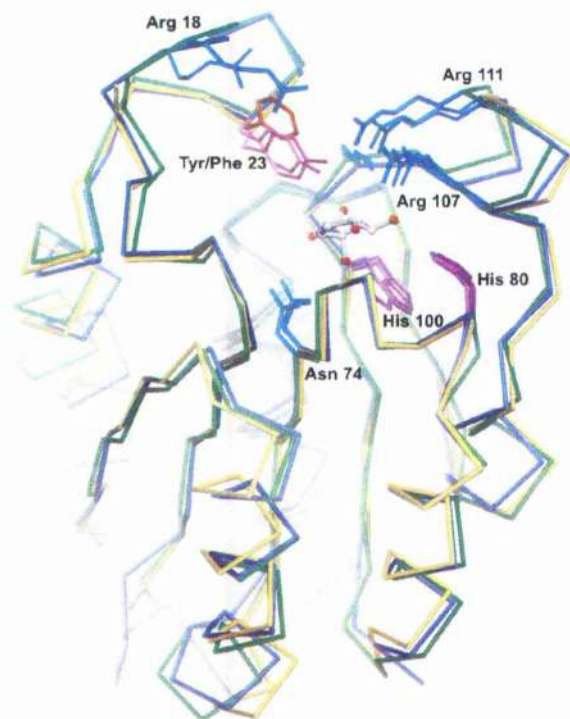


Figure 25. Overlay of subunits from *Bacillus subtilis* (green), *Mycobacterium tuberculosis* (orange) and *Streptomyces coelicolor* (blue). Residues thought to be involved in catalysis are highlighted using the numbering system from *B. subtilis*. Dehydroshikimate is bound in the active site.

Microarray data from *B. subtilis* (derivative 168) grown in aerobic conditions showed that mRNAs for both the type I dehydroquinase (*aroC*) and the *yqhS* gene are present during aerobic vegetative growth (personal communication from Rick W. Ye). In order to study whether YqhS is expressed *in vivo*, Western blots were performed using antibodies raised against F23Y mutant YqhS to probe cell extracts from *B. subtilis*.

4.2 Construction, over expression and purification of site-directed mutant of *B. subtilis* type II dehydroquinase related protein (YqhS)

A two-stage site directed mutagenesis strategy was followed as outlined in section 2.6.3.1, using a construct of pTB361 with *B. subtilis yqhS* inserted into the multiple cloning site between the *NdeI* and *KpnI*, (gifted by A. Herbert) as the template for the amplification. The four primers for the procedure were as follows:

P1 5'GAT CCC GCG AAA TTA ATA CGA CTC ACT ATA 3'

P2 5'GAG GAT GCA TTA CAG ATC TGG TAC 3'

P3 5'CGG CCG TAT ACT TCA GGC TCA 3'

P4 5'TGA AGT ATA CGG CCG CCA GAC ACT 3'

The mutagenesis primers (P3+4) were designed with the desired codon change (shown in bold) to allow the substitution of the phenylalanine by a tyrosine. The first step generated two fragments of *yqhS* cDNA, the first fragment was 171 bp (P1+3) and the second was 411 bp (P2+4). The PCR reactions for both fragments contained ≈ 3 ng of template DNA, 50 pmol of both primers, 0.2 mM of each dNTPs, 2 units Vent_R[®] polymerase (Life technologies), 1 \times ThermoPol reaction buffer (10mM KCl, 10mM ammonium sulphate, 20mM Tris-HCl pH 8.8, 2mM MgSO₄ and 0.1% (v/v) Triton X-100) an additional 1 μ l of 2mM MgSO₄ in a total volume of 50 μ l made up with sterilised water. The BioRad Gene cycler program included 3 elements: a hot start at 94°C for 5 minutes, 30 cycles of amplification consisting of an annealing temperature of 55°C for one minute, an extension period of 1minute at 72°C and a denaturation step of 94°C for one minute followed by a segment of annealing for 1 minute and elongation for 4 minutes. 4 μ l of PCR product was separated and analysed by agarose gel electrophoresis using EZ Load 100bp molecular Ruler (BioRad) (Figure 16). Fragments of the appropriate size were purified by extraction from the gel (2.7.4).

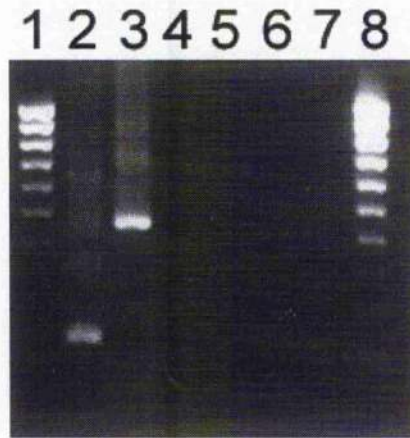


Figure 26. 1% DNA agarose gels of pTB361 *B. subtilis* *yqhS* construct, two-stage site-directed mutagenesis, first round of PCR. Lane 1: EZ Load 100 bp Molecular Ruler (BioRad), lane 2: PCR fragment P1 + P3 (171 bp), lane 3: PCR fragment P2 + P4 (411 bp), lanes 4– 7: failed PCR, lane 8: EZ Load 100 bp Molecular Ruler (BioRad) (5 μ l of PCR product).

The two small fragments of PCR product were used as the template for the second stage of PCR. The second stage PCR reaction contained ≈ 5 ng of both of the fragments from the first stage, 50 pmol of both external primers (P1+2), 0.2 mM of each of dNTP, 1% (v/v) DMSO, 2 enzyme units Vent_R[®] polymerase, 1 \times ThermoPol reaction buffer with an additional 1 μ l of 0.5mM MgSO₄ in a total volume of 50 μ l made up with sterilised water. The BioRad Gene cycler program included 3 elements: a hot start at 94 $^{\circ}$ C for 5 minutes, 30 cycles of amplification consisting of an annealing temperature of 65 $^{\circ}$ C for one minute, an extension period of 1minute at 72 $^{\circ}$ C and a denaturation step of 94 $^{\circ}$ C for one minute followed by a final segment of annealing for 1 minute and elongation for 5 minutes. 4 μ l of PCR product was separated and analysed by agarose gel electrophoresis using Marker X (Promega) and EZ Load 100bp molecular Ruler (BioRad) (Figure 27).

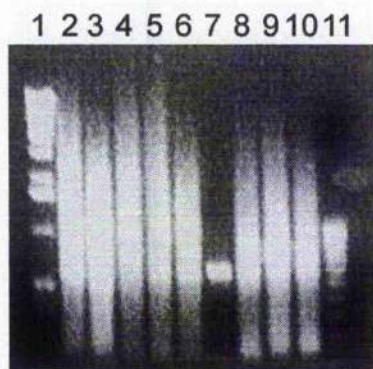


Figure 27. 1% DNA agarose gels of pTB361 *B. subtilis* *yqhS* construct, two-stage site-directed mutagenesis, second round of PCR. Lane 1: DNA Marker X (Roche), lanes 1-6, 8- 10: unsuccessful PCRs, lane 7: fused PCR fragments amplified using P1 and P2 primers. Lane 11: EZ Load 100 bp Molecular Ruler (BioRad) (4 μ l of PCR product).

Mutated *yqhS* F23Y was ligated into expression vector pTB361 using the restriction sites *NdeI* and *KpnI*. Both pTB361 plasmid and the PCR product were digested in a reaction containing 45 μ l of PCR product or 15 μ g of plasmid DNA, 40 units of *NdeI* (NEB) and 20 units of *KpnI* (NEB) with 1 \times digestion buffer 1 (NEB). The digestion reaction was incubated at 37°C for 3 hours and purified by gel electrophoresis to be used in the ligation reaction (2.7.5). The ligation reaction consisted of \approx 100 ng of insert DNA (*yqhS* F23Y), \approx 50 ng of vector DNA (pTB361), 1 unit of T4 DNA ligase with 1 \times T4 ligase buffer (Boehringer Mannheim) in a total volume of 20 μ l and was incubated for 16 hours at room temperature. 10 μ l of the ligation reaction was transformed into DH5 α competent cells (2.8.2). Plasmid purifications were performed on colonies resistant to tetracycline and restriction digest analysis was used to identify successful ligations. The preliminary confirmation of the mutation was by restriction digest analysis, using 5 Units *BstZ17I*, an endonuclease, which would only cut when the mutation was present. Plasmids that it was possible to cut were then sent for sequencing at the University of Glasgow Functional Genomics Sequencing Facility (2.9).

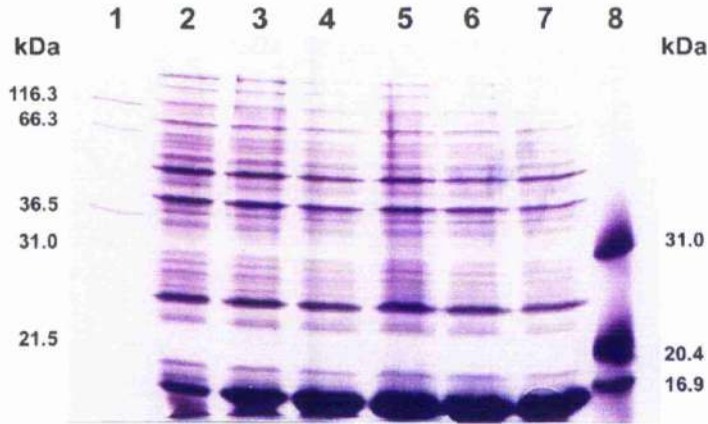


Figure 28. SDS PAGE analysis of the time course expression of expression of *B. subtilis* dehydroquinase related protein YqhS (F23Y) in pTB361-BL21 (DE3) pLysS construct. Lane 1: Novex™ mark 12 Wide range protein standard. Lanes 2 to 7: samples induced by addition of 0.8 mM IPTG from 0-5 hours (one hour increments). Lane 8: Promega low-range protein molecular weight marker.

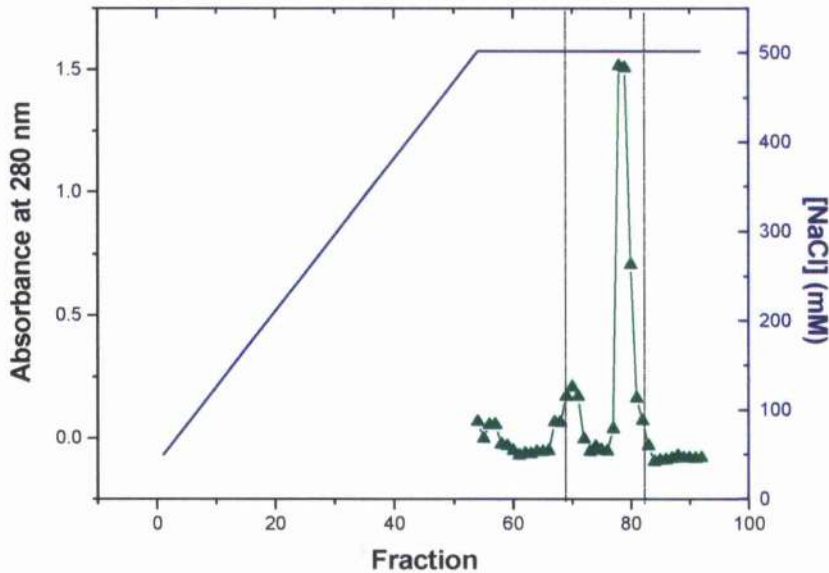


Figure 29. The elution profile from Q sepharose column during purification of *B. subtilis* YqhS mutant F23Y. Absorbance at 280 nm represented by green triangles. The linear NaCl gradient is represented by the blue line. Fractions that were pooled are shown between the dash black lines.



Figure 30. SDS PAGE analysis of the purification of *B. subtilis* YqhS (F23Y) from Q Sepharose. Lane 1: Promega low-range protein molecular weight marker. Lanes 2 to 12: fractions 67, 70, 77 to 83 and 85, respectively. Lane 13: Novex™ mark 12 Wide range protein standard.

The PTB361 *yqhS* F23Y construct was transformed into the over expression strain BL21 (DE3) pLysS. When the A_{600} reached 0.6, the expression of protein was induced by addition of 0.8mM IPTG; Figure 28 shows a time course of the induction, yielding 16 gm wet weight of cells. The purification protocol is described in section 2.12.2. Step 2 consisted of Q Sepharose anion exchange chromatography; the elution profile can be seen in Figure 29. Pooled fractions were analysed by SDS PAGE (Figure 30). The pooled protein fractions were concentrated and then split into two 1.5ml volumes, which were applied to the Sephacryl S200 gel filtration column with a 24-hour interval. 3 ml fractions were collected and the absorbance at 280 nm was recorded (data not shown). Fractions with A_{280} measurements over 0.5 were analysed by SDS PAGE (Figure 31) to check the purity fraction were then pooled and concentrated using an AMICON® protein concentrator with a 30 kDa cut-off membrane. The protein concentration of the purified YqhS F23Y was determined as 57.3 mg/ml by the Lowry method (2.13) giving a total of 573 mg of protein.

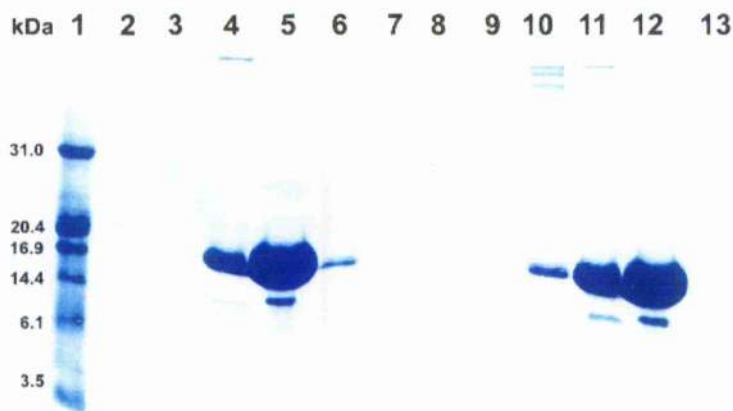


Figure 31. SDS PAGE analysis of the purification of *B. subtilis* YqhS (F23Y) from Sephacryl 200. Lane 1: Promega low-range protein molecular weight marker. Lanes 2 to 13: fractions 110, 114, 117, 122, 127, 131, 134, 138, 147 and 157, respectively.

4.3 Structural studies of YqhS using circular dichroism, fluorescence and dynamic light scattering

4.3.1 Unfolding experiments on YqhS

4.3.1.1 Circular Dichroism results

Experiments on the unfolding of *B. subtilis* YqhS by GdmCl were performed; YqhS at 0.13 mg/ml was incubated for 24 hours at 20°C with varying concentrations of GdmCl (0 to 6 M) in Tris-acetate buffer pH 7.5. Far UV spectra were recorded using a cuvette with a pathlength of 0.05 cm (2.22). The far UV CD spectra showed that there was no significant loss in secondary structure up to at least 4.75 M GdmCl, and even at 6 M, 50% of the native signal at 222 nm still remains (Figure 32). Unfolding studies on the type II dehydroquinase from *M. tuberculosis*, have shown that only 13% of the native signal at 222 nm remains at 6 M GdmCl (Price *et al.*, 1999). This residual CD signal of the *M. tuberculosis* DHQase is likely to be due to other structural elements.

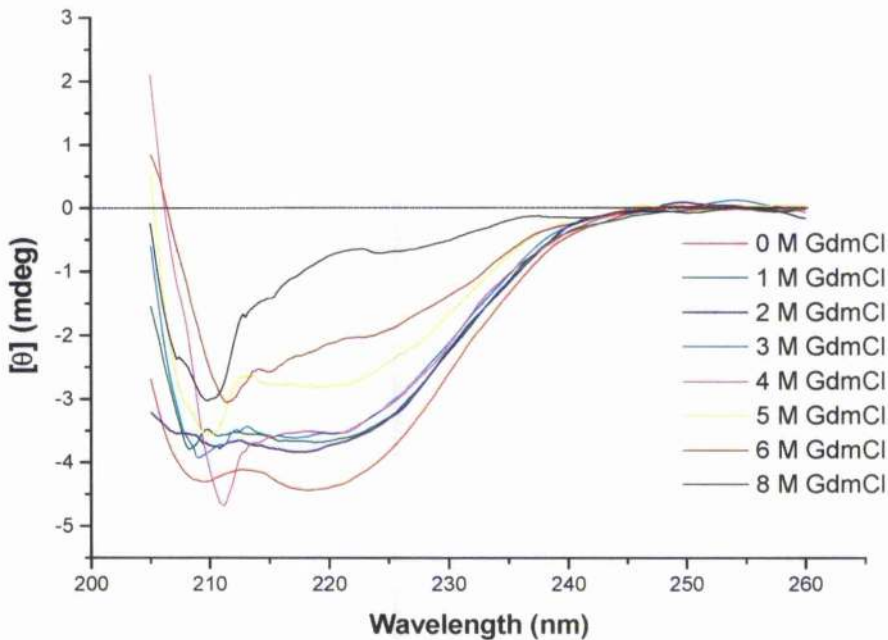


Figure 32. Far UV circular dichroism spectra of the unfolding of *B. subtilis* YqhS by guanidine hydrochloride (GdmCl) see figure insert for concentration of GdmCl.

Further unfolding experiments on *B. subtilis* YqhS in 8 M GdmCl required the GdmCl to be dissolved directly into the protein solution. 0.5448 g of GdmCl was slowly added to 0.3 ml of 255 $\mu\text{g/ml}$ YqhS giving a final concentration of 107 $\mu\text{g/ml}$ of protein and 8 M GdmCl in a volume of 0.713 ml. The solution was incubated for 24 hours at 20°C along with a native protein solution of the same concentration. The far UV CD spectrum was recorded as reported above. In 8 M GdmCl only 20% of the native YqhS signal at 225 nm is preserved (Figure 32).

4.3.1.2 Fluorescence spectroscopy results

The *B. subtilis* YqhS protein has no tryptophan residues so the fluorescence signals arise from the six tyrosine residues per subunit. When excited at 290 nm, the emission peak is at 308 nm. On addition of GdmCl, three distinct phases are noted (Figure 33):

There is a large increase in fluorescence (85%) in the range of 0-1 M GdmCl. In this range the far UV CD spectra indicate there is no change in the secondary structure. It

is possible that this change in fluorescence might be associated with dissociation of the dodecameric structure into trimers (Price *et al.*, 1999).

Between 1 and 4.75 M GdmCl there is effectively no change in the signal, which is consistent with the results of the far UV CD spectra.

Above 4.75 M GdmCl, there is a decline in fluorescence occurring over the same range as the changes in the far UV CD.

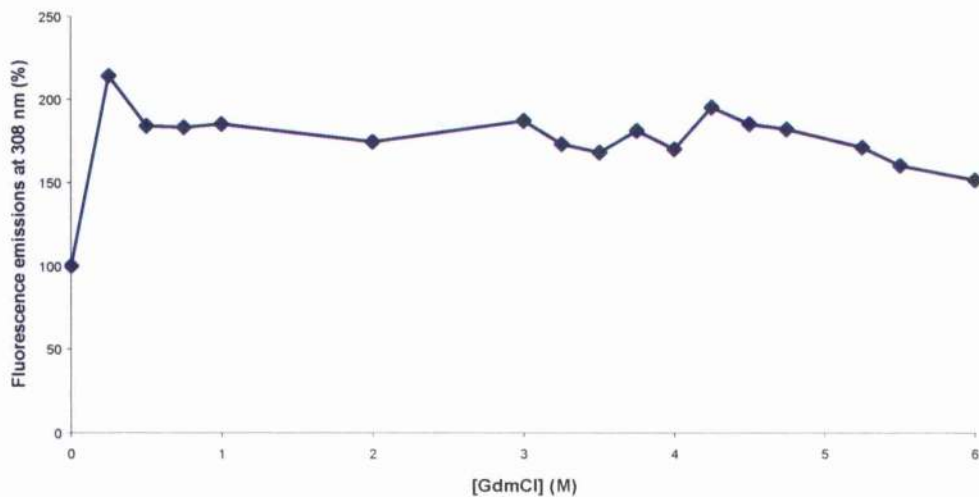


Figure 33. Percentage change in fluorescence emissions at 308 nm during unfolding of *B. subtilis* YqhS protein by guanidine hydrochloride (GdmCl) denaturation. The values have been corrected for Raman scattering.

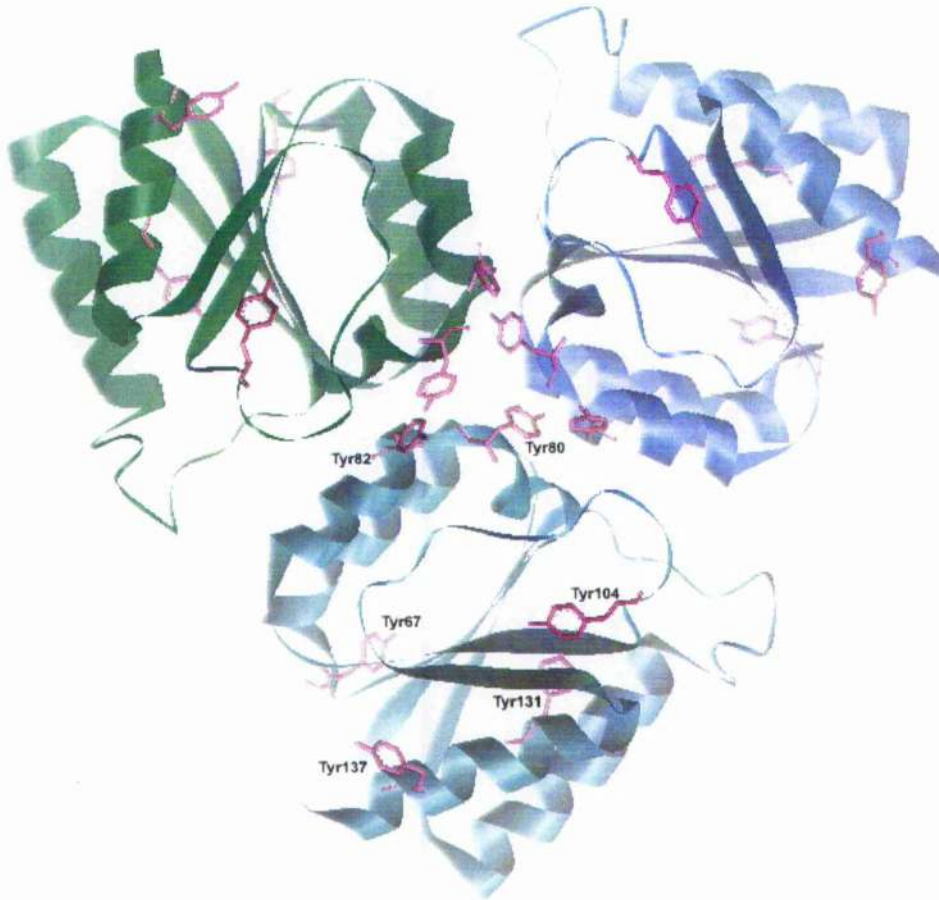


Figure 34. *B. subtilis* YqhS protein trimer of subunits, tyrosine side chains are shown in pink.

Two of the six tyrosines in the subunit are found at the trimer interface (Tyr80 and 82). Tyr67, 131 and 137 are buried within their individual subunits and Tyr104 is solvent exposed (*B. subtilis* YqhS numbering system) (Figure 34).

4.3.2 Dynamic light scattering of YqhS in the presence of low concentrations of guanidine hydrochloride

Dynamic light scattering was used (2.23) to investigate the quaternary structure and any structural changes in the presence of low concentrations of GdmCl and NaCl. These experiments were carried out to test whether low concentrations of denaturant disrupted the dodecamer of the YqhS protein to form trimers causing the observed increase in fluorescence.

The YqhS protein was studied at a protein concentration of 0.75 mg/ml in 50 mM Tris-HCl (pH 7.0). Where indicated GdmCl and NaCl were added to a concentration of 0.5 M. All dynamic light scattering experiments were incubated at 20°C for 30 minutes prior to analysis. 200 µl of each solution was injected into the dynamic light scattering cell.

Table 8. Dynamic light scattering data of *B. subtilis* YqhS protein

<i>B. subtilis</i> YqhS protein			
	Radius (nm)	Estimated MW (kDa)	SOS Error
50 mM Tris-acetate	4.7	126	8.89
50 mM Tris-acetate 0.5 M GdmCl	4.5	114	12.44
50 mM Tris-acetate 0.5 M NaCl	4.6	121	2.49

The estimated molecular weight of the dodecamer 126 kDa is significantly lower than expected (190 kDa) (Table 8), this would give an estimated molecular weight for each subunit of only 10.5 kDa, or imply less subunits being involved in the quaternary structure. This seems unlikely as the YqhS X-ray crystal structure reveals the protein forming dodecamers, the assumptions made about protein density in estimating the molecular weight are unlikely to be true for the YqhS protein. The presence of 0.5 M GdmCl does not significantly affect the quaternary of the YqhS protein.

4.3.3 Interaction of YqhS with dehydroquinone as revealed by fluorescence

To investigate whether dehydroquinone binds to the YqhS protein fluorescence binding experiments were performed using N-Acetyl-L-tyrosinamide (NATA) to

investigate the possible quenching effect of dehydroquinone. Fluorescence measurements were carried out using 0.1 mg/ml of protein in 50 mM Tris-acetate (pH 7.0) at 20°C in a 1 ml volume cell with a 1 cm path length cell and with the slits set at 5.0 nm bandpass. The dehydroquinone concentration was increased from 0 to approximately 6 mM by the addition of 10 μ l aliquots of solution of 14 mM and 70 mM dehydroquinone in 50 mM Tris-acetate (pH 7.0). The fluorescence emissions values were corrected by using the model compound NATA (5 μ M). Samples were excited at 280 nm and their emissions were monitored at 308 nm. Emission values were corrected for Raman scattering, NATA quenching and the dilution effect of titration.

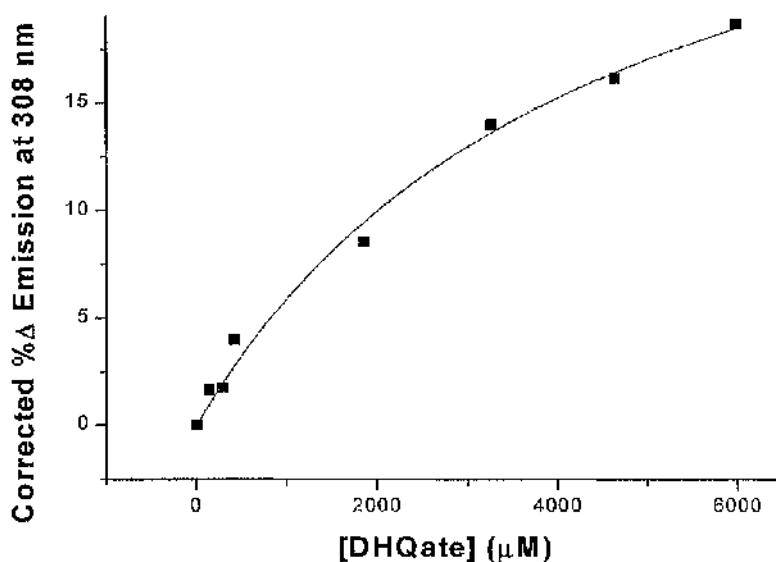


Figure 35. Fluorescence binding of *B. subtilis* YqhS protein corrected using results of N-Acetyl-L-tyrosinamide quenching by dehydroquinone and dilution effect.

The corrected percentage change in emission values (where 0% is defined to 0 mM dehydroquinone) were fitted using a non-linear regression fit and are shown in Figure 35. The K_d value for *B. subtilis* YqhS is $4500 \mu\text{M} \pm 1000$. It may be possible to get a more accurate measure of the K_d value using isothermal titration calorimetry (ITC).

4.3.4 Comparison of YqhS with site-directed mutant F23Y YqhS by circular dichroism

Far UV CD was used to establish that the secondary structure of the site-directed mutant was not affected by the substitution of F23Y. Spectra of 0.1mg/ml solutions of both the wild type and mutant YqhS protein in Tris-HCl buffer (pH 7.5) were measured as described in section 2.22. The F23Y mutant of YqhS has an identical secondary structure to the wild type (Figure 36). The differences in the percentage distribution of secondary structural features were calculated using the SELCON procedure (Sreerama and Woody, 1994a) and are shown in Table 9.

Table 9. Secondary structure estimates (%) of *B. subtilis* YqhS and YqhS F23Y mutant using the SELCON procedure of Sreerama and Woody (1994a).

	Alpha helix	Antiparallel beta sheet	Parallel beta sheet	Turns	Other
Wildtype	45.1	9.0	6.7	14.7	24.2
F23Y	45.4	8.5	6.5	14.0	24.3

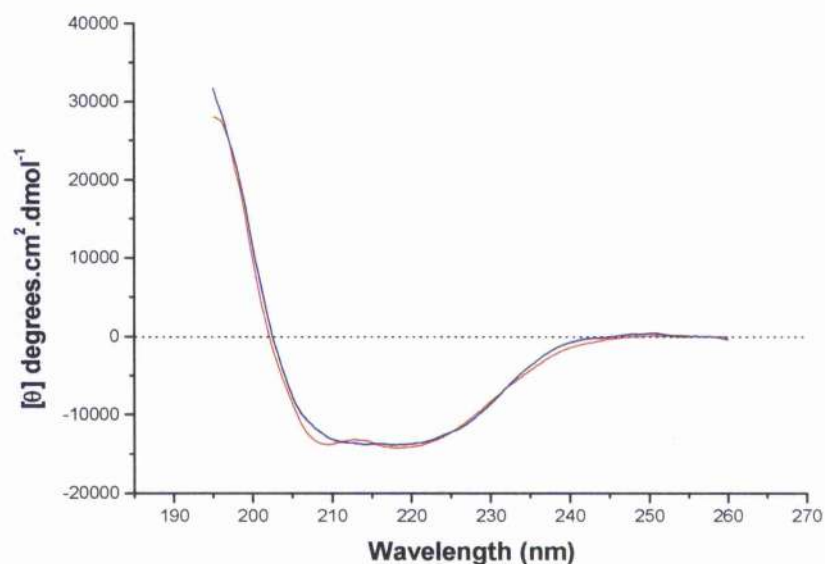


Figure 36. The far UV CD spectra of *B. subtilis* wild type YqhS protein (red) and mutant F23Y YqhS (blue).

4.4 Kinetic comparison of wild type and mutant enzymes

Assays of *B. subtilis* YqhS and the mutant F23Y YqhS were performed in a 1 ml quartz cuvette with a 1cm pathlength containing 34 μg of enzyme, 100 μM dehydroquinate, 50 mM Tris-acetate buffer; (pH 7.0) at 25°C (2.16.1). The enzymic reaction was followed by monitoring an increase in absorbance at 234 nm. The YqhS protein was shown to have an extremely low level of catalytic activity ($k_{\text{cat}} < 10^{-4} \text{ s}^{-1}$). It was only possible to observe this very low activity because of the purity of the substrate prepared by Lorna Noble, A. Herbert had previously failed to find activity but his substrate was not pure. The site-directed mutant F23Y YqhS shows at least a 2000-fold increase in activity (Figure 37). K_m and V_{max} values were obtained for F23Y YqhS by varying the substrate concentration in the assays between 0.1 mM and 2 mM. The $\Delta A_{234\text{min}^{-1}}$ was fitted to a non-linear regression plot (2.18) to yield values for k_{cat} of 0.18 s^{-1} and K_m of 730 μM .

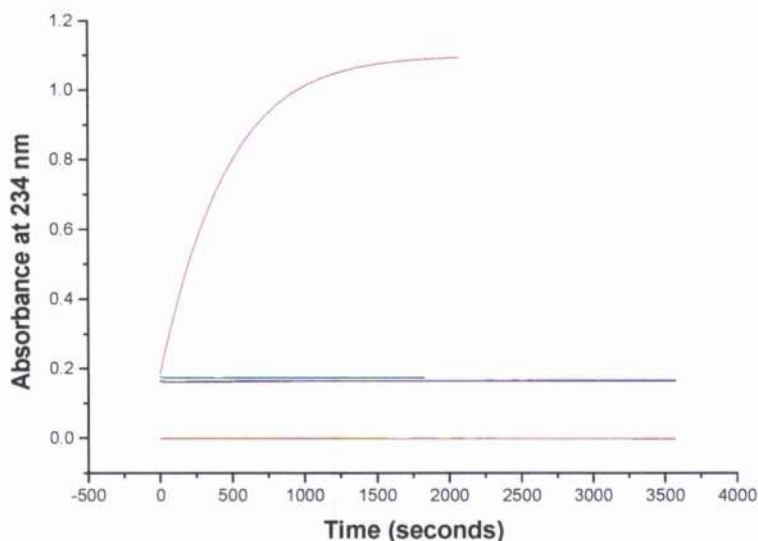


Figure 37. Activity assay of *B. subtilis* YqhS wild type and F23Y mutant measuring the increase in absorbance at 234 nm. The stability of the substrate over the time course is shown in red. The wild type *B. subtilis* YqhS protein in assay buffer is shown in green. The wild type YqhS protein is shown in blue and the F23Y mutant is shown in magenta.

4.5 Detection of YqhS in *B. subtilis* cell extract

4.5.1 Western blotting

In order to study whether YqhS is expressed *in vivo*, western blots were performed using antibodies raised against the F23Y YqhS mutant as described in section 2.14.1. The antibodies had been raised against the mutant, as there was more of this protein available than of the wild type. Circular dichroism analysis showed no significant differences in secondary structure between the wild type and mutant YqhS (4.3.4). The polyclonal antibodies were tested against both the mutated and wild type YqhS protein (Figure 38).

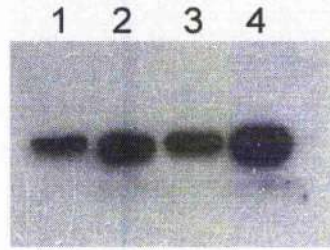


Figure 38. Western blot of purified *B. subtilis* wild type and F23Y mutant YqhS protein using polyclonal antibodies raised against the F23Y YqhS mutant protein. Lanes 1,2: purified wild type YqhS, 5 and 1 μ g, respectively. Lanes 3,4: purified F23Y mutant YqhS, 5 and 1 μ g, respectively.

B. subtilis was grown in nutrient broth (NB) and Spizizen minimal medium (SMM) (2.5.2) for 24 or 48 hours at 37°C. The growth was categorised and checked for contamination by further growth on NB agar for 24 hours at 37°C and colonies were checked for phenotypic characteristics. 1.5 ml of the *B. subtilis* culture was centrifuged at 16,000 \times g for 5 minutes and prepared for SDS PAGE as described in section 2.11. Western blots were performed on the SDS PAGE gels as described in section 2.14 with polyclonal antibodies raised against the F23Y YqhS and the denatured *E. coli* type I dehydroquinase (2.14.1).

The results of the western blot for the YqhS protein show high affinity binding to a protein with a molecular weight of 22.5 kDa; approximately 6 kDa larger than YqhS and slightly lower affinity binding to another protein of approximately 39 kDa (Figure 39). The western blot for the type I dehydroquinase showed some non-specific high affinity binding to a protein the same size as the *E. coli* type I dehydroquinase control (25 kDa) (Figure 39).

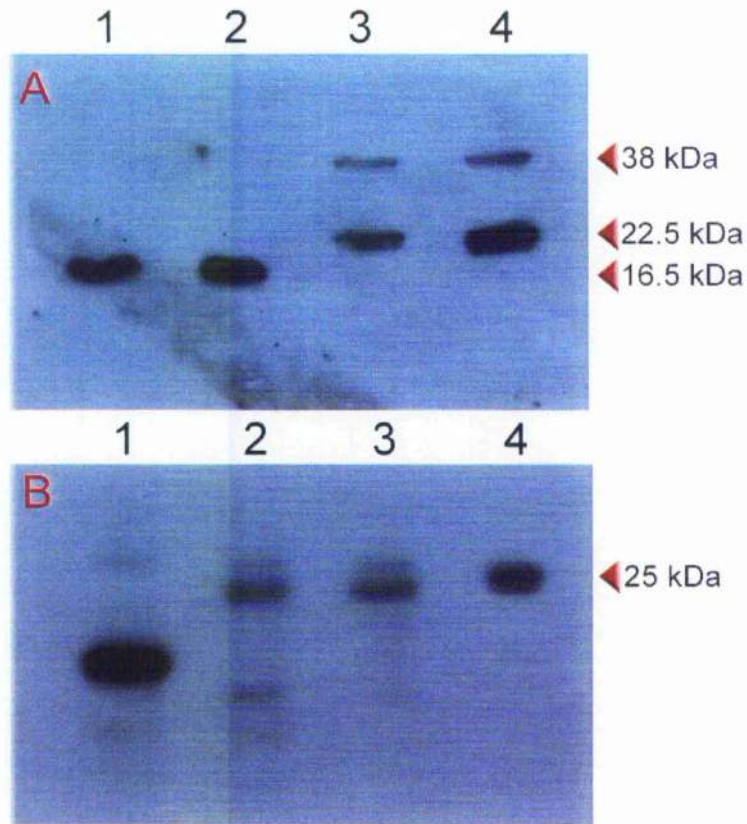


Figure 39. Western blots of *B. subtilis* (derivative 168) cell extract. (A) Using antibodies raised against F23Y YqhS protein. Lanes 1,2: purified YqhS and F23Y YqhS, respectively. Lanes 3,4: *B. subtilis* cell extract grown in NB medium and minimal medium, respectively. (B) Using antibodies raised against *E. coli* type I dehydroquinase. Lane 1: Boehringer Mannheim marker low-range. Lanes 2,3: *B. subtilis* cell extract grown in NB medium and minimal medium, respectively. Lane 4: purified *E. coli* type I dehydroquinase.

4.5.2 Proteomics approach

In an attempt to identify the 22.5 kDa protein which had a high affinity to the antibodies raised against the YqhS mutant, two approaches were used to separate the 22.5 kDa protein 2D SDS PAGE:- electrophoresis and immunoprecipitation. While these methods were being attempted the disruption mutant (YqhSd) was sent by Prof. Sato of the Tokyo University of Agriculture and Technology. The approaches used

to separate and identify the 22.5 kDa protein results are described below. There was insufficient time to optimise the procedures.

4.5.2.1 2-DE of *B. subtilis* cell extract

2-DE was carried out as described in section 2.15.1 on samples taken from a 3 ml culture of *B. subtilis* (derivative 168) culture grown in nutrient broth for 48 hours at 37°C and disrupted by ultrasonication (2.15.1). Characterisation of *B. subtilis* proteins by 2-DE during exponential growth and glucose starvation show a decrease in the relative synthesis rate of chorismate mutase (*AroA*) when limiting amounts of glucose were used (0.05%) (Schmid *et al.*, 1997). Four 2-dimensional gels were run: two were loaded with approximately 200 µg of *B. subtilis* cell extract protein (gels 1,2) and one 'control' was loaded with 100 µg of purified *B. subtilis* YqhS (gifted by A. Herbert) (gel 3). The fourth gel was loaded with approximately 100 µg of *B. subtilis* cell extract protein and 100 µg *B. subtilis* YqhS (gel 4). Protein samples were separated in the first dimension using a pII 4-7 linear gradient immobilisation strip from Amersham Pharmacia Biotech and in the second dimension by 15% (w/v) SDS PAGE (2.11).

After the second dimension separation western blots were performed on gels 2, 3 and 4 using antibodies raised against F23Y YqhS (2.14) and gel 1 was stained with Coomassie Blue (2.11.1). The gels and western blots are shown in Figure 40.

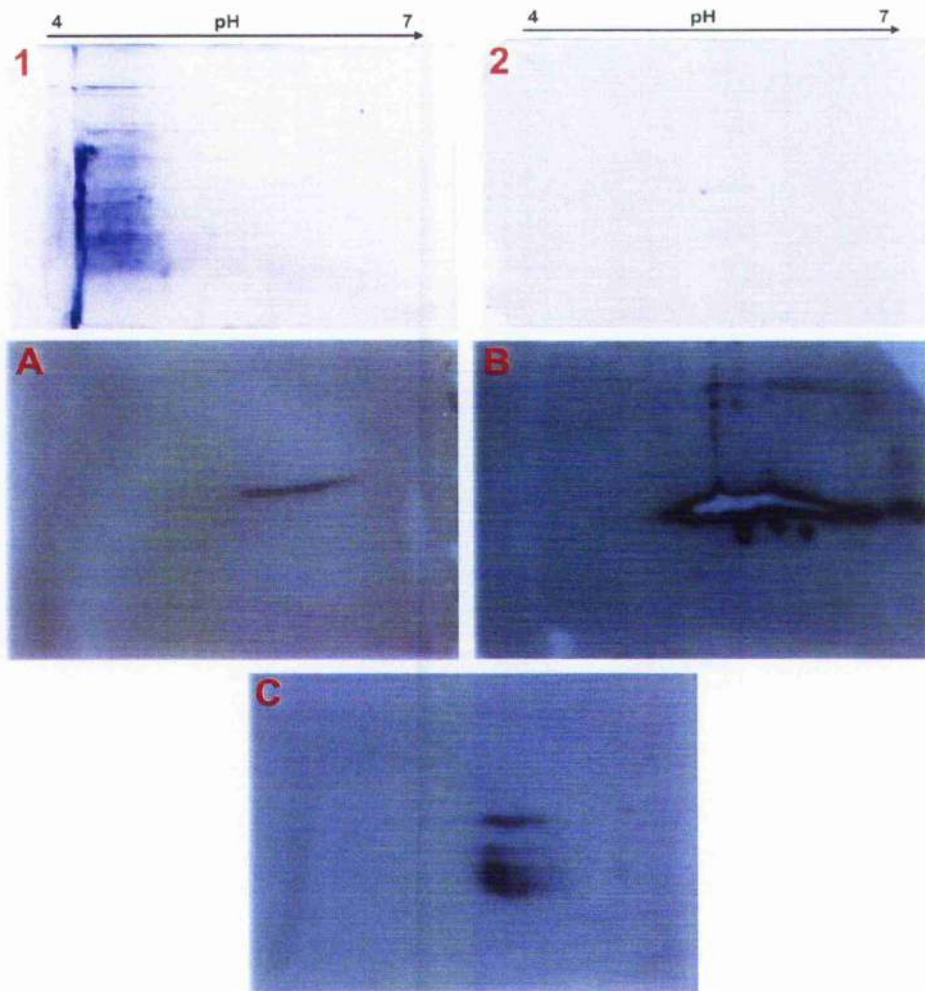


Figure 40. 2-dimensional SDS PAGE of *B. subtilis* (derivative 168) crude extract (1) and purified YqhS protein (2) separated by pH 4 to 7 isoelectric gradient and then by SDS PAGE. Western blots using antibodies raised against the YqhS mutant (F23Y) on 2-dimensional SDS PAGE: (A) 200 μg of *B. subtilis* (derivative 168) crude extract, (B) 100 μg of purified YqhS protein, (C) 100 μg of *B. subtilis* (derivative 168) crude extract and 100 μg of purified YqhS protein.

Both the YqhS and 22.5 kDa protein seemed to focus at approximately pH 5.5 (suggesting that the pI of the two protein is similar). However, there was a 6 kDa difference in molecular weight. Although gels 1 and 2 were run in parallel in the same electrophoresis tank there were slight differences in the way in which they separated the proteins. The separation of the proteins from the *B. subtilis* cell extracts show some smearing of the spots; this could be a result of the ionic strength being too

high in the *B. subtilis* growth medium (2.3.1) causing poor focusing of the isoelectric first dimension step. This made the excising spots that had affinity to the F23Y YqhS antibodies difficult. Nonetheless, the spots were excised and digested with trypsin (2.15.3) and prepared for MALDI mass spectroscopy (2.15.4).

4.5.2.2 Protein A immunoprecipitation of *B. subtilis* cell extract

Protein A immunoprecipitation was carried out as described in section 2.15.2 using the Pierce Seize™ Classic (A) immunoprecipitation kit. 3 ml of *B. subtilis* (168) culture grown in nutrient broth for 48 hours at 37°C was disrupted (2.5.3). 40 µl of F23Y YqhS antibody serum (approximately 60 µg of antibody) was added to 200 µl of supernatant and incubated for 1 hour at 20°C. Elution and wash fractions were collected and separated by SDS PAGE (Figure 41).

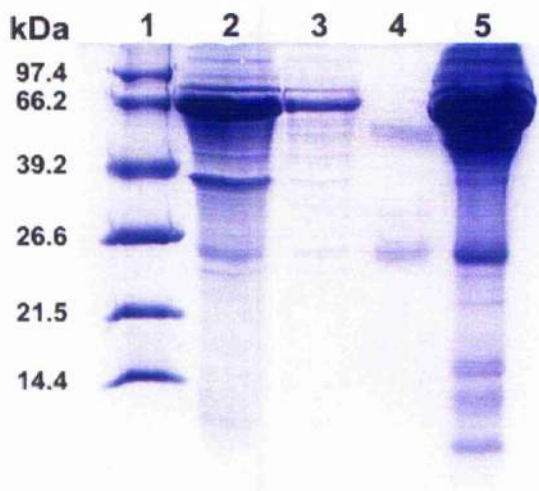


Figure 41. SDS PAGE (15% acrylamide) analysis of protein A immunoprecipitation of *B. subtilis* cell extract. Lane 1: Boehringer Mannheim marker low-range, lane 2 and 3: wash fractions. Lane 4 elution fraction. Lane 5: primary polyclonal antibody (immunoglobulin G) raised against YqhS F23Y.

The results from the polyacrylamide gel show that there are several contaminating proteins within the antibody serum. The majority of the proteins found in the wash fractions of the protocol are likely to be from the antibody serum. Without the use of detergent, which was omitted due to possible interaction with the antibody, the disruption of *B. subtilis* cells may have been compromised.

In the elution fractions of the immunoprecipitation the heavy chain (~50 kDa) and light chain (~25 kDa) of the antibody are clearly visible. Due to the light chain being of a similar molecular weight to the 22.5 kDa protein the Pierce Seize™ X Protein A immunoprecipitation kit was used to avoid antibody contamination in the elution fraction.

The Pierce Seize™ X Protein A immunoprecipitation kit overcomes this problem by immobilising the primary antibody to protein A via the Fc region of the antibody, using a cross-linking reagent Disuccinimidyl subcrate (DSS). Preliminary experiments failed to cross-link the primary antibody to protein A (results not shown) and this approach to purify YqhS was abandoned.

4.5.2.3 Mass Spectrometry

MADI-tof Mass spectrometry was carried out by Sharon Kelly; this proved inconclusive as there were insufficient quantities of peptide to detect.

4.5.3 Disruption mutant (YqhSd)

The complete genome sequence of *B. subtilis* was published in 1997 (Kunst *et al.*, 1997) this revealed approximately 1800 genes with no established function (~43% of the entire genome). The International *Bacillus* Consortium has studied the functionality of these genes, using gene disruption techniques followed by the monitoring of the effect on cell fitness under different growth conditions. A network of 18 European and 12 Japanese laboratories have completed a gene-by-gene inactivation procedure of >95% of all the genes with unknown functions (Ogasawara, 2000; Kobayashi *et al.*, 2003). This was achieved by using the pMUTIN vectors, which allow insertion mutagenesis. Some of the other benefits of the pMUTIN vectors are that they possess a reporter *lacZ* gene, to facilitate the measurement of the expression of the target gene and an inducible promoter to allow controlled expression of the genes downstream of, and found in the same operon as, the target gene (Vagner *et al.*, 1998). The target gene is inactivated by the insertion of the pMUTIN vector within the gene in a single crossover event (Figure 42).

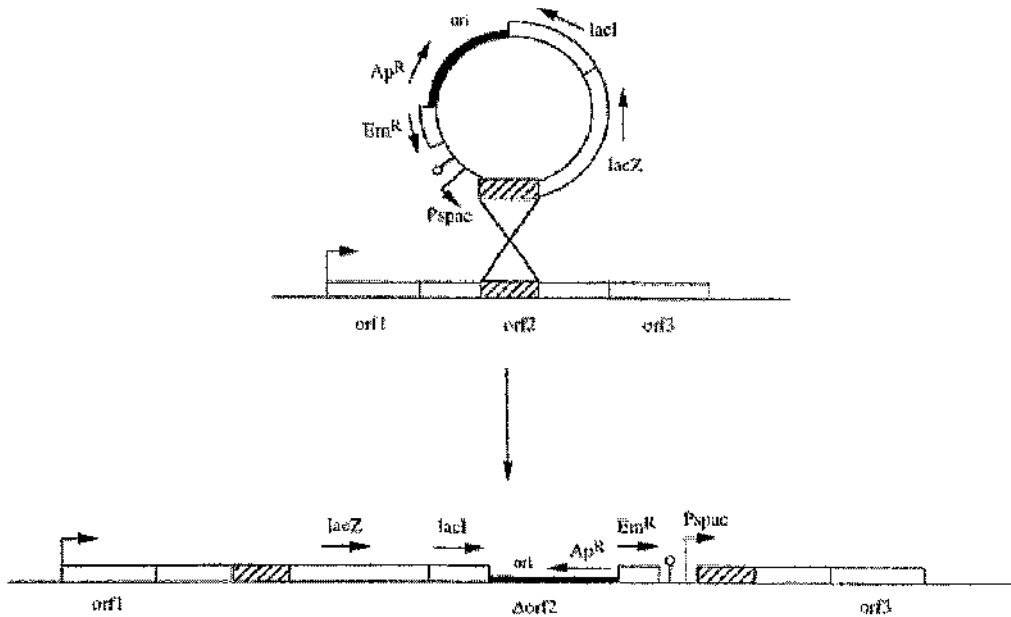


Figure 42. Integration of pMUTIN vector into a target gene. Genes of the *orf1-orf3* operon are indicated as white boxes. Hatched box corresponds to the internal segment of the target gene. The vector is integrated in *orf2* by a single crossover event. Arrows indicate direction of transcription, broken arrows denote the promoter of the operon and *Pspac*, and the lollipop strand is for the transcription termination. This figure is from Vagner *et al.*, 1998.

Among the $\approx 4,100$ genes in *B. subtilis* only 192 were found to be essential and another 79 genes were predicted to be essential. About 80% of the functions that the essential genes encode fall into a few large categories; namely, information processing, cell envelope, shape, division, and energetics. (Kobayashi *et al.*, 2003). The *yqhS* gene was not among the group of genes thought to be essential in *B. subtilis* for growth in LB.

Prof. Sato from Tokyo University of Agriculture and Technology (part of the Japanese *Bacillus* Consortium) gifted the *B. subtilis* (168) disruption mutant for YqhS (YqhS Δ). Growth experiments on the YqhS Δ strain by the Japanese *Bacillus* Consortium had shown that the disruption mutant was able to grow in Schaffer's medium but not in minimal media. Independent growth experiments were performed to test these findings (4.5.3.1). The sporulation frequency was found to be $>2.0 \times 10^{-1}$ (Prof. Sato and Michio Takeuchi personal communication).

The YqhSd strain given by Prof. Sato was tested for erythromycin resistance by growing the strain at 37°C for 24 hours in the presence of 1 µg/ml of erythromycin. The YqhSd strain was then western blotted using the F23Y YqhS antibodies as described in section 4.5.1.

The western blot of the YqhSd cell extract revealed high affinity for the 22.5 kDa protein (Figure 43). This proves that the 22.5 kDa protein is not a modified YqhS and is more likely to represent non-specific binding to the antibody.

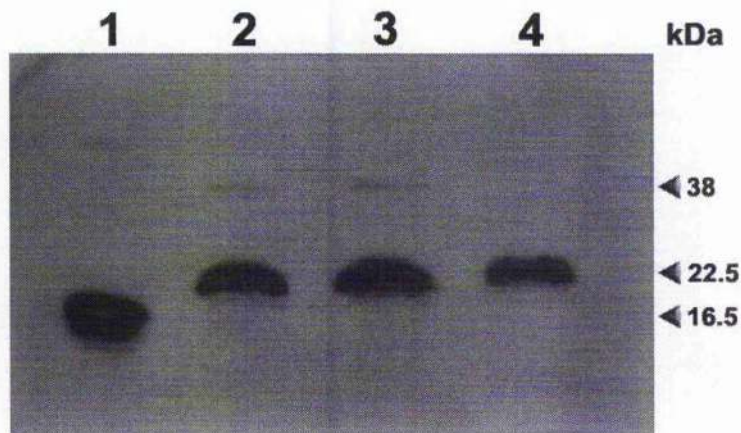


Figure 43. Western blot of *B. subtilis* derivative 168 and YqhSd cell extracts using antibodies raised against YqhS F23Y protein. Lane 1: purified wild type *B. subtilis* YqhS protein. Lanes 2,3: *B. subtilis* (derivative 168) cell extract grown in NB medium and minimal medium, respectively. Lane 4: *B. subtilis* (YqhSd) cell extract grown in NB medium.

4.5.3.1 Growth experiments on the YqhSd mutant.

Independent growth experiments were performed on the YqhS disruption mutant to support growth studies performed by the Japanese *B. subtilis* Consortium. 100 ml cultures were set up from an overnight culture of both the disruption mutant and derivative 168 in nutrient broth (NB) and minimal medium (SMM) (Anagnostopoulos and Spizizen, 1960) with and without glucose (2.3.1). When glucose was utilised it was added to a final concentration of 0.5% (w/v). Cultures were grown under aerobic conditions shaking at 200 rpm at 37°C. The initial absorbance at 600 nm was calculated to be approximately 0.009. Absorbance at 600 nm was measured of *B. subtilis* growth experiments growth at various time intervals; the results are shown in Table 10.

Table 10. *B. subtilis* disruption mutant (YqhSd) growth experiment.⁴

B.subtilis strain	Medium	Hours of growth	A ₆₀₀ measurement
YqhSd	NB ³	15	1.177
		18	1.178
		44	0.533 ^w
WT	NB	15	1.418
		18	1.420
		44	0.680 ^w
YqhSd	SMM ⁴ + Glucose	15	0.087
		18	0.104
		44	0.083
WT	SMM + Glucose	15	1.289
		18	1.386
		44	1.479
YqhSd	SMM	15	0.025
		18	0.058
		44	0.062
WT	SMM	15	0.169
		18	0.212
		44	0.266

³ NB, Nutrient Broth^wCarbon starvation⁴ SMM, Minimal Medium

There does not appear to be any growth of the disruption mutant (YqhSd) in minimal medium and very little growth if any in minimal medium including 0.5% glucose. The wild type *B. subtilis* grows well in minimal medium with 0.5% glucose and only very slowly in minimal medium without glucose. Reduction in growth of both the wild type and mutant in nutrient broth is thought to be due to carbon starvation leading to cell death.

4.6 Inactivation of *B. subtilis* type I dehydroquinase from cell extract

To establish whether the dehydroquinase activity from *B. subtilis* cell extract was due to a type I enzyme, sodium borohydride (NaBH_4) reduction and heat treatment studies were performed on the extract. Sodium borohydride (NaBH_4) was used in an attempt to trap the Schiff base intermediate produced by the type I dehydroquinase mechanism (Butler *et al.*, 1974; Chaudhuri *et al.*, 1991; Kleanthous *et al.*, 1991).

200 ml cultures were set up of *B. subtilis* 168, *B. subtilis* disruption mutant (YqhSd) and *E. coli* DH5 α (which possess only a type I dehydroquinase); these were grown at 37°C for 18 hours in NB and LB, respectively (2.5). Cells were harvested by centrifugation at $5,000 \times g$ for 15 minutes, yielding approximately 0.5g wet weight of *B. subtilis* 168 and YqhSd and approximately 0.75 g wet weight of *E. coli* DH5 α . Harvested cells were split between potassium phosphate buffer (100 mM; pH 7.0) and Tris:acetate buffer (100mM; pH 7.0). This was because type I dehydroquinase catalytic activity is assayed in phosphate buffer but type II dehydroquinase activity is assayed in Tris:acetate since phosphate is a competitive inhibitor of the latter enzymes (5.4.5). The resuspended cells were homogenised by a French pressure cell (2.5.3) in a total volume of 0.75 ml and centrifuged at $16,000 \times g$ for 15 minutes at 4°C. For the chemical modification experiments a 10 mg/ml solution of NaBH_4 (in 40 mM NaOH) was added 10 seconds after the addition of dehydroquinase and then incubated for 20 minutes at 20°C. *E. coli* cells extracts were diluted 5-fold and *B. subtilis* cells extracts were diluted 1.1-fold, incubated in 1 mM dehydroquinase with either 0 mM, 0.1 mM or 0.5 mM NaBH_4 . Additional incubations were performed using purified *E. coli* (strain reference code: AB2848/PKD203) type I dehydroquinase (gifted by John Greene) and *S. coelicolor* type II dehydroquinase (2.12.1). Incubations of the purified *E. coli* type I dehydroquinase (0.1 mg/ml) and *S.*

coelicolor (0.01 mg/ml) were only performed in their assay buffers, in 1 mM dehydroquinate followed by the addition of either 0 mM or 0.5 mM NaBH₄.

The volume of each of the incubations was kept equal by the addition of distilled water (200 µl total volume). 20 µl of each incubation was assayed for dehydroquinase activity by monitoring the increase at 234 nm (2.16.1), using 1 mM dehydroquinase in either potassium phosphate or Tris-acetate buffers in a total volume of 1 ml. All assays were performed in duplicate.

The results of the chemical modification with NaBH₄ are shown in Table 11 below.

There is a 95.5% reduction in catalytic activity of the purified *E. coli* type I dehydroquinase by treatment with NaBH₄ in the presence of substrate. The purified type II dehydroquinase shows only a 21% reduction in activity. The activities of extracts in different buffers could not be compared directly with each other because no steps were taken to ensure that the degree of cell lysis was constant. For each extract, activities are referred to the value obtained in the absence of added NaBH₄. In all cases NaBH₄ significantly reduced the catalytic activity of the cell extracts. It is likely that the dehydroquinase reaction is catalysed via a Schiff base intermediate in *B. subtilis*, and therefore the type I dehydroquinase from *B. subtilis* is likely to contribute the catalytic activity. The *B. subtilis* YqhSd strain showed catalytic activity, confirming that the YqhS protein is not involved in the dehydroquinase reaction.

Table 11. Sodium borohydride (NaBH_4) chemical modification experiments on *E. coli* and *B. subtilis* cell extracts and purified *E. coli* type I dehydroquinase and *S. coelicolor* type II dehydroquinase.

	Buffer (100 mM; pH 7.0)	[NaBH_4] (mM)	Average activity ($\Delta\Lambda_{234}\text{min}^{-1}$)	% Activity loss in respect to 0 mM NaBH_4
<i>E. coli</i> cell extract	K phosphate	0	0.03522	-
		0.1	0.02097	40.5
		0.5	0.00373	89.4
	Tris:acetate	0	0.03996	-
		0.1	0.02201	45
		0.5	0.00306	92.3
<i>B. subtilis</i> 168 cell extract	K phosphate	0	0.01583	-
		0.1	0.00209	87
		0.5	0.0	100
	Tris:acetate	0	0.01178	-
		0.1	0.0	100
		0.5	0.0	100
<i>B. subtilis</i> YqhSd cell extract	K phosphate	0	0.02131	-
		0.1	0.00188	91
		0.5	0.0	100
	Tris:acetate	0	0.01329	-
		0.1	0.0	100
		0.5	0.0	100
<i>E. coli</i> type I dehydroquinase	K phosphate	0	5.479	-
		0.5	0.2456	95.5
<i>S. coelicolor</i> type II dehydroquinase	Tris:acetate	0	1.399	-
		0.5	1.108	21

The thermostability of type I dehydroquinases (57°C in *E. coli*) is significantly lower than the type II dehydroquinases (82°C in *A. nidulans*) (Kleanthous *et al.*, 1992). This difference in stability was used to explore the properties of the catalytically active dehydroquinase in *B. subtilis* cell extracts. Cell extracts of *E. coli* and *B. subtilis* were prepared as described previously. 200 µl of each cell extract was subjected to heat treatment of 65°C for 5 minutes. Assays were performed using 20 µl of sample and 1 mM dehydroquinone in both potassium phosphate and Tris-acetate buffers, 1 ml volume. Upon heat treatment of the *B. subtilis* and *E. coli* cell extract there was a complete loss of catalytic activity (data not shown). This study also points towards the catalytic activities observed in *B. subtilis* cell extracts being entirely contributed by the type I dehydroquinase from *B. subtilis*.

4.7 Chapter summary

B. subtilis YqhS was shown to have an extremely low level of catalytic activity and is therefore not a functional dehydroquinase. The site-directed mutant F23Y of YqhS shows at least 2000-fold increase in activity from the wild type, confirming the importance of this residue. F23Y YqhS displays a K_m of 730 µM and k_{cat} of 0.18 s⁻¹; k_{cat}/K_m is 2.5×10^2 M⁻¹s⁻¹. Compared with other type II dehydroquinases such as *S. coelicolor* (K_m of 100 µM and k_{cat} of 120 s⁻¹; k_{cat}/K_m is 1.2×10^6 M⁻¹s⁻¹) this is still an extremely low level of activity. Although, it is broadly within the range observed for the type II dehydroquinases from *Helicobacter pylori* (K_m of 205.75 µM and k_{cat} of 0.94 s⁻¹), *M. tuberculosis* (K_m of 170.8 µM and k_{cat} of 5.17 s⁻¹) and *Neurospora crassa* (K_m of 70 µM and k_{cat} of 0.08 s⁻¹) (Hautala *et al.*, 1975, Kleanthous *et al.*, 1992); there must be other factors involved in improving the catalytic efficiency of the high activity DHQases. The 3-dimensional structure shows that the potential active site is much shallower in the *B. subtilis* enzyme than in any other functional type II dehydroquinase.

The type I dehydroquinase is the catalytically active dehydroquinase as shown by inactivation experiments (4.6) chemical modification using NaBH₄ to react with an essential lysine in type I DHQ forming a Schiff base. Heat treatment of the cell extract also suggested that a type I DHQase was the active DHQase in *B. subtilis*.

If YqhS is expressed although catalytically compromised, it must still confer some evolutionary advantage indicating a possible second function for AroQ. DNA

microarray experiments in *B. subtilis* showed higher levels of the mRNA for the *yqhS* (the Type II DHQase) than for *aroC* (the Type I DHQase) (personal communication from Rick W. Ye). Direct investigation of the expression of the YqhS protein using antibodies proved to be inconclusive. This does not mean that the YqhS protein is not expressed; YqhS may be expressed under different conditions than those investigated here. Further western blot experiments of *B. subtilis* cell extract under different growth and stress conditions including heat shock, salt and ethanol stress and glucose and phosphate starvation may provide direct evidence of expression. It should be noted that the *B. subtilis* microarray experiments were conducted with 2 × YT medium, while the western blot experiments were conducted using Nutrient broth. This difference only came to light late during the investigations and a direct comparison should be performed. It would also be useful to carry out western blots on *B. subtilis* cell extracts that have been exposed to different stress conditions. The YqhS protein is extremely thermostable and retains 50% of its secondary structure in 6 M GdmCl (4.3.1.1). It is possible that it may play a role in heat or salt stress response. The high resolution 3D X-ray crystallography structure (D. Robinson, 2003) shows that there is a large cavity in the middle of the YqhS dodecameric structure which is also seen in all other type II dehydroquinases. This could provide a possible clue to the proposed second function of type II dehydroquinases. There are a number of conserved side chains within the cavity of the dodecamer, including His85, Glu59 and Asp64 (*S. coelicolor* DHQase numbering system); it is unclear whether these side chains are purely structural or are involved in an as yet unknown function. This cavity may be suitable to assist protein folding even though it is not hydrophobic; thus YqhS could be a molecular chaperonin or a heat shock protein. If YqhS is expressed in response to either heat or salt stress, it could also be linked to the formation of endospores.

B. subtilis can differentiate to form heat-resistant endospores in response to starvation of carbon, nitrogen or phosphorus. Spore formation can be divided into a basic sequence of morphological changes: at the start of differentiation (stages 0 to II) there is one cell type; two complete chromosomes are formed, an asymmetrically sited septum is formed separating the two genomes of the cell. In the second phase (stages II to III) the differentiation becomes fixed and the two distinct genomes start to function differently. The junction of the septum and the outer surface of the

sporangium migrates to the pole of the sporangium and the developing forespore is then engulfed by the mother cell. At stage III *B. subtilis* has irreversibly differentiated into two different cell types, and the forespore can only return to vegetative growth by spore formation and then germination. The forespore develops resistance and dormancy properties to form the mature spore within the mother cell (stages III to VII). The cortex and primordial germ cell wall are formed (stage IV) followed by the development of a proteinaceous spore coat around the forespore at stage V. The two final stages are the maturation of the spore (stage VI) and the release of the mature spore by the lysis of the mother cell (stage VII) (Errington, 1993).

The inactivation procedure using pMUTIN vector system incorporates the *lacZ* gene (2.8.3) as part of the disruption of the target gene. The Japanese *Bacillus* consortium have used this gene during growth experiments on the disruption mutant YqhSd to monitor the expression of the target operon. YqhSd shows an increase in β -galactoside activity during exponential growth, this indicates that the open reading frame in which *yqhS* is situated is expressed.

The *yqhS* gene is located in the genome close to a series of genes which when mutated block sporulation after engulfment (*spoIIIAA-AH*) (Sharp and Pogliano, 1999). Directly downstream of the *yqhS* gene is a gene encoding for a Xaa-Pro dipeptidase followed by a gene encoding for elongation factor P. Directly upstream of the *yqhS* is a conserved protein of unknown function (*yqhT*). The arrangement of these genes is the same as in *B. anthracis* and *B. halodurans* both of which possess a type II dehydroquinase. *Oceanohacillus theyensis* possess a type I dehydroquinase, but also possesses the genetic region containing the genes encoding for the Xaa-Pro dipeptidase, elongation factor P and conserved protein of unknown function; however the gene encoding for a type II dehydroquinase is not present. This seems to suggest that the *Bacillus* family members that possess a type II dehydroquinase share a common ancestor which has had the *yqhS* gene inserted into this region without the incorporation of any other genes. Studies on the *SpoIIA* gene (Piggott *et al.*, 1984) revealed that polycistronic transcription units are involved in sporulation of *B. subtilis*. This helps to organise and regulate the complex process of sporulation. YqhS may be within the polycistronic unit that transcribes the *spoIIIAA-AH* genes. It is still possible that YqhS performs some role during sporulation, although first level

phenotype analysis of the YqhSd strain by the Japanese *Bacillus* consortium, reveals that the YqhSd strain is able to produce spores. The shikimate pathway genes; *aroE*, *H*, *B* and *F* are also grouped together (Kunst *et al* 1997) and may also be expressed as a polycistronic transcription unit; however it should be noted that the *aroA* (chorismate mutase) and *C* (type I DHQase) are not grouped. The location of the type I dehydroquinases in *B. subtilis*, *O. iheyensis* and *B. stearothermophilus* are not analogous.

B. subtilis contains several different σ factors which play an important role in reprogramming the cell in response to different environmental conditions. Vegetative growth is controlled by σ^A , other responses included the formation of an endospore controlled by σ^H , σ^E , σ^F , σ^G and σ^K , motility, chemotaxis and autolysin controlled by σ^D and the expression of general stress proteins controlled by σ^B (Horsburgh *et al.*, 2001). Stress response is activated by two discrete stress classifications: energy stresses such as carbon, phosphorus or oxygen limitation and environmental stresses such as acid, ethanol, heat or salt stress (Akbar *et al.*, 2001). In several studies of stress response in *B. subtilis* particularly in relation to σ^B YqhS has not been identified as being involved including; microarray profiles of *B. subtilis* grown under anaerobic conditions (Ye *et al.*, 2000) and high resolution 2-DE monitoring the changes in expression levels of proteins under different stress conditions: salt, heat, ethanol, oxidative stress and glucose starvation. This latter comprehensive study of general stress proteins in *B. subtilis* and σ^B mutants was performed by Bernhart *et al.* (1997). The 2-DE studies identified 42 general stress protein which require σ^H , but seven which did not. It is possible that YqhS is expressed in stress conditions that have not been characterised and is not regulated by σ^B .

Expression of the disrupted gene was found to increase at the end of exponential growth in the enriched medium. It has been confirmed that, unlike the wild-type strain of *B. subtilis*, the *yqhS*-disrupted mutant will not grow on minimal medium with either glucose or citrate as a carbon source. While the *B. subtilis* wild type is able to grow on minimal medium with glucose and shows poor growth on citrate as a carbon source. *B. subtilis* growth experiments on TCA cycle intermediates as the sole carbon source show that citrate is a viable carbon source for *B. subtilis* as measured by optical density at 600 nm and involves the Mg^{2+} -citrate transporter CitM

(Warner and Lolkema, 2002). The disruption mutant and wild type both grow very well on nutrient broth. Although nutrient broth does not contain major amounts of carbohydrate or fatty acids, growth on nutrient broth by amino acid degradation provides energy and allows incorporation of many preformed polymer precursors. Energy produced via the tricarboxylic acid (TCA) cycle oxidation provides precursors for gluconeogenesis which is essential to supply glycerol, hexoses, hexosamines and pentoses. The disruption mutant must have the gluconeogenic pathway and at least some reactions of TCA cycle as the YqhSd strain is operating to degrade amino acids (Dr. Fixter, personal communication). Analysis of the *B. subtilis* genome revealed nine genes associated with citrate regulation, transport and metabolism.

Thus although YqhS protein is functional, the precise role of this protein is still unclear. Auxotrophic studies on the disrupted mutant should be performed, in order to establish the precise nature of the YqhSd strain and to define more clearly the role of the YqhS protein in *B. subtilis*. These studies might provide the opportunity to dissect out an additional function for proteins with the type II DHQase structure. This study offers an insight into how new functions may evolve in existing protein families.

CHAPTER 5 KINETIC AND STRUCTURAL STUDIES OF TYPE II DEHYDROQUINASES FROM DIFFERENT BACTERIAL SPECIES

5.1 Introduction

The type II dehydroquinase (DHQases) which have been characterised kinetically appear to fall into two main groups. The enzymes from organisms such as *S. coelicolor* and *Aspergillus nidulans* have relatively high values of k_{cat} , in the range 100 to 1000 s⁻¹ at pH 7.0 and 25°C (Klcanthous *et al.*, 1992; Krell *et al.*, 1996). By contrast, the enzymes from *Helicobacter pylori*, *M. tuberculosis* and *Neurospora crassa* have much lower values of k_{cat} in the range 10 s⁻¹ or lower (Hautala *et al.*, 1975; Bottomley *et al.*, 1996a; Price *et al.*, 1999). There appears to be no obvious correlation between the values of k_{cat} and K_m for these enzymes. Sequence alignments of these show strict sequence conservation of all the amino acid residues implicated in catalysis (Appendix C; **Error! Reference source not found.**) with the exception of Ser 56 which is a threonine in *H. pylori* (*S. coelicolor* numbering of amino acids). Comparisons of the orientations of the residues within the active site by X-ray crystallographic data (Figure 44) shows there are no large differences in the orientation of the residues within the active site, apart from the finding that the lid domain (residues 19 to 26 in *M. tuberculosis* DHQase) of two of the lower activity species (*H. pylori* and *M. tuberculosis*) is not resolved.

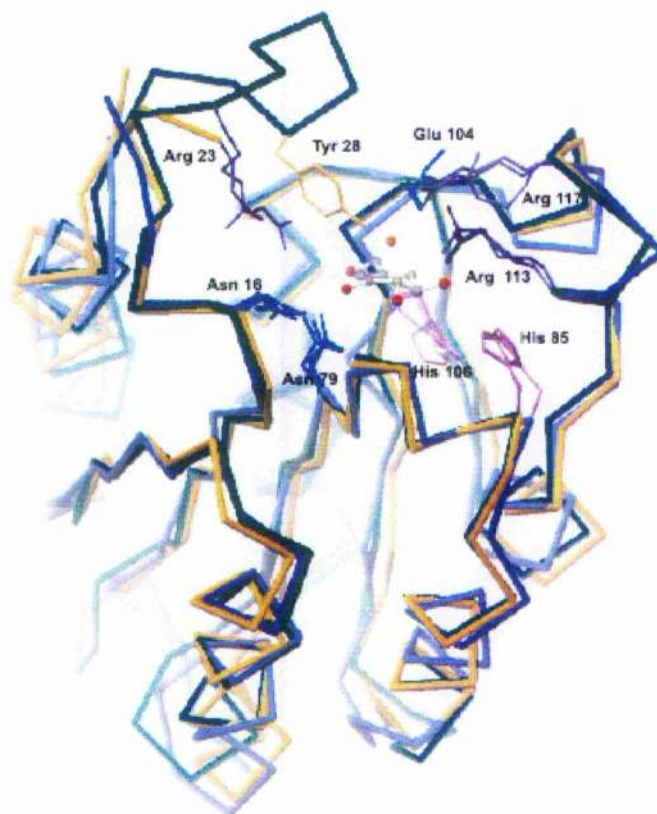


Figure 44. Overlay of subunits from *Streptomyces coelicolor* (green), *Mycobacterium tuberculosis* (orange) and *Helicobacter pylori* (blue). Residues thought to be involved in catalysis are highlighted using the numbering system from *S. coelicolor*. Dehydroshikimate is bound in the active site.

The activity of *Aspergillus nidulans* and *M. tuberculosis* DHQases were shown to be pH-dependent, activity increased with pH (Kleanthous *et al.*, 1992; Harris *et al.*, 1996a) over the range 6.3 to 9.0. Above pH 8.0 it is possible that a decrease in the stability of the substrate may affect the interpretation of the results. In this chapter, the pH-dependence of the activities of *S. coelicolor*, *H. pylori* and *M. tuberculosis* type II DHQases and the *B. subtilis* YqhS F23Y mutant were investigated over a pH range of 6.5 to 8.0, in order to characterise the differences in catalytic properties in greater detail.

It had been originally speculated that the differences in the levels of catalytic activity were due to variations in flexibility of the structures especially within the lid domain

of the active site. Unfolding experiments on *S. coelicolor* and *M. tuberculosis* DHQase showed a complete loss in activity of the *S. coelicolor* enzyme at 3.75M guanidinium chloride (GdmCl) but also revealed a significant activation of the *M. tuberculosis* enzyme by low concentrations of GdmCl (0.5-1.0M) at pH 7.5 in Tris-HCl (Price *et al.*, 1999). This type of activation in the presence of moderate concentrations of denaturant had been previously observed in a number of systems including *Thermotoga maritima* glyceraldehyde 3 phosphate dehydrogenase which is activated by 300% in 0.5M GdmCl (Rehaber and Jaenicke, 1992) and adenylate kinase from rabbit muscle which shows a 60% increase in activity in 1M urea (Zhang *et al.*, 1997). Human phenylalanine hydroxylase is transiently activated by 10 and 100-minute incubations of between 0 and 4 M urea in the absence of the substrate L-phenylalanine (Kleppe *et al.*, 1999). It has been suggested that the activation by denaturants of dehydroquinases may be due to increasing conformational flexibility at the active site (Price *et al.*, 1999). Denaturation experiments using GdmCl and Urea (NaCl was used as a control) were performed to investigate the relative stability and activity of type II DHQases from *S. coelicolor*, *H. pylori* and *M. tuberculosis* and the YqhS F23Y mutant from *B. subtilis*. The structural stability of *H. pylori* type II DHQase towards denaturation was further characterised using fluorescence and circular dichroism. During the denaturation experiments it was observed that there appeared to be a difference in the effect of chloride anion on the activities of the high and low k_{cat} families of DHQase. This apparent effect of chloride ions was investigated further by performing activity studies in the presence of different anions: parallel studies were carried out on the effect of urea in place of GdmCl.

The effect of phosphate on type II DHQases was first characterised during experiments comparing the steady-state parameters of the two types of DHQase (Kleanthous *et al.*, 1992). Preliminary results obtained by Deka (1993) indicated that phosphate behaves as a competitive inhibitor of the type II DHQase from *A. nidulans*, with a K_i of 10 mM at pH 7.0 and 25°C. The effect of the polyanionic ligands sulphate and phosphate on the type II DHQases of *M. tuberculosis*, *H. pylori*, *S. coelicolor* and the *B. subtilis* YqhS F23Y mutant was investigated.

All kinetics assays were carried out as described in section 2.16.1 in 50mM Tris acetate pH 7.0 unless otherwise stated.

5.2 Structural comparison of Type II dehydroquinases

Sequence alignments demonstrate high homology between the type II DHQases from different bacterial species. The primary structures of type II DHQases are strongly conserved with 13 % of residues invariant and 65 % conserved over the 47 sequences shown in Appendix C; **Error! Reference source not found.** The *H. pylori*, *A. nidulans*, *M. tuberculosis* DHQases and the *B. subtilis* protein YqhS show a percentage identity of 43, 56, 44, and 47% respectively, to the *S. coelicolor* DHQase. Using the *S. coelicolor* numbering system for amino acids all of the residues thought to be involved in catalysis are conserved in these DHQase apart from serine 56, which is a threonine in *H. pylori* and tyrosine 28 which as already highlighted in chapter 4 (4.1) is a phenylalanine in *B. subtilis* YqhS. The subunit of the type II DHQases has a flavodoxin-like fold (Burnett *et al.*, 1974). The C terminal α -helix of *H. pylori* is significantly extended compared to the other DHQases discussed in this chapter. The overlay of the structures of *S. coelicolor*, *M. tuberculosis* and *H. pylori* DHQase (Figure 44) shows that there is no significant difference in the orientation of the residues involved in catalysis. There are subtle differences at the floor of the active sites of the type II DHQase X-ray structures. Amino acid side chains at positions 81 and 82 (SCDHQase numbering system) are found on the floor of the active site and are highly conserved as either a glycine or alanine. Ala81 is thought to cause a steric clash with the oxime inhibitor in the SCDHQase (Table 5). It is also noteworthy that the flexible loop that forms a lid to the active site (residues 21-31) is not resolved in the *H. pylori* or the *M. tuberculosis* DHQases which are both of which are low k_{cat} enzymes. This region may be more flexible in these two bacterial species, although there are no indications from the primary structure as to why this might be the case nor whether this extra flexibility may contribute to the lower activity of these enzymes.

5.3 Unfolding of Type II dehydroquinase from *H. pylori*

The type II DHQases from both *S. coelicolor* and *M. tuberculosis* have both been studied by unfolding experiments in the presence of GdmCl (Kleanthous *et al.*, 1992; Price *et al.*, 1999). A denaturation curve of the *H. pylori* was determined using concentrations of GdmCl from 0M to 6M. 0.2 mg/ml of enzyme was incubated at

room temperature for 24hrs. The samples were then analysed using far UV circular dichroism, fluorescence and by measuring catalytic activity (2.22; 2.21; 2.16.1).

5.3.1 Structural analysis using circular dichroism

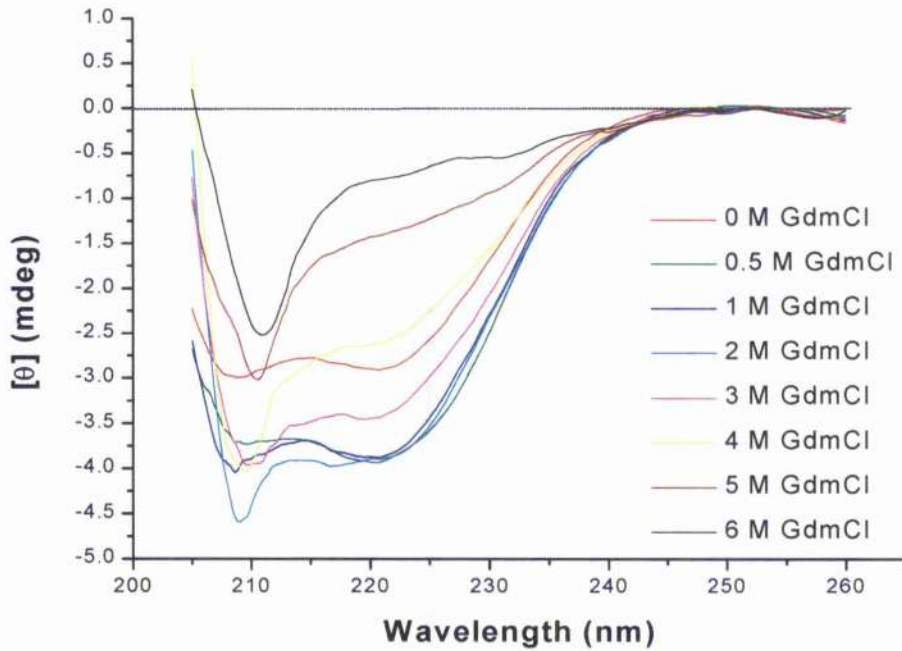


Figure 45. Far UV circular dichroism spectra of the unfolding of *H. pylori* type II DHQase by guanidine hydrochloride (GdmCl) see figure insert for concentration of GdmCl.

CD spectra show the changes in secondary structural features. *H. pylori* DHQase is very stable in GdmCl and shows approximately 40% of the native CD signal at 225nm in 6M GdmCl. At low concentrations (up to 2M) GdmCl there is some evidence for a modest increase in secondary structure (Figure 32). It could be possible that this may reflect a change in the quaternary structure with dissociation of the dodecamer into trimers, but no further experiments have been undertaken to check this suggestion.

5.3.2 Structural analysis using fluorescence

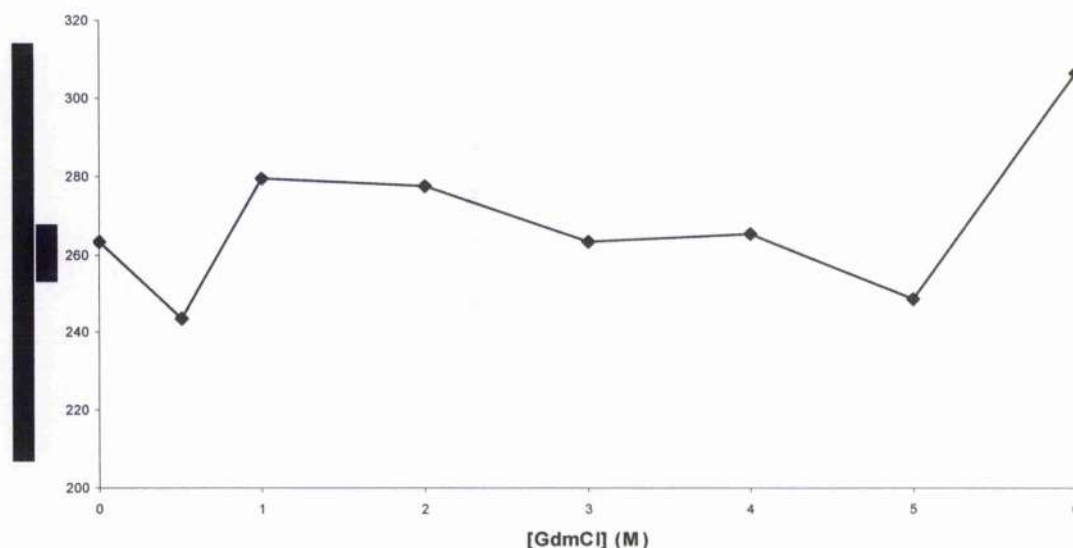


Figure 46. Fluorescence data of the unfolding of *H. pylori* type II dehydroquinase by guanidine hydrochloride (GdmCl). Values are corrected for Raman scattering.

Fluorescence scans were carried out on *H. pylori* DHQase with low concentrations of denaturant; guanidine hydrochloride. *H. pylori* DHQase does not possess any tryptophans so the fluorimeter was set up to selectively excite tyrosine residues at a wavelength of 280 nm. The fluorescence data show no large-scale changes in emission at 308 nm with an increase in GdmCl concentration. At 0.5M GdmCl there is a minor rise in emission; the overall trend is slight increase in emission with GdmCl concentration (Figure 46). This indicates the environment of each of the tyrosines is not significantly altered and the tertiary structure is unchanged by low concentrations of GdmCl. This is consistent with the CD data, which show that the *H. pylori* DHQase is extremely stable towards the denaturant.

5.3.3 Catalytic activity

At low levels of GdmCl (0.5 M and 1 M) there is a significant increase in enzyme activity. It was originally hypothesised that this increase in activity was due to either an increase in flexibility in the structure or was a consequence of the dodecameric

quaternary structure dissociating into trimers (Price *et al.*, 1999). This is explored further in section 5.4.2.

5.3.4 Structural analysis using dynamic light scattering

To investigate any structural changes in the presence of low levels of GdmCl, urea, sodium chloride, sodium phosphate (pH 7.0) and sodium sulphate, dynamic light scattering was used to monitor any changes in quaternary structure. Two catalytically different DHQases, *S. coelicolor* and *H. pylori* were studied at a protein concentration of 0.5 mg/ml. Each protein sample was incubated at 20°C for 1 hour with the test reagents in 50 mM Tris acetate buffer pH 7.0. 200 µl of each solution was injected into the dynamic light scattering cell.

The estimated molecular weight of *S. coelicolor* DHQase is much lower than the actual value as determined by White *et al.*, (1990). This is likely to be due to the assumptions about the density and shape of the protein made by the software of the DynaPro™ system (2.23). There is only a slight change in the radius of the protein and the estimated molecular weight in the presence of the low levels of denaturant and salt tested. This is not thought to be significant as the SOS (sum of squares) is increased in the presence of all the reagents tested which is likely to be due to a slight aggregation (Table 12).

The *H. pylori* results show large amounts of aggregation in the presence of all the reagents tested. In the presence of Tris acetate buffer pH 7.0 the estimated molecular weight is much closer to the actual molecular weight than with the value obtained from the *S. coelicolor* dynamic light scattering data (Kwak *et al.*, 2001). In the presence of 0.5 M urea and 0.17 M sodium sulphate it was not possible to acquire enough counts to make any measurements and the SOS of all the results was >5.0 so their data are likely to be unreliable (2.23).

The dynamic light scattering data do not show any evidence that type II DHQases dissociate into trimers in the presence of low levels of denaturant. All of the reagents tested seem to cause aggregation of the low activity DHQase of *H. pylori*.

Table 12. Dynamic light scattering data for type II dehydroquinases in the presence of various denaturants and salts.

	<i>S. coelicolor</i> dehydroquinase			<i>H. pylori</i> dehydroquinase		
	Radius (nm)	Estimated MW (kDa)	SOS Error	Radius (nm)	Estimated MW (kDa)	SOS Error
[50mM]						
Tris acetate	4.4	106	1.788	5.8	209	8.190
[0.5 M]						
GdmCl	4.4	104	5.548	7.4	383	25.124
[0.5 M]						
Urea	4.7	128	2.399	-	-	-
[1.0 M]						
Urea	4.8	129	4.271	*	*	*
[0.5 M]						
NaCl	4.7	128	2.525	*	*	*
[0.28 M]						
NaPi	5.3	166	7.472	6.3	254	13.682
[0.17 M]						
Na ₂ SO ₄	4.9	142	3.725	-	-	-

5.3.5 Structural analysis using differential scanning calorimetry (DSC)

Differential scanning calorimetry was used to determine the thermal stability of the bacterial type II DHQases from *S. coelicolor*, *M. tuberculosis* and *H. pylori*, the YqhS protein from *B. subtilis* was also tested. Experiments were carried using 0.1 mg/ml of protein in 100 mM Tris:acetate buffer (pH 7.0) in the Biophysical Chemistry

* Insufficient counts

* Sample aggregation.

Laboratory, University of Glasgow (Prof. Cooper). All the proteins were stable to over 100°C whereupon all the protein samples aggregated (data not shown).

5.4 Kinetic characterisation of type II dehydroquinases

5.4.1 pH dependence of the kinetic parameters of type II dehydroquinases

The pH dependence of the kinetic parameters was studied in four type II DHQases; *S. coelicolor*, *M. tuberculosis*, *H. pylori*, and *B. subtilis* protein YqhS mutant F23Y. DHQase activity was measured as described in section 2.16.1. Reactions were initiated by the addition of enzyme (0.015 µg, 0.5 µg, 3 µg, and 40 µg of *S. coelicolor*, *M. tuberculosis*, *H. pylori*, and *B. subtilis* protein YqhS F23Y respectively). Assays were performed over a series of pH values from 6.5 to 8.0. Data at each substrate concentration were measured in quadruplicate.

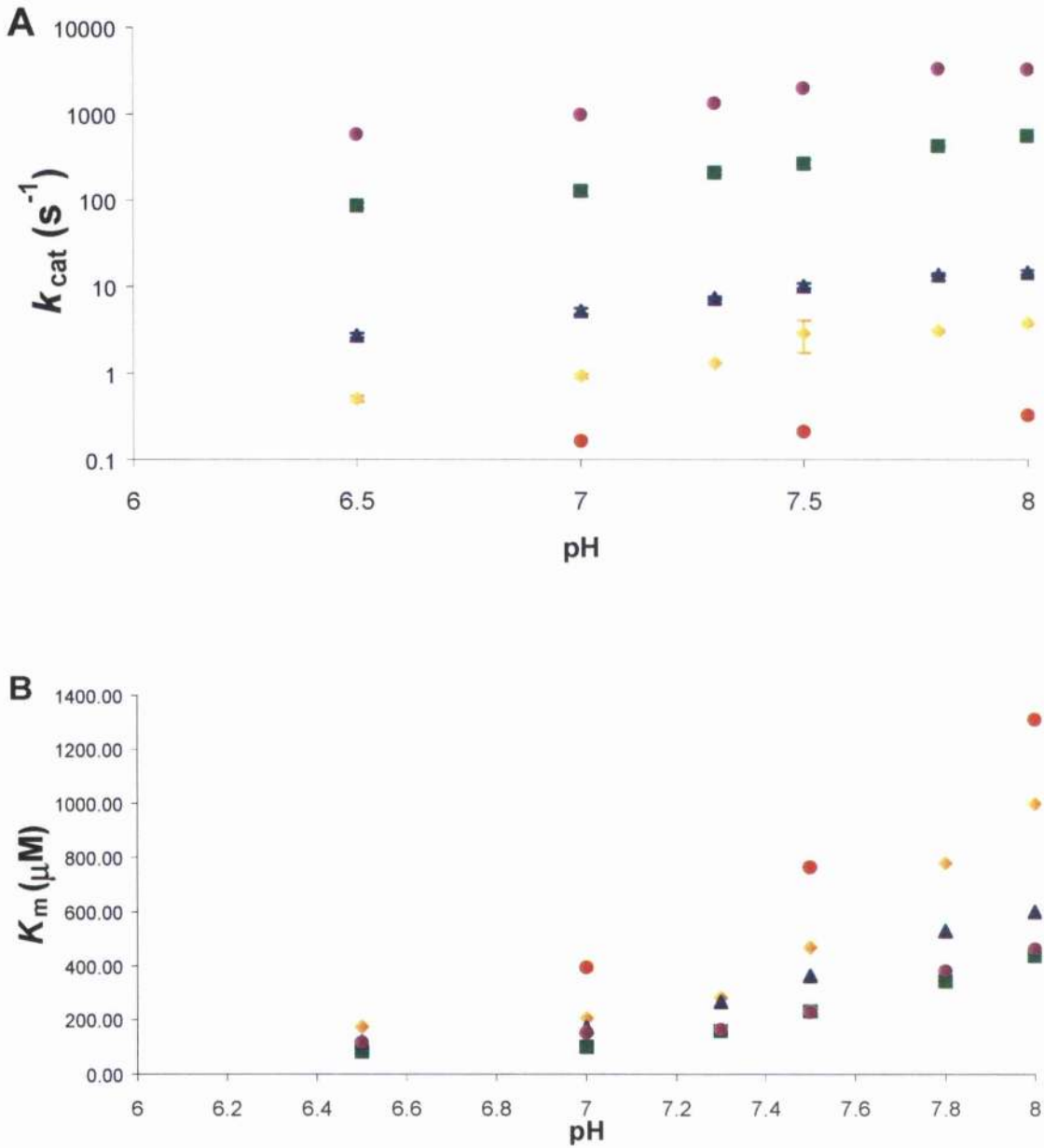


Figure 47. Steady-state kinetics pH-dependence studies effect on (A) k_{cat} and (B) K_m of type II DHQases from *S. coelicolor* (green), *H. pylori* (blue), *M. tuberculosis* (orange), *A. nidulans* (purple) and *B. subtilis* YqhS F23Y mutant (red) (*A. nidulans* data from Dr. Deka 1993).

Table 13. pH-dependence steady-state kinetics studies on bacterial type II DIIQases (*A. nidulans* data from Deka (1993)).

pH	<i>S. coelicolor</i> dehydroquinase				
	k_{cat} (s ⁻¹)	±	K_m (μM)	±	k_{cat}/K_m (s ⁻¹ M ⁻¹)
6.5	84.85	2.92	81.99	8.58	1.03 × 10 ⁶
7.0	124.79	2.78	99.17	7.67	1.26 × 10 ⁶
7.3	205.24	5.31	157.44	11.91	1.30 × 10 ⁶
7.5	260.04	6.76	229.92	16.05	1.15 × 10 ⁶
7.8	416.03	16.33	341.48	31.21	1.23 × 10 ⁶
8.0	480.76	21.13	428.18	43.03	1.13 × 10 ⁶
<i>H. pylori</i> dehydroquinase					
6.5	0.51	2.92	173.05	15.35	2.95 × 10 ³
7.0	0.94	2.24	205.75	13.78	4.55 × 10 ³
7.3	1.31	3.66	281.87	17.94	4.66 × 10 ³
7.5	2.88	6.54	469.71	25.74	6.08 × 10 ³
7.8	3.06	15.07	779.40	41.23	3.93 × 10 ³
8.0	3.76	12.24	999.05	32.00	3.76 × 10 ³
<i>M. tuberculosis</i> dehydroquinase					
6.5	2.72	3.08	18.84	2.39	1.44 × 10 ⁵
7.0	5.17	3.00	23.79	1.97	2.18 × 10 ⁵
7.3	7.30	4.72	45.16	3.96	1.62 × 10 ⁵
7.5	8.50	10.09	54.83	8.87	1.64 × 10 ⁵
7.8	8.76	6.33	58.98	5.46	1.56 × 10 ⁵
8.0	11.38	19.50	87.98	18.44	1.45 × 10 ⁵
<i>A. nidulans</i> dehydroquinase					
6.5	579	ND	116	ND	4.99 × 10 ⁶
7.0	973.2	ND	153	ND	6.36 × 10 ⁶
7.3	1326.6	ND	163	ND	8.14 × 10 ⁶
7.5	1981.8	ND	229	ND	8.65 × 10 ⁶
7.8	3285.3	ND	382	ND	8.60 × 10 ⁶
8.0	3224.1	ND	464	ND	6.95 × 10 ⁶
<i>B. subtilis</i> YqhS F23Y mutant					
7.0	0.194	0.0089	731.79	77.66	2.65 × 10 ²
7.5	0.21	0.0034	765.26	28.22	2.77 × 10 ²
8.0	0.33	0.0448	1310.85	335.60	2.51 × 10 ²

ND Not determined.

The results show that there is a dramatic increase in k_{cat} as the pH increases (Figure 47A) with approximately a seven-fold increase in catalytic activity between pH 6.5 and 8.0 in all the DHQases tested. Similar results were obtained for the *A. nidulans* enzyme (Deka, 1993) (Table 13). As the pH dependence of k_{cat} is similar in all the DHQases tested it is likely that they all share the same catalytic mechanism. There is also an increase in K_m as pH increases although the relationship between pH and K_m varies across the DHQases tested (Figure 47B) (Table 13).

The hydroxyl of free tyrosine (as a free amino acid) has a pK_a of 10.0 and therefore would be expected to be fully protonated at pH 7.0: therefore its environment must significantly shift the pK_a of tyrosine 28 to allow proton abstraction. The proximity of arginine 113 and to a lesser extent arginine 23 would be expected to have a significant effect on the pK_a of tyrosine 28 (Roszak *et al.*, 2002), as has been shown to be the case in human aldose reductase (Tarle *et al.*, 1993). This is consistent with the pH dependence data which show; an increase in activity with increasing pH, specifically related to the increased deprotonation of tyrosine 28.

5.4.2 Stopped flow assay experiments

To investigate any differences in the pre-steady state kinetics of bacterial type II DHQases stopped flow experiments were performed on *S. coelicolor*, *H. pylori* and *B. subtilis* (F23Y) DHQases. Assays were performed using an Applied Photosystems Stopped flow apparatus. No lag or burst phase was observed for HPDHQase or SCDHQase (data not shown).

5.4.3 Effects of salts on catalytic activity

Low concentrations of GdmCl were shown to increase the catalytic activity of two type II DHQases significantly during unfolding experiments (5.3.3) this effect had been previously documented for the *M. tuberculosis* enzyme (Price *et al.*, 1999). Further experiments were carried out using low concentrations of GdmCl, urea and sodium chloride on both the high k_{cat} (*S. coelicolor*) and low k_{cat} (*M. tuberculosis*, *H. pylori*, *B. subtilis* F23Y) type II DHQases (Figure 48, Table 13).

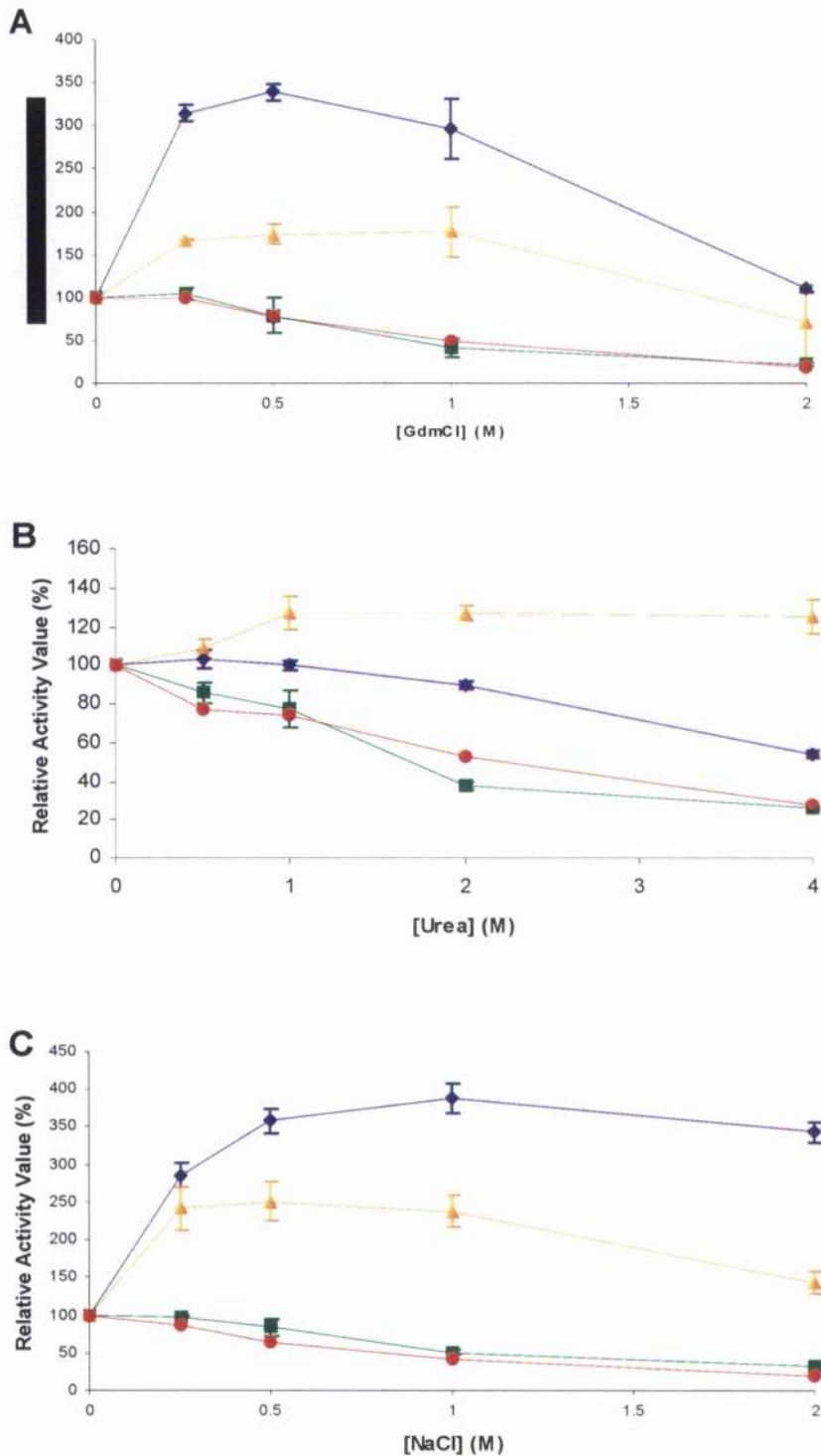


Figure 48. Catalytic activity of *S. coelicolor* (green), *H. pylori* (blue), *M. tuberculosis* (orange) DHQase and *B. subtilis* YqhS F23Y mutant (red) in the presence of low concentration denaturants and salt (A) GdmCl (B) Urea (C) NaCl.

There is a 240% increase in activity of *H. pylori* DHQase at 0.5 M GdmCl and a 77% increase in activity of *M. tuberculosis* DHQase at 1.0 M GdmCl. The same effect was not observed with the higher k_{cat} DHQase from *S. coelicolor* and the *B. subtilis* mutant F23Y where low GdmCl concentrations lead to a small decrease in activity (Figure 48A). These experiments were repeated using comparable concentrations of urea and sodium chloride. As urea is not as strong a denaturant as GdmCl the concentration chosen was double that of the GdmCl used in the assays. The catalytic activity of the *M. tuberculosis* DHQase increased by 27% in 1.0 M urea, but the *H. pylori* DHQase did not increase significantly in low concentrations of urea. The *S. coelicolor* and the *B. subtilis* mutant F23Y DHQases both showed a decline in catalytic activity as the concentration of urea increased (Figure 48B). All four enzymes were also assayed using low levels of sodium chloride and the activity of the DHQases followed the same trend as the GdmCl assay results (Figure 48C). The *M. tuberculosis* and *H. pylori* DHQases showed a 150% (0.5 M NaCl) and 288% (1.0 M NaCl) increase in catalytic activity respectively. The *S. coelicolor* and the *B. subtilis* mutant F23Y DHQases showed a decrease in catalytic activity as the concentration of sodium chloride increased. The catalytic parameters of the bacterial DHQases studied in this chapter in the presence of 0.5 M GdmCl and of sodium chloride are shown in Table 14. All assays were performed in duplicate or in the case of *B. subtilis* (F23Y) quadruplicate.

Table 14. Catalytic kinetic parameters of bacterial type II DHQases in the presence of 0.5 M NaCl and GdmCl.

Bacterial strain of type II DHQase	Salt tested [0.5 M]	k_{cat} (s^{-1})	\pm	K_m (μM)	\pm	k_{cat} / K_m $\text{M}^{-1}\text{s}^{-1}$
<i>S. coelicolor</i>	No salt	124.79	2.78	99.17	7.67	1.26×10^6
	NaCl	78.97	2.54	201.89	19.90	3.91×10^5
	GdmCl	96.92	7.27	339.94	56.20	2.85×10^5
<i>H. pylori</i>	No salt	0.94	2.24	205.75	13.78	4.55×10^3
	NaCl	3.52	0.07	306.85	19.54	1.15×10^3
	GdmCl	3.76	0.07	418.05	23.07	8.99×10^3
<i>M. tuberculosis</i>	No salt	5.17	3.00	23.79	1.97	2.18×10^5
	NaCl	5.44	0.11	36.26	3.01	1.50×10^5
	GdmCl	4.20	0.08	36.89	3.22	1.14×10^5
<i>B. subtilis</i> (F23Y)	No salt	0.194	0.009	731.79	77.66	2.65×10^2
	NaCl	0.097	0.006	930.3	112.0	1.05×10^2
	GdmCl	0.071	0.004	780.5	91.4	9.16×10^1

The k_{cat} of *H. pylori* DHQase (low k_{cat} enzyme) shows a significant increase in the presence of both 0.5 M NaCl and 0.5 M GdmCl (Table 14). The k_{cat} of the *M. tuberculosis* DHQase (low k_{cat} enzyme) shows a moderate increase in the presence of 0.5 M NaCl and a small decrease in the presence of 0.5 M GdmCl. The effect on the K_m is similar between the two low k_{cat} enzymes; the K_m increases by approximately the same order of magnitude in the presence of both NaCl and GdmCl. This evidence suggests that the increase in activity in the *M. tuberculosis* and *H. pylori* DHQases is not due to increased flexibility caused by low concentrations of denaturant as previously thought, and is more likely to be due to a salt effect on the turnover of the substrate.

The activity of the *S. coelicolor* DHQase and *B. subtilis* YqhS F23Y mutant enzyme both decrease in the presence of both 0.5 M NaCl and 0.5 M GdmCl. The K_m of the *S. coelicolor* DHQase is increased approximately 2-fold in the presence of 0.5 M NaCl and 3-fold in the presence of GdmCl (Table 14). The K_m of the *B. subtilis* enzyme is less affected by both 0.5 M NaCl and 0.5M GdmCl. The K_m of the *B. subtilis* enzyme increased by 1.3-fold in the presence of NaCl. There was only a moderate increase in the K_m of the *B. subtilis* enzyme in the presence of 0.5 M GdmCl.

Originally thought to be devoid of life the Dead Sea is native to a number of halophilic archaea including *Haloarcula marismortui*, the enzymes malate dehydrogenase and 2Fe-2S protein ferredoxin of this halophilic archaean were studied by Mevarch *et al.*, 2000. Halophilic enzymes require high salt concentrations for catalytic activity and stability and it is argued that high negative surface charge of halophilic proteins make them more soluble and renders them more flexible at high salt concentrations.

The effect of the chloride ions and other salts on type II DHQases was investigated using a number of salts from the Hofmeister series. The Hofmeister series was originally drawn up on the basis of the effects of various ions on the solubility of proteins (Hofmeister, 1888; Collins and Washabaugh, 1985). It has been shown that the salts of this series can alter enzyme activity by disrupting the organised structure of protein macromolecules (Baldwin, 1996). Bovine liver β -galactosidase and sweet potato β - amylase among others were found to be inhibited by the higher ranking of anions of the Hofmeister series (Warren and Cheatum, 1966). Acetoacetic decarboxylase from *C. acetobutylicum* is also inhibited by anions in a manner which follows the pattern of the Hofmeister series and the size of anion (Fridovich, 1963). The effect of the series of salts on the catalytic activity of the type II DHQase was compared to a control in the absence of added salt. The salts used were sodium bromide, sodium chloride, potassium chloride, sodium fluoride, sodium acetate, GdmCl and sodium thiocyanate; urea was added as a control. The DHQases were incubated for 1 hour in each of the salts tested prior to the activity measurements. The ionic strength was kept constant; 0.5 M in all assays and all the assays were performed at pH 7.0 with 1 mM dehydroquinone. The pH was adjusted for the NaF and NaAc assays to pH 7.0 with glacial acetic acid. The ionic strength (I) is defined

as half of the total sum of the concentration (c_i) of every ionic species in the solution (i) times the square of its charge (z_i). The equation for the ionic strength of a solution is shown below:

$$I = 0.5 \sum (c_i z_i^2)$$

The relative catalytic activity of the two low k_{cat} species of DHQases (*M. tuberculosis* and *H. pylori*) increased significantly in sodium bromide, sodium chloride (previously observed), potassium chloride, sodium fluoride and GdmCl. The *M. tuberculosis* DHQase also showed a significant increase in relative catalytic activity in the presence of sodium acetate and sodium sulphate. The *S. coelicolor* DHQase was inhibited by all the salts tested, as was the *B. subtilis* F23Y DHQase with the exception of a 41% increase in relative catalytic activity in the presence of sodium acetate and no significant change in activity in the presence of sodium fluoride. All the DHQases tested were inhibited by sodium thiocyanate (Figure 49). None of the DHQases follow the precise pattern of the Hofmeister series. The interactions of salts and macromolecules appears to be very complex; ionic species can potentially affect hydrogen bonds, hydrophobic interactions and electrostatic interactions. Interestingly there seems to be a correlation between a rise in catalytic activity in the low k_{cat} type II DHQases and the presence of chloride ions. Detailed studies of *M. tuberculosis* DHQase X-ray crystallographic data have revealed chloride binding sites.

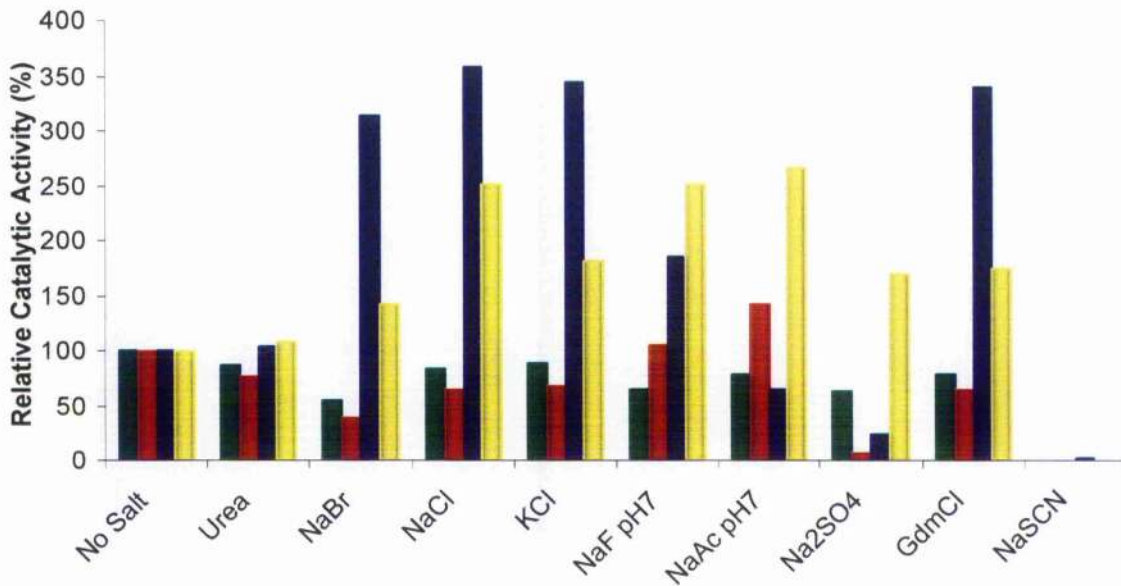


Figure 49. The affect of salts from the Hofmeister series on the catalytic activity of *S. coelicolor* (green), *B. subtilis* YqhS F23Y mutant enzyme (red), *H. pylori* (blue), and *M. tuberculosis* (yellow) dehydroquinases.

5.4.4 Temperature effect on catalytic activity

Preliminary steady-state kinetics experiments were carried out on SCDHQase, MTDHQase and HPDHQase at 37°C. Both MTDHQase and HPDHQase showed an increase in activity at 37°C, while SCDHQase showed a minor decrease (data not shown).

5.4.5 Characterisation of effects of phosphate and sulphate on type II dehydroquinases

The inhibitory effect of polyanions; sodium sulphate and sodium phosphate on type II DHQases was used to give an insight into the differences in substrate specificity of the low and high k_{cat} enzymes. Preliminary results (Frederickson *et al.*, 1999) had indicated that phosphate behaves as a competitive inhibitor of the type II DHQase from *A. nidulans*, with a K_i of 10 mM at pH 7.0 and 25°C. Studies of bisulphonamides by Arrow therapeutics (2001) revealed moderate inhibition of type II DHQase and dehydroquinase synthase. The anti-microbial effect was also tested and shown to have an inhibitory effect on growth on methicillin resistant *Staphylococcus aureus*. Theorell and Nygaard (1954) have also documented the

strong inhibitory effect of polyanions in flavoprotein systems. The inhibition is caused by the tendency of these anions to interact with positive groups of the protein, which are essential for the attachment of FMN. Polyanions have been shown to be bind more strongly to proteins than monovalent anions (Theorell and Nygaard, 1954).

These studies were extended to other type II enzymes for the polyanionic ligands sulphate and phosphate using a combination of kinetic and structural approaches.

Kinetic parameters were obtained by varying substrate concentrations over the appropriate range (between 20 μM and 2 mM) in the presence and absence of sodium phosphate or sodium sulphate.

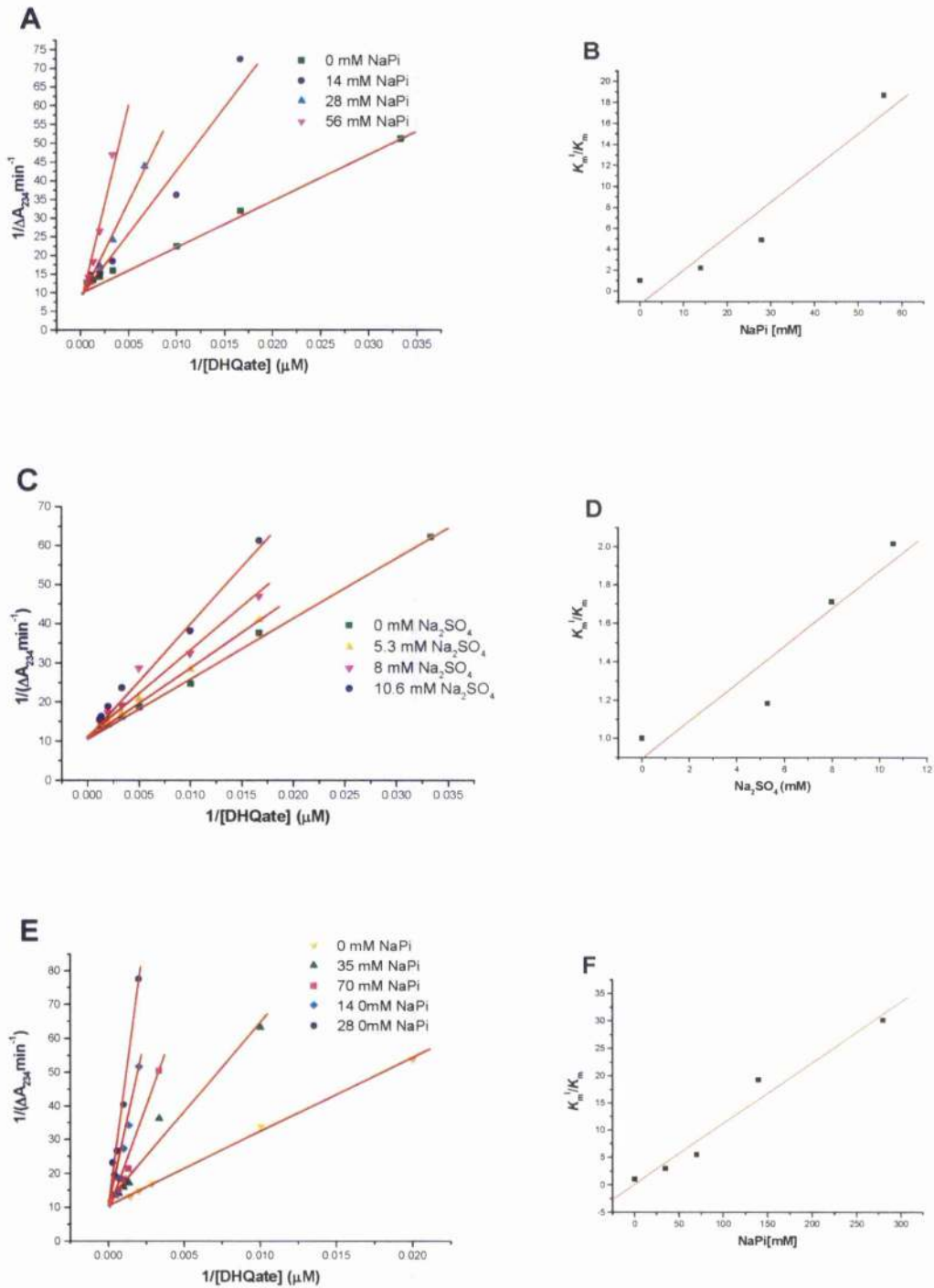
Table 15. Inhibition by polyanions on the kinetic properties of type II DHQases

Enzyme	k_{cat} (s^{-1})	K_m (μM)	K_i (phosphate) (mM)	K_i (sulphate) (mM)
SCDHQase	124.79	99.17	7	11
HPDHQase	0.94	205.75	9	9
MTDHQase	5.17	23.79	ϕ	ψ
BSYqhS (F23Y)	0.194	731.79	9	Ψ

ϕ In the presence of phosphate, a complex pattern is observed in which V_{max} and K_m are both raised; see Figure 51A.

ψ In the presence of sulphate, the V_{max} remains essentially unchanged, but the dependence of K_m on sulphate concentration is markedly non-linear, indicating that the anion may bind to multiple sites on the enzyme.

Ψ In the presence of sulphate, The K_m is not significantly affect, while V_{max} decreases as the concentration of sulphate increases, indicating non-competitive inhibition.



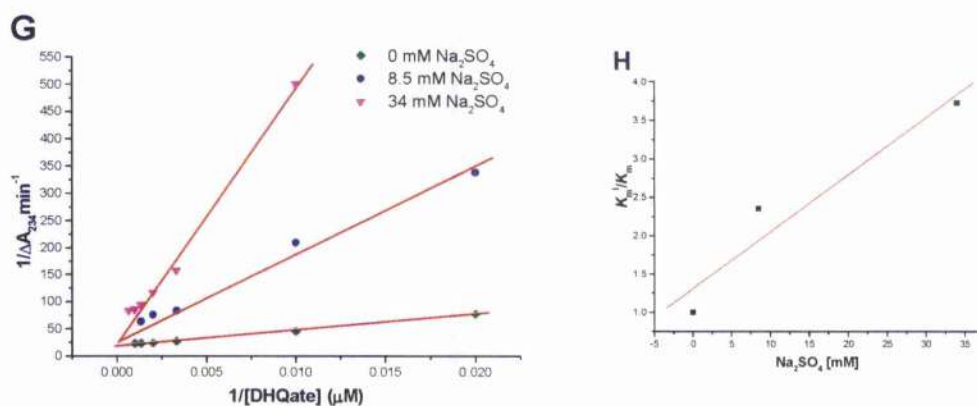
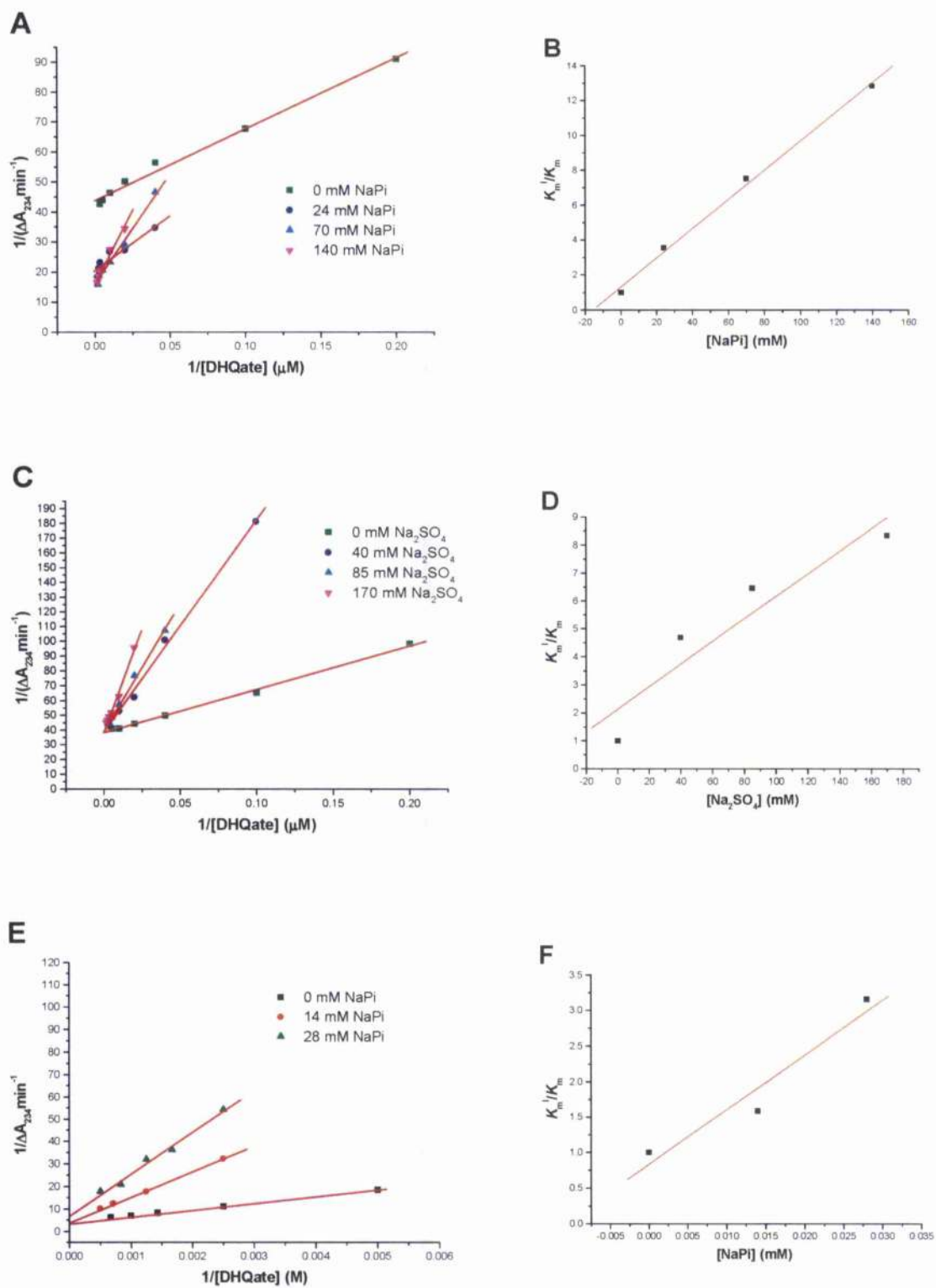


Figure 50. Inhibition of *S. coelicolor* and *H. pylori* type II dehydroquinases by phosphate and sulphate. **A:** Lineweaver-Burk plot for inhibition of SCDHQase by phosphate. **B:** Ratio of K_m^i/K_m vs. [phosphate] for SCDHQase. **C:** Lineweaver-Burk plot for inhibition of SCDHQase by sulphate. **D:** Ratio of K_m^i/K_m vs. [sulphate] for SCDHQase. **E:** Lineweaver-Burk plot for inhibition of HPDQase by phosphate. **F:** Ratio of K_m^i/K_m vs. [phosphate] for HPDQase. **G:** Lineweaver-Burk plot for inhibition of HPDQase by sulphate. **H:** Ratio of K_m^i/K_m vs. [sulphate] for HPDQase. K_m and K_m^i values are the Michaelis constants for dehydroquininate in the absence and presence of either phosphate or sulphate.



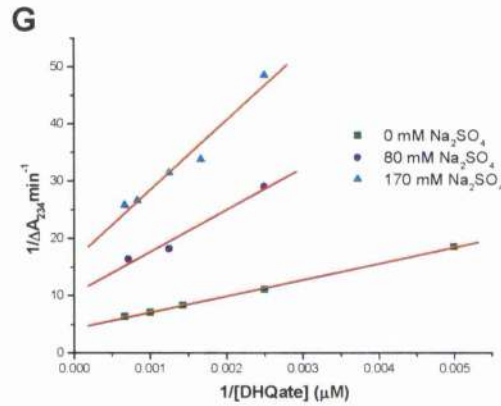


Figure 51. Inhibition of *M. tuberculosis* type II dehydroquinases and *B. subtilis* YqhS (F23Y) by phosphate and sulphate. **A:** Lineweaver-Burk plot for inhibition of MTDHQase by phosphate. **B:** Ratio of K_m^i/K_m vs. [phosphate] for MTDHQase. **C:** Lineweaver-Burk plot for inhibition of MTDHQase by sulphate. **D:** Ratio of K_m^i/K_m vs. [sulphate] for MTDHQase. **E:** Lineweaver-Burk plot for inhibition of *B. subtilis* YqhS (F23Y) by phosphate. **F:** Ratio of K_m^i/K_m vs. [phosphate] for *B. subtilis* YqhS (F23Y). **G:** Lineweaver-Burk plot for inhibition of *B. subtilis* YqhS (F23Y) by sulphate. K_m and K_m^i values are the Michaelis constants for dehydroquinate in the absence and presence of either phosphate or sulphate.

The effects of phosphate and sulphate on the kinetic properties of DHQase are shown in Table 15, Figure 50 and Figure 51. The polyanions both behave as simple competitive inhibitors with respect to dehydroquinate for SCDHQase and HPDHDQase (Figure 50 A-H). In contrast, in the case of *M. tuberculosis* DHQase, the effects of the anions were more complex. Although sulphate did not change the V_{max} , and thus appeared to act as a competitive inhibitor (Figure 51C), the dependence of the K_m on the anion concentration did not follow the expected linear model for simple competitive inhibition. In the presence of phosphate, both V_{max} and K_m were increased (Figure 51A). These results indicate that the anions may bind to more than one site in *M. tuberculosis* DHQase, leading to multiple effects on the kinetic properties of the enzyme.

Phosphate is also a simple competitive inhibitor of *B. subtilis* (F23Y) YqhS (Figure 51E). The inhibition of *B. subtilis* (F23Y) YqhS by sulphate is more complex; the K_m

is not significantly altered at all concentrations of sulphate tested while the V_{\max} decreases with an increase in sulphate concentration. Both Lineweaver-Burk plot (Figure 51G) and direct non-linear fitting point towards sulphate being a non-competitive inhibitor of the YqhS mutant enzyme. This would indicate that sulphate binds at a distinct site from dehydroquininate in the YqhS mutant enzyme. However, in view of the limited amount of data collected and the low activities observed, it would be inappropriate to over interpret these data.

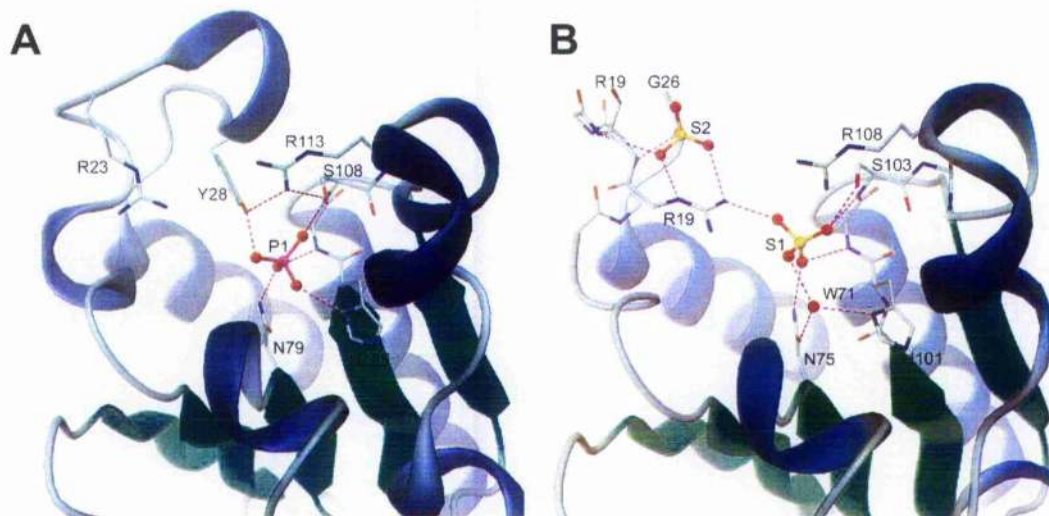


Figure 52. Comparison of the two active sites of the two DHQases. Solid Ribbon representation of the active sites of (A) phosphate (P1) bound within the active site of the *S. coelicolor* DHQase. (B) *M. tuberculosis* DHQase with sulphate ions (S1 and S2) bound within the active site. Amino acid residues important for ligand binding are shown in stick and coloured according to atom type, hydrogen bonds are shown as dashed lines coloured magenta (Evans *et al.*, 2002).

The crystal structures of *S. coelicolor* and *M. tuberculosis* DHQase in complex with phosphate and sulphate respectively, were compared in order to try and interpret the effects of these polyanions on the kinetic parameters of the enzymes. The protein folds are very similar and overlay well. The *M. tuberculosis* DHQase structure has two sulphates in the active site compared with the single phosphate in *S. coelicolor* DHQase, this is consistent with the more complicated kinetics seen in the former enzyme. Unexpectedly, the single phosphate bound to *S. coelicolor* DHQase does

not correspond to either of the sulphates bound in the active site of *M. tuberculosis* DHQase. This finding could be interpreted structurally as the result of the differences between the two ligands. The phosphate ion possesses a protonated oxygen (hydroxyl) while sulphate does not, this protonated oxygen of the phosphate could bind in the analogous position to the C1 hydroxyl of the substrate while this conformation would not be as favourable for sulphate. However, the structure of the *S. coelicolor* DHQase structure with sulphate bound has been solved at 2.8 Å resolution and the anion occupies exactly the same position as is observed in the higher resolution phosphate structure (Roszak *et al.*, 2002). Figure 52 shows a comparison of the two active sites of the two DHQases. The phosphate bound within the active site of the *S. coelicolor* DHQase (Figure 52A) forms several hydrogen bonds with key catalytic residues and occupies an analogous position to the carboxylate and C1 hydroxyl of the substrate. In the structure of *M. tuberculosis* DHQase (Figure 52B), the S1 sulphate is located in this region, but adopts a different conformation from the P1 phosphate seen in the *S. coelicolor* enzyme. The S1 sulphate forms hydrogen bonds with the catalytically important residues Ser103 and Asn75 representing the common position of two of the oxygens of the phosphate anion. However, His101 hydrogen bonds to a water molecule rather than the sulphate, and the catalytically important tyrosine in the lid domain does not close over the active site and interact with the sulphate. Instead Arg19 has moved much further into the active site than observed in the *S. coelicolor* DHQase structures, and is able to form a hydrogen bond with the sulphate. The second sulphate ion also interacts with this arginine and also with residues at the N-terminal end of the flexible lid domain.

5.5 Chapter summary

Type II DHQases fall broadly into two categories: high and low k_{cat} enzymes. Protein sequence alignments and analysis of the 3-dimensional X-ray structures of type II DHQases show high homology between the structures of the high and the low activity DHQases. They also seem to share several biophysical properties including high stability in the presence of denaturant and no observed lag or burst phase using stopped-flow kinetics. pH dependence studies provided evidence that all the type II DHQases tested shared a common catalytic mechanism. However, studies on *M. tuberculosis* and *A. nidulans* type II DHQase performed by Harris *et al.* (1996b)

showed significant differences in solvent and substrate isotope effects between these enzymes. The relationship between the V_n/V_0 ratio and the fraction of ^2H in the solvent of the assay (n) (V_n is the rate of reaction when the a fraction of deuterium (^2H) in the solvent is n and V_0 is the rate when $n = 0$) suggests that a single proton contributes to the isotope effect in the MTDHQase, whilst the results for *A. nidulans* enzyme suggest that at least two protons contribute to the observed effects. Substrate isotope effects also reveals differences in V_{\max} and V_{\max}/K_m between the two enzymes. The step in the mechanism that contributes to the substrate isotope effect is thought to occur at different points on the free-energy profile of the MTDHQase and *A. nidulans* dehydroquinase reactions; the highest point and the transition state with the highest energy, respectively (Harris *et al.*, 1996a). Unfortunately it was not possible to determine $\text{p}K_a$ values for the DHQases tested as there were problems caused by substrate instability at pH values higher than 8.0 (L. Noble, personal communication). It was originally thought that subtle structural changes especially in the lid domain caused by low levels of denaturant were responsible for the observed increases in the catalytic activity in the presence of 1M GdmCl. The 3-dimensional X-ray structures of two low k_{cat} enzymes (MTDHQase and HPDHQase) show that both have disordered lid domains. The lid domain is thought to be more flexible in these enzymes. Analysis of the protein sequence of the lid domain of all the type II DHQases tested shows no significant differences between the amino acid side chains which would account for the extra flexibility in this domain (Appendix C; **Error! Reference source not found.**). Unfolding studies using urea as a denaturant indicated that increased activity caused by guanidine hydrochloride is not due to an increase in flexibility, but rather to the presence of chloride ions. In contrast *B. subtilis* YqhS mutant (F23Y), a low k_{cat} enzyme, does not show an increase in activity in the presence of low concentrations of chloride. This indicates that not all low k_{cat} enzymes show the same chloride effect. However it should be noted that the *B. subtilis* YqhS enzyme is not a true DHQase (CHAPTER 4) and it is possible that different factors are responsible for the low catalytic activity of the YqhS (F23Y) that are not involved in the evolution of the other low k_{cat} DHQases.

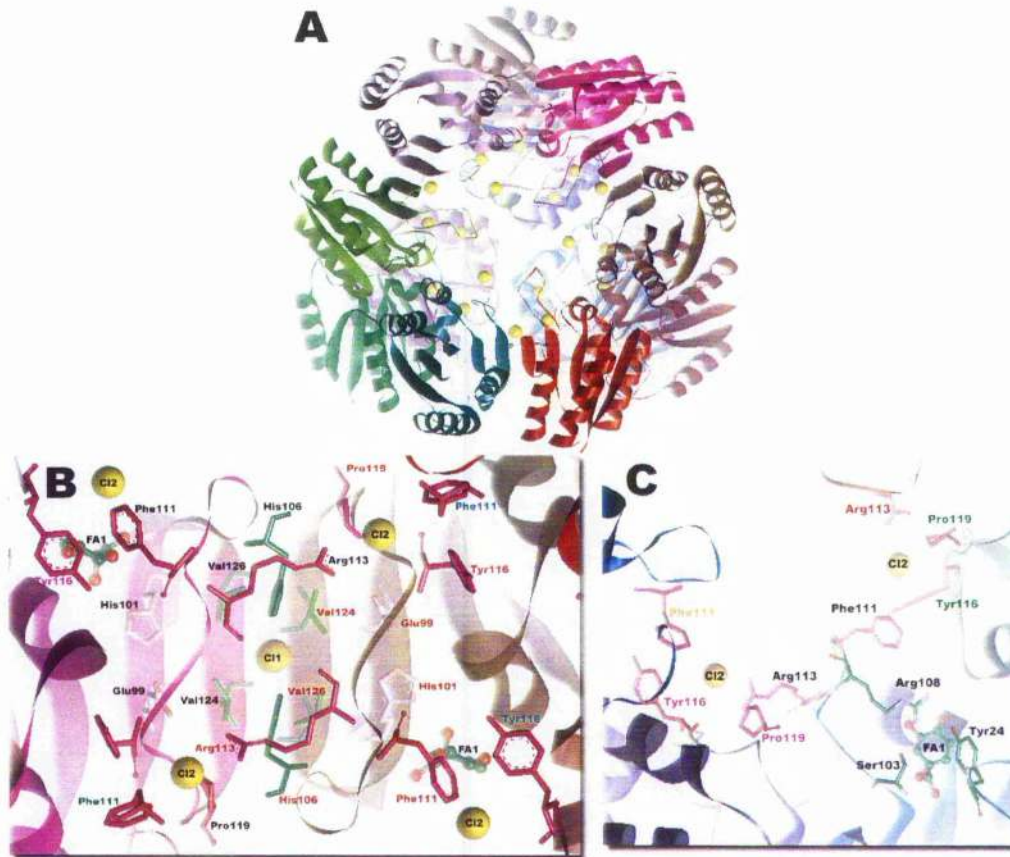


Figure 53. 3-dimensional structure of *M. tuberculosis* dehydroquinase in complex with 2,3-anhydro-quinic acid and chloride ions. (A) *M. tuberculosis* DHQase dodecamer, secondary structural features are represented in flat ribbon and strands, subunits are individually coloured, chloride ions are shown as yellow balls. (B) Interactions of chloride ions (Cl1, 2) at subunit interface: amino acids highlighted in green are involved in the coordination chloride 1 (Cl1) and highlighted in magenta are residues which interact with chloride 2 (Cl2). Catalytic side chains (H101 and E99) are represented by their electrostatic charge. (C) The potential stabilisation of the minor loop domain by two chloride 2 ions involving 5 subunits. 2,3-anhydro-quinic acid (FA1) is shown as a ball and stick representation while the catalytic side chains are represented as colour-coded stick models (carbon atoms are shown in green, oxygen atoms shown in red and nitrogen atoms shown in blue). Amino acids are labelled according to the *M. tuberculosis* numbering system and numbers are coloured according to their respective subunit.

Several differences between the type II DHQases have been identified in this study. Low concentrations of chloride have been shown to increase the catalytic activity of both MTDHQase and HPDHQase while the same concentration of chloride lowers the catalytic activity of SCDHQase and *B. subtilis* YqhS (F23Y). Chloride ions are present in the X-ray structure of the *M. tuberculosis* enzyme in complex with the inhibitor 2,3-anhydro-quinic acid (FA1); as a result of the crystallisation conditions used to obtain crystals for diffraction. In total there are 18 chloride ions within the dodecamer (Figure 53A), 1.5 per subunit. The chloride ions are found in two distinct orientations within the dodecamer. Six chloride ions (chloride 1, Cl1) are located at subunit interfaces (Figure 53B) and form hydrogen bonds with the imidazole rings of a pair of histidine residues (His106), Val124 and Val 126 are approximately 4.5 Å (using the *M. tuberculosis* numbering system for amino acids) from neighbouring subunits. The other twelve chloride ions (chloride 2, Cl2) are located behind the minor loop domain of the active site (Figure 53C); this loop domain contains the catalytic residue Arg108, responsible for the localised pK_a effect on Tyr24 (thought to be involved in proton abstraction, CHAPTER 3). Chloride 2 forms hydrogen bonds with Arg113 and is 4 Å away from Phe111 both of which are located on the minor loop domain, but interact with different chloride 2 ions. Pro116 from the neighbouring subunit is 3.7 Å away from chloride 2 and possibly forms weak Van der Waals interactions. The main chain amide group of Tyr116 from the same neighbouring subunit is 5 Å away from the chloride 2 ion.

Chloride 1 is thought to have a role in the stabilisation of the quaternary structure of MTDHQase. It is also possible that chloride 1 has some indirect effect on the catalytic residues His101 and Glu99 (likely candidates to be involved in donation of a proton to the hydroxyl at C1 of dehydroquinone, CHAPTER 3) on the neighbouring β-strand (Figure 53B). Two Cl2 ions are thought to be involved in an increase in the stability of the minor loop domain of the active site. The orientation of Arg108 is important for catalytic activity and the extra stability of the minor loop domain may account for the moderate increase in activity observed in MTDHQase in the presence of 0.5 M chloride ions.

The B-factors of Cl1 and Cl2 in the X-ray structure of *M. tuberculosis* are 37 and 28 Å², respectively giving an indication of their mobility and consequently order in the structure. This suggests that Cl2 is more precisely located and therefore more likely

to be involved in the increase in catalytic activity. In contrast Cl1 interacts weakly with Val124 and 126 and the indirect effect on His101 and Glu99 is less likely. Cl2 may bind more tightly so be present at low chloride concentrations and therefore represent the site of binding for chloride.

Without 3-dimensional structural data on the binding of chloride to SCDHQase it is difficult to propose a reason for the reduction in catalytic activity observed. In the SCDHQase 3-dimensional structures reported by Roszak *et al.*, (2002) histidine residues (H111, H106 in MTDHQase) from neighbouring subunits make the largest single contribution (83 \AA^2) to the buried surface area at the dimer interface. As in the MTDHQase structure the two imidazole rings of the histidines point toward each other, restricting the size of the solvent cavity, which is occupied by water. In the presence of chloride ions it is conceivable that these interactions maybe disrupted causing the observed decrease in catalytic activity.

The polyanions, sulphate and phosphate were found to be simple competitive inhibitors with respect to dehydroquinate for SCDHQase and HPDHQase as previously observed in *A. nidulans* (Frederickson *et al.*, 1999). In contrast the effect of polyanions on MTDHQase was more complex. The results of MTDHQase kinetic studies in the presence of phosphate indicated that the anions bind to more than one site, leading to multiple effects on the kinetic properties of the enzyme. Phosphate is a simple competitive inhibitor with respect to dehydroquinate and sulphate is surprisingly a non-competitive inhibitor for *B. subtilis* YqhS (F23Y) protein, although it should be noted that errors associated in measuring the low activity of the YqhS mutant and the limited amount of data that was collected may have affected these data. The X-ray crystallographic data on the enzymes from *S. coelicolor* and *M. tuberculosis* with phosphate and sulphate bound respectively identify significant differences in both the mode of binding and number of polyanions bound by the two enzymes. The differences in binding of the anion to the carboxylate recognition site of the enzymes may account for the relative potencies of several rationally designed inhibitors (Frederickson *et al.*, 1999). A greater understanding of the differences in binding of known inhibitors of type II DHQases may lead to further selectivity.

Analysis of the crystal structure of *S.coelicolor* DHQase with various ligands bound in the active site, such as phosphate, the transition state analogue 2,3-anhydro-quinic acid and dehydroshikimate (R23A mutant SCDHQase) reveals that the main chain

amide nitrogens of Ser108 and Ile107 to bond to the carboxylate group. Phosphate, which is a competitive inhibitor of *S. coelicolor* DHQase, mimics the carboxylate group. Ser108 binds to the carboxylate of dehydroquinate. Ser108 is probably responsible for substrate recognition and orientation (Roszak *et al.*, 2002; Evans *et al.*, 2002; 3.5).

Four sulphate molecules were identified in the MTDHQase structure, with two lying in the active site of the enzyme. Neither binding position of the sulphate molecules was analogous to the location of the phosphate molecule in the SCDHQase structure. The catalytic lid domain is disordered as in the apoenzyme structure. The first sulphate molecule (S1, Figure 52) in the active site is positioned in the carboxylate binding site as identified from the SCDHQase-inhibitor complexes, the second sulphate molecule (S2, Figure 52) interacts with the amide nitrogens of residues 17-19 and the side chain of Arg19. The binding of a second anion in the position of the lid domain of the *M. tuberculosis* DHQase structure may help to explain the complex kinetic effects of the polyanions observed for this enzyme. The finding that the sulphate anion does not occupy the same position as the C1 hydroxyl and carboxylate of the substrate helps to explain differences in the inhibition of type II DHQases. A number of selective inhibitors have been synthesized by Frederickson *et al.*, (1999) including the transition state analogue 2,3-anhydroquinic acid and its oxime derivative. These inhibitors contain all the structural features of the substrate and transition state respectively, with the exception of the C3 carbonyl which is absent. The K_i values for these inhibitors were two-fold and nine-fold lower respectively for SCDHQase than for MTDHQase therefore polyanions do not bind as tightly to MTDHQase. As the K_m of MTDHQase is lower than SCDHQase, polyanions are less effective inhibitors of MTDHQase than SCDHQase. This suggests that while recognition of the C1 carboxylate and hydroxyl is the major component necessary for the specific binding of substrate to SCDHQase, the C3 carbonyl also plays a significant role in substrate binding in MTDHQase, quite possibly by interacting with Arg19.

The differences between sulphate and phosphate with respect to both the potency and type of inhibition suggest that the X-ray structures of SCDHQase in complex with phosphate and MTDHQase in complex with sulphate may not be directly comparable. However, a low resolution X-ray structure of SCDHQase in complex with phosphate,

shows phosphate occupies the same location as sulphate in the SCDHQase-sulphate structure. The effects of the two polyanions on HPDQase are analogous to SCDHQase. It would be valuable to produce a 3-dimensional structure of HPDQase in complex with polyanions or either a higher resolution structure of SCDHQase-phosphate or MTDHQase in complex with sulphate.

During the course of evolution, the catalytic activity of an enzyme is presumably optimised by an organism to suit its environment. The availability of the substrate and the relative need for the product govern the catalytic parameters. *H. pylori* and *M. tuberculosis* are both human pathogens which grow at 37°C in contrast to *S. coelicolor* and *A. nidulans* which both grow at lower fluctuating temperatures found in soil where the concentration of quinate (utilised in the catabolic quinate pathway) is high.

The effect of salts and polyanions on type II DHQases is complex and does not seem to fall into a simple pattern with low and high k_{cat} enzymes. The type of inhibition of type II DHQases by polyanions can vary and structural data indicate that mode of binding can differ. It would be beneficial to extend this study by analysing type II DHQases from other species, for example the *Campylobacter jejuni* DHQase which has been cloned by Prof. Hunter and co-workers at the University of Strathclyde (CHAPTER 7). In view of the complexity of effects observed, it is unlikely that one single factor is important in determining whether a DHQase has a low or high k_{cat} . Rather it is likely that a variety of factors including the flexibility of the active site and the nature and orientation of the residues involved in substrate binding and catalysis have been employed during evolution in order to match the catalytic properties of each enzyme with the metabolic needs of the particular organism.

CHAPTER 6 HAEMOPHILUS INFLUENZAE**SHIKIMATE DEHYDROGENASE AND RELATED****YdiB PROTEIN****6.1 Introduction**

Shikimate dehydrogenase coded by the *aroE* gene is present as a monomer in *E. coli* (ECAroE) (Chaudhuri and Coggins, 1985) and exclusively uses NADPH as a cofactor (Yaniv and Gilvarg, 1955). In plants shikimate dehydrogenase occurs as a bifunctional enzyme (on a single polypeptide chain) with a type I dehydroquinase (Koshiha, 1978; Polley, 1978; Mousdale *et al.*, 1987; Deka *et al.*, 1994) this enzyme also requires NADPH as a cofactor. Fungi such as *Aspergillus nidulans* possess a pentafunctional *arom* polypeptide (Charles *et al.*, 1985), the C terminal domain of which carries the shikimate dehydrogenase activity. The organisation of the enzymes of the shikimate pathway within different organisms is described further in section 1.1.3.

Quinate dehydrogenase (*gutB*) catalyses the conversion of quinate to dehydroquinone, which is then connected to protocatechuate via the catabolic quinate utilisation pathway (1.2). This pathway shares two metabolites of the shikimate pathway, namely dehydroquinone and dehydroshikimate (Giles *et al.*, 1967; Hawkins *et al.*, 1993). Some shikimate dehydrogenases are also able to catalyse the quinate dehydrogenase reaction. To date three independent families of quinate/shikimate dehydrogenases have been identified. The first group are NAD⁺ dependent dehydrogenases and are widespread amongst microorganisms (Lopez Barea and Giles, 1978; Hawkins *et al.*, 1993), the second is found in gymnosperms such as *Pinus taeda* and utilises NADPH as a cofactor (Ossipov *et al.*, 2000), whilst the third use pyrrolo-quinoline (PQQ) as a cofactor and are almost exclusively found in gram-negative bacteria and are often membrane-associated dehydrogenases (Duine, 1991).

Protein sequence analysis of AroE from *E. coli* using BLAST (Altschul *et al.*, 1997) identified approximately 150 sequences, predominantly designated as putative shikimate dehydrogenases (Appendix C; **Error! Reference source not found.**). The BLAST analysis also revealed that shikimate dehydrogenases have significant sequence homology to NAD⁺-dependent quinate/shikimate dehydrogenases.

Several organisms including *E. coli*, *H. influenzae* and *Deinococcus radiodurans* possess a second analogue of the shikimate dehydrogenase denoted as YdiB function unknown. The existence of a second shikimate dehydrogenase could affect the design of potential drugs directed at AroE as YdiB may compensate for any inhibition of AroE. There are significant differences in sequence between AroE and YdiB in the N-terminal region, which is thought to be involved in the binding of the C1 carboxylate of dehydroshikimate and in forming the dimer interface (Michel *et al.*, 2003). Based on the N-terminal region the YdiB proteins broadly fall in to two groups (6.1.1). The first group, which includes the *E. coli* YdiB protein (ECYdiB), are more closely related to the majority of the AroE proteins than the second group, which includes one of the proteins in this study namely YdiB from *H. influenzae* (HIYdiB). The differences between the two groups are discussed in detail below.

pH dependence studies on the bifunctional plant shikimate dehydrogenase family have been performed including *Pisum sativum* (Balinsky and Davies, 1961a; Dennis and Balinsky, 1972), *Camellia sinensis* L. (Sanderson, 1966) and *Pinus taeda* (Ossipov *et al.*, 2000). These showed the rate of the reverse reaction (formation of dehydroshikimate from shikimate) to be maximal at pH 10.0-10.6. The overall trend of pH dependence points towards a similar mechanism being adopted in each of the enzymes tested. pH dependence experiments on *Phaseolus aureus* showed an optimum rate at pH 8.0 although the enzyme was only partially purified (Nandy and Ganguli, 1961). pH dependence experiments performed on the crude ECARoE (Yavin and Gilvarg, 1955) indicated a pH optimum of 8.5. The difference in the pH optima for the plant and bacterial enzymes could be due to the fact that the bacterial enzyme was not fully saturated with the cofactor (Balinsky and Davies, 1961b).

The catalytic properties of ECARoE and ECYdiB were determined for the reaction in reverse direction (shikimate to dehydroshikimate) in 100mM Tris-HCl (pH 9.0) by Michel *et al.*, (2003). ECARoE oxidises shikimate exclusively using NADP⁺ as a cofactor with a K_{NADP} of 0.056 mM, K_{SHK} of 0.065 mM and the k_{cat} was found to be 260 s⁻¹. Unusually ECYdiB is able to oxidise both shikimate and quinate with either NAD⁺ or NADP⁺ as the cofactor. The K_{NAD} and K_{NADP} were found to be 0.087 mM and 0.1 mM respectively using shikimate as substrate and 0.116 mM and 0.5 mM respectively using quinate as substrate. The cofactor also has an effect on the binding of the substrate in the presence of NAD⁺. The K_{SHK} and K_{QUT} values are 0.0205 mM

and 0.041 mM respectively, while in the presence of NADP^+ the values are much higher 0.12 mM (K_{SHK}) and 0.555 mM (K_{QUT}). Using shikimate as a substrate the activity of ECYdiB is ~1700-fold lower than ECARO E with k_{cat} values of 0.0624 and 0.156 s^{-1} using NAD^+ and NADP^+ as substrate respectively. The catalytic activity with quinate is also extremely low for both NAD^+ and NADP^+ (k_{cat} : 0.0416 and 0.0625 s^{-1} , respectively).

The *E. coli* *ydiB* and *aroE* proteins share 25% sequence identity, and X-ray structures of both the proteins have been reported (Michel *et al.*, 2003). Despite there being relatively low sequence homology between *E. coli* AroE and YdiB, the two enzymes have highly similar 3-dimensional structures and adopt the same fold. The ECYdiB protein has an extended loop region (residues 176-182), which is typical of the first group of YdiB proteins. It is unclear what role the extended loop region plays in the protein, since X-ray structural data show that the loop is not close to either the substrate or the cofactor. Dynamic light scattering experiments on the ECYdiB revealed that it has a hydrodynamic radius consistent with a globular protein of approximately 60 kDa, indicating that ECYdiB occurs as dimers (Michel *et al.*, 2003). The dimer interface contains several hydrophobic residues that are not present in the monomeric ECARO E.

6.1.1 Substrate binding domain and reaction mechanism

To date there is no X-ray structure of a substrate analogue bound to any enzyme of the shikimate dehydrogenase family. The active site has been identified by the position of the nicotinamide ring of the cofactor. The presence of a sulphate or phosphate ion within the substrate-binding pocket of the ECARO E and ECYdiB, and a DTT molecule in the ECARO E structure are the result of the crystallisation conditions (Figure 54). These reagents give clues to the orientation of the substrate in the enzyme binding site. The X-ray structures reveal a closed conformation only in the presence of the DTT molecule (ECARO E, molecule A) and it is proposed that the conformational change which closes the central cleft occurs on substrate binding (Michel *et al.*, 2003). Studies on glyceraldehyde-3-phosphate dehydrogenase from rabbit muscle provided strong evidence for ligand-induced conformational changes which cause negative cooperativity in binding of cofactors of different subunits (Henis and Levitzki, 1980). Chemical modification experiments of ECARO E

(Chackrewarthy, 1995) identified Lys65 and His13 as either being involved in the catalytic mechanism or being close to the binding site for shikimate.

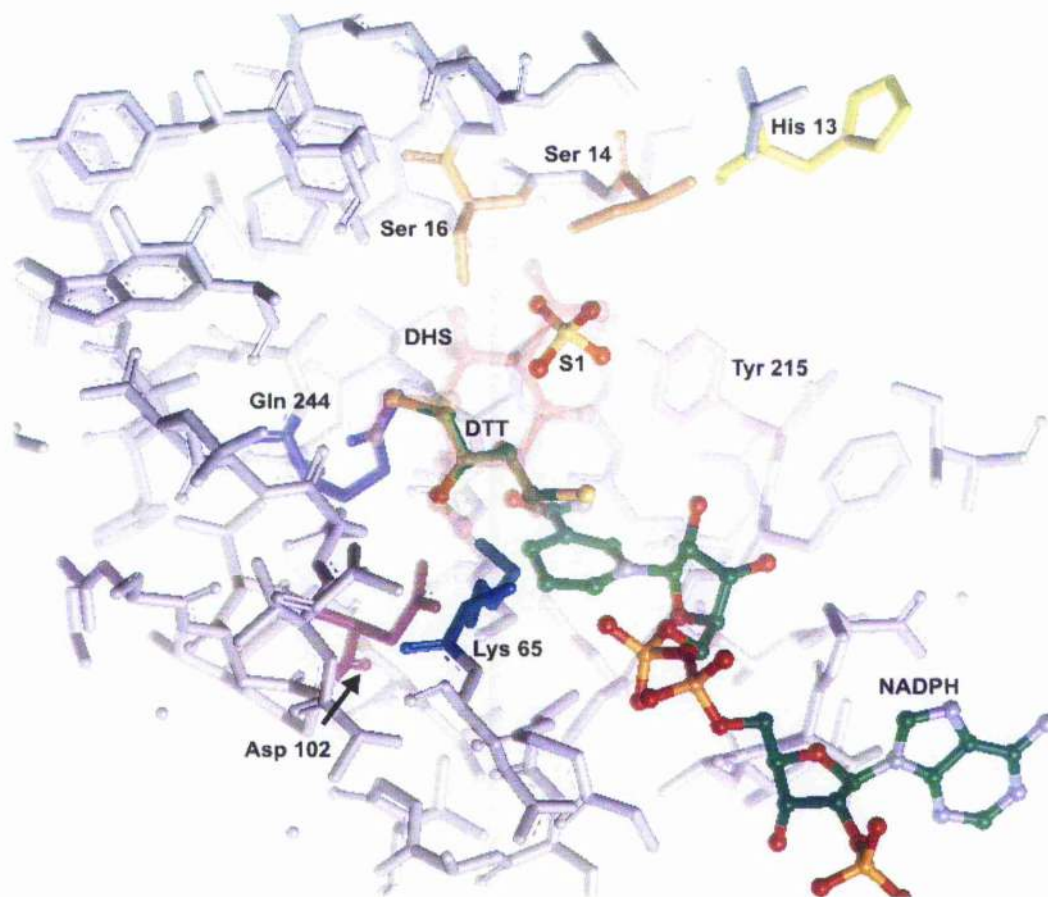


Figure 54. X-ray structure of EC AroE-NADP⁺ complex substrate binding pocket with bound sulphate (S1) and DTT molecules represented as ball and stick (carbon atoms in green), highlighted protein side chains are colour coded according to the type of amino acid and labelled according to the EC AroE sequence. The proposed position of dehydroshikimate is represented by the red ghost overlay.

The N-terminal domain is involved in substrate binding and recognition and typically the sequence pattern for shikimate dehydrogenase (AroE) is G-N-P-I-X-[H,q]-S-K-S-P (where X is variable). The ECYdiB was chosen for further analysis as it is closely related to the AroE group and represents one group of YdiB proteins characterised by the sequence pattern [M,i]-[A/G]-[Y,t]-P-I-H-S-[L,k]-S-P within the N-terminal region. HIYdiB represents the second group; the substrate binding domain deviates

quite considerably from the AroE shikimate dehydrogenases with the N-terminal sequence being: C-[M/I]-S-L-[A,s]-[A,g]-R-P. However, there are similarities between these regions, the S-[L,k]-S and C-[M/I]-S sequences in EcydIB and HIYdiB, respectively may perform the same role in these proteins, it would be valuable to produce an X-ray structure of HIYdiB to determine the orientation of specific residues. The second group of YdiB proteins also has a highly conserved insertion of four amino acids after the substrate binding domain: [R,t,a,q]-F-H-N.

Using stereospecifically labeled cofactors and substrate it was possible to determine that hydride transfer takes place from the A-side of the nicotinamide ring of NADPH (Dansette and Azerad, 1974), which is consistent with the orientation of the cofactor in the X-ray structure of both ECARoE and EcydIB (Michel *et al.*, 2003). The C3 of either dehydroshikimate or quinate must be positioned to accept/receive the hydrogen from C4 of the nicotinamide ring.

The conserved serine side chains near the N-terminus of the AroE enzymes (S14 and S16 in ECARoE) are expected to be involved in the binding of the carboxyl at C1. Tyr215 of ECARoE is also thought to establish an additional hydrogen bond with the carboxylate group (Figure 54). The serine and tyrosine residues are present in the HIAroE and EcydIB, but there are significant differences in the HIYdiB substrate-binding pocket. There is only one conserved serine residue in the N-terminal domain and an alanine side chain replaces the tyrosine side chain. The C5 hydroxyl of the substrate is expected to form hydrogen bonds with a glutamine residue (Q244 in ECARoE) present in all the shikimate dehydrogenase family.

The invariant residues Lys65 and Asp102 are the most likely candidates to donate a proton to the C3 carbonyl of the substrate, as they are orientated toward the substrate-binding pocket in which the DTT molecule is present (Figure 54). Another contender for the role of proton donor is His13; this residue was highlighted by pH dependence of the inactivation of ECARoE by diethylpyrocarbonate (DEPC), which is a histidine-specific reagent (Chackrewarthy, 1995). However, in the X-ray structure His13 is not correctly orientated to perform this role and is some distance away from the cofactor (Michel *et al.*, 2003).

6.1.2 Binding specificity of the cofactor

Interestingly unlike most dehydrogenases that utilise NAD or NADP as a cofactor (Carugo and Argos, 1997a), the shikimate dehydrogenase family does not show a strong preference for either cofactor. NAD and NADP are stereochemically similar the only difference being a phosphomonoester on the C2 of the ribose attached to the adenine ribose of NADP. They both show different biochemical reactivities with NAD⁺ behaving being almost exclusively involved in oxidative catabolism and NADPH serving as a reductant, confined with few exceptions to the reactions of reductive biosynthesis (Carugo and Argos, 1997a).

The comparison of the cofactor binding sites within the shikimate dehydrogenase family is of interest as it reveals the structural features necessary to discriminate between NADP and NAD. The amino acid sequence of ECARoE between residues 121 and 151 exhibits the characteristic 'finger print' of an ADP-binding $\beta\alpha\beta$ -fold (Anton and Coggins, 1988). The charge of the side chain of the residue in the final position of this 'fingerprint' determines whether the enzyme is able to accommodate the 2' phosphate group of the adenosine moiety (Wierenga *et al.*, 1986). Chemical modification experiments using PGO on ECARoE revealed that an arginine side chain either forms part of, or is situated close to, the NADP binding site (Chackrewarthy, 1995). The protein sequences (Appendix C; **Error! Reference source not found.**) of the *H. influenzae* homologues were analysed using the X-ray structure data for ECARoE and ECYdiB (Figure 55). An invariant arginine side chain stacks against the A face of the adenine ring of the cofactor. The B face of the adenine ring is orientated by a serine side chain in the NADPH-dependent ECARoE (S190) and *H. influenzae* shikimate dehydrogenase (HIAroE S189). This is replaced by a valine in the NAD-dependent ECYdiB (V206) and an isoleucine in *H. influenzae* YdiB protein (HIYdiB I185). The substitution of the serine to valine causes a shift in the position of the A face arginine and affects the arrangement of the adenosine moiety recognition and binding loop (Michel *et al.*, 2003). Ile185 of the HIYdiB could also cause a shift in the position of this loop.

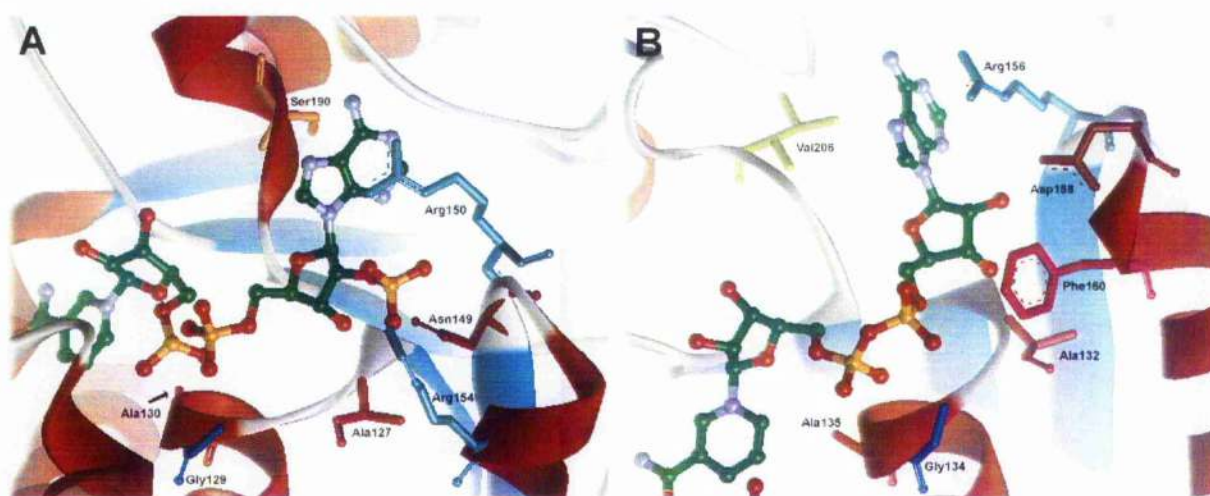


Figure 55. Comparison of the cofactor recognition and binding site of ECARoE (A) and ECYdiB (B). NADP^+ and NAD^+ are represented as ball and stick (carbon atoms in green), protein side chains colour coded according to the type of amino acid and labelled according to their appropriate protein sequence. The protein backbone and secondary structural features are represented by a solid ribbon.

In the ECARoE structure the invariant arginine side chain (R150) also forms an “electrostatic clamp” with another arginine (R154) and plays a crucial role in the binding of the adenosine phosphate of NADP^+ (Michel *et al.*, 2003). Arg154 is replaced by a lysine in both the *H. influenzae* AroE and YdiB. The X-ray structure of the ECARoE- NADP^+ complex (Figure 55A) shows that the invariant asparagine residue (N149) forms a hydrogen bond with the hydroxyl group at the O3' position of the adenosine ribose. In the ECYdiB- NAD^+ complex (Figure 55B), the asparagine side chain (N155) adopts a different position and together with an aspartic acid side chain (D158 in ECYdiB), forms hydrogen bonds to the O2' hydroxyl of the adenosine ribose. In the HIYdiB sequence Arg150 and Asn149 are in the reverse order (Arg151 and Asn152, HIYdiB numbering of amino acids) this may cause shifts in the orientation of the residues around this region.

NADP binding is thought to be favoured by the HIAroE as it retains a threonine (Thr151) which creates a polar environment for the phosphate group of the adenosine moiety. In the ECYdiB this residue is replaced by a phenylalanine (Phe160) which creates a neutral environment for the O2' hydroxyl group of NAD^+ (Michel *et al.*,

2003). HIYdiB possess a valine in place of the threonine that could potentially affect the polar environment of the phosphate-binding pocket, since the valine side chain is hydrophobic. However, due to the difference in the order of the amino acid residues this is unlikely.

The binding of the nicotinamide and pyrophosphate moieties of the cofactor should be analogous in ECARoE and ECYdiB. The amide group of the nicotinamide ring is hydrogen bonded to an invariant glycine side chain and a methionine or cysteine side chain in ECARoE and ECYdiB respectively. Both the *H. influenzae* homologues possess a methionine in this position.

Throughout the shikimate dehydrogenase family the pyrophosphate moiety binds to a glycine rich loop (residues 126-131 in ECARoE) (Michel *et al.*, 2003). The sequence pattern is a modification of the canonical pattern identified in NAD⁺-dependent dehydrogenases (Carugo and Argos, 1997b). Interestingly the group of YdiB proteins (which includes HIYdiB) with a lower sequence homology to the AroE, has a conserved serine (S127) and a methionine (M130) within the pyrophosphate binding motif; however detailed analysis of both the X-ray structures suggests that this is unlikely to affect binding of the pyrophosphate moiety. The glycine rich loop also forms a hydrogen bond with the O3' hydroxyl group of the adenosine ribose unit.

6.1.3 Inhibitor and analogue studies of shikimate dehydrogenase

Balinsky and Davics (1961b) performed inhibitor studies using a variety of phenolic compounds. These studies revealed that the *Pisum sativum* bifunctional enzyme bound to the substrate by means of the C1 carboxyl and the hydroxyl groups at C4 and C5 and identified vanillin, gallic acid and *p*-hydroxybenzoic acid as inhibitors. On the basis of this evidence, Baillic *et al.*, (1972) synthesized various novel dehydroshikimate analogues from 1,6-dihydroxy-2-oxoisonicotinic acid (Figure 56). The analogues were tested for inhibition of the *Pisum sativum* enzyme and couch grass enzyme. Several of these analogues were found to be reversible competitive inhibitors with K_i values ranging from 0.07-0.8 mM for the *Pisum sativum* enzyme. Intriguingly compounds found to be competitive in the reverse direction for the bifunctional enzyme of *Pisum sativum* such as 1,6-dihydroxy-2-oxoisonicotinic acid, were shown to have no inhibition in the forward reaction despite the structure of the

compound being more closely related to dehydroshikimate than to shikimate (Baillie *et al.*, 1972). This anomaly was attributed to the difference in the binding of the substrate in the presence of NADP⁺ and NADPH (Dowsett *et al.*, 1972).

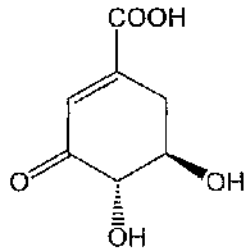
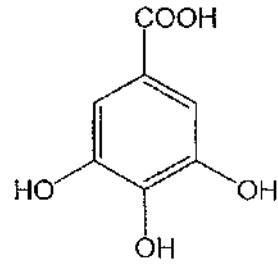
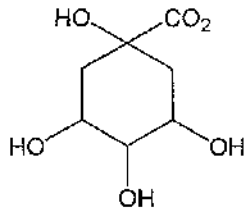
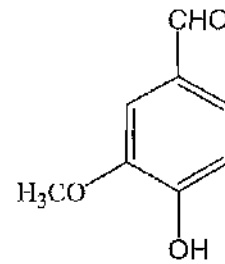
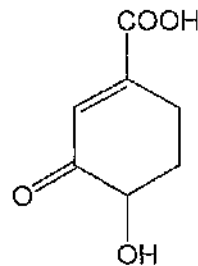
Several structural analogues of shikimate were tested as possible inhibitors of the *Pisum sativum* bifunctional enzyme. Methyl vanillate, syringate and *p*-hydroxybenzaldehyde (Figure 56) were found to be competitive inhibitors (73, 61 and 17% loss in activity respectively) these studies highlighted the importance of the C4 hydroxyl for substrate binding and revealed that substitutions larger than -OCH₃ in the C3 position and -CO₂H in the C1 position were not inhibitory because of steric hindrance to binding (Dennis and Balinsky, 1972).

Gallic acid, thought to be an inhibitor of the plant bifunctional enzyme of *Pisum sativum*, has been shown to be a substrate for the production of hydrolysable tannin synthesis. In the case of mountain birch (*Betula pubescens* ssp. *czerepanovii*) shikimate dehydrogenase (Ossipov *et al.*, 2003) these studies used HPLC to analyse the concentration of gallic acid formed from dehydroshikimate. Assays were stopped by the addition of 6 M HCl followed by centrifugation.

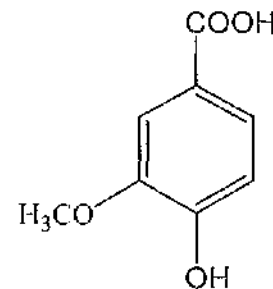
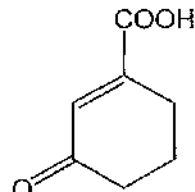
Product inhibition and isotope studies on the *Pisum sativum* bifunctional enzyme and the dissociation constants of the cofactor of this enzyme have shown an ordered BiBi mechanism with NADP likely to bind first followed by dehydroshikimate (Dowsett *et al.*, 1972; Balinsky *et al.*, 1971).

Figure 56. Substrate analogues and inhibitors of the shikimate dehydrogenase family.**Dehydroshikimate acid**

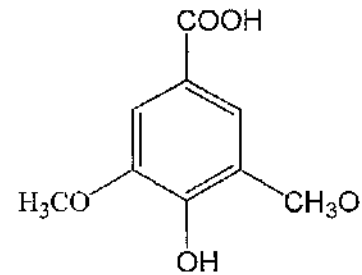
Yavin and Gilvarg, 1955

**Gallic acid**Baillie *et al.*, 1972; Ossipov *et al.*, 2003**Quinic acid**Hawkins *et al.*, 1993**Vanillin**Balinsky and Davies, 1961b; Baillie *et al.*, 1972**5-deoxy analogue**Bugg *et al.*, 1988**Vanillic acid**

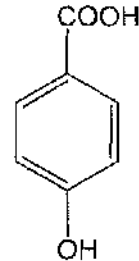
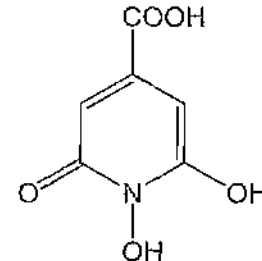
Dennis and Balinsky, 1972

**Dideoxy-dihydro analogue**Bugg *et al.*, 1988**Syningic acid**

Dennis and Balinsky, 1972

***p*-hydroxybenzoic acid**

Dennis and Balinsky, 1972

**1,6-dihydroxy-2-oxoisonicotinic acid**Baillie *et al.*, 1972

Substrate analogues which lacked either the C5 or both the C5 and C4 hydroxyl groups were tested on ECAroE by steady state kinetics in the forward direction (Bugg *et al.*, 1988). On removal of the C5 hydroxyl group (producing 5-deoxy-analogue Figure 56) only moderate specificity was lost between the substrate and the enzyme, a 1.56-fold increase in K_m and 25% reduction in k_{cat} . There is a substantial increase in K_m to 17 mM (a 189-fold increase) on the removal of both the C5 and C4 hydroxyl group (dideoxy analogue Figure 56) (Bugg *et al.*, 1988). Apparent binding energies (ΔG_{app}) were calculated from the ratio k_{cat}/K_m for each of the analogues. ΔG_{app} can be used as an approximation of the true enzyme-substrate binding interaction and the classification of hydrogen bond interactions which fall into two groups: uncharged (2.0-7.5 kJ mol⁻¹) and charged (12.5-25 kJ mol⁻¹) donor/acceptor interactions (Fersht, 1988). The removal of the C-4 hydroxyl group gives a ΔG_{app} value of 29.0 kJ mol⁻¹ suggesting that the C4 hydroxyl forms important hydrogen bond interactions with a charged residue such as a lysine or a cysteine (Bugg *et al.*, 1988), X-ray data suggests that this is most likely to be Lys65 (Michel *et al.*, 2003).

6.2 Construction, over expression and purification of *H. influenzae* shikimate dehydrogenase and the related YdiB protein

6.2.1 Purification of *H. influenzae* shikimate dehydrogenase

The pTB361 *aroE* construct was gifted by S. Campbell (University of Glasgow). The *aroE* construct was transformed into *E. coli* over-expression strain BL21 (DE3) pLysS (2.10). Cell growth was monitored by measuring A_{600} ; once the absorbance had reached 0.6, the expression of protein was induced by addition of 0.8 mM IPTG. The time course of the induction is shown in Figure 57. The pTB361 *H. influenzae* *aroE* construct was grown for a further 6 hours after induction, yielding 10.4 g wet weight of cells from 11 × 0.5 litres of LB medium. Shikimate dehydrogenase was purified using the methods of Chaudhuri and Coggins, (1985) and Maclean *et al.*, (2000), as outlined in section 2.12.3. The elution profile of the DEAE Sephacel column is shown in Figure 58. The final purification step (ADP affinity column) was omitted as the protein was considered to be of a sufficient purity after gel filtration on Sephacryl 200 (Figure 59). The enzyme was then dialysed against 50mM Tris HCl, 200 mM KCl, 50% glycerol (v/v) and stored at -20°C. The protein concentration was 18 mg/ml as determined by absorption at 280 nm (2.13).

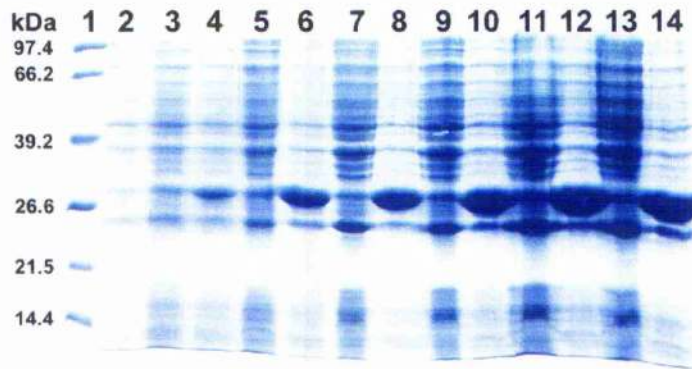


Figure 57. SDS PAGE analysis of the time course of expression of *H. influenzae* shikimate dehydrogenase (HIAroE) in pTB361-BL21 (DE3) pLys S construct. Lane 1: Boehringer Mannheim marker low-range, lanes 3,5,7,9,11 and 13: Control without 0.8 mM IPTG from 0-6 hours. Lanes 2,4,6,8,10,12 and 14: Induced by addition of 0.8 mM IPTG from 0-6 hours (one hour increments).

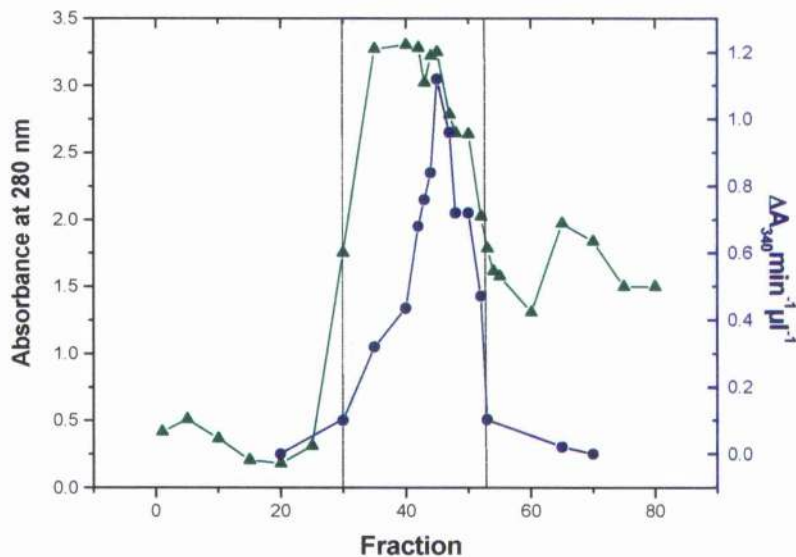


Figure 58. The elution profile from DEAE Sephacel column during purification of *H. influenzae* shikimate dehydrogenase (HIAroE). Absorbance at 280 nm represented by green triangles. Shikimate dehydrogenase activity is shown as blue circles. Fractions that were pooled are shown between the dash black lines.

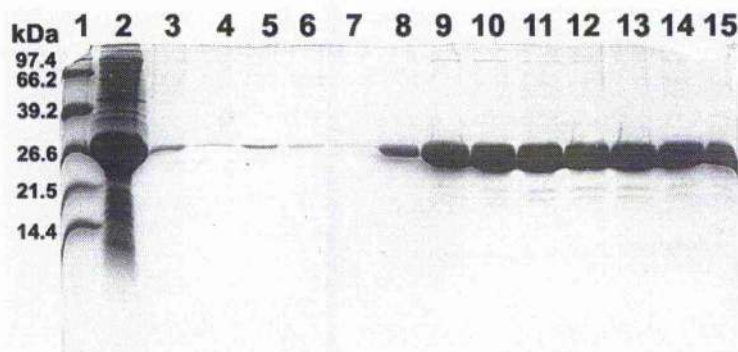


Figure 59. SDS PAGE of Sephacryl 200 fractions during purification of *H. influenzae* shikimate dehydrogenase. Lane 1: Boehringer Mannheim marker low-range, lane 2: *E. coli* pTB361 *aroE*-BL21 (DE3) pLys S construct crude extract. Lanes 3-8: fractions 50 to 75 with (5 fraction increments) eluted from Sephacryl 200. Lanes 9-15: fractions 80 to 87 eluted from Sephacryl 200.

6.2.2 Cloning and over-expression of *H. influenzae* of YdiB protein

The *ydiB* gene was cloned from *H. influenzae* genomic DNA (2.2.4) using PCR (2.6). Two PCR primers were designed by S. Campbell and are shown below:

P1. 5' TATAAGGAGAC**CA**TATGATCAACAAAG 3'

P2. 5' AACACAATGTACCAGATCTTTATTTC 3'

The PCR primers were designed with mismatches incorporated into them to (shown in bold) to add in endonuclease restriction sites, *Nde* I and *Bgl* II respectively, at either end of the *ydiB* gene. The mismatches did not effect the sequence of the gene. The PCR reaction contained 0.5 ng of genomic DNA as the template for amplification, 50 pmol of each primer P1 and P2, 0.2 mM of each dNTPs, 5 units *Taq* DNA polymerase (Promega), 1:10 dilution of 10× *Taq* reaction Buffer (500 mM KCl, 100 mM Tris·HCl, pH 9.0, 1.0% Triton[®] X-100) an additional 0.5 µl of 50 mM MgSO₄ in a total volume of 50 µl made up with sterilised water.

The BioRad Gene Cyclor program included 3 elements: a hot start at 95°C for 7 minutes, 35 cycles of amplification consisting of an annealing temperature of 54°C

for one minute, an extension period of 1 minute at 72°C and a denaturation step of 95°C for 1 minute followed by annealing for 1 minute and elongation for 7 minutes. 4 µl of PCR product was separated and analysed by agarose gel electrophoresis using XIV DNA marker (Roche) (Figure 16). Fragments of the appropriate size were purified by extraction from the gel (2.7.4).

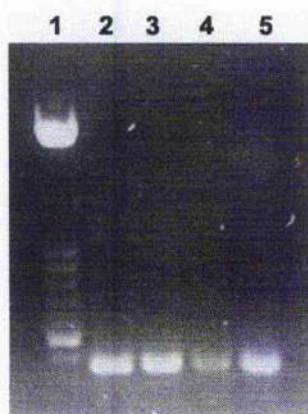


Figure 60. 1% DNA agarose gel of *H. influenzae* PCR. Lane 1: XIV DNA marker (Roche), lanes 2-5: 4 µl of PCR product.

Originally the primers were designed to ligate the *ydiB* gene directly into an expression vector. This approach was found to be unreliable as it was difficult to confirm whether the PCR product had been digested properly prior to ligation. The pUni/V5-His-TOPO[®] Echo[™] Cloning system from Invitrogen was utilised to clone the PCR product containing the *ydiB* gene. The TOPO[®] cloning reaction included 1.5 µl of gel purified PCR product (50 ng), 1 µl of pUni/V5-His-TOPO[®] (1 ng) and 1 µl of salt solution (1.2 M NaCl; 0.06 M MgCl₂) in a total volume of 6 µl made up with sterilised water. TOPO[®] cloning reactions were incubated at 20°C for 25 minutes. 2µl of the TOPO[®] cloning reaction was transformed into *E. coli* competent cells strain; PIR1 (supplied by Invitrogen). The transformation protocol is described in section 2.8.2 and then checked by restriction digest with endonucleases: *Nde* I, *Sac* I and *Bgl* II. Once the pUni/V5-His-TOPO[®] *ydiB* construct had been generated, it was ligated into pTB361 using the restriction sites *Nde* I and *Sac* I. The ligation reaction consisted of approximately 5 ng of digested vector, 80 ng of digested insert DNA (*ydiB* gene), 1 unit of T4 DNA ligase with 1×T4 ligase buffer (Boehringer Mannheim) with sterilised water added to a total volume of 20µl. The reaction was incubated for 16 hours at room temperature. 10µl of the ligation reaction was

transformed into JM109 competent cells (2.8.2). Plasmid purifications were performed on colonies resistant to tetracycline (12.5 µg/ml). Restriction digest analysis was used to identify successful ligations. The pTB361 *ydiB* construct was sequenced by the University of Glasgow Functional Genomics Sequencing Facility (2.9).

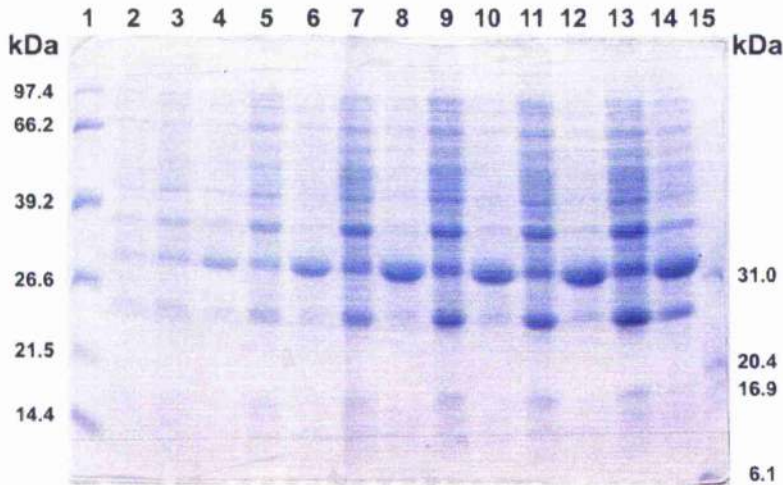


Figure 61. SDS PAGE analysis of the time course expression of expression of *H. influenzae* shikimate dehydrogenase related protein YdiB (HIYdiB) in pTB361-BL21 (DE3) pLysS construct. Lane 1: Boehringer Mannheim marker low-range, lanes 3,5,7,9 and 11: Control without 0.8 mM IPTG from 0-6 hours. Lanes 2,4,6,8,10 and 12: Induced by addition of 0.8 mM IPTG from 0-6 hours (one hour increments). Lanes 13 and 14: overnight control; and induced, respectively. Lane 15: Promega low-range protein molecular weight marker.

The pTB361 *H. influenzae ydiB* construct was transformed into the over expression strain BL21 (DE3) pLysS (2.10). Cell growth was monitored by A_{600} ; once the absorbance had reached 0.6, the expression of protein was induced by addition of 0.8 mM IPTG: Figure 19 shows the time course of the induction. The pTB361 *H. influenzae ydiB* construct was grown for a further 6 hours after induction, yielding 15.25 g wet weight of cells from 11 × 0.5 litres of LB medium.

6.2.3 Purification of YdiB protein

The purification protocol of *H. influenzae* YdiB was based on the protocol described in section 2.12.3. The *H. influenzae* YdiB protein has a significantly different predicted pI (8.59) from the *E. coli* shikimate dehydrogenase (predicted pI = 5.35), for which the protocol had been optimised. Therefore several of the steps were not as effective when applied to the purification of *H. influenzae* YdiB. The ammonium sulphate cuts for HYdiB were optimised as follows. 100ml of induced the *H. influenzae ydiB* construct (BL21 (DE3) pLysS) was centrifuged at $5,000 \times g$ for 15 minutes and resuspended in 5 ml of extraction buffer (2.12.3.1). Cells were lysed using a French pressure cell at 3,500 psi. 0.1mg of DNase was added and the lysate was stirred on ice for 30 minutes. The lysate was then centrifuged at $40,000 \times g$ for 30 minutes. Samples of the resulting soluble and insoluble fractions were taken for analysis on SDS PAGE. Benzamidine was added to the soluble fraction to a final concentration of 1 mM and then solid ammonium sulphate was added to increase the concentration from 10% to 55% saturation in 5% increments. At each level of saturation the solution was stirred for 15 minutes at 0°C and then centrifuged at $40,000 \times g$ for 15 minutes. The supernatant was collected for further analysis. 20 μ l samples were taken after each centrifugation of both the supernatant and resuspended pellet, so that analysis by SDS PAGE could be performed (Figure 62). Most of the *H. influenzae* YdiB protein precipitates between 20% and 25% saturation $(\text{NH}_4)_2\text{SO}_4$. This is significantly different from the *E. coli* shikimate dehydrogenase protein purification which utilised $(\text{NH}_4)_2\text{SO}_4$ cuts between 30% and 55% saturation.

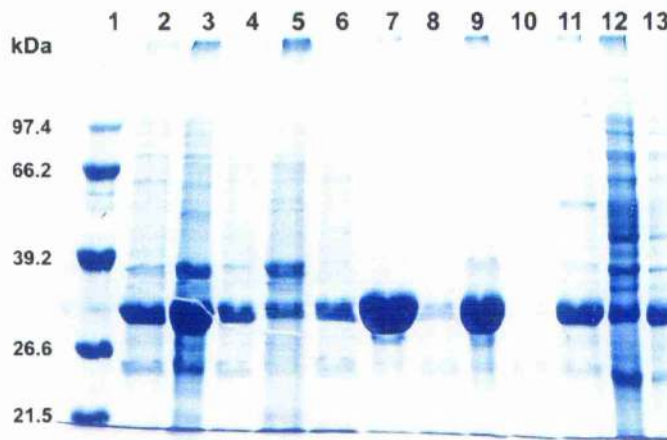


Figure 62. SDS PAGE analysis of ammonium sulphate saturation experiment. Lane 1: Boehringer Mannheim marker low-range, lanes 2,4,6,8 and 10: supernatant fractions of $(\text{NH}_4)_2\text{SO}_4$ saturations from 10% to 30% saturation. Lanes 3,5,7,9 and 11: redissolved pellets of $(\text{NH}_4)_2\text{SO}_4$ saturations from 10% to 30% saturation (5% increments). Lanes 12 and 13: *E. coli H. influenzae* YdiB construct crude extract control and induced, respectively.

The *E. coli* shikimate dehydrogenase protein purification also included an anion exchange step on DEAE Sephacel; this purification step was omitted from the YdiB protein purification since preliminary experiments revealed that YdiB did not bind to the column.

The purification of *H. influenzae* YdiB was performed as follows; cells were lysed and centrifuged as described in section 2.5.3. The soluble supernatant was adjusted to 25% saturation $(\text{NH}_4)_2\text{SO}_4$ and centrifuged as described in section 2.12.3.2. The resulting precipitate was re-dissolved in 0.5 M NaCl 100 mM Tris·HCl pH 7.0 (buffer A) and dialysed overnight in the same buffer. The dialysed soluble protein was then concentrated to a volume of 20 ml and applied to an affinity chromatography column (2',5'-ADP Sepharose) that had been pre-equilibrated in buffer A at a flow rate of 10ml/hour. The column was washed in 100 ml of buffer A and 4 ml fractions of the eluant were taken. A 20 ml portion of 1mM NADP^+ in buffer A (flow rate of 1ml/hour: 1ml fractions) was then applied to the column to elute the YdiB protein. Fractions were assayed as described in section 6.6 except; 100 mM sodium carbonate buffer (pH 10.6) was used instead of the 100 mM glycine·Tris·NaOH buffer (pH10.0) later used in kinetic analysis. The capacity of the column was not large enough and

consequently a large fraction of the YdiB protein did not bind to the affinity column. This meant that fractions with activity were found before and after the NADP⁺ elution step (data not shown). In the future it will be preferable to use a larger column of the same material or a less expensive option could be to use a Resource Q or Phenyl-Sepharose column. Fractions containing shikimate dehydrogenase activity were pooled and concentrated to a volume of 2 ml and applied to a Sephacryl 200 (gel filtration) column (165 × 2.5 cm diameter), which had been equilibrated in 100 mM Tris-HCl, pH 7.5 containing 0.5 M NaCl (buffer B) at a flow rate of 10ml/hour; 5ml fractions were collected. The protein was eluted using buffer B. The A₂₈₀ of the eluant was monitored and assays for shikimate dehydrogenase activity were performed: Figure 63 shows the elution profile. Samples that possessed shikimate dehydrogenase activity were analysed by SDS PAGE (Figure 64) to assess the level of purity of the YdiB protein; appropriate fractions were pooled and concentrated to approximately 10 mg/ml. The concentration of Tris-HCl (pH 7.5) was adjusted to 300 mM. The concentrated YdiB protein was divided into two aliquots; to one an equal volume of glycerol was added prior to storage at -20°C. The second aliquot was concentrated by using a 0.5 ml Vivaspin 500 centricon with a 10 kDa cut-off (Viva Science) which was centrifuged at 16,000 × g for 15 minutes at 4°C. The concentrated solution was then adjusted to 300 mM Tris-HCl (pH 7.5), 15mg/ ml YdiB protein and used in crystallisation screens (6.4).

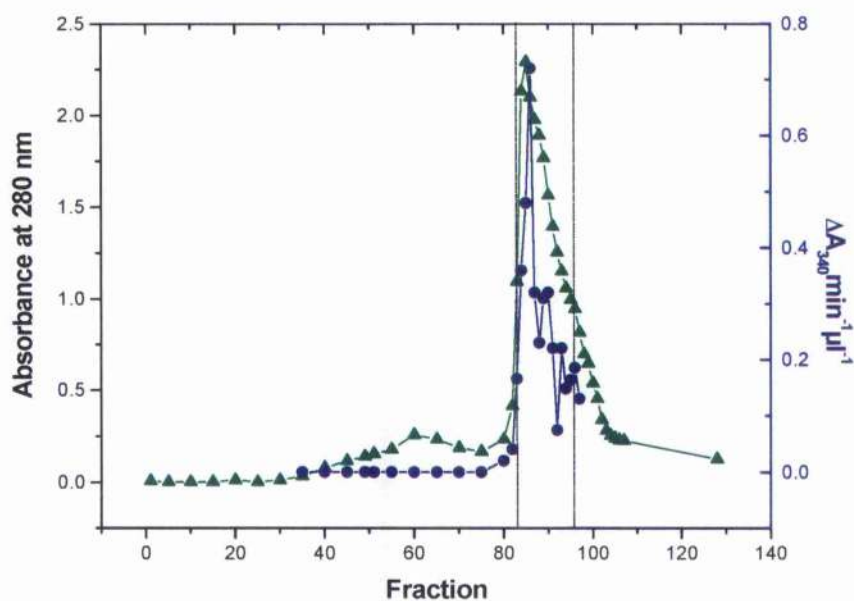


Figure 63. Elution profile of the purification of *H. influenzae* shikimate dehydrogenase related protein YdiB (HIYdiB) on Sephacryl 200 column. The A_{280} of the eluant is shown as green triangles. Shikimate dehydrogenase activity is shown as blue circles. Fractions that were pooled are shown between the dash black lines.

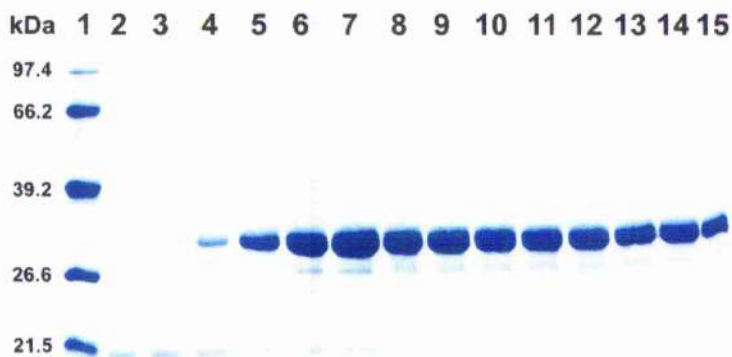


Figure 64. SDS PAGE analysis of Sephacryl 200 elution fractions. Lane 1: Boehringer Mannheim marker low-range, lanes 2-15: S200 fractions 80 to 94.

6.3 Dynamic light scattering of HIAroE and HIYdiB

Dynamic light scattering was used (2.23) to investigate the quaternary structure and any structural changes in the presence cofactor, substrate and the potential inhibitor vanillin. The ECAroE has been shown to be a monomeric protein by gel filtration (Chaudhuri and Coggins, 1985) and by dynamic light scattering analysis (Maclean *et al.*, 2000). Dynamic light scattering of ECYdiB indicated that the predominant species was ~60 kDa indicating that ECYdiB forms dimers. This was confirmed by size exclusion chromatography where the apo protein eluted as a single species of 64 kDa (Michel *et al.*, 2003). Sequence analysis of both the *H. influenzae* AroE and YdiB proteins reveal hydrophobic side chains in the same positions as ECYdiB suggesting that both HIAroE and HIYdiB form dimers.

The HIAroE protein was studied at a protein concentration of 2.5 mg/ml in 50 mM Tris·HCl, 200 mM KCl (pH 7.0). The HIYdiB protein was analysed at a protein concentration of 1 mg/ml in 300 mM Tris·HCl (pH 7.0). Where indicated NADP⁺ was added to a concentration of 2 mM, shikimate and vanillin were added to a final concentration of 4 mM. All protein-ligand experiments were incubated at 20°C for 5 minutes prior to analysis. 200 µl of each solution was injected into the dynamic light scattering cell.

The estimated molecular weight of HIAroE in the presence of NADP⁺ and shikimate is ~32 kDa which is consistent with HIAroE being monomeric in a similar fashion to the ECAroE protein (Maclean *et al.*, 2000). Without NADP⁺ and shikimate the sum of squares (SOS) increased significantly; this is likely to arise from aggregation of the enzyme. In the presence of NADP⁺ and vanillin the SOS shows the data to be unreliable reflecting greater polydispersity of the protein, (Table 8).

Table 16. Dynamic light scattering data of *H. influenzae* shikimate dehydrogenase and YdiB protein⁵.

	<i>H. influenzae</i> shikimate dehydrogenase			<i>H. influenzae</i> YdiB protein		
	Radius (nm)	Estimated MW (kDa)	SOS Error	Radius (nm)	Estimated MW (kDa)	SOS Error
300 mM Tris·HCl	ND	ND	ND	3.5	60	1.326
50 mM Tris·HCl, 200 mM KCl	29.9	11041	131.1	ND	ND	ND
2 mM NADP	ND	ND	ND	3.3	54	0.583
2 mM NADP ⁺ , 4 mM Shikimate	2.7	32	6.49	3.3	55	0.678
2 mM NADP ⁺ , 4 mM Vanillin	4	87	60.28	ND	ND	ND

The estimated molecular weight of HIYdiB in buffer is 60 kDa (Table 8), consistent with the formation of dimeric units as observed for ECYdiB (Michel *et al.*, 2003). In the presence of NADP and shikimate the hydrodynamic radius of HIYdiB is slightly reduced which is most probably due to a closing of the protein conformation

⁵ ND = Not determined.

caused by the binding of the ligands. Various closed conformation are seen in the X-ray structure of ECARoE and ECYdiB (Michel *et al.*, 2003). The diameter of the ECYdiB in 300 mM Tris·HCl is approximately 70 Å in the presence of 2 mM NADP⁺ and 4 mM shikimate the diameter decreased to 66 Å.

6.4 Crystallization of HIAroE and HIYdiB

AroE and YdiB from *H. influenzae* have been crystallized by the sitting drop vapour-diffusion method at 20°C (2.24). Crystallisation trails were set up with protein freshly purified. The HIAroE and HIYdiB were concentrated to 20 mg/ml by using a 0.5 ml Vivaspın 500 centricon with a 10 kDa cut-off (Viva Science). 1 µl of HIAroE in 1 mM NADP, 200 mM KCl, 50 mM Tris·HCl, (pH 7.0) was added to 1 µl each of the crystallisation reagents to be tested, trials of HIAroE with 0.5 mM vanillin included in the primary buffer were also set up. The primary buffer for HIYdiB was 1 mM NADP, 300 mM Tris·HCl (pH 7.0). Sparse screen matrices of HIAroE were set up using a comprehensive range of conditions including commercial screens such as Wizard II (Emerald Biostructures), and local sparse screen matrices such as Magic 50, M-screen, N-screen and CAS screen (Hampton research) overall a total of 672 crystallisation conditions were set up. The sparse screen matrices Wizard I, Wizard II, M- screen and magic 50 were set up for HIYdiB, overall a total of 312 crystallisation conditions were set up.

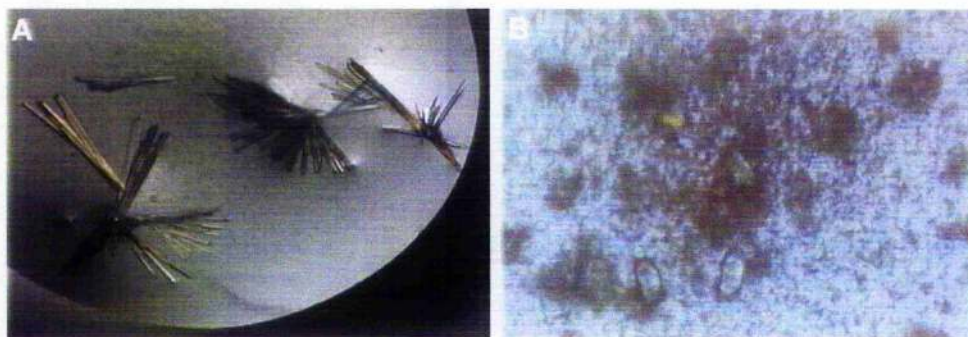


Figure 65. Crystals of HIAroE 10 mg/ml HIAroE in 1 mM NADP, 200 mM KCl, 50 mM Tris·HCl, (pH 7.0). Formed by the sitting-drop vapour diffusion method (A). 0.2 M sodium nitrate, 20% (w/v) PEG 3350 yielded large needle forms. (B) Small rhombus shaped crystals were found in 0.1 CaCl₂, 10% (w/v) PEG 8000, 0.1 M HEPES (pH7.5) without vanillin.

Several conditions gave promising results for HIAroE, 0.2 M sodium nitrate, 20% (w/v) PEG 3350 yielded large needle forms both in the presence and absence of 0.5 mM vanillin (Figure 65A). Small rhombus shaped crystals were found in 0.1 CaCl₂, 10% (w/v) PEG 8000, 0.1 M HEPES (pH7.5) (Figure 65B) without vanillin.

HIYdiB crystallised under several different conditions as summarised in Table 17.

Table 17. Crystallisation conditions for HIYdiB.

Crystallisation (number)	screen	Crystallisation conditions	Morphology of crystals
Wizard I (6)		30% (w/v) PEG 3000, 0.1 M citrate (pH 6.0)	Large needle like crystals
Wizard II (36)		0.2 M NaCl, 10% (w/v) PEG 3000, phospho/citrate buffer (pH 4.2)	Large cubic crystals (Figure 66)
M-Screen (2)		0.1 M LiSO ₄ , 10% (w/v) PEG 8000, 0.1 M acetate (pH 4.6)	Large hexagonal prisms (Figure 66)
M-Screen (76)		0.2 MgCl ₂ , 15% (w/v) PEG 4000, 0.1 M acetate (pH 4.57)	Large cubic crystals
M-Screen (82)		30% Mono-methylether PEG 2000, 0.1 M citrate (pH 5.38)	Large needle like crystals
Magic 50 (20)		0.2 (NH ₄) ₂ SO ₄ , 25% (w/v) PEG 4000, 0.1 M acetate (pH 4.6)	Small cubic crystals some precipitation

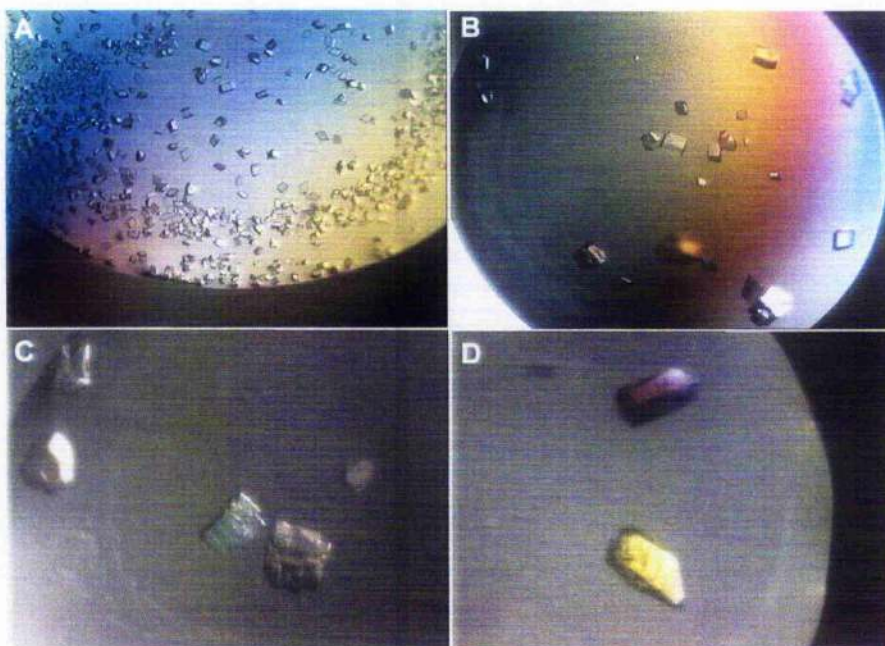


Figure 66. Crystals of *H. influenzae* shikimate dehydrogenase related protein YdiB (HIYdiB) 10 mg/ml in 1 mM NADP, 300 mM Tris·HCl (pH 7.0). Formed by the sitting-drop vapour diffusion method (A) 0.2 M NaCl, 10% (w/v) PEG 3000, phospho/citrate buffer (pH 4.2). (B) 0.1 M LiSO₄, 10% (w/v) PEG 8000, 0.1 M acetate (pH 4.6). (C) 0.1 M Li₂SO₄, 0.1 M acetate buffer 10% (w/v) PEG 8000, (pH 5.0 and 5.2). (D) 0.2 M MgCl₂, 0.1 M acetate buffer 10.5% and 12% (w/v) PEG 4000, (pH 5.0).

HIYdiB crystallised predominately in the presence of low concentrations of NaCl, Li₂SO₄ or MgCl₂ salts, 10-25% (w/v) PEG 3000-8000 and in either acetate or citrate buffer at a pH of between 4 to 5. Three optimisation matrices were set up for HIYdiB. In the first optimisation the protein drop size was adjusted, under the crystallisation conditions already determined. The 1: 1 µl ratio of protein solution to crystallisation reagent was repeated and ratios of, 1.5: 1.5 µl, 2: 2 µl and 1: 2 µl were also set up. Most of the conditions of optimisation 1 still yielded crystals of various sizes. The second optimisation matrix varied both the concentration of PEG 8000 from 4-14% (w/v) and the pH from 4.4 to 5.2 (0.1 M Li₂SO₄, 0.1 M acetate buffer) across 24 wells, yielding irregular cubic crystal forms in 10% (w/v) PEG 8000, pH 5.0 and 5.2 (Figure 66). Crystals were also found in 12% (w/v) PEG 8000 pH 5.2. The third optimisation matrix varied both the concentration of PEG 4000 from 10.5-

18% (w/v) and the pH from 3.8 to 5.0 (0.2 M MgCl₂, 0.1 M acetate buffer) over 24 wells, yielding small cubic crystal forms in 10.5% and 12% (w/v) PEG 4000, pH 5.0 (Figure 66). Optimisations were not carried out on HIARoE as K. Stewart continued this part of the project.

Protein crystals were tested by X-ray diffraction at the Daresbury synchrotron on Beam Line 9.6 by B. Lohkamp and A. McEwen. Preliminary diffraction experiments showed that HIYdiB crystals diffracted to approximately 8.0 Å. These crystals were more than 2 months old and it is possible that newer crystals may diffract significantly better.

6.5 Structural comparisons using circular dichroism

The CD spectrum of the HIARoE and HIYdiB was recorded in both the near UV and far UV at protein concentrations of 1.38 mg/ml and 0.5 mg/ml respectively and in cells of 0.5 cm and 0.02 cm path length respectively in 50mM potassium phosphate buffer pH 7.0. From the far UV CD spectra it was clear that the secondary structures of HIARoE and HIYdiB are very similar (Figure 67A). There is a slight increase in the peak at 195 nm is likely to be due to higher content of alpha helix in HIARoE. The secondary structural contents were calculated using the SELCON procedure (Sreerama and Woody, 1994b) and are shown in Table 18.

Table 18. Secondary structure estimates (%) using the SELCON procedure of Sreerama and Woody (1994b).

	Alpha helix	Antiparallel beta sheet	Parallel beta sheet	Turns	Other
HIAROE	32.6	10.5	9.2	15.7	31.6
HIYdiB	28.1	12.4	8.4	16.8	34.1

The near UV CD spectrum shows differences in the environments of the aromatic amino acids between HIARoE and HIYdiB. There are no tryptophan side chains in the HIYdiB sequence; this is reflected in the near UV CD where there is only a low signal at 290 nm compared with the HIARoE which possesses three tryptophan side chains, which contribute to the signal at 290 nm (Figure 67B).

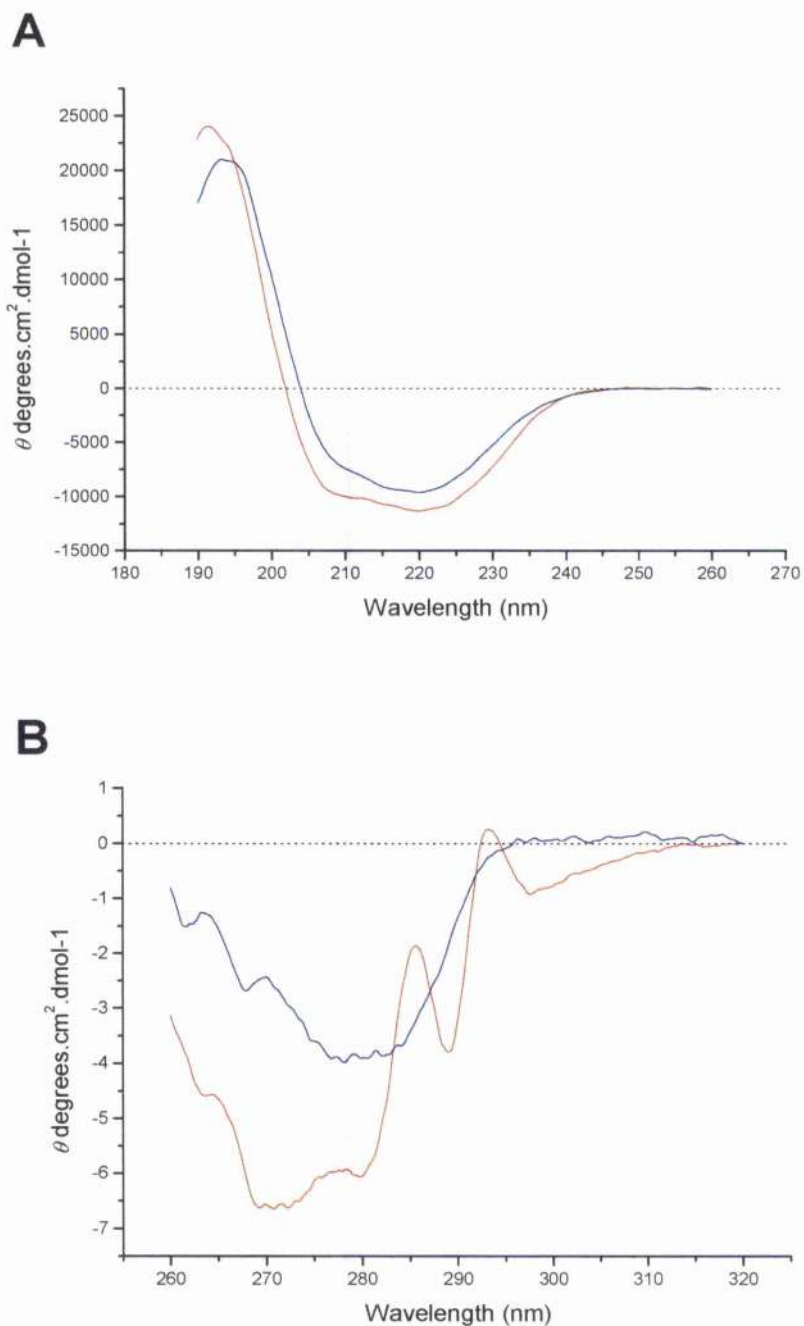


Figure 67. CD spectra of HIAroE (red) and HIYdiB (blue) in 50mM potassium phosphate buffer pH 7.0. (A) Far UV CD spectra of *H. influenzae* analogues (0.5 mg/ml; 0.02 cm path length). (B) Near UV spectra UV of *H. influenzae* analogues (1.38 mg/ml; 0.5 cm path length).

Overall the HIYdiB structure has more aromatic residues than HIAroE, although the HIAroE signal is substantially stronger this is could either be due to a greater structural rigidity in the tertiary structure or neighbouring aromatic side chains that are quenching each other's signal. It would be interesting to use CD to study the effect of NADP on the tertiary structure in solution, since changes in the tertiary structure could correspond to formation of the closed conformation observed in the X-ray structure of HIAroE-complexed with NADP⁺ and DTT. However the strong absorption by NADP⁺ at 260 nm could complicate the interpretation of the CD spectra.

6.6 Kinetic Comparisons of AroE and YdiB enzymes

At physiological pH (7.0) the reaction equilibrium favours production of shikimate over dehydroshikimate, i.e. the direction of the biosynthetic route of the shikimate pathway. However it is more convenient to follow the reverse reaction at the non-physiological pH (10.0), because dehydroshikimate is not readily available.

Steady-state kinetics experiments were performed on HIAroE and HIYdiB. The formation of dehydroshikimate from shikimate or the formation of dehydroquininate from quinate was monitored by measuring the formation of the reduced form of the cofactor (NADH or NADPH) by observing the increase in absorbance at 340 nm (2.16.2). Assays were performed in a 1 ml quartz cuvette, 1 cm path length with 100mM glycine adjusted to pH 7.0 with 2 M Tris and then additionally adjusted to pH 10.0 with 10 M NaOH (assay buffer) at 25°C using either 0.05-5 µg of HIAroE or 1-10 µg of HIYdiB. All assays were performed in duplicate. The concentrations of cofactors: NAD⁺ and NADP⁺ and the substrates shikimate and quinate were both varied in systematic fashion to give a matrix of 25 two-substrate assays. Stock solutions of substrates were made up in assay buffer and adjusted to pH 10.0. The concentration range of each of the substrates is summarised in Table 19.

Table 19. Summary of concentration ranges used for two substrate assays performed on HIAroE and HIYdiB the range in conjunction with the other substrate present (*) (mM).

*	Shikimate		Quinate		NADP		NAD	
	NADP (mM)	NAD (mM)	NADP (mM)	NAD (mM)	SHK (mM)	QUIN (mM)	SHK (mM)	QUIN (mM)
HIAroE	0.025- 1.5	0.07- 1.	10- 200	20- 200	0.025- 1.5	0.05- 1.5	5-20	2.5-20
HIYdiB	5-80	5-60	N/A	N/A	(0.05- 1.5	N/A	5-20	N/A

Double reciprocal graphs (2.18) were plotted for all of the two-substrate matrices. In addition V_{\max} and K_m values were determined by hyperbolic regression fits of individual groups of assays where one substrate was kept constant (substrate A) and the other varied (substrate B). These values were converted to give the intercept and slope values using the as two substrate steady-state kinetics equations shown below (Price and Stevens, 1999):

$$\text{Intercept} = \frac{1}{V_{\max}}$$

$$\text{Slope} = \frac{K_m}{V_{\max}}$$

The intercept and slope values were plotted against the reciprocal values of the concentration of substrate A (Figure 68). The final kinetic parameters were calculated from the intercept and slope of the secondary plots, as shown in the equation below. Values of k_{cat} were calculated from the actual V_{\max} values using the extinction coefficient for NAD(P) of $6270 \text{ M}^{-1} \text{ cm}^{-1}$ and the theoretical molecular weights of HIAroE (29.76 kDa) and HIYdiB (29.9 kDa). The results of the steady-state kinetic analysis of *H. influenzae* AroE and YdiB are summarised in Table 20.

$$K'_B = \frac{V_{\max} \times \text{Slope}}{K_A}$$

Determination of K' values from double reciprocal plot data (Price and Stevens, 1999).

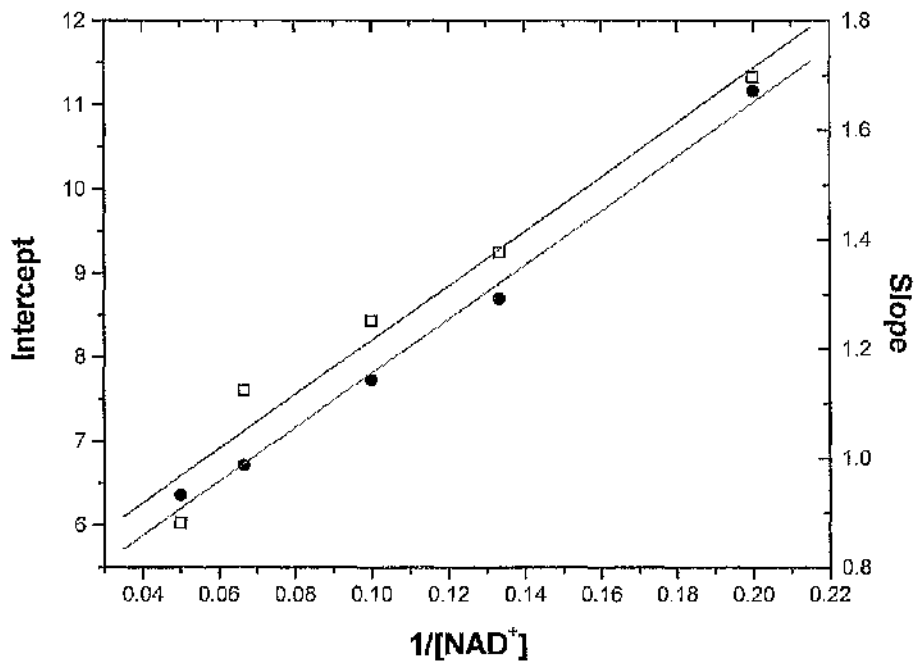


Figure 68. Steady state kinetics double reciprocal plot of *H. influenzae* shikimate dehydrogenase (HIAroE) with NAD^+ and shikimate.

Table 20. Steady-state kinetic analysis of *H. influenzae* shikimate dehydrogenase (HIAroE) MW = 29.76 kDa.

		K_m (mM)	K' (mM)	$\mu\text{mol}/\text{min}/\mu\text{g}$	μg of Enz.	k_{cat} s^{-1}	k_{cat}/K_m $\text{M}^{-1} \text{s}^{-1}$
Shikimate	NADP ⁺	0.0196	-	-	-	-	9.92×10^6
	NAD ⁺	8.558	-	-	-	-	-
	Shikimate (+NADP ⁺)	0.18	0.09075	391.87	0.1	194.37	1.08×10^6
	Shikimate (+NAD ⁺)	0.18	0.0925	719.94	0.05	357.09	1.98×10^6
Quinate	NADP ⁺	0.024	-	-	-	-	2.07×10^6
	NAD ⁺	16.946	-	-	-	-	4.60×10^2
	Quinate (+NADP ⁺)	89.7	98.7	100.13	0.5	49.66	5.54×10^2
	Quinate (+NAD ⁺)	18.94	77.49	15.71	5	7.79	4.11×10^2

Table 21. Steady-state kinetic analysis of *H. influenzae* shikimate dehydrogenase related protein (HIYdiB) (MW = 29.9 kDa).

		K_m (mM)	K' (mM)	$\mu\text{mol}/\text{min}/\mu\text{g}$	μg of Fenz.	k_{cat} s^{-1}	k_{cat}/K_m $\text{M}^{-1} \text{s}^{-1}$
Shikimate	NADP ⁺	0.3761	-	-	-	-	5.09×10^4
	NAD ⁺	13.58	-	-	-	-	4.46×10^1
Shikimate (+NADP ⁺)		64.15	6.989	38.44	1	19.15	2.99×10^2
Shikimate (+NAD ⁺)		11.85	25.04	1.22	10	0.61	5.11×10^1
Quinate	NADP ⁺	*	-	-	-	-	-
	NAD ⁺	*	-	-	-	-	-
Quinate (+NADP ⁺)		^	-	-	10	-	-
Quinate (+NAD ⁺)		^	-	-	10	-	-

HIYdiB only exhibited a very low level of catalytic activity with quinate as substrate in the presence of either cofactor. Assays were performed using 100 mM quinate, either 10 mM NADP⁺ or 15 mM NAD⁺ and 10 μg of HIYdiB in the standard assay buffer. The $\Delta A_{340} \text{min}^{-1}$ was 0.005 (approximately $5 \times 10^{-3} \text{ s}^{-1}$) and 0.0024 (approximately $2 \times 10^{-3} \text{ s}^{-1}$), for NADP⁺ and NAD⁺ respectively so it was not possible to obtain kinetic parameters for HIYdiB with quinate as a substrate.

* 0.005 $\Delta A_{340} \text{min}^{-1}$ for 10mM NADP 100mM Quinate 10 μg of enzyme.

^ 0.0024 $\Delta A_{340} \text{min}^{-1}$ for 10mM NADP 100mM Quinate 10 μg of enzyme.

The inhibitory effect of vanillin on HIARoE was investigated. The concentration of the cofactor was kept constant (1.5 mM) while both shikimate and vanillin were varied to generate data for a Lineweaver-Burk plot. Preliminary experiments revealed that vanillin absorbed substantially at 340nm. Figure 69 shows the absorbance spectrum of 0.1 mM vanillin at pH 9.0 showing that the absorbance at 340 nm is 1.2 using a cuvette with a 1 cm path length. Further inhibition studies were performed using a cuvette of 4 mm path length and monitoring the increase in absorbance at 366 nm. No inhibitory effect was observed for vanillin at a concentration of 0.1 mM (note the absorbance of 0.1 mM vanillin at 366nm in a 4 mm path length was 0.58). These inhibition experiments were not performed using a layer of toluene to stop the oxidation of vanillin as described by Balinsky and Davies, (1961b). It might be possible to use this method to study higher concentrations of vanillin and observe an inhibitory effect. However, inhibition studies on the *P. sativum* shikimate dehydrogenase revealed a K_i value of 93 μM for vanillin (Balinsky and Davies, 1961b), the concentration of vanillin (0.1 mM) used in the inhibition studies on HIARoE would be expected to have some inhibitory affect.

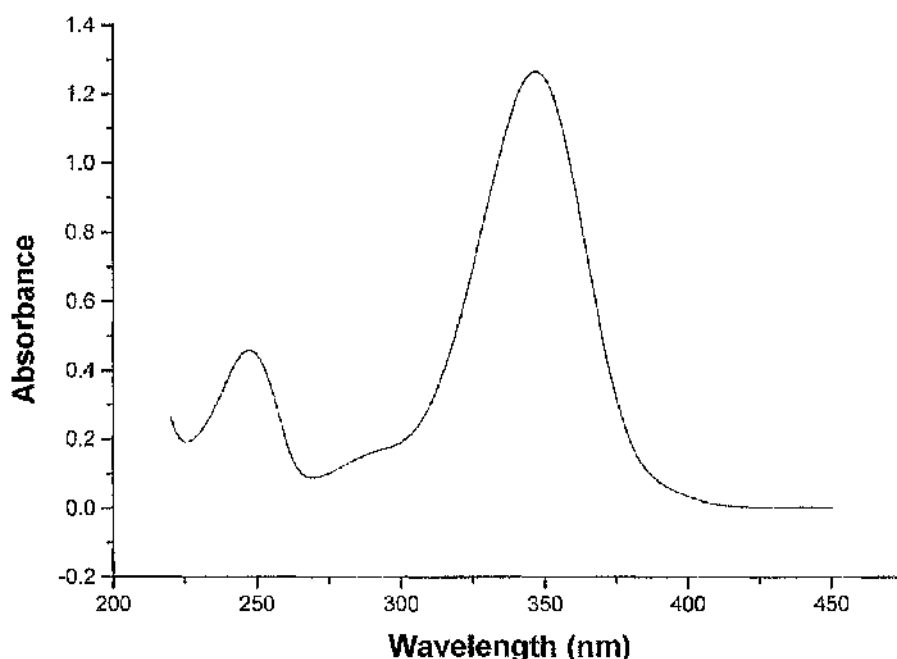


Figure 69. Absorbance spectrum of 0.1 mM vanillin at pH 9.0, 1 cm path length.

6.7 Fluorescence binding experiments of *H. influenzae* shikimate dehydrogenase

To investigate whether the HIARoE follows a BiBi ordered mechanism like the bifunctional *P. sativum* (Dowsett *et al.*, 1972) fluorescence binding experiments were performed using shikimate in the absence of NADP⁺. Fluorescence measurements were carried out in 100 mM glycine-NaOH buffer (pH 10.0) at 20°C in a 1 ml volume cell with a 1 cm path length cell and with the slits set at 5.0 nm bandpass. The shikimate concentration was increased from 0 to 540 μM by the addition of 10 μl aliquots of solution of 3 or 15 mM shikimate. Shikimate was not found to quench any emission at 312 nm and there it was not necessary to correct the fluorescence results by using a model compound such as N-Acetyl-L-tyrosinamide. Samples were excited at 290 nm and their emissions were monitored at 312 nm. Emission values were corrected for both Raman scattering and the dilution effect of titration.

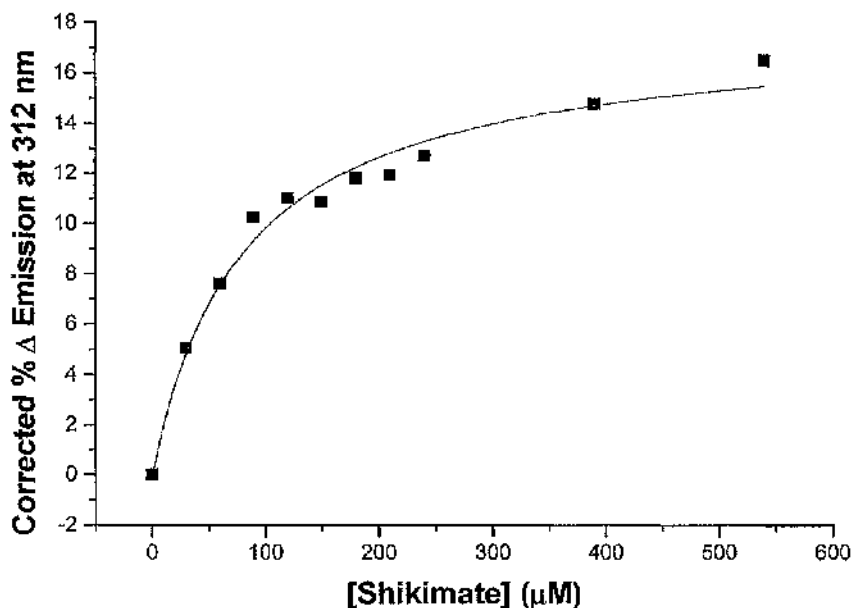


Figure 70. Fluorescence binding of *H. influenzae* shikimate dehydrogenase (HIARoE) corrected for Raman scattering and dilution effect.

The corrected percentage change in emission values (where 0% is defined to 0 mM shikimate) were fitted using a non-linear regression fit and are shown in Figure 35. The K_{SHIK} value for HIARoE in the absence of NADP⁺ is $82 \mu\text{M} \pm 11$. The K_{SHIK}

value is comparable to the K'_{SHIK} observed in the steady state kinetics results (90 μM). This shows that shikimate is able to bind to HIAroE irrespective of the presence of NADP^+ . Further evidence that the mechanism of HIAroE is not ordered in contrast with the BiBi mechanism of *P. sativum* (Balinsky *et al.*, 1971).

6.8 Chapter summary

HIAroE and HIYdiB are both NADPH-dependent dehydrogenases. However, they are both able to utilise shikimate in the presence of NAD^+ and HIAroE is able to utilise quinate in the presence of both cofactors. HIAroE appears to bind NADP^+ (K_{NADP} 20 μM) more tightly than NAD^+ (K_{NAD} 8500 μM). This is consistent with the results of sequence analysis that revealed similar residues within the cofactor recognition site to those in the NADP-dependent ECAroE (K_{NADP} 56 μM). On this basis Thr151 in HIAroE is likely to play an important role in cofactor recognition. HIYdiB also appears to bind more tightly to NADP^+ (K_{NADP} 380 μM) than NAD^+ (K_{NAD} 1400 μM). It is probable that the cofactor-recognition site of HIYdiB is broadly similar to both ECAroE and HIAroE. The hydrophobic valine side chain (V154) could be responsible for some of the loss in binding affinity observed in HIYdiB compared with HIAroE. However, it is also possible that Val154 could be orientated to face away from the cofactor, with some alterations in the relevant part of the amino acid sequence of HIYdiB, a 3-dimensional X-ray structure would clearly resolve these issues.

Since HIAroE is able to catalyse the reduction of both shikimate and quinate, it is possible to assign HIAroE as a putative shikimate/quininate dehydrogenase. The K_{SHIK} values for HIAroE in the presence of either cofactor are identical (180 μM). The HIAroE K' values for shikimate (K' of ~ 90 μM) with either cofactor are lower than the K_{SHIK} values. This was unexpected as it was originally thought that binding of the cofactor would aid the binding of substrate, although substrate binding maybe related to the release of the product, as there is a trade off between binding specificity and catalytic activity. The fluorescence studies revealed that shikimate is able to bind to HIAroE irrespective of the presence of a cofactor with a K_{SHIK} of 82 μM which is very close to the K' value reported. On this basis it would appear that the enzyme mechanism is not ordered as in *P. sativum* (Balinsky *et al.*, 1971). It is thought that the non-cooperative binding observed may be related to product release as tight

binding of the enzyme-cofactor-substrate complex could decrease the turnover of the enzyme (personal communication from Prof. Paul Engel, University College Dublin).

The catalytic activities of HIAroE in the presence of shikimate with either NADP⁺ (k_{cat} 194 s⁻¹) or NAD⁺ (k_{cat} 357 s⁻¹) are comparable; the k_{cat} of HIAroE may reflect the precise binding mode of the cofactor. The 2-fold difference in k_{cat} may be explained in part if the release of the cofactor is the limiting factor within the catalytic reaction, as the $K_{\text{NAD(P)}}$ is higher for NAD⁺ than NADP⁺. Release of the product has been shown to be the rate-limiting step in a number of dehydrogenases such as lactate dehydrogenase (Price and Stevens, 1999; Südi, 1974a; 1974b).

The catalytic properties of HIAroE for quinate in the presence of either NADP⁺ (k_{cat} 50 s⁻¹) or NAD⁺ (k_{cat} 8 s⁻¹), do not follow the same pattern as for oxidation of shikimate. The HIAroE K_{QUIN} values for quinate in the presence of either NADP⁺ and NAD⁺ are 90 and 19 mM respectively. In these circumstances it appears that the release of dehydroquinone may be the limiting factor in this catalytic reaction. In contrast to the HIAroE K' values for shikimate the HIAroE K' values for quinate (99 and 78 mM in the presence of NADP⁺ and NAD⁺, respectively) are higher than the K_{QUIN} values, suggesting that the cofactor promotes binding of quinate although the high K values point to weak binding of this substrate. The ECroE catalyses the oxidation of both shikimate and quinate, but the catalytic activities are much lower than for HIYdiB. Interestingly the catalytic activity of ECYdiB in the presence of NAD⁺ is higher for quinate and lower for shikimate, the reverse of the trend observed in HIAroE. ECYdiB is unlikely to be a true quinate/shikimate dehydrogenase due to its extremely low catalytic activity with quinate as substrate, although the true substrate of this protein may share some of the same structural features of both dehydroshikimate and quinate.

The analogue HIYdiB is only able to catalyse the oxidation of shikimate, and although the catalytic activity is higher than for ECYdiB it is unlikely that HIYdiB is a true shikimate dehydrogenase, since the k_{cat} values of 19 and 0.6 s⁻¹ are 10 and 600-fold (for NADP⁺ and NAD⁺, respectively) lower than for HIAroE. Interestingly shikimate appears to bind tighter to HIYdiB in the presence of NAD⁺ (K_{SHIK} 12 mM) than NADP⁺ (K_{SHIK} 64 mM). A similar pattern is observed with the HIAroE-quinone results, where tighter binding is accompanied by lower catalytic activity. The extremely low catalytic activity observed using quinate as substrate in the presence of

either NAD⁺ or NADP⁺ is likely to result from differences in the amino acid sequence near the N-terminus. The kinetic data suggests that the true substrate of HIYdiB and the other members of this subset of the shikimate dehydrogenase family are unlikely to possess a carboxylate and a hydroxyl group at C1. The conserved insert of four amino acids near the N terminus ([R,t,a,q]-F-H-N) may well play some catabolic role possible in binding some small hydrophobic group. A 3-dimensional X-ray structure would be valuable in discovering the true substrate of HIYdiB. The preliminary crystals obtained here could provide the basis for such a structural determination. Equally screening a series of dehydroshikimate analogues could identify the important components for binding which could be used in a wide search for the true substrate.

It would be beneficial to study the conversion of dehydroshikimate to shikimate (forward reaction). This could be achieved either by performing a coupled assay with a dehydroquinase enzyme or dehydroshikimate could be chemically synthesized via the dichloro-dicyano-benzoquinone (DDQ) oxidation of commercially available shikimate as described by T. Bugg (1989). pH dependence profiles of both the forward and reverse reactions of shikimate dehydrogenase would be very valuable. The pI of HIYdiB is 8.59 and protein incubated at a high pH (10.0) and at a high protein concentration (~10 mg/ml) for extended periods of time (>4 hours) tended to precipitate. It is therefore possible that these non-physiological conditions may have affected the kinetic properties of HIYdiB. In the future it would be informative to repeat these experiments at pH 7.0.

The inhibition studies of HIAroE show no inhibitory effect of vanillin. Most of the previously reported inhibition studies were performed on the plant bifunctional enzymes such as that from *Pisum sativum*, where several analogues including vanillin were found to be competitive inhibitors. The substrate-binding domain of these bifunctional enzymes may well adopt a different conformation from that of the bacterial shikimate dehydrogenases. Gallic acid was found to be a competitive inhibitor of the *Pisum sativum* enzyme (Baillie *et al.*, 1972), but recent studies have shown it to be a substrate of the mountain birch bifunctional enzyme which is involved in the formation of hydrolysable tannins (Ossipov *et al.*, 2003). It is possible that these early studies were complicated by the high absorbance of many of these potential inhibitors, although Balinsky and Davies (1961b) did take measures to

limit the oxidation of vanillin and some other potential inhibitors. Further crystallisation trials of both HIAroE and HIYdiB should be performed with other potential inhibitors such as *p*-hydroxybenzaldehyde acid; with an aim of obtaining a tertiary complex of the enzyme. This would shed light on the mode of binding of the substrate to the enzymes.

The protein purification method used for HIYdiB (pI of 8.59) could be further developed; instead of using an anion exchange column at pH 7.5, a cation exchange mono or resource Q column at pH 7.5 could be used. This is likely to increase the purity, and yield of the protein purification, although it should be noted that the protein obtained from the method described (6.2.3) was of a high purity as judged by SDS-PAGE.

The existence of two isoforms of shikimate dehydrogenases in many bacterial species evokes evolutionary and metabolic questions, and also affects the design of any potential inhibitors. The location of the *aroE* gene within the *H. influenzae* genome is between a gene coding for a DNA-3-methyladenine glycosidase I and a conserved hypothetical protein of function unknown. The loci of the *ydiB* gene is close to a serine acetyltransferase and a conserved hypothetical protein. The location of these genes within the *E. coli* genome is different; the *aroE* gene is surrounded by genes with unknown or putative functions and *ydiB* (subset more closely related gene to *aroE*) is located between a gene thought to encode an amino acid transport protein, and the *aroD* gene coding for a type I dehydroquinase. It is postulated that this *ydiB-aroD* cluster is the ancestral precursor to the bifunctional enzyme found in plants and some bacteria (Michel *et al.*, 2003). Since *H. influenzae* possesses a type II DHQase rather than a type I DHQase a bifunctional enzyme would not be expected.

The dynamic light scattering data shows that HIYdiB forms dimers of approximately 60 kDa, in contrast to HIAroE which is apparently monomeric. A site-directed mutagenesis strategy could be used to identify the key residues likely to be involved in dimer formation, especially residues Leu9, Met40 and Phe42 in ECYdiB.

The crystallisation trails of HIAroE and HIYdiB, yielded encouraging results. Only a few crystals were tested at the Daresbury synchrotron and it is expected that further X-ray diffraction experiments using fresher crystals will give a better diffraction pattern. The X-ray structure of HIYdiB is currently on hold at the Protein Data Bank

(PDB identifier: 1NPY) (<http://www.rcsb.org/pdb/>) submitted by Korolev *et al.* at the Feinberg School of Medicine, Northwestern University, Chicago this data should be very useful in understanding the precise nature of the substrate-binding pocket in the enzyme.

CHAPTER 7 GENERAL DISCUSSION

In this chapter I would like to highlight some of the major conclusions concerning the bacterial type II dehydroquinases and shikimate dehydrogenases.

Site-directed mutagenesis of the active site residues of SCDHQase: R113A, H106A, E104A, S108A and Y28F all significantly decrease the catalytic activity of the enzyme (Table 7 page no. 108). The mutation Y28F and R113A gave the largest effects with 4700-fold and 2190-fold reductions in k_{cat} . CD evidence confirmed that none of the mutations significantly altered the secondary or tertiary structure of the enzyme (Table 6 page no. 106). This indicates that the enzyme structure was not significantly altered and strongly suggests that the mutations altered the catalytic mechanism of SCDHQase. pH studies of SCDHQase, HPDIHQase, MTDHQase and *B. subtilis* YqhS mutant F23Y show that as pH increases from 6.5 to 8.0 there is a seven-fold increase in catalytic activity (k_{cat}) (Figure 47 page no. 155). This implies that all of these type II DHQases share a common catalytic mechanism. This is confirmed by the 3-dimensional X-ray structure data for each of the type II DIIHQases which show that the key active site residues are all arranged in a similar manner in each structure (Figure 44 page no. 147). The two exceptions to this statement are: (1) HPDHIHQase possesses a threonine in the place of serine 108 and (2) the precise orientation of tyrosine 28 (*S. coelicolor* numbering system) thought to be involved in proton abstraction, varies among the structures. In the low k_{cat} enzymes (HPDHIHQase, MTDHIHQase) the lid domain in which this tyrosine residue is situated is not ordered. It was hypothesised that these structures were more flexible in the lid domain and this may account for the lower activity observed in these type II DHQases compared with the high k_{cat} enzymes SCDHIHQase and the QutE from *A. nidulans*. However, denaturation studies with low concentrations of urea did not confirm this proposal. There was a significant difference in the effect of chloride ions; 0.5 M chloride decreased the catalytic activity of the high k_{cat} enzyme from SCDHIHQase and increased the catalytic activity of low k_{cat} enzymes, HTDHIHQase and HPDHIHQase. The exact role of the flexibility of the lid domain in promoting catalysis remains to be established.

More evidence is needed including characterisation of at least another high k_{cat} enzyme. Prof. Iain Hunter at the University of Strathclyde has recently produced a

construct of the *Campylobacter jejuni* type II DHQase. It is not yet known whether the *C. jejuni* enzyme will be in the high k_{cat} category. However, analysis of its sequence shows that the *C. jejuni* DHQase overall has higher homology to HPDHQase and *B. subtilis* YqhS than to the two high k_{cat} enzymes SCDHQase and *A. nidulans* QutE. Out of the five DHQases analysed MTDHQase had the lowest homology to *C. jejuni* DHQase. The lid domain of the *C. jejuni* is slightly different from the other DHQase studied in the present work. Biochemical analysis of the *C. jejuni* DHQase may help explain some of the reasons for the low and high k_{cat} type II DHQases. It is likely that environmental factors may influence the level of catalytic activity observed in different type II DHQases. *S. coelicolor* and *A. nidulans* are both saprophytes found in soil and function at different temperatures according to the weather where as *M. tuberculosis* and *H. pylori* are found in humans and operate specifically at mammalian body temperatures. The temperature and concentration of quininate in the two environments differ considerably. All enzymes must make a 'trade off' between K_m and k_{cat} to maximise efficiency within the cell. If the availability of a particular substrate is low in the environment of the microorganism in question then it would be expected that the K_m would also be low, at the expense of the k_{cat} . This seems to be the case for *M. tuberculosis* (K_m 23 μ M at pH 7.0) but not *H. pylori* (K_m 200 μ M at pH 7.0).

Further crystallographic studies are required on the mutants of SCDHQase. This would be especially true for the E104A mutation this should reveal the exact role of this residue is still unclear. It may also be possible to soak substrate into crystals of the E104A mutant, giving more information on the mode of substrate binding. It would also be useful to study the kinetic parameters of various inhibitors of type II DHQase like vinyl fluoride (Frederickson et al, 2002) and the effect of polyanion binding on the S108A mutant.

The presence of two types of DHQase raises several evolutionary questions. To date *B. subtilis* is the only organism known to possess genes homologous to both type I and type II DHQases. This is of interest as it may offer an insight into how new functions may evolve in existing protein families. Other members of the *Bacillus* family are split between either possessing either a type I or type II DHQase (Figure 24 page no 113). There does not seem to be any evolutionary or environmental pattern to the distribution of the two types of enzyme. This suggests that there has

been gene transfer between microorganisms, as evolutionary distinct organisms possess genes encoding for DHQases, which have high identity. This may have occurred by the ability of bacteria to acquire plasmid DNA from other bacterial species by conjugation (Heinemann, 1991). Analysis of the genomes of *Bacillus* family members reveals that when the type II DHQase is present it is found in the same location. In *Oceanobacillus theyensis* possess a type I DHQase the region in which the type II DHQase would be found is analogous apart from the absence of the type II DHQase. This suggests that *Bacillus* family members that possess a type II DHQase share a common ancestor which acquired the type II DHQase without any other genes. The start codon of the *yqhS* gene is GTG, which is quite rare in *B. subtilis* 9% of genes start with this codon (Kunst *et al.*, 1997); this also suggests that the *yqhS* gene has been acquired. It seems likely that *B. subtilis* originally possessed only a type I DHQase, as NaBH_4 experiments showed this to be the active form of the enzyme. The organisation of shikimate pathway enzymes in *B. subtilis* is quite different from that in any organism studied to date.

B. subtilis YqhS was shown to have an extremely low level of catalytic activity and is therefore not a functional DHQase. The site-directed mutant F23Y of YqhS shows at least 2000-fold increase in activity from the wild type. The increase in activity is comparable with the decrease in activity observed in the Y28F mutant of SCDHQase, confirming the importance of this residue. The extremely low catalytic activity observed of the F23Y *B. subtilis* YqhS protein shows that other factors must be important in optimising catalytic efficiency. It seems that the YqhS protein may represent a case of divergent evolution (Gerlt and Babbitt, 2001) and that YqhS must have another function that may be common to other type II DHQases, as there is such high identity between the *B. subtilis* YqhS and other functional type II DHQases. The growth experiments with minimal medium performed on wild-type *B. subtilis* (derivative 168) and the disruption mutant (dYqhS) established the importance of the *yqhS* gene under these conditions. Unlike the wild-type strain of *B. subtilis*, the *yqhS* disrupted mutant will not grow on minimal medium with either glucose or citrate as a carbon source (Table 10 page no. 137). Presently auxotrophic studies are underway in an attempt to establish the nature of the disruption mutant, in order to define more clearly the role of the YqhS protein in *B. subtilis*. Quaternary structural analysis reveals a large cavity formed by the assembly of the tetramer of trimers. There are

several conserved residues within the cavity of type II DHQases including His 85, Glu59 and Asp64 (Appendix C; **Error! Reference source not found.**) (*S. coelicolor* numbering system). This cavity may be involved in the second function. However, no homologous motifs were found using the 3-dimensional motif modelling program PINTS (<http://www.russell.embl.de/pints/>).

The paralogs; *H. influenzae* shikimate dehydrogenase (HIAroE) and the *H. influenzae* shikimate dehydrogenase related protein (HIYdiB) are both NADPH-dependent dehydrogenases although they are able to catalyse reactions in the presence of NAD⁺. The function of HIYdiB is still unclear as the catalytic activity of the HIYdiB protein is significantly lower than the HIAroE enzyme for all the substrates tested (Table 20; Table 21 page no. 206, 207). Using fluorescence quenching it has been shown that shikimate can bind to HIAroE in the absence of the cofactor. The K_{SHIK} value for HIAroE in the absence of NADP⁺ is $82 \mu\text{M} \pm 11$. This K_{SHIK} fluorescence value is equivalent to the K' value observed in the steady state kinetics results ($90 \mu\text{M}$). HIAroE is likely to follow a random sequential mechanism rather than the ordered BiBi mechanism proposed for bifunctional plant enzymes such as bifunctional *P. sativum* (Dowsett *et al.*, 1972).

The YdiB family of proteins seem to comprise two groups that may have diverged from the shikimate dehydrogenases. The *E. coli* YdiB protein (ECYdiB) is an NAD⁺-dependent dimer and catalyses the oxidation of both shikimate and quinate, placing it in the quinate-shikimate dehydrogenase category (1.4.1). The HIYdiB protein is an NADP⁺-dependent dimer with an unknown function. The N terminal region is thought to be very important in the binding of the substrate and sequence analysis gives small clues about the substrate-binding pocket. HIYdiB was able to catalyse the oxidation of shikimate but not of quinate. The structures of shikimate and quinate are similar, with quinate possessing an extra hydroxyl group at C1. It can be hypothesised that the substrate of HIYdiB does not have a hydroxyl group in this position. However, assays should be performed in the forward direction at a more physiological pH. Additional fluorescence binding studies should be performed on HIYdiB to establish whether quinate is able to bind to the enzyme. The X-ray structure of HIYdiB is currently on hold at the Protein Data Bank (PDB identifier: 1NPY) (<http://www.rcsb.org/pdb/>); this 3-dimensional structure may reveal more detail about the substrate binding pocket.

The emergence of bacterial resistance to established antibiotics in hospital-acquired infections is a matter of ever-growing concern. In particular *Staphylococcus*, *Enterococcus* and *Streptococcus aureus* and *M. tuberculosis*, have all evolved resistant strains over the last few years (Nachega and Chaisson, 2003). The appearance of glyphosate resistance in Goose grass is also a matter of concern for the production of food to an ever-increasing world population (Baerson *et al*, 2002). For these reasons, there is an urgent need for new antibacterial and herbicide agents, particularly those that act on novel targets. The discovery of several paralogs of the shikimate pathway enzymes such as the YdiB protein, in a variety of bacterial and plant species raises questions about using shikimate pathway inhibitors as antibiotics. Where possible it may be beneficial to study the binding properties of potential antibiotics to these paralogs, so that organisms that are not being targeted are not affected.

There are several important factors in designing inhibitors for type II DHQase. The C1 carboxylate group is very important for correct binding of the substrate and inhibitors. It is thought that only one alanine side chain in SCDHQase (Ala81) is responsible for the differences in binding affinity of the oxime inhibitor observed between MTDHQase (K_i 20 μ M) and SCDHQase (K_i 500 μ M). The *C. jejuni* DHQase also possess a alanine in the same position. It would be interesting to perform studies of the inhibition of *C. jejuni* DHQase by oxime. It also may be worthwhile to test some of the inhibitors of DHQase on shikimate dehydrogenases and vice versa, since the substrate of the two enzymes have very similar structures.

In conclusion this study has highlighted a number of important aspects of shikimate pathway enzymology, and indicated a number of directions for further investigation.

REFERENCES

(1-272)

1. Ahmad S, Jensen RA. The Stable Phylogenetic Distribution of the Recently Evolved L- Phenylalanine-Inhibited Isozyme of 3-Deoxy-D-Arabino- Heptulosonate 7-Phosphate Synthase in Enteric Bacteria. *Current Microbiology* 1989;18(6):341-349.
2. Akbar S, Gaidenko TA, Kang CM, O'Reilly M, Devine KM, Price CW. New family of regulators in the environmental signaling pathway which activates the general stress transcription factor sigma(B) of *Bacillus subtilis*. *J. Bacteriol.* 2001;183(4):1329-1338.
3. Alibhai MF, Stallings WC. Closing down on glyphosate inhibition - with a new structure for drug discovery. *Proc. Natl. Acad. Sci. U. S. A.* 2001;98(6):2944-2946.
4. Altschul SF, Madden TL, Schaffer AA, Zhang J, Zhang Z, Miller W, et al. Gapped BLAST and PSI-BLAST: a new generation of protein database search programs. *Nucleic. Acids. Res.* 1997;25(17):3389-3402.
5. Anagnostopoulos C, Spizizen J. Requirements for transformation in *Bacillus subtilis*. *Journal of Bacteriology* 1960;81:741-746.
6. Anderson KS, Johnson KA. Kinetic and Structural-Analysis of Enzyme Intermediates - Lessons from Epsp Synthase. *Chemical Reviews* 1990;90(7):1131-1149.
7. Anton IA, Duncan K, Coggins JR. A Eukaryotic Repressor Protein, the Qa-1s Gene-Product of *Neurospora-Crassa*, Is Homologous to Part of the Arom Multifunctional Enzyme. *J. Mol. Biol.* 1987;197(2):367-371.
8. Anton IA, Coggins JR. Sequencing and overexpression of the *Escherichia coli* *aroE* gene encoding shikimate dehydrogenase. *Biochem. J.* 1988;249(2):319-26.
9. Arrow-Therapeutics. Bissulfonamides as inhibitors of the dehydroquinase synthetase enzyme AroB and of the type II dehydroquinase enzyme AroQ. *Expert Opin. Ther. Patents.* 2001;11:1797-1799.

10. Bacron SR, Rodriguez DJ, Tran M, Feng Y, Biest NA, Dill GM. Glyphosate-resistant goosegrass. Identification of a mutation in the target enzyme 5-enolpyruvylshikimate-3-phosphate synthase. *Plant Physiol.* 2002;129(3):1265-1275.
11. Baillie AC, Corbett JR, Dowsett JR, McCloskey P. Inhibitors of shikimate dehydrogenase as potential herbicides. *Biochem. J.* 1972;126(3):113-120.
12. Balasubramanian S, Davis GM, Coggins JR, Abell C. Inhibition of chorismate synthase by (6*R*)- and (6*S*)-6-fluoro-5-enolpyruvylshikimate 3-phosphate. *J. Am. Chem. Soc.* 1991;113:8945-8946.
13. Baldwin RL. How Hofmeister ion interactions affect protein stability. *Biophys. J.* 1996;71(4):2056-2063.
14. Balinsky D, Davis BD. Aromatic biosynthesis in higher plants 1. Preparation and properties of dehydroshikimic reductase. *Biochem. J.* 1961a;80:292-296.
15. Balinsky D, Davis BD. Aromatic biosynthesis in Plants 2. Mode of attachment of shikimic acid and dehydroshikimic acid to dehydroshimic reductase. *Biochem. J.* 1961b;80:296-300.
16. Balinsky D, Davis BD. Aromatic biosynthesis in higher plants 3. Preparation and properties of dehydroquinase. *Biochem. J.* 1961c;80:300-304.
17. Balinsky D, Dennis AW, Cleland WW. Kinetic and isotope-exchange studies on shikimate dehydrogenase from *Pisum sativum*. *Biochemistry* 1971;10(10):1947-52.
18. Banerji S, Wakcfield AE, Allen AG, Maskell DJ, Peters SE, Hopkin JM. The Cloning and Characterization of the Arom Gene of *Pneumocystis carinii*. *J. Gen. Microbiol.* 1993;139:2901-2914.
19. Bartlett PA, Maitra U, Chouinard PM. Synthesis of "iso-EPSP" and evaluation of its interaction with chorismate synthase. *J. Am. Chem. Soc.* 1986;108:8068-8071.
20. Bartlett PA, Satake K. Does Dehydroquinase Synthase Synthesize Dehydroquinase. *J. Am. Chem. Soc.* 1988;110(5):1628-1630.

21. Bartlett PA, McLaren KL, Marx MA. Divergence between the Enzyme-Catalyzed and Noncatalyzed Synthesis of 3-Dehydroquinate. *Journal of Organic Chemistry* 1994;59(8):2082-2085.
22. Bello CG, Harris JM, Manthey MK, Coggins JR, Abell C. Irreversible inhibition of type I dehydroquinase by substrates for type II dehydroquinase. *Bioorganic & Medicinal Chemistry Letters* 2000;10(5):407-409.
23. Bender SL, Widlanski T, Knowles JR. Dehydroquinase synthase: the use of substrate analogues to probe the early steps of the catalyzed reaction. *Biochemistry* 1989;28(19):7560-7572.
24. Bentley R. The shikimate pathway--a metabolic tree with many branches. *Crit Rev. Biochem. Mol. Biol.* 1990;25(5):307-384.
25. Beri RK, Grant S, Roberts CF, Smith M, Hawkins AR. Selective overexpression of the QUTB gene encoding catabolic 3- dehydroquinase in multicopy transformants of *Aspergillus nidulans*. *Biochem. J.* 1990;265(2):337-342.
26. Bernhardt J, Volker U, Volker A, Antelmann H, Schmid R, Mach H, et al. Specific and general stress proteins in *Bacillus subtilis*-a two- dimensional protein electrophoresis study. *Microbiology* 1997;143(3):999-1017.
27. Birnboim HC, Doly J. A rapid alkaline extraction procedure for screening recombinant plasmid DNA. *Nucleic Acids Res.* 1979;7(6):1513-23.
28. Boam DJ, Price NC, Kelly SM, Krell T, Coggins JR. Evidence that the active site in type II dehydroquinase from *Streptomyces coelicolor* is near the single tryptophan. *Biochem. Soc. Trans.* 1997;25(1):348; replaces 93S.
29. Bondinell WE, Vnek J, Knowles PF, Sprecher M, Sprinson DB. On the mechanism of 5-enolpyruvylshikimate 3-phosphate synthetase. *J. Biol. Chem.* 1971;246(20):6191-6196.
30. Bonner CA, Jensen RA. Cloning of cDNA encoding the bifunctional dehydroquinase.shikimate dehydrogenase of aromatic-amino-acid biosynthesis in *Nicotiana tabacum*. *Biochem. J.* 1994;302(Pt 1):11-14.
31. Boocock MR, Coggins JR. Kinetics of 5-enolpyruvylshikimate-3-phosphate synthase inhibition by glyphosate. *FEBS Lett.* 1983;154(1):127-133.

32. Bornemann S, Ramjee MK, Balasubramanian S, Abell C, Coggins JR, Lowe DJ, et al. *Escherichia coli* chorismate synthase catalyzes the conversion of (6S)-6-fluoro-5-enolpyruvylshikimate-3-phosphate to 6-fluorochorismate. Implications for the enzyme mechanism and the antimicrobial action of (6S)-6-fluoroshikimate. *J. Biol. Chem.* 1995;270(39):22811-22815.
33. Bottomley JR, Clayton CL, Chalk PA, Kleanthous C. Cloning, sequencing, expression, purification and preliminary characterization of a type II dehydroquinase from *Helicobacter pylori*. *Biochem. J.* 1996a;319(Pt 2):559-565.
34. Bottomley JR, Hawkins AR, Kleanthous C. Conformational changes and the role of metals in the mechanism of type II dehydroquinase from *Aspergillus nidulans*. *Biochem. J.* 1996b;319(Pt 1):269-278.
35. Boys CW, Bury SM, Sawyer L, Moore JD, Charles IG, Hawkins AR, et al. Crystallization of a type I 3-dehydroquinase from *Salmonella typhi*. *J. Mol. Biol.* 1992;227(1):352-355.
36. Bradford MM. A rapid and sensitive method for the quantitation of microgram quantities of protein utilizing the principle of protein-dye binding. *Anal. Biochem.* 1976;72:248-254.
37. Bruce NC, Cain RB. Hydroaromatic metabolism in *rhodococcus rhodochromus*: purification and characterisation of its NAD-dependent quinate dehydrogenase. *Arch. Microbiol.* 1990;154:179-186.
38. Bugg TDH, Abell C, Coggins JR. Affinity Labeling of *Escherichia coli* Dehydroquinase. *Tetrahedron Lett.* 1988;29(51):6783-6786.
39. Bugg TDH. Active Site Studies on Enzymes of the Shikimate Pathway.: University of Cambridge; 1989.
40. Bullock WO, Fernandez JM, Short JM. X11-Blue - A High-Efficiency Plasmid Transforming RecA *Escherichia-Coli* Strain With Beta-Galactosidase Selection. *Biotechniques* 1987;5(4):376-378.
41. Burnett RM, Darling GD, Kendall DS, LeQuesne ME, Mayhew SG, Smith WW, et al. The structure of the oxidized form of clostridial flavodoxin at 1.9-A resolution. *J. Biol. Chem.* 1974;249(14):4383-4392.

42. Butler JR, Alworth WL, Nugent MJ. Mechanism of dehydroquinase catalyzed dehydration. I. Formation of a Schiff base intermediate. *J. Am. Chem. Soc.* 1974;96(5):1617-1618.
43. Carpenter EP, Hawkins AR, Frost JW, Brown KA. Structure of dehydroquinase synthase reveals an active site capable of multistep catalysis. *Nature* 1998;394(6690):299-302.
44. Carter P, Wells JA. Dissecting the Catalytic Triad of a Serine Protease. *Nature* 1988;332(6164):564-568.
45. Carugo O, Argos P. NADP-dependent enzymes. II: Evolution of the mono- and dinucleotide binding domains. *Proteins* 1997a;28(1):29-40.
46. Carugo O, Argos P. NADP-dependent enzymes. I: Conserved stereochemistry of cofactor binding. *Proteins* 1997b;28(1):10-28.
47. Case ME, Giles NH, Doy CH. Genetical and biochemical evidence for further interrelationships between the polyaromatic synthetic and the quinate-shikimate catabolic pathways in *Neurospora crassa*. *Genetics* 1972;71(3):337-348.
48. Chackrewarthy S. Studies on the active-site of *Escherichia coli* shikimate dehydrogenase: University of Glasgow; 1995.
49. Chakrabarti R, Schutt CE. Novel sulfoxides facilitate GC-Rich template amplification. *Biotechniques* 2002;32:866-874.
50. Chaleff RS. The inducible quinate-shikimate catabolic pathway in *Neurospora crassa*: induction and regulation of enzyme synthesis. *J. Gen. Microbiol.* 1974;81(2):357-372.
51. Charles IG, Keyte JW, Brammar WJ, Hawkins AR. Nucleotide sequence encoding the biosynthetic dehydroquinase function of the penta-functional arom locus of *Aspergillus nidulans*. *Nucleic Acids Res.* 1985;13(22):8119-8128.
52. Chaudhuri S, Coggins JR. The purification of shikimate dehydrogenase from *Escherichia coli*. *Biochem. J.* 1985;226(1):217-223.
53. Chaudhuri S, Duncan K, Graham LD, Coggins JR. Identification of the active-site lysine residues of two biosynthetic 3- dehydroquinases. *Biochem. J.* 1991;275(1):1-6.

-
54. Cline J, Braman JC, Hogrefe HH. PCR fidelity of pfu DNA polymerase and other thermostable DNA polymerases. *Nucleic Acids Res.* 1996;24(18):3546-3451.
 55. Coggins JR, Boocock MR, Campbell MS, Chaudhuri S, Lambert JM, Lewendon A, et al. Functional domains involved in aromatic amino acid biosynthesis. *Biochem. Soc. Trans.* 1985;13(2):299-303.
 56. Coggins JR, Boocock MR. The *arom* multifunctional enzyme. *Multidomain Proteins Structure and Evolution* 1986;Chapter 8:259-281.
 57. Coggins JR, Duncan K, Anton IA, Boocock MR, Chaudhuri S, Lambert JM, et al. The anatomy of a multifunctional enzyme. *Biochem. Soc. Trans.* 1987;15(4):754-9.
 58. Collins KD, Washabaugh MW. The Hofmeister effect and the behaviour of water at interfaces. *Q. Rev. Biophys.* 1985;18(4):323-422.
 59. Corpet F. Multiple Sequence Alignment with Hierarchical-Clustering. *Nucleic Acids Res.* 1988;16(22):10881-10890.
 60. Da Silva AJ, Whittington H, Clements J, Roberts C, Hawkins AR. Sequence analysis and transformation by the catabolic 3-dehydroquinase (QUTE) gene from *Aspergillus nidulans*. *Biochem. J.* 1986;240(2):481-488.
 61. Dansette P, Azerad R. The shikimate pathway : II. Stereospecificity of hydrogen transfer catalyzed by NADPH-dehydroshikimate reductase of *E. coli*. *Biochimie* 1974;56(5):751-755.
 62. Daugherty M, Vonstein V, Overbeek R, Osterman A. Archaeal shikimate kinase, a new member of the GHMP-kinase family. *J. Bacteriol.* 2001;183(1):292-300.
 63. Davies GM, Barrett-Bee KJ, Jude DA, Lehan M, Nichols WW, Pinder PE, et al. (6S)-6-fluoroshikimic acid, an antibacterial agent acting on the aromatic biosynthetic pathway. *Antimicrob. Agents Chemother.* 1994;38(2):403-406.
 64. DeFeyter RC, Davidson BE, Pittard J. Nucleotide sequence of the transcription unit containing the *aroL* and *aroM* genes from *Escherichia coli* K-12. *J. Bacteriol.* 1986;165(1):233-239.

-
65. DeFeyter RC, Pittard J. Genetic and molecular analysis of *aroL*, the gene for shikimate kinase II in *Escherichia coli* K-12. *J. Bacteriol.* 1986a;165(1):226-232.
 66. DeFeyter RC, Pittard J. Purification and properties of shikimate kinase II from *Escherichia coli* K-12. *J. Bacteriol.* 1986b;165(1):331-333.
 67. Deka RK, Kleanthous C, Coggins JR. Identification of the essential histidine residue at the active site of *Escherichia coli* dehydroquinase. *J. Biol. Chem.* 1992;267(31):22237-22242.
 68. Deka R. Studies of the shikimate pathway enzyme, 3-dehydroquinase. University of Glasgow; 1993.
 69. Deka RK, Anton IA, Dunbar B, Coggins JR. The characterisation of the shikimate pathway enzyme dehydroquinase from *Pisum sativum*. *FEBS Lett.* 1994;349(3):397-402.
 70. DeLeo AB, Sprinson DB. Mechanism of 3-deoxy-D-arabino-heptulosonate 7-phosphate (DAHP) synthetase. *Biochem. Biophys. Res. Commun.* 1968;32(5):873-877.
 71. DeLeo AB, Dayan J, Sprinson DB. Purification and kinetics of tyrosine-sensitive 3-deoxy-D-arabino-heptulosonic acid 7-phosphate synthetase from *Salmonella*. *J. Biol. Chem.* 1973;248(7):2344-2353.
 72. Dennis AW, Balinsky D. The effect of pII on the kinetic parameters of shikimate dehydrogenase from *Pisum sativum*. *Int. J. Biochem.* 1972;3:93-102.
 73. Dewick PM. The biosynthesis of shikimate metabolites. *Nat. Prod. Rep.* 1998;15(1):17-58.
 74. Dowsett JR, Middleton B, Corbett JR, Tubbs PK. The anomalous inhibition of shikimate dehydrogenase by analogues of dehydroshikimate. *Biochim. Biophys. Acta* 1972;276(2):344-9.
 75. Doy CH. Control of aromatic biosynthesis particularly with regard to the common pathway and the allosteric enzyme, 3-deoxy-D-arabino heptulosonate 7-phosphate synthetase. *Rev. Pure and Appl. Chem.* 1968;18:41-78.

-
76. Duggan PJ, Parker E, Coggins J, Abell C. Enzymatic-Synthesis of (6r)-Fluoroshikimic Acid and (6s)- Fluoroshikimic Acid. *Bioorganic & Medicinal Chemistry Letters* 1995;5(20):2347-2352.
77. Duine JA. Quinoproteins: enzymes containing the quinonoid cofactor pyrroloquinoline quinone, topaquinone or tryptophan-tryptophan quinone. *Eur. J. Biochem.* 1991;200(2):271-284.
78. Duncan K, Lewendon A, Coggins JR. The purification of 5-enolpyruvylshikimate 3-phosphate synthase from an overproducing strain of *Escherichia coli*. *FEBS Lett.* 1984a;165(1):121-127.
79. Duncan K, Lewendon A, Coggins JR. The Complete Amino-Acid-Sequence of *Escherichia coli* 5- Enolpyruvylshikimate 3-Phosphate Synthase. *Febs Lett.* 1984b;170(1):59-63.
80. Duncan K, Chaudhuri S, Campbell MS, Coggins JR. The overexpression and complete amino acid sequence of *Escherichia coli* 3-dehydroquinase. *Biochem. J.* 1986;238(2):475-483.
81. Duncan K, Edwards RM, Coggins JR. The Pentafunctional Arom Enzyme of *Saccharomyces cerevisiae* Is a Mosaic of Monofunctional Domains. *Biochem. J.* 1987;246(2):375-386.
82. Edelhoch H. Spectroscopic determination of tryptophan and tyrosine in proteins. *Biochemistry* 1967;6(7):1948-1954.
83. Eflink MR, Shastry MC. Fluorescence methods for studying kinetics of protein-folding reactions. *Methods Enzymol.* 1997;278:258-286.
84. Elsemore DA, Ornston LN. The *pca-pob* supraoperonic cluster of *Acinetobacter calcoaceticus* contains *quiA*, the structural gene for quinate-shikimate dhydrogenase. *J. Bacteriol.* 1994;176(24):7659-66.
85. Elsemore DA, Ornston LN. Unusual ancestry of dehydratases associated with quinate catabolism in *Acinetobacter calcoaceticus*. *J. Bacteriol.* 1995;177(20):5971-5978.
86. Ely B, Pittard J. Aromatic amino acid biosynthesis: regulation of shikimate kinase in *Escherichia coli* K-12. *J. Bacteriol.* 1979;138(3):933-943.

-
87. Errington J. *Bacillus subtilis* Sporulation - Regulation of Gene-Expression and Control of Morphogenesis. *Microbiological Reviews* 1993;57(1):1-33.
88. Evans LD, Roszak AW, Noble LJ, Robinson DA, Chalk PA, Matthews JL, et al. Specificity of substrate recognition by type II dehydroquinases as revealed by binding of polyanions. *FEBS Lett.* 2002;530(1-3):24-30.
89. Ewart CD, Jude DA, Thain JL, Nichols WW. Frequency and mechanism of resistance to antibacterial action of ZM 240401, (6S)-6-fluoro-shikimic acid. *Antimicrob. Agents Chemother.* 1995;39(1):87-93.
90. Eykman JF. Sur le principes constituants de l'*Illicium religiosum* (Sieb.) (Shikimi-no-ki en japonais). *Rec. Trav. Chim.* 1885;4:32-54.
91. Eykman JF. Ueber die Shikimisaure. *Chem. Ber.* 1891;24:1278-1303.
92. Fersht AR. Relationships between Apparent Binding-Energies Measured in Site-Directed Mutagenesis Experiments and Energetics of Binding and Catalysis. *Biochemistry* 1988;27(5):1577-1580.
93. Florova G, Denoya CD, Morgenstern MR, Skinner DD, Reynolds KA. Cloning, expression, and characterization of a type II 3-dehydroquinase gene from *Streptomyces hygroscopicus*. *Arch. Biochem. Biophys.* 1998;350(2):298-306.
94. Floss HG, Onderka DK, Carroll M. Stereochemistry of the 3-deoxy-D-arabino-heptulosonate 7-phosphate synthetase reaction and the chorismate synthetase reaction. *J. Biol. Chem.* 1972;247(3):736-744.
95. Fredrickson M, Parker EJ, Hawkins AR, Coggins JR, Abell C. Selective Inhibition of Type II Dehydroquinases. *J. Org. Chem.* 1999;64(8):2612-2613.
96. Frederickson M, Coggins JR, Abell C. Vinyl fluoride as an isoelectronic replacement for an enolate anion: inhibition of type II dehydroquinases. *Chem. Commun.* 2002(17):1886-1887.
97. Fridovich I. Inhibition of Acetoacetic Decarboxylase by Anions. *J. Biol. Chem.* 1963;238(2):592-598.

-
98. Ganem B. Tetrahedron Report Number 59. From Glucose to Aromatics: Recent Developments in natural products of the shikimic acid pathway. Tetrahedron 1978;34:3353-3383.
99. Gerlt JA, Babbitt PC. Divergent evolution of enzymatic function: mechanistically diverse superfamilies and functionally distinct suprafamilies. Annu. Rev. Biochem. 2001;70:209-246.
100. Giles NH, Case ME, Partridge CW, Ahmed SI. A gene cluster in *Neurospora crassa* coding for an aggregate of five aromatic synthetic enzymes. Proc. Natl. Acad. Sci. U. S. A. 1967;58(4):1453-1460.
101. Giles NH, Partridge CW, Ahmed SI, Case ME. The occurrence of two dehydroquinases in *Neurospora crassa*, one constitutive and one inducible. Proc. Natl. Acad. Sci. U. S. A. 1968;58(5):1930-1937.
102. Giles NH, Case ME, Baum J, Geever R, Huiet L, Patel V, et al. Gene organization and regulation in the qa (quinic acid) gene cluster of *Neurospora crassa*. Microbiol. Rev. 1985;49(3):338-358.
103. Grolach J, Schmid J, Amrhein N. Differential Expression of Tomato (*Lycopersicon-Esculentum* L) Genes Encoding Shikimate Pathway Isoenzymes .2. Chorismate Synthase. Plant Molecular Biology 1993;23(4):707-716.
104. Gourley DG, Coggins JR, Isaacs NW, Moore JD, Charles IG, Hawkins AR. Crystallization of a type II dehydroquinase from *Mycobacterium tuberculosis*. J. Mol. Biol. 1994;241(3):488-491.
105. Gourley DG, Shrive AK, Polikarpov I, Krell T, Coggins JR, Hawkins AR, et al. The two types of 3-dehydroquinase have distinct structures but catalyze the same overall reaction. Nat. Struct. Biol. 1999;6(6):521-525.
106. Grewe R, Haendler H. 5-Dehydroquinic acid. Biochemical Preparations 1966;11:21-26.
107. Grimshaw CE, Sogo SG, Knowles JR. The fate of the hydrogens of phosphoenolpyruvate in the reaction catalyzed by 5-enolpyruvylshikimate-3-phosphate synthase. Isotope effects and isotope exchange. J. Biol. Chem. 1982;257(2):596-598.
-

-
108. Gupta RS. Protein Phylogenies and Signature Sequences: A Reappraisal of Evolutionary Relationships among Archaeobacteria, Eubacteria, and Eukaryotes. *Microbiology And Molecular Biology Reviews* 1998;62(4):1435-1491.
109. Hanahan D, Meselson M. Plasmid screening at high colony density. *Gene* 1980;10:63-67.
110. Hanahan D, Lane D, Lipsich L, Botchan M. Characteristics of an SV40-Plasmid recombinant and its movement into and out of the genome of murine cell. *Cell* 1980;21:127-139.
111. Hanahan D, Meselson M. Plasmid screening at high colony density. *Methods Enzymol.* 1983;100:333-342.
112. Harris J, Kleanthous C, Coggins JR, Hawkins AR, Abell C. Different Mechanistic and Stereochemical Courses for the Reactions Catalyzed by Type-I and Type-II Dehydroquinases. *J. Chem. Soc.-Chem. Commun.* 1993(13):1080-1081.
113. Harris JM, Gonzalez-Bello C, Kleanthous C, Hawkins AR, Coggins JR, Abell C. Evidence from kinetic isotope studies for an enolate intermediate in the mechanism of type II dehydroquinases. *Biochem. J.* 1996a;319(Pt 2):333-336.
114. Harris JM, Watkins WJ, Hawkins AR, Coggins JR, Abell C. Comparison of the substrate specificity of type I and type II dehydroquinases with 5-deoxy- and 4,5-dideoxy-dehydroquinic acid. *Journal of the Chemical Society-Perkin Transactions 1* 1996b(19):2371-2377.
115. Haslam E, Turner MJ, Sargent D, Thompson RS. The Shikimate Pathway. Part I. Introduction; Preparation of Stereo-specifically Labelled 2-Deuterio-derivatives of 3-Dehydroquinic acid. *J. Chem. Soc. (C)* 1971:1489-1495.
116. Haslam E. The shikimate pathway. John Wiley & Sons, New York 1974.
117. Hautala JA, Jacobson JW, Casc ME, Giles NH. Purification and characterization of catabolic dehydroquinase, an enzyme in the inducible quinic acid catabolic pathway of *Neurospora crassa*. *J. of Biol. Chem.* 1975;250(15):6008-6014.
118. Hawkes TR, Lewis T, Coggins JR, Mousdale DM, Lowe DJ, Thorneley RN. Chorismate synthase. Pre-steady-state kinetics of phosphate release from 5-enolpyruvylshikimate 3-phosphate. *Biochem. J.* 1990;265(3):899-902.
-

-
119. Hawkins AR, Giles NH, Kinghorn JR. Genetical and biochemical aspects of quinate breakdown in the filamentous fungus *Aspergillus nidulans*. *Biochem. Genet.* 1982;20(3-4):271-286.
120. Hawkins AR, Lamb HK, Moore JD, Charles IG, Roberts CF. The pre-chorismate (shikimate) and quinate pathways in filamentous fungi: theoretical and practical aspects. *J. Gen. Microbiol.* 1993;139(Pt 12):2891-9.
121. Hedstrom L, Abeles R. 3-Deoxy-D-manno-octulosonate-8-phosphate synthase catalyzes the C-O bond cleavage of phosphoenolpyruvate. *Biochem. Biophys. Res. Commun* 1988;157(2):816-820.
122. Heinemann JA. Genetics of Gene-Transfer between Species. *Trends in Genetics* 1991;7(6):181-185.
123. Hellman U, Wernstedt C, Gonez J, Heldin CH. Improvement of an "In-Gel" digestion procedure for the micropreparation of internal protein fragments for amino acid sequencing. *Anal. Biochem.* 1995;224(1):451-455.
124. Henis YI, Levitzki A. The Sequential Nature of the Negative Cooperativity in Rabbit Muscle Glyceraldehyde-3-Phosphate Dehydrogenase. *Eur. J. Biochem.* 1980;112:59-73.
125. Higuchi R, Krummel B, Saiki RK. A general method of *in vitro* preparation and specific mutagenesis of DNA fragments: study of protein and DNA interactions. *Nucleic Acids Res.* 1988;16(15).
126. Hill RK, Newkome GR. Stereochemistry of chorismic acid biosynthesis. *J. Am. Chem. Soc.* 1969;91(21):5893-4.
127. Hofmiester F. *Arch. Exptl. Pathol. Pharmacol.* 1888;24:247.
128. Horsburgh MJ. Chorismate synthase from *Staphylococcus aureus*.: University of Glasgow; 1995.
129. Horsburgh MJ, Thackray PD, Moir A. Transcriptional responses during outgrowth of *Bacillus subtilis* endospores. *Microbiology* 2001;147(Pt 11):2933-2941.
130. Huang CY. Derivation of initial velocity and isotope exchange rate equations. *Methods in Enzymol.* 1979;63:54-85.
-

-
131. Jaworski EG. Mode of action of *N*-Phosphonomethylglycine: inhibition of aromatic amino acid biosynthesis. *J. Agr. Food Chem.* 1972;20(6):1195-1198.
132. Jude DA, Ewart CDC, Thain JL, Davies GM, Nichols WW. Transport of the antibacterial agent (6*S*)-6-fluoroshikimate and other shikimate analogues by the shikimate transport system of *Escherichia coli*. *Biochim. Biophys. Acta-Biomembranes* 1996;1279(2):125-129.
133. Kelly SM, Price NC. The use of circular dichroism in the investigation of protein structure and function. *Curr. Protein. Pept. Sci.* 2000;1(4):349-384.
134. Kikuchi Y, Tsujimoto K, Kurahashi O. Mutational analysis of the feedback sites of phenylalanine-sensitive 3-deoxy-D-arabino-heptulosonate-7-phosphate synthase of *Escherichia coli*. *Appl. Environ. Microbiol.* 1997;63(2):761-762.
135. Kim CG, Kirschning A, Bergon P, Ahn Y, Wang JJ, Shibuya M, et al. Formation of 3-Amino-5-Hydroxybenzoic Acid, the Precursor of Mc(7)N Units in Ansamycin Antibiotics, by a New Variant of the Shikimate Pathway. *J. Am.Chem. Soc.* 1992;114(12):4941-4943.
136. Kim CG, Yu TW, Fryhle CB, Handa S, Floss HG. 3-Amino-5-hydroxybenzoic acid synthase, the terminal enzyme in the formation of the precursor of mC7N units in rifamycin and related antibiotics. *J. Biol. Chem.* 1998;273(11):6030-6040.
137. Kleanthous C, Campbell DG, Coggins JR. Active site labeling of the shikimate pathway enzyme, dehydroquinase. Evidence for a common substrate binding site within dehydroquinase and dehydroquinase synthase. *J. Biol. Chem.* 1990a;265(19):10929-10934.
138. Kleanthous C, Coggins JR. Reversible alkylation of an active site methionine residue in dehydroquinase. *J. Biol. Chem.* 1990b;265(19):10935-10939.
139. Kleanthous C, Reilly M, Cooper A, Kelly S, Price NC, Coggins JR. Stabilization of the shikimate pathway enzyme dehydroquinase by covalently bound ligand. *J. Biol. Chem.* 1991;266(17):10893-10898.
140. Kleanthous C, Deka R, Davis K, Kelly SM, Cooper A, Harding SE, et al. A comparison of the enzymological and biophysical properties of two distinct classes of dehydroquinase enzymes. *Biochem. J.* 1992;282(Pt 3):687-695.
-

-
141. Kleppe R, Uhlemann K, Knappskog PM, Haavik J. Urea-induced denaturation of human phenylalanine hydroxylase. *J. Biol. Chem.* 1999;274(47):33251-33258.
142. Knaggs AR. The biosynthesis of shikimate metabolites. *Nat. Prod. Rep.* 2001;18(3):334-55.
143. Kobayashi K, Ehrlich SD, Albertini A, Amati G, Andersen KK, Arnaud M, et al. Essential *Bacillus subtilis* genes. *Proc. Natl. Acad. Sci. U. S. A.* 2003;100(8):4678-4683.
144. Koshiha T. Purification of two forms of the associated 3-dehydroquinate hydro- lyase and shikimate:NADP⁺ oxidoreductase in *Phaseolus mungo* seedlings. *Biochim. Biophys. Acta* 1978;522(1):10-18.
145. Krell T, Pitt AR, Coggins JR. The use of electrospray mass spectrometry to identify an essential arginine residue in type II dehydroquinases. *FEBS Lett.* 1995;360(1):93-96.
146. Krell T, Horsburgh MJ, Cooper A, Kelly SM, Coggins JR. Localization of the active site of type II dehydroquinases. Identification of a common arginine-containing motif in the two classes of dehydroquinases. *J. Biol. Chem.* 1996;271(40):24492-24497.
147. Krell T, Coggins JR, Laphorn AJ. The three-dimensional structure of shikimate kinase. *J. Mol. Biol.* 1998;278(5):983-997.
148. Krell T, Maclean J, Boam DJ, Cooper A, Resmini M, Brocklehurst K, et al. Biochemical and X-ray crystallographic studies on shikimate kinase: the important structural role of the P-loop lysine. *Protein Sci.* 2001;10(6):1137-1149.
149. Kunst F, Ogasawara N, Moszer I, Albertini AM, Alloni G, Azevedo V, et al. The complete genome sequence of the gram-positive bacterium *Bacillus subtilis*. *Nature* 1997;390(6657):249-256.
150. Kuwajima K. Circular Dichroism. In: *Methods in Molecular Biology*; 1995. p. 115-135.
151. Kwak JE, Lee JY, Han BW, Moon JJ, Sohn SH, Suh SW. Crystallization and preliminary X-ray crystallographic analysis of type II dchydroquinase from *Helicobacter pylori*. *Acta Crystallogr D Biol Crystallogr.* 2001;57(Pt 2):279-80.
-

-
152. Laemmli UK. Cleavage of structural proteins during the assembly of the head of bacteriophage T4. *Nature* 1970;227(259):680-685.
153. Lakshman DK, Jian J, Tavantzis SM. A double-stranded RNA element from a hypovirulent strain of *Rhizoctonia solani* occurs in DNA form and is genetically related to the pentafunctional AROM protein of the shikimate pathway. *Proc. Natl. Acad. Sci. U. S. A.* 1998;95(11):6425-9.
154. Lalonde G, O'Hanley PD, Stocker BA, Denich KT. Characterization of a 3-dehydroquinase gene from *Actinobacillus pleuropneumoniae* with homology to the eukaryotic genes qa-2 and QUTE. *Mol. Microbiol.* 1994;11(2):273-80.
155. Lamb HK, van den Hombergh JP, Newton GH, Moore JD, Roberts CF, Hawkins AR. Differential flux through the quinate and shikimate pathways. Implications for the channelling hypothesis. *Biochem. J.* 1992;284(Pt 1):181-187.
156. Lamb HK, Moore JD, Lakey JH, Levett LJ, Wheeler KA, Lago H, et al. Comparative analysis of the QUTR transcription repressor protein and the three C-terminal domains of the pentafunctional AROM enzyme. *Biochem. J.* 1996;313(Pt 3):941-50.
157. Lambert JM, Boocock MR, Coggins JR. The 3-dehydroquinase synthase activity of the pentafunctional arom enzyme complex of *Neurospora crassa* is Zn²⁺-dependent. *Biochem. J.* 1985;226(3):817-29.
158. Le Marechal P, Froussios C, Level M, Azerad R. Enzymic properties of phosphonic analogues of D-erythrose 4-phosphate. *Biochem. Biophys. Res. Commun.* 1980;92(4):1097-103.
159. Leech AP, James R, Coggins JR, Kleanthous C. Mutagenesis of active site residues in type I dehydroquinase from *Escherichia coli*. Stalled catalysis in a histidine to alanine mutant. *J. Biol. Chem.* 1995;270(43):25827-36.
160. Leech AP, Boetzel R, McDonald C, Shrive AK, Moore GR, Coggins JR, et al. Re-evaluating the role of His-143 in the mechanism of type I dehydroquinase from *Escherichia coli* using two-dimensional ¹H,¹³C NMR. *J. Biol. Chem.* 1998;273(16):9602-7.
161. Levin JG, Sprinson DB. The Enzymatic Formation and Isolation of 3-Enolpyruvylshikimate 5-phosphate. *J. Biol. Chem.* 1964;239(4):1142-1150.
-

-
162. Lineweaver H, Burk D. The Determination of Enzyme Dissociation Constants. *Am. J. Chem. Soc.* 1934;56:658-666.
163. Lobner-Olesen A, Marinus MG. Identification of the gene (*aroK*) encoding shikimic acid kinase I of *Escherichia coli*. *J. Bacteriol.* 1992;174(2):525-9.
164. Lopez Barea J, Giles NH. Purification and characterization of quinate (shikimate) dehydrogenase, an enzyme in the inducible quinic acid catabolic pathway of *Neurospora crassa*. *Biochim. Biophys. Acta* 1978;524:1-14.
165. Lourenco EJ, Neves VA. Partial purification and some properties of shikimate dehydrogenase from tomatoes. *Phytochemistry* 1984;23(3):497-499.
166. Lowry OH, Rosebrough NR, Farr AL, Randall RJ. Protein Measurement with Folin Phenol Reagent. *J. Biol. Chem.* 1951;193:265-275.
167. Lumsden J, Coggins JR. The subunit structure of the arom multienzyme complex of *Neurospora crassa*. A possible pentafunctional polypeptide chain. *Biochem. J.* 1977;161(3):599-607.
168. Maclean J, Campbell SA, Pollock K, Chackrewarthy S, Coggins JR, Laphorn AJ. Crystallization and preliminary X-ray analysis of shikimate dehydrogenase from *Escherichia coli*. *Acta Crystallogr. D Biol. Crystallogr.* 2000;56(4):512-515.
169. Matsudaira P. Sequence from picomole quantities of proteins eletroblotted onto polyvinylidene difluoride membranes. *J. Biol. Chem.* 1987;262(21):10035-10038.
170. McConkey GA. Targeting the shikimate pathway in the malaria parasite *Plasmodium falciparum*. *Antimicrob Agents Chemother* 1999;43(1):175-177.
171. McPherson A. *Preparation and Analysis of Proteins Crystals*: Krieger Publishing; 1989.
172. Mevarech M, Frolow F, Gloss LM. Halophilic enzymes: proteins with a grain of salt. *Biophys. Chem.* 2000;86(2-3):155-164.
173. Michaelis L, Menten ML. *Biochem. Z.* 1913;49:1333.
174. Michel G, Roszak AW, Sauve V, McLean J, Matte A, Coggins JR, et al. Structures of shikimate dehydrogenase AroE and its paralog YdiB: A common structural framework for different activities. *J. Biol. Chem.* 2003;12:19463-19472.
-

-
175. Millar G, Coggins JR. The complete amino acid sequence of 3-dehydroquinase synthase of *Escherichia coli* K12. FEBS Lett. 1986;200(1):11-7.
176. Millar G, Lewendon A, Hunter MG, Coggins JR. The cloning and expression of the *aroL* gene from *Escherichia coli* K12. Purification and complete amino acid sequence of shikimate kinase II, the *aroL*-gene product. Biochem. J. 1986;237(2):427-37.
177. Mitsuhashi S, Davis BD. Aromatic Biosynthesis XII. Conversion of 5-Dehydroshikimic Acid by 5-Dehydroquinase. Biochimica Et Biophysica Acta 1954;15:54-61.
178. Moffatt BA, Studier FW. T7 Lysozyme Inhibits Transcription by T7 RNA-Polymerase. Cell 1987;49(2):221-227.
179. Moore JD, Lamb HK, Garbe T, Servos S, Dougan G, Charles IG, et al. Inducible overproduction of the *Aspergillus nidulans* pentafunctional AROM protein and the type-I and -II 3-dehydroquinases from *Salmonella typhi* and *Mycobacterium tuberculosis*. Biochem. J. 1992;287(Pt 1):173-81.
180. Moral CH, Del Castillo EF, Fierro PL, Cortes AV, Castillo JA, Soriano AC, et al. Molecular characterization of the *Aeromonas hydrophila* *aroA* gene and potential use of an auxotrophic *aroA* mutant as a live attenuated vaccine. Infection and Immunity 1998;66(5):1813-1821.
181. Morell H, Clark MJ, Knowles PF, Sprinson DB. The enzymic synthesis of chorismic and prephenic acids from 3-enolpyruvylshikimic acid 5-phosphate. J. Biol. Chem. 1967;242(1):82-90.
182. Mousdale DM, Coggins JR. Detection and Subcellular-Localization of a Higher-Plant Chorismate Synthase. FEBS Lett. 1986;205(2):328-332.
183. Mousdale DM, Campbell MS, Coggins JR. Purification and characterisation of the bifunctional dehydroquinase-shikimate: NADP oxidoreductase from pea seedlings. Phytochemistry 1987;26(10):2665-2670.
184. Mousdale DM, Coggins JR. The Shikimate Pathway. Methods in Plant Biology 1993;9:1-23.
185. Nachega JB, Chaisson RE. *Tuberculosis* drug resistance: a global threat. Clin Infect Dis 2003;36(Suppl 1):S24-30.
-

-
186. Nakatsukasa WM, Nester EW. Regulation of aromatic amino acid biosynthesis in *Bacillus subtilis* 168. I. Evidence for and characterization of a trifunctional enzyme complex. *J. Biol. Chem.* 1972;247(18):5972-9.
187. Nandy M, Ganguli NC. Studies on 5-dehydroshikimic reductase from Mung bean seedlings (*Phaseolus aureus*). *Arch. Biochem. Biophys.* 1961;92:399-408.
188. Nguyen VT, Baker DP, Tricot C, Baur H, Villeret V, Dideberg O, et al. Catabolic ornithine carbamoyltransferase of *Pseudomonas aeruginosa*. Importance of the N-terminal region for dodecameric structure and homotropic carbamoylphosphate cooperativity. *Eur. J. Biochem.* 1996;236(1):283-293.
189. Niven GW, Kerby NW, Rowell P, Stewart WDP. The Regulation of Aromatic Amino-Acid Biosynthesis in Amino- Acid Liberating Mutant Strains of *Anabaena-Variabilis*. *Arch. Microbiol.* 1988;150(3):272-277.
190. Nozaki Y. The preparation of guanidine hydrochloride. *Methods Enzymol* 1972;26(PtC):43-50.
191. O'Farrell PH. High resolution two-dimensional electrophoresis of proteins. *J. Biol. Chem.* 1975;250(10):4007-21.
192. Oefner C, D'Arcy A, Daly JJ, Gubernator K, Charnas RL, Heinze I, et al. Refined crystal structure of beta-lactamase from *Citrobacter freundii* indicates a mechanism for beta-lactam hydrolysis. *Nature* 1990;343(6255):284-288.
193. Ogasawara N. Systematic function analysis of *Bacillus subtilis* genes. *Res. Microbiol.* 2000;151(2):129-134.
194. Onderka DK, Floss HG. Steric course of the chorismate synthetase reaction and the 3-deoxy-D- arabino-heptulosonate 7-phosphate (DAHP) synthetase reaction. *J. Am. Chem. Soc.* 1969;91(21):5894-5896.
195. Osborne A, Thorneley RN, Abell C, Bornemann S. Studies with substrate and cofactor analogues provide evidence for a radical mechanism in the chorismate synthase reaction. *J. Biol. Chem.* 2000;275(46):35825-35830.
196. Ossipov V, Bonner C, Ossipova S, Jensen R. Broad-specificity quinate (shikimate) dehydrogenase from *Pinus taeda* needles. *Plant Physiology and Biochemistry* 2000;38(12):923-928.
-

-
197. Ossipov V, Salminen JP, Ossipova S, Haukioja E, Pihlaja K. Gallic acid and hydrolysable tannins are formed in birch leaves from an intermediate compound of the shikimate pathway. *Biochemical Systematics and Ecology* 2003;31(1):3-16.
198. Pace CN. Determination and analysis of urea and guanidine hydrochloride denaturation curves. *Methods Enzymol.* 1986;131:266-80.
199. Pace CN, Vajdos F, Fee L, Grimsley G, Gray T. How to measure and predict the molar absorption coefficient of a protein. *Protein Sci* 1995;4(11):2411-23.
200. Padgett SR, Re DB, Gasser CS, Eichholtz DA, Frazier RB, Hironaka CM, et al. Site-Directed Mutagenesis of a Conserved Region of the 5- Enolpyruvylshikimate-3-Phosphate Synthase Active-Site. *J. Biol. Chem.* 1991;266(33):22364-22369.
201. Parish T, Stoker NG. The common aromatic amino acid biosynthesis pathway is essential in *Mycobacterium tuberculosis*. *Microbiology* 2002;148:3069-3077.
202. Parker EJ, Gonzalez Bello C, Coggins JR, Hawkins AR, Abell C. Mechanistic studies on type I and type II dehydroquinase with (6R)- and (6S)-6-fluoro-3-dehydroquinic acids. *Bioorg. Med. Chem. Lett.* 2000;10(3):231-234.
203. Payne DJ, Wallis NG, Gentry DR, Rosenberg M. The impact of genomics on novel antibacterial targets. *Current opinion in Drug discovery and development* 2000;3(2):177-190.
204. Piggot PJ, Curtis CA, De Lencastre H. Use of integrational plasmid vectors to demonstrate the polycistronic nature of a transcriptional unit (*spoIIA*) required for sporulation of *Bacillus subtilis*. *J. Gen. Microbiol.* 1984;130(8):2123-2136.
205. Pilch PF, Somerville RL. Fluorine-containing analogues of intermediates in the Shikimate pathway. *Biochemistry* 1976;15(24):5315-20.
206. Pittard AJ. Biosynthesis of the Aromatic Amino Acids. In: F.C. N, editor. *Escherichia coli and Salmonella cellular and molecular biology*. Second Edition ed: ASM Press; 1987. p. 458-484.
207. Polley LD. Purification and characterization of 3-dehydroquinic acid hydrolase and shikimate oxidoreductase. Evidence for a bifunctional enzyme. *Biochim. Biophys. Acta* 1978;526(1):259-66.

-
208. Pomp D, Medrano JF. Organic solvents as facilitators of polymerase chain reaction. *Biotechniques* 1991;10(1):58-59.
209. Price NC, Boam DJ, Kelly SM, Duncan D, Krell T, Gourley DG, et al. The folding and assembly of the dodecameric type II dehydroquinases. *Biochem. J.* 1999;338(Pt 1):195-202.
210. Price NC, Stevens I. *Fundamentals of enzymology: The cell and molecular biology of catalytic proteins.* 3rd ed: Oxford University Press; 1999.
211. Ranganathan G, Mukkada AJ. Ubiquinone biosynthesis in *Leishmania major* promastigotes. *Int J Parasitol* 1995;25(3):279-84.
212. Ray JM, Yanofsky C, Bauerle R. Mutational analysis of the catalytic and feedback sites of the tryptophan-sensitive 3-deoxy-D-arabino-heptulosonate-7-phosphate synthase of *Escherichia coli*. *J. Bacteriol.* 1988;170(12):5500-6.
213. Rehder V, Jaenicke R. Stability and reconstitution of D-glyceraldehyde-3-phosphate dehydrogenase from the hyperthermophilic eubacterium *Thermotoga maritima*. *J. Biol. Chem.* 1992;267(16):10999-1006.
214. Roberts F, Roberts CW, Johnson JJ, Kyle DE, Krell T, Coggins JR, et al. Evidence for the shikimate pathway in apicomplexan parasites. *Nature* 1998;393(6687):801-5.
215. Robinson DA. Thesis in Progress: University of Glasgow; 2003.
216. Roszak AW, Robinson DA, Krell T, Hunter IS, Fredrickson M, Abell C, et al. The structure and mechanism of the type II dehydroquinase from *Streptomyces coelicolor*. *Structure (Camb)* 2002;10(4):493-503.
217. Rotenberg SL, Sprinson DB. Isotope effects in 3-dehydroquinase and dehydratase. Mechanistic implications. *J. Biol. Chem.* 1978;253(7):2210-5.
218. Salomon II, Davis BD. Aromatic Biosynthesis. IX The Isolation of a Precursor of Shikimic Acid. *J. Am. Chem. Soc.* 1953;75:5567-5571.
219. Sampathkumar P, Morrison JF. Chorismate mutase-prephenate dehydrogenase from *Escherichia coli*. Purification and properties of the bifunctional enzyme. *Biochim Biophys Acta* 1982;702(2):204-11.
-

-
220. Sanderson GW. 5-Dehydroshikimate reductase in the tea plant (*Camellia sinensis* L.). Properties and distribution. *Biochem. J.* 1966;98(1):248-252.
221. Santos NC, Castanho MA. Teaching light scattering spectroscopy: the dimension and shape of tobacco mosaic virus. *Biophys. J.* 1996;71(3):1641-1650.
222. Scharf KH, M.H. Z, Onderka DK, Carroll M, Floss HG. Stereochemistry of the enzymatic and non-enzymatic conversion of 3-dehydroshikimate into protocatechuate. *Chem. Commun.* 1971:765-766.
223. Schmid J, Schaller A, Leibinger U, Boll W, Amrhein N. The in-vitro synthesized tomato shikimate kinase precursor is enzymatically active and is imported and processed to the mature enzyme by chloroplasts. *Plant. J.* 1992;2(3):375-83.
224. Schmidt CL, Danneel HJ, Schultz G, Buchanan BB. Shikimate Kinase from Spinach-Chloroplasts - Purification, Characterization, and Regulatory Function in Aromatic Amino- Acid Biosynthesis. *Plant Physiology* 1990;93(2):758-766.
225. Schneider TR, Hartmann M, Braus GH. Crystallization and preliminary X-ray analysis of 3-deoxy-D-arabino- heptulosonate-7-phosphate synthase (tyrosine inhibitable) from *Saccharomyces cerevisiae*. *Acta Crystallogr D Biol Crystallogr* 1999;55(Pt 9):1586-8.
226. Schoner R, Herrmann KM. 3-Deoxy-D-arabino-heptulosonate 7-phosphate synthase. Purification, properties, and kinetics of the tyrosine-sensitive isoenzyme from *Escherichia coli*. *J. Biol. Chem.* 1976;251(18):5440-7.
227. Selvapandiyar A, Majumder K, Fattah FA, Ahmad S, Arora N, Bhatnagar RK. Point mutation of a conserved arginine (104) to lysine introduces hypersensitivity to inhibition by glyphosate in the 5- enolpyruvylshikimate-3-phosphate synthase of *Bacillus subtilis*. *FEBS Lett* 1995;374(2):253-6.
228. Sharp MD, Pogliano K. An *in vivo* membrane fusion assay implicates SpoIIIE in the final stages of engulfment during *Bacillus subtilis* sporulation. *Proc. Natl. Acad. Sci. U. S. A.* 1999;96(25):14553-14558.
229. Shneier A, Harris J, Kleanthous C, Coggins JR, Hawkins AR, Abell C. Evidence for the opposite stereochemical courses for the reactions catalysed by type I
-

- and type II dehydroquinases. *Bioorganic & Medicinal Chemistry Letters* 1993;3(7):1399-1402.
230. Shumilin IA, Kretsinger RH, Bauerle RH. Crystal structure of phenylalanine-regulated 3-deoxy-D-arabino-heptulosonate-7-phosphate synthase from *Escherichia coli*. *Structure Fold Des.* 1999;7(7):865-875.
231. Shuttleworth WA, Pohl ME, Helms GL, Jakeman GL, Evans JNS. Site-directed mutagenesis of putative active site residues of 5-enolpyruvylshikimate-3-phosphate synthase. *Biochemistry* 1999;38(1):296-302.
232. Smith DD, Coggins JR. Isolation of a bifunctional domain from the pentafunctional arom enzyme complex of *Neurospora crassa*. *Biochem. J.* 1983;213(2):405-15.
233. Sprinson DB, Rothschild J, Sprecher M. The Synthesis of 3-Deoxy-D-arabino-heptulosonic Acid 7-Phosphate. *J. Biol. Chem.* 1963;238(3170-3175).
234. Sreerama N, Woody RW. Poly(pro)II helices in globular proteins: identification and circular dichroic analysis. *Biochemistry* 1994a;33(33):10022-10025.
235. Sreerama N, Woody RW. Protein secondary structure from circular dichroism spectroscopy. Combining variable selection principle and cluster analysis with neural network, ridge regression and self-consistent methods. *J. Mol. Biol.* 1994b;242(4):497-507.
236. Srinivasan PR, Katagiri M, Sprinson DB. The Enzymatic Synthesis of Shikimic Acid from D-Erythrose-4-Phosphate and Phos-Phoenolpyruvate. *J. Am. Chem. Soc.* 1955;77:4943-4944.
237. Srinivasan PR, Katagiri M, Sprinson DB. The conversion of Phosphoenolpyruvic Acid and D-Erythrose 4-Phosphate to 5-Dehydroquinic Acid. *J. Biol. Chem.* 1958;234:713-715.
238. Srinivasan PR, Rothschild J, Sprinson DB. The Enzymic Conversion of 3-Deoxy-D-arabino-heptulosonic Acid 7-Phosphate to 5-Dehydroquinic Acid. *J. Biol. Chem.* 1963;238(10):3176-3182.
239. Stallings WC, Abdel-Meguid SS, Lim LW, Shieh HS, Dayringer HE, Leimgruber NK, et al. Structure and topological symmetry of the glyphosate target 5-

- enolpyruvylshikimate-3-phosphate synthase: a distinctive protein fold. Proc. Natl. Acad. Sci. U. S. A. 1991;88(11):5046-5050.
240. Steinrucken HC, Amrhein N. The herbicide glyphosate is a potent inhibitor of 5-enolpyruvyl-shikimic acid-3-phosphate synthase. Biochem. Biophys. Res. Commun. 1980;94(4):1207-1212.
241. Stephens CM, Baucarle R. Analysis of the metal requirement of 3-deoxy-D-arabino-heptulosonate-7-phosphate synthase from *Escherichia coli*. J. Biol. Chem. 1991;266(31):20810-20817.
242. Stephens RS, Kalman S, Lammel C, Fan J, Marathe R, Aravind L, et al. Genome sequence of an obligate intracellular pathogen of humans: *Chlamydia trachomatis*. Science 1998;282(5389):754-759.
243. Studier FW, Moffatt BA. Use of Bacteriophage-T7 RNA-Polymerase to Direct Selective High-Level Expression of Cloned Genes. J. Mol. Biol. 1986;189(1):113-130.
244. Sudi J. The lactate dehydrogenase--reduced nicotinamide--adenine dinucleotide--pyruvate complex. Kinetics of pyruvate binding and quenching of coenzyme fluorescence. Biochem. J. 1974a;139(1):251-9.
245. Sudi J. Macroscopic rate constants involved in the formation and interconversion of the two central enzyme--substrate complexes of the lactate dehydrogenase turnover. Biochem. J. 1974b;139(1):261-71.
246. Summerton J, Atkins T, Beswick R. A Rapid method for Preparation of Bacterial Plasmids. Anal Biochem 1983;133:79-84.
247. Sutherland JK, Watkins WJ, Bailey JP, Chapman AK, Davies GM. The Synthesis of 6-Alpha-Fluoroshikimic and 6-Beta-Fluoroshikimic Acids. Journal of the Chemical Society-Chemical Communications 1989(18):1386-1387.
248. Suzuki N, Sakuta M, Shimizu S. Purification and characterization of a cytosolic isozyme of 3-deoxy-D-arabino-heptulosonate 7-phosphate synthase from cultured carrot cells. Journal of Plant Physiology 1996;149(1-2):19-22.
249. Szabo AG. Fluorescence principles and measurement. In: Gore MG, editor. Spectrophotometry and spectrofluorimetry: a practical approach.: Oxford University Press; 2000. p. 33-43.

-
250. Tabor S, Richardson CC. A bacteriophage T7 RNA polymerase/promotor system for controlled exclusive expression of specific genes. Proc. Natl. Acad. Sci. U. S. A. 1985;82:1074-1078.
251. Tarle I, Borhani DW, Wilson DK, Quioco FA, Petrash JM. Probing the active site of human aldose reductase. Site-directed mutagenesis of Asp-43, Tyr-48, Lys-77, and His-110. J. Biol. Chem. 1993;268(34):25687-25693.
252. Theorell H, Nygaard P. Kinetic and equilibria in flavoprotein systems II. The effect of pH, anions and temperature on the dissociation and reassociation of the old yellow enzyme. Acta chemica Scandinavica 1954;8:1649-1658.
253. Thomas MG, Lawson C, Allanson NM, Leslie BW, Bottomley JR, McBride A, et al. A series of 2(Z)-2-Benzylidene-6,7-dihydroxybenzofuran-3[2H]-ones as inhibitors of chorismate synthase. Bioorg. Med. Chem. Lett. 2003;13(3):423-426.
254. Vagner V, Dervyn E, Ehrlich SD. A vector for systematic gene inactivation in *Bacillus subtilis*. Microbiology 1998;144(11):3097-3104.
255. Valone JA, Jr., Case ME, Giles NH. Constitutive mutants in a regulatory gene exerting positive control of quinic acid catabolism in *Neurospora crassa*. Proc. Natl. Acad. Sci. U. S. A. 1971;68(7):1555-1559.
256. Villeret V, Tricot C, Stalon V, Dideberg O. Crystal-Structure of *Pseudomonas-Aeruginosa* Catabolic Ornithine Transcarbamoylase at 3.0-Angstrom Resolution - a Different Oligomeric Organization in the Transcarbamoylase Family. Proc. Natl. Acad. Sci. U. S. A. 1995;92(23):10762-10766.
257. Vinella D, Gagny B, Joseleau-Petit D, D'Ari R, Cashel M. Mecillinam resistance in *Escherichia coli* is conferred by loss of a second activity of the AroK protein. J. Bacteriol. 1996;178(13):3818-3828.
258. Warner JB, Lolkema JS. Growth of *Bacillus subtilis* on citrate and isocitrate is supported by the Mg²⁺-citrate transporter CitM. Microbiology-Sgm 2002;148:3405-3412.
259. Warren JC, Cheatum SG. Effect of neutral salts on enzyme activity and structure. Biochemistry 1966;5(5):1702-1707.
-

-
260. Whipp MJ, Pittard AJ. A reassessment of the relationship between *aroK*- and *aroL*-encoded shikimate kinase enzymes of *Escherichia coli*. *J. Bacteriol.* 1995;177(6):1627-1629.
261. White PJ, Millar G, Coggins JR. The overexpression, purification and complete amino acid sequence of chorismate synthase from *Escherichia coli* K12 and its comparison with the enzyme from *Neurospora crassa*. *Biochem. J.* 1988;251(2):313-322.
262. White PJ, Young J, Hunter IS, Nimmo HG, Coggins JR. The purification and characterization of 3-dehydroquinase from *Streptomyces coelicolor*. *Biochem. J.* 1990;265(3):735-738.
263. Widlanski TS, Bender SL, Knowles JR. Stereochemical Course of the Cryptic Elimination and Cyclization Steps in the Reaction Catalyzed by Dehydroquinase Synthase. *J. Am. Chem. Soc.* 1987;109(6):1873-1875.
264. Widlanski T, Bender SL, Knowles JR. Dehydroquinase synthase: the use of substrate analogues to probe the late steps of the catalyzed reaction. *Biochemistry* 1989a;28(19):7572-7582.
265. Widlanski T, Bender SL, Knowles JR. Dehydroquinase Synthase - a Sheep in Wolf's Clothing. *J. Am. Chem. Soc.* 1989b;111(6):2299-2300.
266. Wierenga RK, De Maeyer MCH, Hol WGJ. Interaction of pyrophosphate moieties with α helices in dinucleotide binding proteins. *Biochemistry* 1985;24:1346-1357.
267. Wilson DJ, Patton S, Florova G, Hale V, Reynolds KA. The shikimic acid pathway and polyketide biosynthesis. *Journal of Industrial Microbiology & Biotechnology* 1998;20(5):299-303.
268. Wright F, Bibb MJ. Codon usage in the G+C-rich *Streptomyces* genome. *Gene* 1992;113(1):55-65.
269. Yanisch-Perron C, Viera J, Messing J. Improved M13 phage cloning vectors and host strains: nucleotide sequences of the M13mpl8 and pUC19 vectors. *Gene* 1985;33:103-119.
270. Yavin H, Gilvarg C. Aromatic biosynthesis XIV. 5-dehydroshikimic reductase. *J. Biol. Chem.* 1955;213:787-795.
-

-
271. Ye RW, Tao W, Bedzyk I, Young T, Chen M, Li L. Global gene expression profiles of *Bacillus subtilis* grown under anaerobic conditions. *J. Bacteriol.* 2000;182(16):4458-4465.
272. Zhang HJ, Sheng XR, Pan XM, Zhou JM. Activation of adenylate kinase by denaturants is due to the increasing conformational flexibility at its active sites. *Biochem. Biophys. Res. Commun.* 1997;238(2):382-386.

Appendix A. TABLE OF BUFFERS

Buffer	Composition per litre
General buffers and solutions	
10% SDS	100 g SDS
0.5M Tris acetate	60.6 g Tris base Adjust to desired pH with glacial acetic acid.
0.5M EDTA pH 8.0	186.1 g EDTA·4H ₂ O ~20 g NaOH Adjust pH with NaOH, EDTA will not go into solution until pH is raised to about 8.0
Agarose gel electrophoresis buffers for analysis of DNA	
TAE (50×)	242 g Tris base 57.1 ml glacial acetic acid 100 ml 0.5 M EDTA, pH 8.0
TBE (10×)	54 g Tris base 27.6 g boric acid 20 ml 0.5 M EDTA, pH 8.0
Composition per 10 ml	
Agarose DNA loading buffer (10×)	25 mg bromophenol blue 3 ml glycerol

 Buffers for preparing *E. coli* competent cells

	Composition per 500 ml
RF1	37.28 g KCl 1.1 g CaCl ₂ ·6H ₂ O 50 ml 1M potassium acetate 4.9g MnCl ₂ ·4H ₂ O 75 ml glycerol Adjust pH to 5.8 with glacial acetic acid and filter sterilise.
RF2	2.1 g MOPS 0.4 g KCl 8.2 g CaCl ₂ ·6H ₂ O 75 ml glycerol Adjust pH to 6.8 with glacial acetic acid and filter sterilise.

 SDS-PAGE Buffers and solutions for analysis of proteins

	Composition per litre
30% acrylamide/ 0.8% bis-acrylamide	300 g acrylamide 8 g bis-acrylamide
Separating gel buffer (2.5×) (1.875 M Tris·Cl, 0.25% SDS)	227.1 g Tris base 2.5 g SDS Adjust pH to 8.8 with HCl.
Stacking gel buffer (5×) (0.5 M Tris·Cl, 0.25% (w/v) SDS)	60.5 g Tris base 2.5 g SDS Adjust pH to 6.8 with phosphoric acid.

SDS-PAGE Buffers and solutions for analysis of proteins

	Composition per litre
Electrophoresis Buffer (10×)	60.5 g Tris base
	144.1 g glycine
	5 g SDS
	pH should be 8.8 without adjustment.
	Composition per 10 ml
SDS-PAGE sample buffer	2.25 ml 1M Tris·Cl, pH 6.8
	5 ml glycerol
	0.5 g of SDS
	5 mg Bromophenol blue
	2.5 ml dithiothreitol (DTT)
Coomassie staining solution	0.5 g coomassie brilliant blue R-250
	400 ml Ethanol
	Dissolve, then add:
	100 ml glacial acetic acid
	500 ml water
Destaining solution	100 ml ethanol
	100 ml glacial acetic acid
	800 ml water

Western transfer and immunodetection buffers and solutions	
	Composition per litre
Transfer buffer (CAPS)	22.1 g cyclohexylaminopropane sulfonic acid (CAPS) (100 mM) 100 ml of Methanol (10% v/v) pH should be 11.0 without adjustment.
PBS (10×)	71.7 ml 0.5M K ₂ HPO ₄ 28.3 ml 0.5M KH ₂ PO ₄ 8.8 g NaCl pH should be 7.2 without adjustment.
Composition for 500 ml	
Blocking and antibody buffer	250 ml PBS 0.25 ml Tween-20 15 g milk powder (Marvel™)
Bradford's Reagent	0.5 mg/ml Coomassie Blue G 25% (v/v) methanol 42.5% (v/v) Phosphoric acid pH -0.01 The solution is stable indefinitely in a dark bottle at 4°C.
Lowry reagents	(A) 2% (w/v) Sodium potassium tartrate (B) 1% (w/v) CuSO ₄ ·5H ₂ O (C) 0.1 M NaOH, 2% (w/v) Na ₂ CO ₃ mixed in a ratio of 1:1:100, respectively.
Folin reagent	50% (v/v) folin

Appendix B. Company names and addresses

Amersham Biosciences (formally Amersham and Pharmacia), 800 Centennial Avenue, P.O. Box 1327, Piscataway, NJ 08855-1327, USA, + 1-732-457-8000

Applied Biosystems, Division Headquarters, 850 Lincoln Centre Drive, Foster City, CA 94404, U.S.A. + 1-650-638-5800, <http://www.appliedbiosystems.com/>

Beckman Coulter (UK) Ltd, Oakley Court, Kingsmead Business park, London Road, High Wycombe, Buckinghamshire, HP11 1JU 0044 0 1494 441181
www.beckman.com

BioRad Laboratories Ltd, BioRad House, Maylands Avenue, Hemel Hempstead, Hertfordshire, HP2 7TD, 0800 181134, www.bio-rad.com

Clare chemical research, 24B station St, Ross on Wye, HR9 7AG, England, UK. +44 1989 565049.

Emerald BioAgriculture Corporation, 3125 Sovereign Dr. Suite B, Lansing, MI 48911-4240, USA 001 517 882 7370 www.emeraldbio.com

F. Hoffmann-La Roche Ltd., Group Headquarters, Grenzacherstrasse 124, CH-4070 Basel, Switzerland, +41-61-688 1111, <http://www.roche.com/>

Fisher Scientific UK Ltd., Bishop Meadow Road, Loughborough, Leicestershire LE11 5RG, UK, 01509 231166, E-mail: info@fisher.co.uk, <http://www.fisher.co.uk/>

Hampton Research, 27632 El Lazo Road, Suite 100, Laguna Niguel, CA 92677-3913, USA 001 949 425 1321 www.hamptonresearch.com

JASCO (UK) Ltd, 18 Oak Industrial Park, Chelmsford Road, Great Dunmow, CM6 1XN, 44 (0) 1371 876988, Email : inbox@jasco.co.uk, www.jasco.co.uk

Millipore (Amicon is a subsidiary) (UK) Limited, Units 3&5 The Courtyards, Hatters Lane, Watford, WD18 8YH, 0870 900 4645, www.millipore.com/

MWG Biotech (UK) Ltd., Mill Court, Featherstone Road, Wolverton Mill South, Milton Keynes, MK12 5RD, United Kingdom, + 44 - 19 08 - 525 - 500, E-mail info@mwg.co.uk.

New England Biolabs (UK) Ltd., 73 Knowl Piece, Wilbury Way, Hitchin, Hertfordshire, SG4 0TY, United Kingdom, 0800 318486, E-mail: info@uk.neb.com, <http://www.neb.com/>

Pierce Scientific (part of Perbio), Knutpunkten 34, SE-252 78 Helsingborg, Sweden, +46 42 26 90 90, E-mail: info@perbio.com, <http://www.perbio.com/>

Promega UK Ltd, Delta House, Chilworth Research Centre, Southampton SO16 7NS
Phone : 0800 378994, www.promega.com

Proxeon Biosystems (formally Protana), Staermosegaardsvej 6, DK-5230 Odense M, Denmark, (+45) 6557 2300, E-mail: info@proxeon.com, www.proxeon.com

Sigma-Aldrich Company Ltd, The Old Brickyard, New Rd, Gillingham, Dorset, SP8 4XT, Phone : 0800 717181, www.sigmaaldrich.com

Stratagene, Gebouw California, Hogehilweg 15, 1101 CB Amsterdam Zuidoost, The Netherlands <http://www.stratagene.com/>

Thermo Orion, Corporate Office, 166 Cummings Centre, Beverly, MA 01915, United States, +1 978-232-6000, Email: info@thermoorion.com, <http://www.thermo.com/>.

Viva Science Ltd. Satorius group Unit 6, Stonedale Road, Stonhouse, Gloucestershire, GL10 3RQ, UK. www.vivascience.com

Appendix C. Protein Sequence Alignments

Figure 71. *S. coelicolor* type II dehydroquinase (SCDHQase) aligned against representatives of type II dehydroquinases. The secondary structural features of SCDHQase are shown at the top of the alignment the alpha (α) and 3₁₀ (η) helices are represented as helices and beta strands (β) represented by arrows, and β turns are marked TT. Sequences important in this study are highlighted in yellow; residues targeted for site-directed mutagenesis are highlighted in green. This sequence alignment was created using the following sequences (organism, designated function) from GeneBank: *Streptomyces coelicolor* (S._coelicolor), *Bradyrhizobium japonicum* (B._japonicum), *Agrobacterium tumefaciens* (A._tumefaciens), *Brucella suis* (Brucella_suis), *Brucella abortus* (Brucella_abortus), *Brucella melitensis* (Brucella_melitensis), *Mesorhizobium loti* (Mesorhizobium_loti), *Sinorhizobium meliloti* (S._meliloti), *Magnetospirillum magnetotacticum* (M._magnetotacticum), *Pseudomonas fluorescens* (P._fluorescens), *Pseudomonas aeruginosa* (P._aeruginosa), *Corynebacterium glutamicum* (C._glutamicum), *Caulobacter crescentus* (C._crescentus), *Pseudomonas putida* (Pseudomonas_putida), *Pseudomonas syringae* (Pseudomonas_syringae), *Xylella fastidiosa* (Xylella_fastidiosa), *Xanthomonas campestris* pv. (X._campestris), *Xanthomonas axonopodis* pv. (X._axonopodis), *Ralstonia solanacearum* (R._solanacearum), *Nitrosomonas europaea* (N._europaea), *Actinobacillus pleuropneumoniae* (A._pleuropneumoniae), *Pasteurella multocida* (P._multocida), *Haemophilus influenzae* (H._influenzae), *Vibrio cholerae* (Vibrio_cholerae), *Vibrio parahaemolyticus* (V._parahaemolyticus), *Emericella nidulans* (Emericella_nidulans), *Buchnera aphidicola* str. (B._aphidicola), *Bacillus halodurans* (Bacillus_halodurans), *Bacillus subtilis* (Bacillus_subtilis), *Bacillus anthracis* (Bacillus_anthraxis), *Deinococcus radiodurans* (D._radiodurans), *Bacteroides thetaiotaomicron* (B._thetaiotaomicron), *Campylobacter jejuni* (Campylobacter_jejuni), *Geobacter metallireducens* (G._metallireducens), *Bifidobacterium longum* (B._longum), *Tropheryma whippelii* (Tropheryma_whipplei), *Corynebacterium pseudotuberculosis* (C.pseudotuberculosis), *Mycobacterium leprae* (M._leprae), *Mycobacterium tuberculosis* (M._tuberculosis), *Helicobacter pylori* (Helicobacter_pylori), *Fusobacterium nucleatum* (F._nucleatum), *Clostridium perfringens* (C._perfringens), *Thermotoga maritima* (T._maritima), *Thermoanaerobacter tengcongensis* (T._tengcongensis), *Neurospora crassa* (Neurospora_crassa), *Chlorobium tepidum* (Chlorobium_tepidum) and *Streptomyces hygroscopicus* (S._hygroscopicus).

Figure 72. *E. coli* shikimate dehydrogenase (ECAroE) aligned against representatives of the shikimate dehydrogenase family. The secondary structural features of ECAroE are shown at the top of the alignment the alpha (α) and 3_{10} (η) helices are represented as helices and beta strands (β) represented by arrows, and β turns are marked TT. Sequences important in this study are highlighted in yellow; shikimate dehydrogenases are highlighted in green; type 1 and type 2 YdiB proteins are highlighted in blue and pink, respectively. This sequence alignment was created using the following sequences (organism, designated function) from GeneBank: *E. coli* K12 AroE (E._coli_AroE), *Salmonella typhimurium* (S._typhimurium_AroE), *Salmonella enterica* (S._enterica_AroE), *Yersinia pestis* (Y._pestis_AroE), *Haemophilus influenzae* (H._influenzae_AroE), *Pasteurella multocida* (P._multocida_AroE), *Haemophilus somnus* (H._somnia_AroE), *Actinobacillus actinomycetemcomitans* (A._actinomycet._AroE), *Vibrio cholerae* (V._cholerae_AroE), *Vibrio vulnificus* (V._vulnificus_AroE), *Pseudomonas syringae* (P._syringae_Hypo), *Azotobacter vinelandii* (A._vinelandii_Hypo), *Nitrosomonas europaea* (N.europaeaQuin/Shik), *Neisseria polysaccharea* (N.polysacchareaAroE), *Neisseria flavescens* (N._flavescens_AroE), *Neisseria meningitidis* (N._meningitidesAroE), *Neisseria gonorrhoeae* (N._gonorrhoeae_AroE), *Buchnera aphidicola* (B._aphidicola_AroE), *Legionella pneumophila* (L._pneumophila_Hypo), *Helicobacter pylori* (H._pylori_AroE), *Escherichia coli* (E._coli_YdiB), *Salmonella typhimurium* (S._typhimurium_YdiB), *Listeria monocytogenes* (L._monocyto._AroEFam), *Listeria monocytogenes* (L._monocyto._YdiB), *Listeria innocua* (L._innocua_oxidoreduct), *Synechocystis* sp. PCC 6803 (Synechocystis_AroE), *Magnetococcus* sp. MC-1 (Magnetococcus_Hypo), *Listeria monocytogenes* (L._monocytoenes_AroE), *Bacillus anthracis* (B.anthraxisQuin/Shik), *Bacillus subtilis* (B._subtilis_AroE), *Leuconostoc mesenteroides* subsp. *mesenteroides* (L._mesenteroid._Hypo), *Lycopersicon esculentum* (tomato) (L._esculentum_BiFAroE), *Deinococcus radiodurans* (D._radiodurans_AroE), *Pseudomonas fluorescens* (P._fluorescens_Hypo2), *Rhodobacter sphaeroides* (R._sphaeroides_Hypo), *Corynebacterium diphtheriae* (C._diphtheriae_AroE), *Pseudomonas putida* (P._putida_AroEFam), *Mycobacterium smegmatis* (M._smegmatis_YdiB), *Brucella melitensis* (B._melitensis_Quin/Shik), *Haemophilus influenzae* (H._influenzae_YdiB), *Actino actinomycetemcomitans* (A._actinomycet_YdiB), *Pasteurella multocida* (P._multocida_YdiB), *Pseudomonas putida* (P._putida_Quin/Shik), *Pseudomonas fluorescens* (P._fluorescens_Hypo1), *Deinococcus radiodurans* (D._radiodurans_YdiB), *Mycobacterium smegmatis* (M._smegmatis_AroE), *Yersinia pestis* (Y._pestis_YdiB), *Salmonella enterica* subsp. *enterica* serovar *Typhi* (S._enterica_YdiB), *Corynebacterium diphtheriae* (C._diphtheriae_YdiB), *Neurospora crassa* (N._crassa_QuinDHG) and *Emericella nidulans* (A._nidulans_QuinDHG).

